Organic Self-Assembled Layer-by-Layer Thin Films for Second-Order Nonlinear Optics

Matthew T. Guzy

Dissertation submitted to the Faculty of the Virginia Polytechnic Institute and State University in partial fulfillment of the requirements for the degree of

Doctor of Philosophy
In
Chemical Engineering

Richey M. Davis, Co-chair
Kevin E. Van Cott, Co-chair
J. Randy Heflin
Harry W. Gibson
Garth Wilkes

July 7, 2003
Blacksburg, VA

Keywords: Layer-by-layer deposition, second order nonlinear optics, polymeric thin films, chromophore orientation, self assembly

Organic Self-Assembled Layer-by-Layer Thin Films for Second-Order Nonlinear Optics

Matthew T. Guzy

(ABSTRACT)

Layer-by-layer deposition techniques were used to fabricate films with second order nonlinear optical (NLO) properties. These materials are key to the development of electro-optic modulators used in fiber optic communication systems. Performance benefits and lower manufacturing costs are driving the development of organic NLO materials as replacements for inorganic crystalline materials such as lithium niobate.

The layer-by-layer deposition technique in which polyelectrolytes are deposited on a surface by electrostatic effects is called the Ionically Self-Assembled Monolayer or ISAM method. The role of the optically inactive polycation's structure on deposition and chromophore orientation was studied by fabricating films with several different polycations. While the specific interactions responsible for chromophore orientation in ISAM films remains unclear, hydrogen bonding and electrostatic effects are ruled out as the sole sources of orientation. The highest values of $\chi^{(2)}$ were observed under pH conditions that resulted in flat and thin layers. The relationship between pH and the optical homogeneity of the film was also explored. Deposition of polymers under pH conditions in which the polymer chains were aggregated in solution results in films that are not suitable for use in devices.

In this work, a new layer-by-layer deposition technique was developed. Coined hybrid deposition, it relies on covalent bonds and electrostatic interactions for film fabrication. Optically inactive polyamines were used as sources of positive charges and as binding sites with optically active low molecular weight chromophores functionalized with a reactive triazine ring and negative charged sulfonate groups. Polar ordering of the chromophores was obtained when the deposition was done under conditions in which covalent bonding was the preferred attachment mechanism for the chromophore molecules. pH conditions in which electrostatic attachment dominated resulted in poorer orientation. The effect of adding ionic salts to the dye solutions was studied, with hopes of increasing the chromophore density in the film by shielding inter-dye electrostatic repulsions. A linear relationship in deposited amount, as characterized by absorbance/bilayer, was observed as the salt concentration was increased. Little effect on $\chi^{(2)}$ was observed for films made with the as-received Procion Red MX-5B chromophore. However, films fabricated from purified Procion Brown MX-GRN showed a definite dependence on added salt. Exceptional $\chi^{(2)}$ values were obtained for Procion Brown films deposited using 0.5 M NaCl and PAH. The importance of depositing from non-aggregated solutions was again highlighted, as films made with the less soluble Procion Orange were significantly less homogeneous than those made from Procion Red and Procion Brown which were highly soluble. The role of polycation structure on the deposition and orientation of Procion Brown and Red was examined.

Acknowledgements

With a majority of the dissertation (almost) behind me, I can take an opportunity to breathe a sigh of relief and reflect on the people and events that have gotten me to where I am now. First and foremost my parents, Thomas and Barbara, as well as my brother, Michael, must be thanked for their unconditional support and encouragement over the years.

In Blacksburg there are a number of people to thank who have contributed to the success I've had. My advisors Kevin Van Cott and Richey Davis have both guided my research and have proofread countless documents. My coworkers in the Davis lab and Van Cott labs have been a source of assistance and entertainment over the years.

There are two individuals who have contributed greatly towards my maintaining any semblance of sanity in Blacksburg. Jody, you were and will always be my partner in crime. Craig, there is not much to say that's not been said already. There are not words to express my gratitude to the both of you.

TABLE OF CONTENTS

TABLE OF FIGURES

TABLE OF TABLES

1 Introduction

1.1 Motivation

The modern world very much depends on the communications industry. Telephones, fax machines, cellular phones, and the internet are essential to life in highly developed societies. At present, long range communications require fiber optic networks which rely upon signal conversion. The next generation of switching equipment will be based on second order nonlinear optical (NLO) materials, which can be used to manipulate light with electricity (see Figure 1.1-1 for a schematic of an electro-optic modulator based on a Mach-Zehnder interferometer).[1] Initially, these materials were limited to a few inorganic crystals such as lithium niobate ($LiNbO_3$). Applications of these inorganic crystals as NLO materials are limited due to manufacturing and processing difficulties which, in many cases, makes these materials prohibitively expensive.

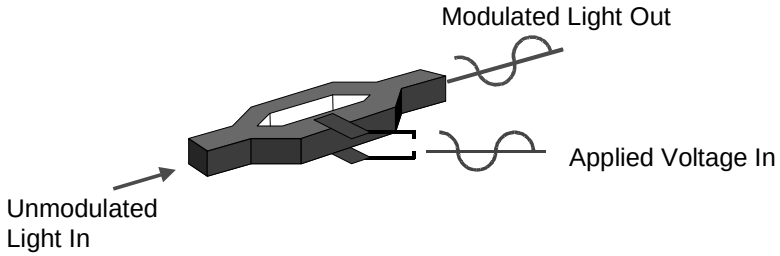

Figure 1.1-1 - Schematic of an electro-optic modulator. Unmodulated light enters the device and is modulated by an applied voltage. A detailed description of how this device works is provided in Chapter 2.

Polymeric NLO materials, first demonstrated as feasible in the late 1980's, represent the next evolutionary step for electro-optic materials.[2,3] Polymeric materials offer substantial performance benefits over traditional inorganic materials in addition to the fabrication and processing benefits inherent with polymeric materials. For any polymeric material to display NLO activity there are two criterion that must be met: 1) a NLO-active chromophore must be present in the material and 2) the NLO-active substituent must possess some net degree of order. Several different classes of materials meet these two requirements.

The first class, first demonstrated in the late 1980's, are guest / host, or poled polymeric materials. In these materials a NLO-active chromophore is doped into a polymeric matrix and oriented by an electric field while the temperature is held above the

glass transition temperature of the matrix. The host is then quenched below its glass transition and the orientation of the chromophore molecules is "locked in". However, the NLO activity is not stable over long periods of time, due to the randomization of the chromophore's orientation. This process is schematically shown in Figure 1.1-2. The randomization process occurs even more quickly at elevated temperatures needed for device fabrication and operation. This lack of stability is the principle roadblock preventing widespread application of these materials.

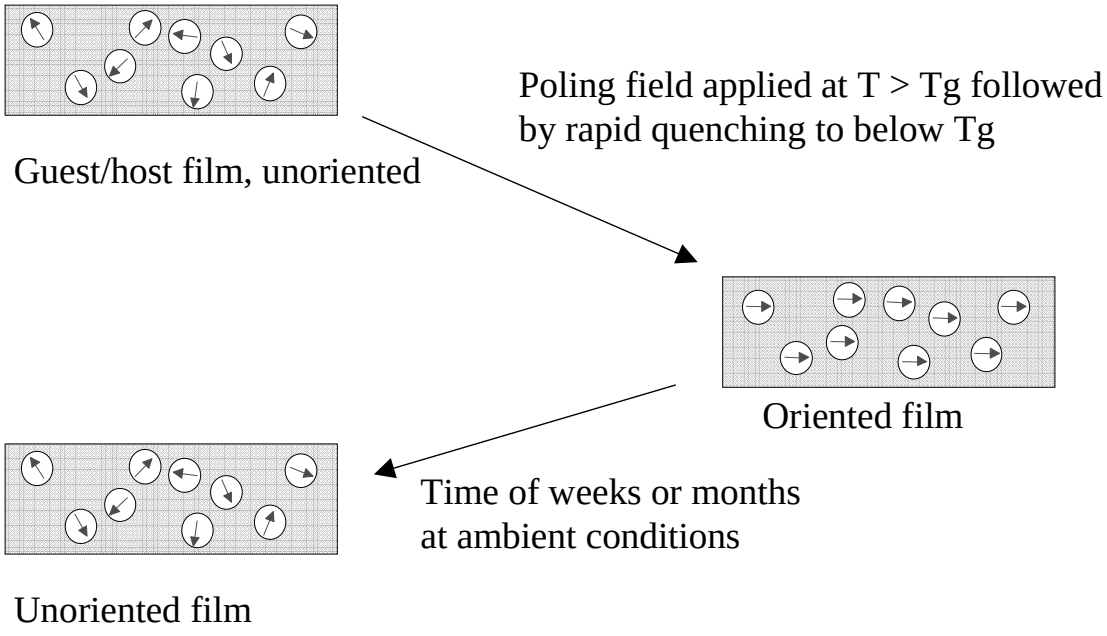

Figure 1.1-2 - Schematic of the poling process showing how orientation arises due to the poling field, yet decays back to the unoriented initial state.

The second class of polymeric materials for NLO applications seeks to overcome the loss of orientation problem by utilizing a system where the chromophore's oriented state is it's intrinsic state. Langmuir-Blodgett films are formed in a layer by layer process in which monolayer of material is deposited on a substrate by dipping the substrate through a compressed monolayer of material suspended on a water surface. High degrees of orientation can be achieved along with very good NLO performance. However, Langmuir-Blodgett films lack the physical robustness needed for application and also are very sensitive to environmental factors, which can lead to degradation of the material.

The third class of materials, and the class this research focuses on, involves the deposition of NLO chromophores in a layer-by-layer manner.[4] The ionically self-

assembled monolayer (ISAM) method is a film fabrication method in which oppositely charged multivalent species including colloidal particles and polymers are deposited on a charged substrate. For a polymer-polymer ISAM where a glass slide is used as the substrate, it is first placed in a solution of polycation. The polyelectrolyte adsorbs to the surface and causes a reversal of the surface charge. The substrate, now positively charged, is well rinsed (to remove any unbound polyelectrolyte) and is then placed in a polyanionic solution. Again, polyelectrolyte adsorbs and the surface undergoes a charge reversal. The substrate is removed from the solution and again rinsed. This process is repeated until the desired number of layers has been deposited. This process is schematically shown below in Figure 1.1-3.

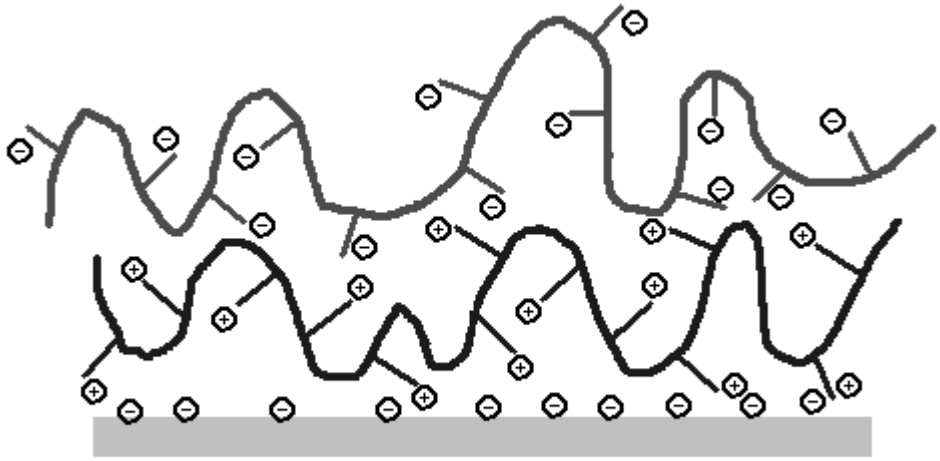

Figure 1.1-3 - Schematic of a deposited ISAM bilayer. Additional layers would then be deposited on the polyanion, creating a multilayer film

This method has been shown as a viable method for fabricating NLO-active films. However, these films do not have a second order susceptibility, $\chi^{(2)}$ (a parameter that characterizes second order NLO), high enough for practical device applications. One of the benefits of the ISAM method is that the films have been shown to have excellent thermal stability.[5] The deposition of NLO films that possess a $\chi^{(2)}$ value high enough for device applications is the fundamental goal of this research. Prior to this work, the deposition of NLO active ISAM films had only been demonstrated for several different polymeric, anionic chromophore molecules. The effects of processing variables as well as polymer and chromophore architecture on the resulting film's orientation had not been

thoroughly examined. However, the promise of high $\chi^{(2)}$ values in addition to the demonstrated exceptional thermal stability provided incentive for further work.

1.2 Specific Research Objectives

While the long-term goal of the project is to develop a film with an appropriately large NLO response for use in a prototype electro-optic modulator, there are several smaller goals which must first be achieved to bring the larger objective closer to fruition. This research specifically aims to improve the orientation of the chromophoric molecules in the films. First-generation ISAM films showed promising values of $\chi^{(2)}$, despite having relatively small degrees of net orientation. With increased orientation, these $\chi^{(2)}$'s should drastically improve. To these ends, this research has three principal research objectives:

1) **Probe the sources of chromophore orientation ISAM films.** Specifically, examine the role of electrostatic, hydrogen bonding and steric effects that drive film self-assembly and chromophore orientation.

2) **Develop a hybrid deposition scheme that, unlike the traditional purely electrostatic ISAM method, relies on both electrostatic interactions and covalent bonds for building ordered layer-by-layer films.**

3) **Determine the process variables needed to make 1-10 μm thick NLO active films with the necessary optical clarity.** For use in any prototype device, films must be homogeneous, or free from any defects which would result in scattering. The effects of ionic strength, pH and solubility of compounds has been examined.

1.3 Thesis Outline

This thesis is organized into the following chapters.

- **Chapter 2. Literature Review**

Chapter 2 begins with an overview of nonlinear optics and reviews second order nonlinear optic phenomena. Following that discussion, the focus moves to the general adsorption of polymers on surfaces. Finally, a review of literature relevant to the ISAM process and ISAM process variables is presented, ending with a review of NLO ISAM work.

- **Chapter 3. Layer-By-Layer Deposition And Ordering Of Low Molecular Weight Dye Molecules For Second Order Nonlinear Optics**

Chapter 3 addresses objectives #2 and #3 in the previous section and provides detail on the materials and reactive mechanism used to fabricate these films. To these ends, a commercially available chromophore (Procion Red MX-5B), whose structure includes a reactive triazine moiety has been used in tandem with the polycation poly(allylamine hydrochloride) to fabricate films. Measurements of the absorbance demonstrate regular layer-by-layer growth of the film. Additionally, NLO characterization reveals that hybrid deposition results in regularly oriented films with $\chi^{(2)}$ values within a factor of 20 to those of $LiNbO_3$. This approach is quite general and its extension is discussed in Chapters 4 and 5. Effects of pH on the deposition of dye, film thickness and $\chi^{(2)}$ are provided.

- **Chapter 4. Effect of Ionic Strength on the Deposition and Orientation of Low Molecular Weight Chromophores**

Chapter 4 continues the development of the hybrid deposition scheme presented in the previous chapter. Films are deposited under high ionic strengths to increase the electrostatic screening that occurs during deposition. This increased screening allows for a higher packing density of dye molecules on the surface, increasing the chromophore density in the film. If orientation is not compromised, this will result in an increase in $\chi^{(2)}$. Additionally, the relationship between Procion chromophore structure and $\chi^{(2)}$ is probed by fabrication of films with three different Procion chromophores.

- **Chapter 5. Effect of Polycation Structure on the Orientation of a Low Molecular Weight Chromophore**

Chapter 5 continues the development of the hybrid deposition scheme using either Procion Red or Brown dyes and four different polycations - poly(allylamine hydrochloride), poly(vinylamine hydrochloride), polyethylimine, and chitosan. These polycations have primary and secondary amines with different spacings between the amine functionality and the polymer backbone, allowing for some insight into the orientation mechanism for films fabricated via hybrid deposition.

- **Chapter 6.Orientation of an Anionic Chromophoric Side Group in Ionically Self-Assembled Films: Effects of pH and Polycation Choice**

Chapter 6 addresses objectives #1 and #3 in the previous section. This was done using commercially available polycations commonly employed in the ISAM method including poly(allylamine hydrochloride), poly(L-lysine), and poly(diallyldimethylammonium chloride). These films were fabricated using the NLO chromophore poly(1-[4-(3-carboxy-4-hydroxylphenylazo)benzensulfonamido]-1,2-ethanediyl, sodium salt) (PCBS). Details on the deposition process as well as quantitative NLO results are presented. In addition to the previously mentioned results regarding orientation, the effects of solution conditions on optical homogeneity of the film are also addressed.

- **Chapter 7. A Continued Examination of the Role of Hydrogen Bonding and Polycation Structure on the Orienting of Side Group Chromophores in Electrostatic Layer-by-Layer Films**

Continuing the work of the previous chapter, the polycations poly(vinylamine), chitosan, and polyethylimine are used to fabricate films with the anionic chromophore PCBS. The comparison between these three polycations provides an insight into the role of the separation distance between the polymer backbone and the charged group in the orientation of the chromophore. The importance of hydrogen bonding for orientation is probed via a comparison of films made with the hydrogen bonding capable poly(4-vinylpyridine) and the non-hydrogen bonding poly(4-vinyl-N-methylpyridinium iodide).

- **Chapter 8. Summary and Future Work**

Chapter 8 summarizes the most significant findings of this research and also details a future course for this project to take.

---

[1] Boyd, Robert W. *Nonlinear Optics*. Academic Press, New York, New York, 1992

[2] Dalton, L.; Harper, A; Ghosn, R.; Steier, W.; Ziari, M.; Fetterman, H.; Shi, Y.; Mustacich, R.; Jen, A.; Shea, K. 'Synthesis and Processing of Improved Organic Second-Order Nonlinear Optical Materials for Applications in Photonics' *Chem. Mater.* **7** (1995) 1060-1081

[3] Lytel, R. 'Applications of Electro-Optic Polymers to Integrated Optics' *SPIE Proceedings* **1216** (1990) 30-40

[4] Decher, G. 'Fuzzy Nanoassemblies: Toward Layered Polymeric Multicomposites' *Science* **277** (1997) 1232-1237

[5] Heflin, J.; Figura, C.; Marciu, D.; Lui, Y.; Claus, R. 'Thickness Dependence of Second-Harmonic Generation in Thin Films Fabricated by Ionically Self-Assembled Monolayers' *Appl. Phys. Lett.* **74** (1999) 495-497

2 Literature Review

2.1 Introduction to Non-Linear Optics

The behavior of light is understood jointly through Maxwell's equations, which govern the propagation of electromagnetic radiation, and quantum mechanics, which govern the interaction of light with matter. Maxwell's equations for a vacuum are:

$$\nabla \cdot \vec{D} = 4\pi\rho \tag{2.1}$$

$$\nabla \cdot \vec{B} = 0 \tag{2.2}$$

$$\nabla \times \vec{E} = -\frac{1}{c}\frac{\partial \vec{B}}{\partial t} \tag{2.3}$$

$$\nabla \times \vec{H} = \frac{1}{c}\frac{\partial \vec{D}}{\partial t} + \vec{J} \tag{2.4}$$

The first of these relations, Equation 2.1, is Gauss' Law which states that the total electric flux through any closed surface equals the net charge inside that surface divided by the permittivity of free space, ε_0. The electric induction, $\vec{D}$, is related to the electric field intensity, $\vec{E}$, through the relation;

$$\vec{D} = \varepsilon_0 \vec{E} \tag{2.5}$$

The next equation (2.2) is Gauss' Law In Magnetism, which precludes the existence of point magnetic poles. The magnetic induction, $\vec{B}$, is related to the magnetic field intensity, $\vec{H}$, with a relationship similar to the one which relates $\vec{D}$ to $\vec{E}$. This relation is:

$$\vec{B} = \mu_0 \vec{H} \tag{2.6}$$

where μ_0 is the permeability of free space. The third Maxwell Equation (2.3) is the differential form of Faraday's Law of Induction, which states that the line integral of an electric field around any closed path is equal to the rate of change of the magnetic flux through any surfaces bounded by that path. The fourth, and final of Maxwell's Equations is Ampere's Law, which states that magnetic fields arise from both circulating electric charges with charge density, $\vec{J}$ and from time variations in $\vec{D}$.

From the third and fourth Maxwell's Equations it is possible to derive the wave equations for electromagnetic waves in free space:

$$\frac{\partial^2 \vec{E}}{\partial x^2} = \mu_0 \varepsilon_0 \frac{\partial^2 \vec{E}}{\partial t^2} \tag{2.7}$$

$$\frac{\partial^2 \vec{H}}{\partial x^2} = \mu_0 \varepsilon_0 \frac{\partial^2 \vec{H}}{\partial t^2} \tag{2.8}$$

Both equations (2.7) and (2.8) have the form of the general wave equation with a speed of $\frac{1}{\sqrt{\mu_0 \varepsilon_0}}$, which is defined as c, the speed of light. These equations have simple solutions of the form (shown in 1 dimension for simplicity):

$$E = E_m \cos(kx - \omega t) \tag{2.9}$$

$$H = H_m \cos(kx - \omega t) \tag{2.10}$$

where E_m and H_m are the maximum values of those quantities. The wave number, k, is defined in equation 2.11:

$$k = \frac{2\pi}{\lambda} \tag{2.11}$$

where λ is the wavelength. The angular frequency , ω, is defined in equation 2.12:

$$\omega = 2\pi f \tag{2.12}$$

where f is the frequency.

When an applied electric field encounters a medium, the bound electrons in the material are disturbed from their equilibrium positions. A net dipole moment in the material is induced, which creates additional lines of induction. In a dielectric material, the total induction is:

$$\vec{D} = \varepsilon_0 \vec{E} + \vec{P} \tag{2.13}$$

where P is the sum of the internal dipole moments induced per volume, or polarization. This polarization is dependent on the applied electric field.

$$P_i = \chi_{ij}^{(1)} E_j + \chi_{ijk}^{(2)} E_j E_k + \chi_{ijkl}^{(3)} E_j E_k E_l + \ldots \tag{2.14}$$

where $\chi_{ij}^{(1)}$ is the linear susceptibility, $\chi_{ijk}^{(2)}$ is the second-order susceptibility, and $\chi^{(3)}_{ijkl}$ is the third order susceptibility. This susceptibility term contains all the dielectric information for a material. For simplicity, only scalar expressions (equivalent to 2D planar waves) will be considered. The induction, D, can then be expressed as;

$$D = \varepsilon_0 (1 + \chi^{(1)}) E \tag{2.15}$$

This is simplified by introducing the dielectric constant for a material, ε, which is defined by;

$$\varepsilon = \varepsilon_0(1+\chi^{(1)}) \tag{2.16}$$

Substitution of (2.16) into (2.15) gives the constitutive relationship for induction of a dielectric.

$$D = \varepsilon E \tag{2.17}$$

It is important to note that while ε is a material property, it does depend on the frequency of the applied electric field.

As the intensity of the applied electric field is increased the linear nature of the relationship between polarization and the applied electric field is lost. The relative magnitudes of the higher order powers are much less than that of the linear susceptibility, which is why these phenomena only occur at high field intensities. The polarization can also be expressed by

$$P = P^{(1)} + P^{(2)} + P^{(3)} + ... \tag{2.18}$$

where $P^{(1)}$ is the linear polarization, $P^{(2)}$ is the second order polarization, etc. These higher order terms are the source for nonlinear optic phenomena. Different orders of nonlinearity have different physical phenomena associated with them. For example, second order nonlinear optic phenomena, related to the $P^{(2)}$ term, are different from third order nonlinear optic phenomena. In equation 2.14, $\chi^{(2)}$ is shown as a second order tensor. However, it is the $\chi^{(2)}_{zzz}$ component that is being referenced unless otherwise noted.

2.2 **Second Order Nonlinear Optic Phenomena.**

The field of nonlinear optics was born in 1961, when the second order nonlinear optic phenomena, second harmonic generation was first observed.[1] Second harmonic generation, as well as the electro-optic effect and wave mixing will all be discussed.

2.2.1 **Second Harmonic Generation.**

A laser beam of electric field strength

$$E(t) = E(e^{-i\omega t} + e^{i\omega t}) \tag{2.19}$$

encounters a material that has a nonzero $\chi^{(2)}$. The induced second order polarization is

$$P^{(2)}(t) = 2\chi^{(2)}E^2 + \chi^{(2)}E^2(e^{-2i\omega t} + e^{2i\omega t}) \tag{2.20}$$

The first term, which is independent of time represents a static electric field created in the NLO active medium and is known as optical rectification. The second, time-dependent term, represents the changing polarization of the medium. Note that the polarization is oscillating at twice the incident frequency. An oscillating polarization can give rise to electromagnetic radiation, as described by the driven wave equation[2].

$$\nabla^2 E - \frac{n^2}{c^2}\frac{\partial^2 E}{\partial t^2} = \frac{4\pi}{c^2}\frac{\partial^2 P}{\partial t^2} \tag{2.21}$$

Under appropriate experimental conditions, the incident radiation at a wavelength of λ will be converted to radiation at a wavelength of $\lambda/2$. This emanating radiation with half the incident wavelength, or twice the incident frequency, is the second harmonic. This frequency doubling process is referred to as second harmonic generation (SHG).

The dependence of the second harmonic intensity ($I_{2\omega}$) on film thickness (l) and $\chi^{(2)}$ is given by:[3]

$$I_{2\omega} \propto \left(l_c \chi^{(2)}\right)^2 \sin^2\left(\frac{\pi l}{2l_c}\right) \tag{2.22}$$

The coherence length, l_c, is related to the refractive indices of the material by:

$$l_c = \frac{\lambda}{4\left(n^{2\varpi} - n^{\omega}\right)} \tag{2.23}$$

This is typically in the range of several microns, significantly thicker than films examined in this study. In this limit, $l \ll l_c$ a quadratic dependence of $I_{2\omega}$ on thickness arises as shown below:

$$I_{2\varpi} \propto \left(\chi^{(2)} l\right)^2 \tag{2.24}$$

2.2.2 **Wave Mixing.**

Wave mixing is the phenomena that occurs when two photons of different frequencies form a third photon of different wavelength. The frequency of the resulting photon is either the sum or the difference of the frequencies of the two incident photons. Consider an electric field governed by the following equation:

$$E(t) = E_1(e^{-i\omega_1 t} + e^{i\omega_1 t}) + E_2(e^{-i\omega_2 t} + e^{i\omega_2 t}) \tag{2.25}$$

The resulting second order polarization would then be:

$$\begin{aligned} P^{(2)}(t) &= \chi^{(2)} {E_1}^2 (2 + e^{-2i\omega_1 t} + e^{2i\omega_1 t}) \\ &+ 2E_1 E_2 (e^{-i(\omega_1+\omega_2)t} + e^{i(\omega_1+\omega_2)t} + e^{-i(\omega_1-\omega_2)t} + e^{i(\omega_1-\omega_2)t}) \\ &+ \chi^{(2)} {E_2}^2 (2 + e^{-2i\omega_2 t} + e^{2i\omega_2 t}) \end{aligned} \tag{2.26}$$

In this expression, there are terms that correspond to four different frequencies, second harmonics of both incident wavelengths, the sum of frequencies, and the difference of frequencies. It is not expected that radiation from all four frequencies will occur, as there are additional requirements for the emission of radiation. The specific frequency that is radiated by the system is generally selected by choosing the appropriate polarization of the incident radiation and the orientation of the nonlinear optic media[4].

2.2.3 **Electro-Optic (Pockel's) Effect.**

A third second order nonlinear optic phenomena is the electro-optic effect. This phenomenon allows the index of refraction of the medium to be controlled by an electric field. This effect governs EO modulator operation. The refractive index for a material can be expressed by:

$$n = \sqrt{\frac{\varepsilon}{\varepsilon_0}} \tag{2.27}$$

at frequencies where the material is transparent[5]. Considering only the time independent terms of the polarization expression, the electric displacement field becomes second order:

$$D = \varepsilon E = E + 4\pi\chi^{(1)}E + 8\pi\chi^{(2)}E^2 \tag{2.28}$$

Through substitution and simplification the following relationship for the refractive index is found:

$$n = \sqrt{{n_o}^2 + 8\pi\chi^{(2)}E} \tag{2.29}$$

where n_o is defined by

$$n_o = \sqrt{1 + 4\pi\chi^{(1)}} \tag{2.30}$$

and is independent of any applied field. This allows for the refractive index of a second order NLO material to be changed by applying an electric field across the material.

The electro-optic coefficient, r_{33}, is an often-cited quantity for an EO modulator as it describes the change in the optical refractive index by an electric field E.[6] Equation 2.31 defines this relationship:

$$\frac{\Delta\varepsilon_{33}}{\varepsilon_{33}^2} = r_{33k} E_k \tag{2.31}$$

The electro-optic coefficient is then related to $\chi^{(2)}$ by means of:

$$\chi_{ijk}^{(2)} = -\frac{1}{2} n_i^2 n_j^2 r_{ijk} \tag{2.32}$$

As previously stated, we are typically interested in the quantity $\chi^{(2)}_{zzz}$.

2.3 **Applications of NLO Materials**

Due to the unique phenomena associated with second order NLO materials, there are equally unique and valuable applications of these materials. Using the second harmonic generation and wave mixing properties, it is possible to tune the wavelength of lasers and other optical devices. This is potentially useful as a way to increase the storage capacity of optical disks by a factor of 4.[7]

A very interesting application involves interferometers that convert electrical signals to optical signals. An electro-optic (EO) modulator lies at the heart of fiber optic communications system. One example of these interferometers is the Mach-Zehnder interferometer, which is pictured in Figure 2.3-1.

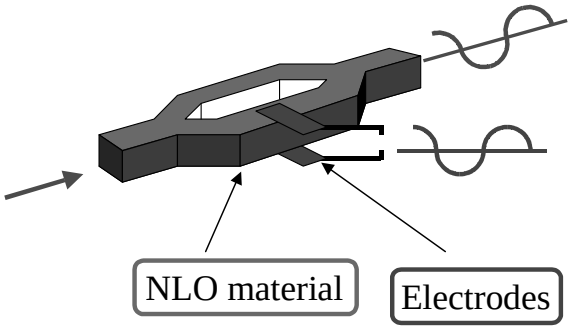

Figure 2.3-1 - Picture of a Mach Zehnder interferometer

This device has two arms of equal length. When a light beam travels down through the device, it is split and travels down each arm. The beams then recombine and interfere

constructively with each other. However, one arm is situated between a pair of electrodes, which allows for an electric voltage to be applied across the arm. Using the electro-optic effect, the applied voltage can be used to change the refractive index of that portion of the arm. This effectively changes the path length of the arm. When the split beam combines, interference occurs, causing variations in the intensity of the beam. The voltage required for the output to have zero intensity upon recombination (which is equivalent to shifting the phase of the wave in the active arm by π radians) or, halfwave voltage (V_π) is:

$$V_\pi = \frac{nd\lambda}{2L\chi^{(2)}} \tag{2.33}$$

where d is the waveguide thickness, λ is the wavelength, L is the length of the waveguide arms and n is the refractive index. Voltages less than this would leave an intensity less than the zero voltage intensity. The halfwave voltage for polymeric and lithium niobate modulators is typically 5 volts.[8]

2.4 **Non-linear Optic Materials**

For any material to display second order non-linear optic activity there is one basic requirement that must be met, the material must be anisotropic. This can be seen by applying an electric field to an isotropic material. The second order polarization is:

$$P^{(2)} = \chi^{(2)}E^2(t) \tag{2.34}$$

However, given that the material is isotropic, the following is true:

$$-P^{(2)} = \chi^{(2)}(-E(t))^2 \tag{2.35}$$

$$-P^{(2)} = \chi^{(2)}E^2(t) \tag{2.36}$$

By comparing the two expressions, the only way $P^{(2)}$ can be equal to $-P^{(2)}$ is if $\chi^{(2)}$ is identically zero. No isotropic material will display any second order non-linear optic properties. This is an important point to note because it automatically excludes 11 of the 32 crystal classes and requires any non-crystalline materials to have a level of molecular orientation. [4]

In terms of materials for incorporation into devices, Ohmer and Pandey set forth several criteria that an ideal second order NLO material should possess.[9] These criteria include: a large second order NLO coefficient, availability of crack-free single crystals,

transparency, high thermal conductivity, environmental stability, good mechanical properties, a large laser-damage threshold, performance in a laser system, commercial availability, and low cost.

2.4.1 **Inorganic NLO Materials**

Essentially all NLO materials used in commercial applications are based on inorganic crystalline materials. These crystals, generally lithium niobate ($LiNbO_3$) or potassium niobate have $\chi^{(2)}$ values on the order of 10^{-7} esu. The electro-optic coefficient (r_{33}) for $LiNbO_3$ is 32 pm/V.[10] The $\chi^{(2)}$ value for quartz is 1.92 X 10^{-9} esu.[11] These materials have several drawbacks, which limit their widespread application. The materials are difficult to grow, requiring long times, high temperatures and extreme pressures. Fully-grown crystals are also difficult to integrate into devices, complicating and limiting device design. Finally, these materials are often susceptible to environmental factors, particularly moisture. For the above reasons these crystalline materials are expensive ($10,000 for a 40 Gb / s modulator), which limits their applications.

2.4.2 **Organic NLO Materials**

2.4.2.1 **Benefits of Polymeric NLO Materials**

Polymer based nonlinear optic materials offer an attractive alternative to inorganic crystalline materials. The electro-optic activity of polymeric materials is approaching, and in some reports has already exceeded, the levels of lithium niobate ($LiNbO_3$). Comparing physical and device properties for $LiNbO_3$ and polymeric based materials allows for advantages to be seen. This is shown in Table 2.4-1.

Table 2.4-1 - Comparison of physical and device properties between $LiNbO_3$ and poled polymer NLO materials[12]

Physical / Device Properties	$LiNbO_3$	Polymers
Electro-optic coefficients (pm/V)	32	10-50*
Dielectric Constant	28	4
Crystal Growth Temperature, °C	1000	NA
Processing Temperature, °C	1000	150-200
Processing Time	10 hr.	10 min.
Multiple Layers Possible	No	Yes
Fabrication and Processing Demonstrated Bandwith	Difficult 40 GHz-cm	Simple >100 GHz-cm
Device Lifetime	Years	Months

* poling-field and wavelength-dependent

The dielectric constant of a material directly effects the response time of the material to an applied electric field. The higher the dielectric constant, the more the material resists the displacement of its electrons by the applied field. By having a lower dielectric constant, polymeric materials can respond faster to the applied field. This translates into a higher bandwidth, which represents the amount of information the material can process in a given amount of time. Inorganic $LiNbO_3$ modulators typically have bandwidth values of 9 GHz·cm, while polymeric materials are capable of bandwidths in excess of 100 GHz·cm[13]. Polymeric materials also have a higher optical damage threshold compared to inorganic counterparts. Also evident from Table 2.4-1 is the clear processing and manufacturing advantages that polymeric materials offer over traditional inorganic materials.

2.4.2.2 **Organic NLO Chromophores.**

In order to impart nonlinear optical activity to the polymeric materials, an NLO active chromophore must be incorporated into the polymeric system. These molecules consist of an electron donating and an electron-withdrawing group connected by a series of conjugated pi bonds. This allows the electrons to travel across the molecule's electron

cloud as an electric field is applied. The molecular level polarization, p_i, in an electric field is given by:

$$p_i = \alpha_{ij} E_j + \beta_{ijk} E_j E_k + \gamma_{ijkl} E_j E_k E_l + ... \tag{2.37}$$

where α_{ij} is the linear polarizability, β_{ijk} and γ_{ijkl} are the first and second hyperpolarizabilities, E_i is the applied electric field. The macroscopic $\chi^{(2)}$ is the sum of all the molecular contributions (β) mapped on the macroscopic unit vectors. This relationship can be written as:

$$\chi^{(2)} = NF\beta\left\langle \cos^3\theta \right\rangle \tag{2.38}$$

where N is the number density of chromophore molecules in the polymer material, F accounts for any local field effects and θ is the tilt angle of the chromophore molecule relative to the surface normal. Figure 2.4-1 illustrates this tilt angle in a schematic of a layer-by-layer film. Again, the need for an asymmetric material is demonstrated. If θ had random values, the value of $\langle\cos^3\theta\rangle$ would be zero, making $\chi^{(2)}$ zero.

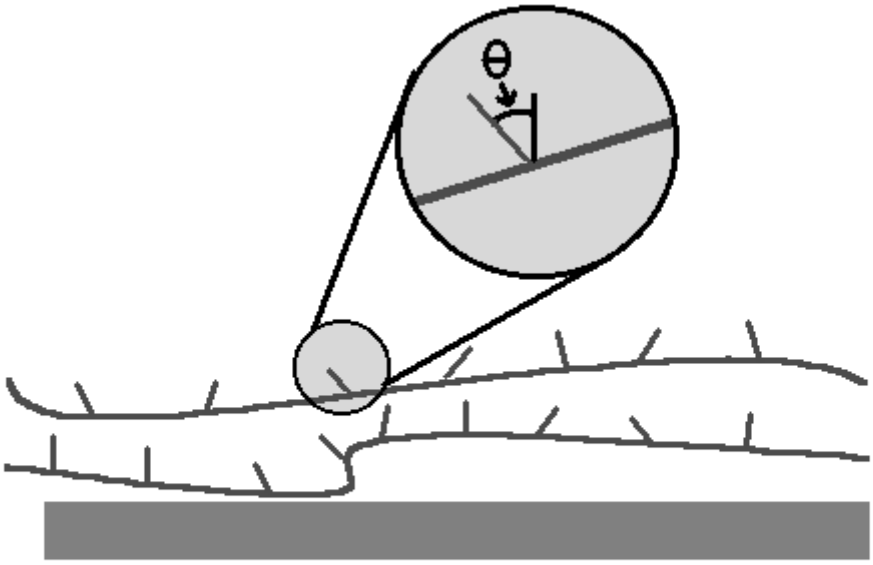

Figure 2.4-1- Schematic showing the orientation angle θ of a chromophore in an ISAM film.

The effects of changing the conjugation length and acceptor / donor groups on the β value for the chromophore are shown for several different systems are shown in Figure 2.4-2.[14] As can be seen, the β value increases with increasing conjugation length and it increases with the strength of the donor / acceptor groups on the molecule.

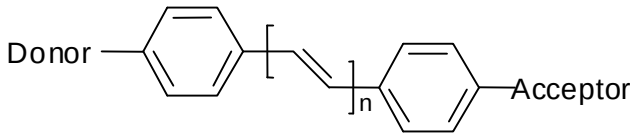

Acceptor	Donor	Solvent	n	λ_{max} (nm)	μ (10^{-18})	β (10^{-30})
CN	OCH_3	Chloroform	1	340	3.8	19.0
			2	360	4.5	27.0
			3	380	4.4	40.0
NO_2	OCH_3	Chloroform	1	376	4.5	34.0
			2	397	4.8	47.0
			3	414	5.1	76.0
			4	430	5.8	101.0
NO_2	$N(CH_3)_2$	Chloroform	1	430	6.6	73.0
			2	442	7.6	107.0
			3	458	8.2	131.0

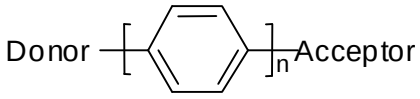

Acceptor	Donor	Solvent	n	λ_{max} (nm)	μ (10^{-18})	β (10^{-30})
NO_2	NH_2	NMP	1	370	7.8	10.0
			2	372	7.8	24.0
			3	360	7.6	16.0
			4	344	10.0	11.0
NO_2	OCH_3	*p*-Dioxane	1	302	4.6	5.1
			2	332	4.5	9.2
			3	340	5.0	11.0

Figure 2.4-2 - Table of β values that shows the effect of increasing the conjugation length and the strength of the donor / acceptor groups[14]

2.4.2.2.1. **Measuring β.**

This β value is measured by one of several techniques. Chromophoric molecules in solution are measured using a technique called electric field-induced second harmonic generation (EFISH). This technique measures the vector projection of the

hyperpolarizability along the molecular dipole (μ). The hyperpolarizability, β, is isolated from the μβ term by dividing by μ, which is obtained from dipole moment measurements.[15] Measurements made of materials in solid form can also be made by either wedge or Maker fringe techniques.

2.4.2.2.2. **Modeling β.**

The calculation of theoretical values for β as a function of molecular structure has been actively explored over the years. If the β value of a molecular structure could be modeled accurately, molecules could be designed to enhance β, which would improve a material's NLO properties. The first model, the bond parameter model, assumed that the total induced polarization was equal to the sum of the polarizations induced in individual chemical bonds between two atoms. This was then extended to the bond additivity model, where it is assumed that bond polarizability is additive. Inorganic crystals and tetrahedrally coordinated semiconductors have been successfully modeled by this technique. The main drawback of this technique is its inability to explain the large NLO activity found in non σ–type crystals or conjugated π systems.[16]

Gott et al. measured β of functionalized benzene rings and found that polarizable and inductive side groups result in molecules with larger β values.[17] Oudar and Chemla developed a quantitative model for a substituent radical (R) interacting with a p electron cloud (M). Their model is shown below.

$$\beta = 3\left(\frac{\gamma_m}{\alpha_m}\right)\mu_R \tag{2.39}$$

where γ and α are the third-order and first-order polarizabilities of the π network and μ_R is the induced dipole moment. Several important things about β are revealed in this model. First, μ_R depends on the strength of the radical-p interactions, so the stronger these interactions, the higher the resulting β. Secondly, γ increases more quickly than α does with increasing π bond length. This accurately reflects β's increasing values with an increasing conjugation length. This model also gives the sign of β.[18]

The next step in the modeling process was to consider doubly substituted benzene molecules with a donor and acceptor group. Levine et al. examined the effect that the substitution positions of nitroaniline on the molecule's β value. The para position

resulted in the highest β followed by the ortho position with the meta position being the lowest. This dependence on position was attributed to intramolecular charge transfer between the donor and acceptor. These values, as measured by Oudar and Chemla, are shown in Figure 2.4-3.[19]

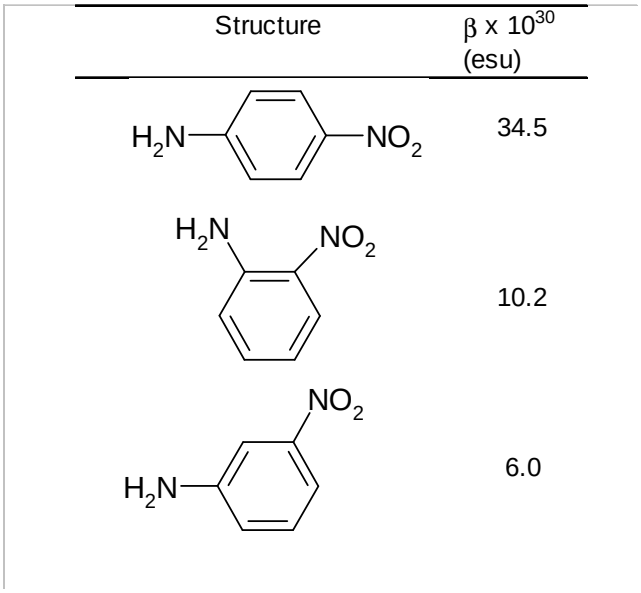

Figure 2.4-3 – Values of β for para, meta and ortho nitroaniline[19]

This dependence on position was attributed to intramolecular charge transfer between the donor and acceptor. They also observed that the β value for the doubly substituted p-nitroaniline was an order of magnitude larger than the mono-substituted nitrobenzene and aniline.[20] Oudar and Chemla quantified this theory by introducing a two-term model for β.

$$\beta = \beta_{ct} + \beta_{add} \tag{2.40}$$

where β_{ct} is a two level model that uses quantum mechanical calculations to determine the charge transfer contribution and β_{add} is the contribution of the benzene ring-substituent interaction. While β_{ct} successfully describes the mechanism of most organic solids, the β_{add} term often makes the value of β incorrect and occasionally gives it the wrong sign.[19]

The effect of the conjugation length of the π network on the β value was explored by Ducic et al. By measuring the β value of several molecules with different number of

double bonded carbon atoms between a donor and an acceptor, it was shown that β was proportional to the conjugation length squared.[21]

Levine and Bethea postulated that inter-molecular interactions between the NLO chromophore and solvent molecules also contributed to the overall β after observing a 20% to 30% difference in measured β values depending on the polar nature of the solvent.[22] A five-term model for the β value of species A in the presence of species B is given in equation 2.41.

$$\beta = \beta_g + \beta_{dip}^{AA} + \beta_{dip}^{AB} + \beta_{hb} + \beta_{IMCT} \qquad (2.41)$$

where β_g is the β of an isolated gas phase molecule, β_{dip}^{AA} is the contribution from the dipole interaction of two A molecules, β_{dip}^{AB} is the contribution from the dipole interaction between an A and B, β_{hb} is the hydrogen bonding contribution and β_{IMCT} is the intermolecular charge transfer contribution. These terms are determined from quantum mechanical calculations. By considering all these contributions, it is possible to obtain a good approximation for the β value of a molecular system.

While the modeling of β continues to be an active research area, the existing models do not predict the β value of large, complicated chromophore molecules very well. These models do continue to evolve and become more accurate. As the accuracy of computational chemistry to improve, it is likely that the β value will be easily estimated in the future.

2.4.3 **Fabrication of Polymeric NLO Materials.**

There are several different ways that polymer-based NLO materials can be made. None of these techniques are viable yet for widespread commercial application, each method having its own drawbacks. The three main classes of polymer NLO materials are guest/host polymers, Langmuir-Blodgett films and ionically self-assembled films.

2.4.3.1 **Guest/Host Polymer Systems**.

This method of fabricating polymer based NLO materials incorporates an NLO active chromophore (guest) into an amorphous polymer matrix (host). The guest chromophore is doped into the polymer matrix. The system is then heated up to a temperature above the glass transition temperature (T_g) of the host. At this point, an

electric field (typically 50-250 V/μm) is applied across the material.[23] This electric field causes the dipole moments of the chromophore molecules to align, imparting orientation to the system. The temperature of the system is then dropped below the glass transition temperature of the matrix, locking in the orientation of the chromophore molecules. The poling field is then removed. This method is often referred to as the "poled polymer" method. This is schematically shown Figure 2.4-4.

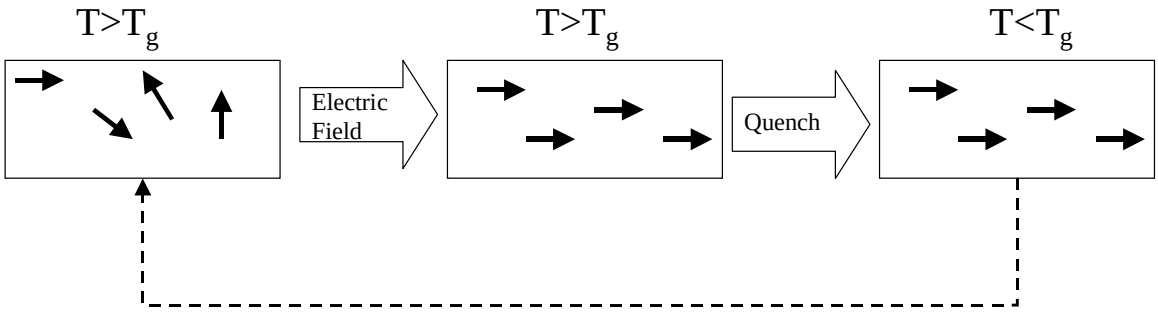

Figure 2.4-4 - Schematic showing the poling process. Guest chromophore molecules are represented by arrows.

There are two principle drawbacks to all guest/host polymer systems. The first is that the guest chromophores and host matrices are typically not very compatible, which limits the amount of chromophore that can be included in the matrix. This has a direct effect on the $\chi^{(2)}$ of the material. The second, larger drawback to these materials is that the oriented state is not the equilibrium state for the system. In guest/host systems there exists a driving force towards the randomization of the chromophore guests. Eventually, as represented by the dashed line in Figure 2.4-4, the oriented system will return to a random configuration. This results in a loss of all second order NLO activity. As the temperature of the system increases, the rate at which the chromophore molecules can randomize also increases. At typical device temperatures (~100°C) this process occurs at a rate that makes these materials doubtful for use in commercial applications (see Figure 2.4-5 for the room temperature decay of a poled polymer system).[23] Additionally, the chromophore molecules act as a plasticizer, lowering the glass transition temperature of the host, increasing this effect.

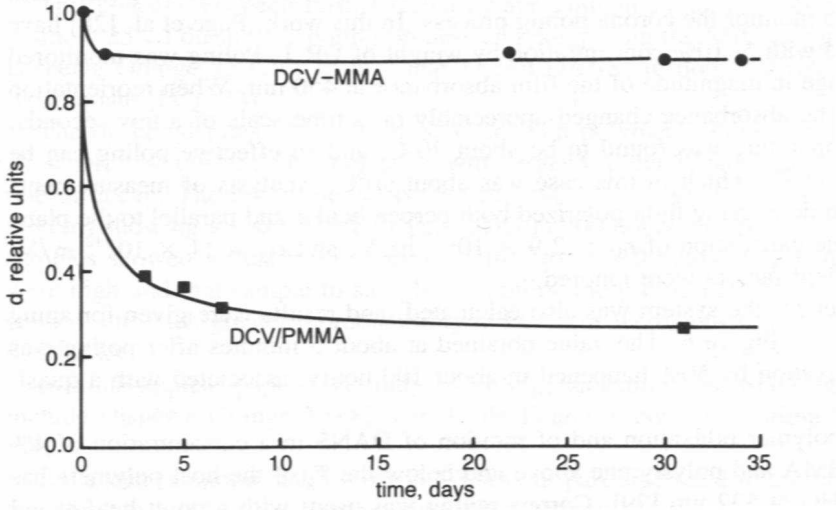

Figure 2.4-5 – Room temperature decay of the second-harmonic coefficient of poled guest / host system DCV in PMMA and side chain copolymer DCV-MMA[24]

Several approaches have been taken to overcome this shortcoming. One of the earliest attempts involved using host matrices that could be crosslinked. Once the host was below its glass transition temperature, it would be exposed to UV light, which would cause the formation of a network in the matrix.[25] While this did improve the stability of guest/host systems, it did not improve the stability to a point where it was practical for device integration. Another difficulty with photo-initiated crosslinking is that the chromophore molecules often interfere with the absorption of light by the photo-initiators, hindering the crosslinking process.[26]

A different approach that was used to improve the stability was the use of host polymers that would react upon heating, again locking in the orientation of the chromophore molecules. One example of these systems is a polyamic acid host.[27] During the poling process, once the chromophores are oriented in the matrix, the temperature is increased to approximately 250°C. At these temperatures the polyamic acid host undergoes a cyclization process, condensing and forming imide rings. A by-product of the condensation reaction is water, so the film is then heated to a higher temperature to remove the water. While the formation of the imide rings and the resulting densification of the film do restrict the motion of the chromophore molecules and increase the thermal

stability, the temperatures required for this process are generally so high that the chromophore molecule is destroyed in the process.

The state-of-the-art in poled polymers is summarized by Dalton et al.[8] In this work, an EO modulator with halfwave voltage below 1 V was fabricated. The modulator, unlike the Mach-Zehnder interferometer shown in Figure 2.3-1, is EO-active on both arms. This allowed the halfwave voltage to be reduced by a factor of two. The polymeric NLO film was a PMMA host matrix with custom chromophores as the guest. These chromophore molecules are designed with bulky groups giving the molecules an ellipsoidal shape, which is predicted to increase the EO activity of the molecules. One of the chromophore structures used in this work is shown in Figure 2.4-6.

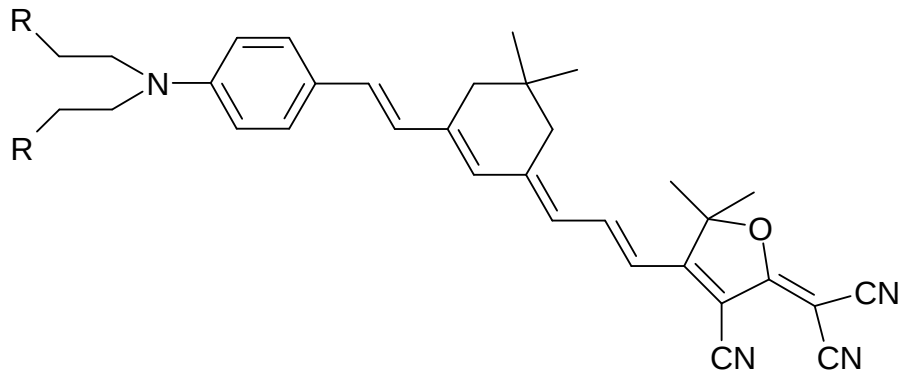

Figure 2.4-6- Structure of the CLD-1 chromophore, where the R group represents the tetrabutyldimethylsiloxane protecting group.[8]

In the poled materials values of roughly 60 pm/V were obtained for r_{33}. This compares to the value of 32 pm/V for lithium niobate. The modulator was thermally stable up to approximately 65°C, the glass transition temperature of the PMMA matrix.

This illustrates how the thermal stability problem prevents these materials from being commercially applied. This was also the case for the first poled polymer film consisting of poly(methyl methacrylate) doped with Disperse Red and remains true for state of the art materials. [28]

2.4.3.2 **Langmuir-Blodgett Films.**

The loss of orientation in poled polymer films results from the fact that the oriented state is not the equilibrium state for the material. Several different approaches to film fabrication can be used, in which the oriented state is the equilibrium state for the material. One such technique is the Langmuir-Blodgett technique.[10]

The general approach to fabricating films with this technique involves using optically active chromophores having a hydrophilic head and a hydrophobic tail. These molecules are spread, as a monolayer, from an immiscible solvent onto a water surface. The solvent is removed and the layer is compressed forming an ordered monolayer. Deposition of the film occurs as the substrate is passed through the monolayer. There are three types of Langmuir-Blodgett films that can be formed.

The first type, known as a 'Y-type' film is formed when a hydrophobic substrate is dipped through a solution of amphiphilic chromophores. The hydrophobic tails associate with the substrate as it is dipped through the monolayer. As the substrate is removed, the hydrophilic heads on the water surface associate with the deposited, exposed, hydrophilic heads. The dipping is repeated building a multi-layered film. 'Y-type' films are inherently centrosymmetric. However, there are several techniques that can be used to impart an overall degree of orientation, allowing the film to have second order NLO activity. Most often optically inactive spacer molecules are incorporated in the film, imparting a noncentrosymmetric 'Z-type' structure.

The other two types of films, 'X-type' and 'Z-type' are inherently noncentrosymmetric and are formed only upon insertion or removal of the substrate through compressed monolayers of chromophore molecules. However, materials appropriate for use in these types of films are less prevalent in nature. Additionally, many 'Z-type' and 'X-type' films degrade to 'Y-type' films, losing their noncentrosymmetry. These three different film types are schematically showing in Figure 2.4-7.

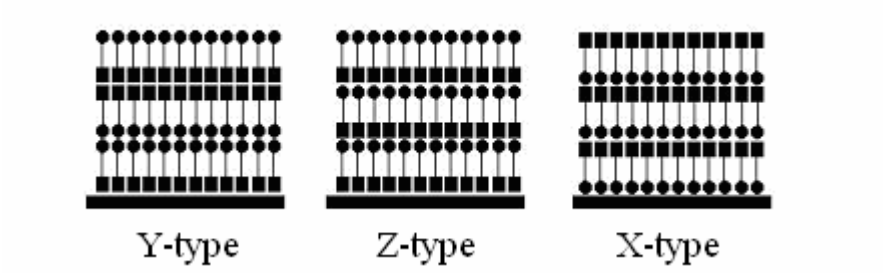

Figure 2.4-7 -Schematic of Y, Z and X-type Langmuir-Blodgett films. The rectangular end of the molecule represents the hydrophobic tail, while the circular end represents the hydrophillic head. This figure demonstrates the centrosymmetry of the Y-type film and the noncentrosymmetry of the Z and X types.

Langmuir-Blodgett films are difficult to manufacture and process. The inclusion of optically inactive materials in 'Y-type' films significantly decreases their NLO activity and materials that adopt 'X-type' or 'Z-type' configurations are not as common. $\chi^{(2)}$ values are typically in the ranges of 10-70 pm/V for Langmuir-Blodgett films.[29] Problems with the long-term stability of these materials have also been reported, as they are susceptible to environmental factors, in particular moisture and heat.[30] Additionally, these films must be fabricated in clean room environments to prevent the inclusion of dust which would cause optic losses and introduce defects to the film. For these reasons, Langmuir-Blodgett films are not suitable for large-scale commercial applications.

2.4.3.3 **Ionically Self-Assembled Monolayer Films.**

Multilayer oriented films can also be made in which electrostatic interactions drive film self-assembly. This technique, pioneered by Iler and subsequently explored by Decher, et al. overcomes many of the shortcomings of other fabrication techniques.[31, 32] The ionically self-assembled monolayer process (ISAM) involves the dipping of a charged substrate in a polycationic solution. The polycation adsorbs to the surfaces and causes a charge reversal to occur. The film is then rinsed to remove any nonadsorbed material. The film is then dipped into an anionic solution, adsorbing a layer of polyanion, again causing a charge reversal. This two-step dipping process creates a bilayer, and is repeated until the film has the desired thickness. Many papers have appeared in the literature demonstrating that this method can be used to incorporate a wide range of materials in nanostructured thin films.[35,36,37] These materials have found applications for sensing, separations, anticorrosion and electronics.[33] Heflin, et al. demonstrated that by incorporating a NLO active chromophore in the anionic or cationic layer, it is possible to impart NLO behavior on the system. Before going into the details of the ISAM process, the topic of polyelectrolyte adsorption on surfaces will first be reviewed.

2.5 **Polyelectrolyte Adsorption**

There are four main scenarios that can occur for the adsorption of polymers on surfaces where some form of electrostatic interactions are present. These four cases are that of an uncharged polymer adsorbing on an charged surface, a charged polymer

adsorbing on an uncharged surface, a charged polymer adsorbing on a charged surface with the same sign and a charged polymer adsorbing on a charged surface with opposite sign.[34] Each case will briefly be considered.

2.5.1 **Neutral Polymers on Charged Surfaces.**

The adsorption of neutral polymers results from χ, the solvency parameter and χ_s, the segmental adsorption energy parameter. By convention, $\chi_s = 0$ means no interactions. As χ_s increases the interactions become increasingly attractive for $\chi_s > 0$. The presence of a charged surface causes an attraction of counter-ions to the surface. These counter-ions then compete with polymer segments, which lowers the adsorbed amount when compared to the situation where both polymer and surface are neutral. This competition has little effect for weakly charged surfaces, but as the charge density increases, this effect becomes more pronounced. The effect of added salts is minimal because the number of counter-ions associating with the surface is limited to the amount needed to counter the surface charge. Figure 2.5-1 and Figure 2.5-2 illustrate these points. In Figure 2.5-1 the excess adsorbed amount in the absorbed number of monolayers, θ^{ex}, is shown as a function of surface charge density, σ_o for two adsorbing polymers. For dilute polymer solutions θ^{ex} is equal to the absorbed amount of monolayers, θ^a. In general θ, the absorbed amount in monolayers is related to the absorbed amount, Γ by:

$$\theta = \frac{\Gamma}{\Gamma_m} \tag{2.42}$$

Here Γ_m is the monolayer capacity in units of mass / area.

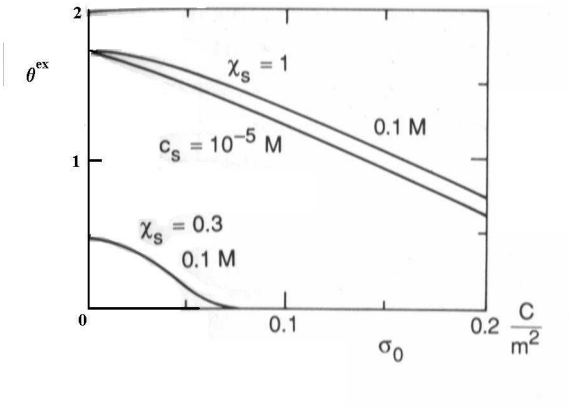

Figure 2.5-1 – Effects of surface charge density (σ_o) on the adsorption of uncharged polymers with χ_s of 1 and 0.3. This demonstrates the reduced adsorption with increasing surface charge.[34]

One polymer has a χ_s value of 1 while the other has a χ_s value of 0.3. For the polymer with χ_s=1, increasing the salt concentration by 4 orders of magnitude causes only a modest increase in θ^{ex}. The effect of surface charge density is more pronounced on the polymer with a χ_s of 0.3 because the counter-ions are more effectively competing with the polymer segments. In the case χ_s=1, the polymer has a significantly higher affinity for the surface compared to the counter-ions, which have no specific interactions. These theoretical points are experimentally examined in Figure 2.5-2 which shows results for the adsorbed amount (Γ) of PEO on silica as a function of the surface charge density.

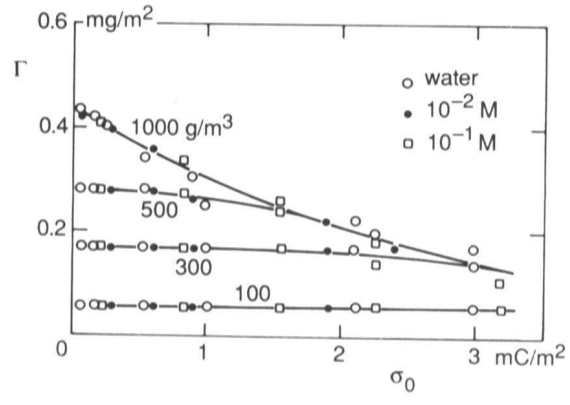

Figure 2.5-2- Experimental data for the adsorption of PEO on Silica. The absorbed amount of PEO (Γ) is given as a function of the surface charge density for 4 different polymer concentrations at 3 salt concentrations.[34]

These experiments were conducted at 4 polymer concentrations (1000 g/m^3, 500 g/m^3, 300 g/m^3 and 100 g/m^3) with 3 different salt concentrations (0M, 10^{-2} M and 10^{-1} M). In the two lower concentrations, the amount of polymer is not sufficient to saturate the surface, so there is no effect of changing the surface charge density. However, in the two cases where there is sufficient polymer available, the expected decrease in adsorbed amount as surface charge increases is observed in addition to this effect being independent of salt concentration. It is noted that it is difficult to be experimentally certain that competition by counter-ions is the only phenomena responsible for this effect.

2.5.2 **Polyelectrolytes on Neutral Surfaces.**

In the adsorption of a charged polyelectrolyte to an uncharged surface, there is no electrostatic contribution to the adsorption energy, χ_s. However, the lack of an electrostatic contribution does not reduce this scenario to that of neutral polymers adsorbing onto neutral surface, where adsorption is governed solely by χ and χ_s. The presence of charges on the chains causes polymer segments to repel one another, which prevents polymer segments from accumulating near the surface. This segment repulsion effectively lowers χ which then lowers the adsorbed amount due to the increased solubility of the polymer. The adsorbed amount of polymer is also affected by the addition of salts. The presence of additional ions in the solution leads to electrostatic shielding of the charges on the polymer chains, causing χ^{eff} to approach χ of the corresponding uncharged case. Physically, the additional salt ions reduce the inter-segment repulsion, which leads to an increase in adsorbed amount. This decrease in adsorption that results from inter-segment repulsion as well as the effect of additional salt is illustrated in Figure 2.5-3.

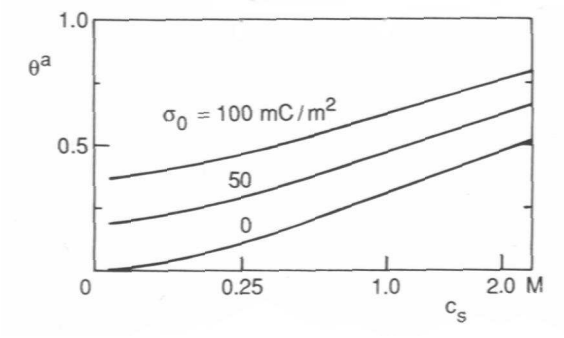

Figure 2.5-3 – Comparison of the adsorbed amount of charged polyectrolyte on three surfaces with different charge densities. The uncharged surface shows significantly lower adsorbed amounts compared to either charged surface. Additionally, the increase in adsorbed amount as the concentration of salt is increased is quite evident. Values were calculated using the multilayer Stern-model.[34]

Here the calculated adsorbed amount of a highly charged polyelectrolyte is plotted as a function of salt concentration, c_s on surfaces with 3 different charge densities (σ_o=100 mC/m^2, 50 mC/m^2 and 0 mC/m^2 (the uncharged case)). The adsorbed amount corresponding to an uncharged surface is significantly lower than its charged counterparts and there is a clear increase in adsorption as the salt concentration is increased. It is significant to note that even under very high salt concentrations, the effect of inter-segment repulsions are still evident. In addition to the increase in the amount of polymer adsorbed as the salt concentration is increased, the manner in which polymer chains are adsorbed also changes. In the low salt limit the chains adsorb in flat, thin layers due to the segment – segment repulsions. As the salt concentration increases, the layers are deposited in thicker layers dominated by loops and tails. The effect of chain length (and thus molecular weight) varies depending on which regime of salt concentration the adsorption is occurring in. In the low salt regime, molecular weight effects are fairly insignificant. Under high salt conditions, however, there is a marked increase in adsorbed amount as the chain's molecular weight is increased. This is illustrated in Figure 2.5-4, where poly(styrene sulfonate) of various molecular weights has been adsorbed on uncharged silica (at pH =2.0) at ionic strengths ranging from 0.5M to 3 M.

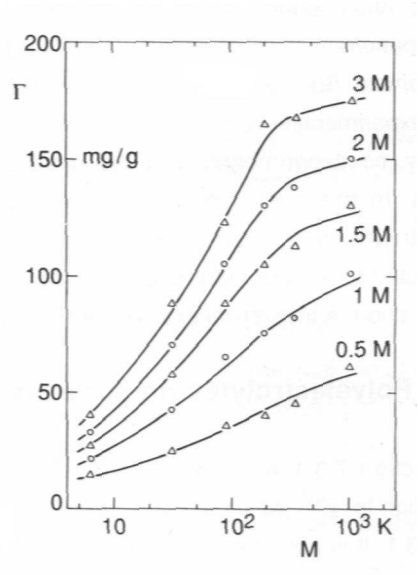

Figure 2.5-4 - Adsorption experiments of PSS on silica (pH =2) for 5 ionic strengths were the adsorbed amount was measured as a function of the chain's molecular weight, M[34]

The experiment conducted at 0.53 M salt shows a weak dependence on ionic strength, while the 3 M case shows three fold increase in adsorbed amount as the molecular weight was increased from 10,000 g/mol to 1,000,000 g/mol.

2.5.3 **Polyelectrolytes on surfaces with the same charge sign.**

At low salt concentrations, it is possible that the repulsions between the polymer chain and surface reduce the χ_s to a degree where no polymer will adsorb on the surface. As the salt concentration is increased, the electrostatic effects are screened and χ_s^{eff} begins to increase and approach χ_s. The χ_s^{eff} term can be approximated to include contributions of the specific interaction χ_s as well as the electrostatic interactions. This approximation is given below:

$$\chi_s^{eff} \approx \chi_s - \frac{\tau\alpha e\sigma_d}{\varepsilon\kappa kT} \tag{2.43}$$

where τ is either +/- 1 and identifies the sign of the polymer segment charge, α is the degree of ionization of the polymer chain, e is the fundamental charge, σ_d is the charge density of the surface (can be either negative or positive), κ is the inverse Debye length, and is proportional to the square root of the concentration of added salts. Once the χ_s^{eff} reaches a critical value (χ_{sc}) the energy of adsorption is large enough to counteract the

repulsion between polymer and surface and adsorption occurs. Eventually, the salt will completely screen the electrostatic effects, and the adsorption will approach the uncharged case. The effect of salt on the adsorption of a charged polymer is shown in Figure 2.5-5.

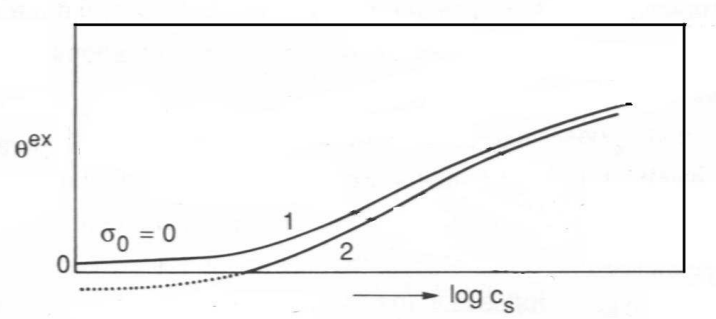

Figure 2.5-5- Schematic comparing the theoretical adsorption of a charged polymer on a neutral surface (curve 1) and a surface with the same sign charge (curve 2). Depletion occurs below a critical salt concentration, and as the salt concentration increases the adsorbed amount approaches the neutral case.[34]

Here curve 1 represents the uncharged surface and curve 2 represents the surface with same sign charge as the polymer chain. The dotted portion of curve 2 represents the depletion range of salt concentrations.

In addition to the salt concentration being important, there are significant effects attributed to both the surface charge density and the degree of ionization for a weak polyelectrolyte. Figure 2.5-6 shows the adsorbed amount of a weak polyacid with a pK_a of 4 as a function of the surface charge density. For the pH = 2 case, the polyacid is relatively uncharged. For the pH =4 case, the polymer is roughly one half charged and at a pH of 6, the polymer is strongly charged.

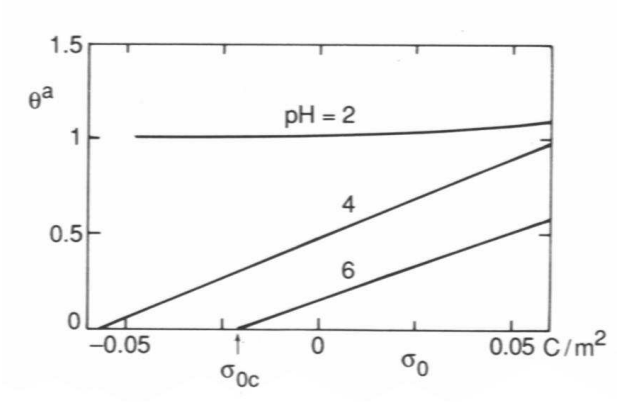

Figure 2.5-6 – Theoretical absorbed amount of a weak polyacid (pK_a = 4) as a function of the pH and the surface charge density, σ_o, χ_s=1.0, χ=0.5 c_s=0.1 M[34]

When the polymer is essentially uncharged, the adsorbed amount is independent of the surface charge density. However, as the charge density on the polymer becomes increasingly negative (moving from pH 4 to 6), the absorbed amount decreases for a fixed surface charge density. Additionally, as the surface charge density moves from a positive value (opposite in charge from the polyacid) to a negative value (same sign charge as the polyacid) the absorbed amount decreases until it eventually reaches zero at a critical surface charge density. It is important to reiterate that despite the fact that the polymer and the surface have the same charge, adsorption can occur within a given range of surface charge densities because the energy of adsorption is significant enough to counteract the repulsive forces.

One example that combines the salt and surface charge effects is a set of experimental data in which poly(l-lysine) (PLL) at a low pH was adsorbed on AgI. Under these conditions, the PLL is fully charged. The AgI surface has a positive charge for pAg < 5.5 and a negative charge where pAg > 5.5. The results are shown below in Figure 2.5-7 for three salt concentrations (10^{-3} M, 10^{-2} M, 10^{-1} M).

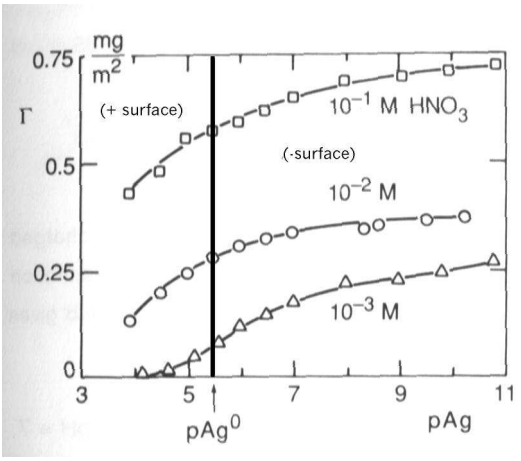

Figure 2.5-7 –Absorbed amount of the polycation poly(L-lysine) on AgIas a function of the surface charge density and the concentration of added salts (HNO_3). Below the pAg of 5.5 the surface is positively charged and above 5.5 it is negatively charged.[34]

For all three salt concentrations, adsorption was observed when the surface was negatively charged. As the surface became positively charged the adsorbed amount decreased as expected. In the 10^{-3} M salt condition, the surface became fully depleted at a pAg of approximately 4. At the higher salt conditions, desorption would occur at lower values of pAg. This behavior is, in fact, due to a large specific affinity for PLL on AgI.

2.5.4 **Polyelectrolytes on Surfaces with Opposite Charge.**

In the previously considered scenarios for polymer adsorption on surfaces where the polymer and / or the surface have been charged, the adsorption of polymer was driven by surface interactions represented by χ_s and the electrostatic effects have retarded the adsorption of polymer. The scenario of polyelectrolytes adsorbing on surfaces of opposite charge has been divided into two sub-categories: pure electrosorption where the surface affinity term, $\chi_s = 0$ and the second case where the χ_s term is non-zero and so surface affinities enhance deposition.

2.5.4.1 **Pure Electrosorption.**

Pure electrosorption is defined as adsorption where there is only one driving force, electrostatic attractions. The specific interaction term χ_s is zero or less than zero. However, due to the electrostatic effects, the effective term (χ_s^{eff}) (refer to Equation 40 in section 2.5.3) is greater than zero. Despite the fact that electrostatic attractions provide the driving force for adsorption, the inter-segment repulsion of accumulated charged segments of the polymer serve to limit the adsorption, as they did in the case of a charged polymer adsorbing on a neutral surface. The presence of salts still affects the adsorption of charged polymer. For low salt concentrations, the adsorbing polymer counteracts the surface charge. However, as the salt concentration increases, the ions begin to displace the polymer segments, thus reducing the adsorbed amount. Another important variable for pure electrosorption is the degree of ionization of the polymer chain, α. At low charge levels, the polymer may not sufficiently compensate for the charged surface. As the charge density increases, segment-segment repulsion becomes increasingly more important, reducing the amount of adsorption that occurs. Regardless of the degree of ionization there will be a critical salt concentration, c_{sc}, where salt ions completely

displace the polymer segments. In fact, the effects of salt concentration and degree of ionization overlap. In the low salt regime, the amount of adsorption is inversely proportional to the degree of ionization ($\theta \propto 1/\alpha$). At the high salt limit, the c_{sc} is roughly proportional to the degree of ionization.

2.5.4.2 **Electrosorption with Surface Affinity.**

This scenario is essentially the same as pure electrosorption except that there is a finite surface affinity that favors adsorption. The combination of surface affinity and electrostatic attractions causes the χ_s^{eff} term to be greater than χ_s which encourages adsorption, while the build-up of charged groups causes χ^{eff} to be less than χ, which opposes adsorption. Figure 2.5-8 shows the results of calculations that demonstrate the influence of a non-zero χ_s on adsorption.

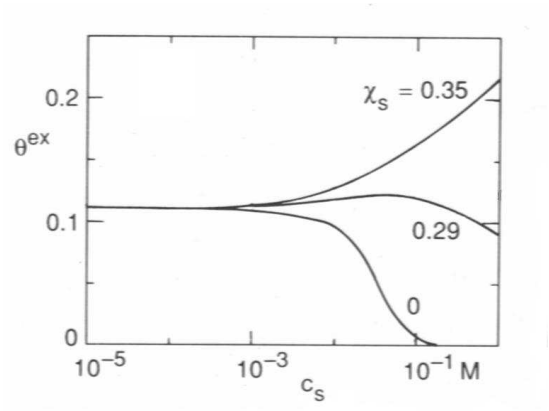

Figure 2.5-8 – The effect of salt concentration on the adsorption of polymers for pure electrosorption, weak surface affinity (χ_s=0.29) and strong surface affinity (χ_s=0.35), polymer charge density α=0.2, surface charge density σ_0=0.01 C/m^2 [34]

In the low salt regime, the surface affinity does not have a large affect on the adsorption. As the concentration of salt increases, the effect of added salts depends on the magnitude of χ_s. For fairly small values of χ_s, the salt ions compete with polymer segments for adsorption sites, causing the adsorbed amount to decrease as the amount of salt present increases. However, comparing the non-zero χ_s case to the case of pure electrosorption, the effect of salts is less drastic in the non-zero case and the c_{sc}, where salt counter-ion replace all the polymer segments, would be significantly higher. In cases where the surface affinity is fairly strong, the addition of salts promotes adsorption of additional polymer. This occurs because the additional salts screen the segment-segment

electrostatic interactions. This causes the adsorbing polymer to adsorb in a loopier conformation. This transition from a flat conformation to a thick, loopy one allows for more polymer to be adsorbed on the surface.

A variation on this situation is for polymers which may not be fully ionized, where the degree of charge, α, is a significant variable. Figure 2.5-9 shows the absorbed amount of polymers with different degrees of ionization as a function of the salt concentration.

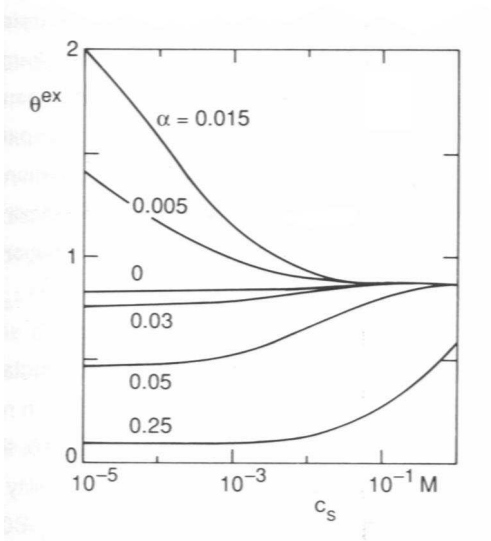

Figure 2.5-9 – Adsorbed amount of polymer with varying degree of ionization as a function of the salt concentration[34]

In the low salt regime, there are two competing effects depending on the degree of ionization. If the degree of ionization is low, electrostatic attraction drives adsorption to the surface. However, if the polymer becomes too highly charged, segment-segment repulsion begins to counteract the χ_s^{eff} term, causing the adsorbed amount to be lower compared to the neutral polymer adsorbing on the charged surface. In the high salt regime, both highly and sparsely charged polymers approach the neutral polymer limit. For the highly charged polymers, which had relatively low adsorption amounts, the addition of salts screens the segment-segment interactions, allowing more polymer to adsorb. In the case of the low charge density, the additional salts compete with the polymer for adsorption sites, which reduces the adsorbed amount.

2.5.5 **Weak Polyelectrolytes.**

A weak polyelectrolyte is one where the degree of ionization depends on the pH of the solution. The Henderson-Hasselbalch equation relates the relative degree of ionization for a weak acid to the pH and the pK_a. The Henderson-Hasselbalch equation is shown in general form for the weak acid HA below.

$$pH = pK_a + \log\frac{[A^-]}{[HA]} \tag{2.44}$$

From $[A^-]$ and [HA], the degree of ionization, α can be calculated. Obviously, the pH is the significant variable in the adsorption of weak polyelectrolytes on a surface.

Figure 2.5-10 shows the theoretical results for the adsorption of a weak polyacid on three surfaces of different surface charge density as a function of pH.

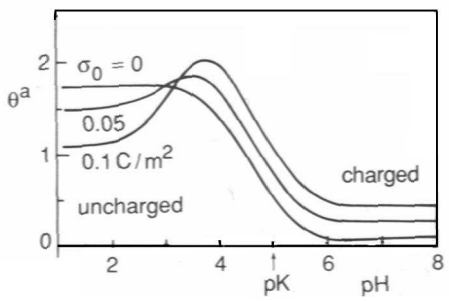

Figure 2.5-10 – Adsorbed amount of a weak polyacid as a function of pH for three surface charge densities. The salt concentration is constant at 0.1 M.[34]

For the neutral surface, the adsorption is high where the chains are uncharged (at a low pH) and the adsorbed amount decreases as the chains become charged with increasing pH. This occurs due to segment-segment repulsions. For the positively charged surface, the uncharged polymers at low pH experience competition with salt ions for adsorption sites. As the pH is increased, the chains become charged and can better compete with the salt ions, causing the adsorbed amount to increase. However, there reaches a point where segment-segment interactions become a hindrance to adsorption and the adsorbed amount decreases. A maximum in the amount absorbed is observed for the cases where the surface is charged. This maximum generally occurs 1~1.5 pH units below the pK_a.

Figure 2.5-11 shows the structural changes that occur in the adsorbed layer with changes in pH for a constant surface charge (σ_o=0.05 C/m^2) and constant salt (c_s=0.1 M).

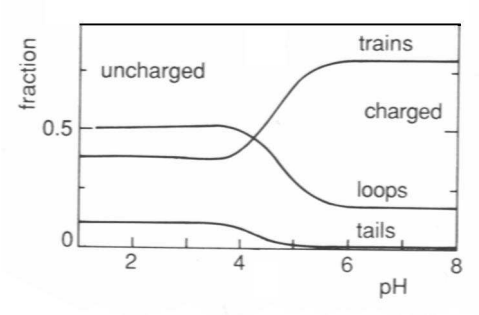

Figure 2.5-11 – The fraction of chains adsorbed as loops, trains and tails as a function of the pH for a constant surface charge density and salt concentration[34]

At low pH values, where the polymer is uncharged, loops and tail are a significant fraction (> 50%) of the adsorbed polymer, resulting in a thick adsorbed layer. As the polymer becomes charged, the polymer chains shift to adsorbing in flat trains (> 80%). In both Figure 2.5-10 and Figure 2.5-11 the transition between these regimes occurs around the pK_a (~5.0), where the polymer is one-half charged.

2.6 **Ionically Self-Assembled Monolayer Films**.

A large body of literature has developed on ISAM films since being reported in the early 1990s. There are certain authors and papers in this field that merit special emphasis. Iler's work depositing alternate layers of charged colloidal particles laid the foundation for the entire field.[31] Decher not only introduced this technique for polyelectrolytes, but along with Lvov and Kunitake has studied some of the core issues regarding film formation. Dubas and Schlenoff, as well as the Stuart and Fleer groups have published extensively on the formation and effects of processing variables on these films. Reviews by Decher, Hammond and Laschewsky condense the most important findings in the field well.[35,36,37]

The buildup of multilayer thin films by means of the deposition of alternately charged polyelectrolytes was developed by Decher et al. and was first reported in 1992.[38] In this study, films were constructed from alternating layers of poly(styrene sulfonate) (PSS) and poly[4-vinylbenzyl-N,N-diethyl-N-methyl-ammonium iodide]. The absorbance was measured at 225 nm every following the deposition of a pair of layers. A linear relationship between the absorbance and the number of layers deposited is seen. This linear increase in absorbance signifies that the amount of polymer deposited per dipping

is the same. In fact, this linear increase is routinely used by many groups as a method to determine if films are being deposited correctly. A set of films was made using polyallyamine hydrocholoride (PAH) and PSS with absorbance and film thicknesses being measured as a function of the number of layers deposited. Again a linear relationship between the absorbance and number of layers was observed. SAX results for film thickness also showed a linear dependence on the number of layers deposited. These results are shown in Figure 2.6-1.

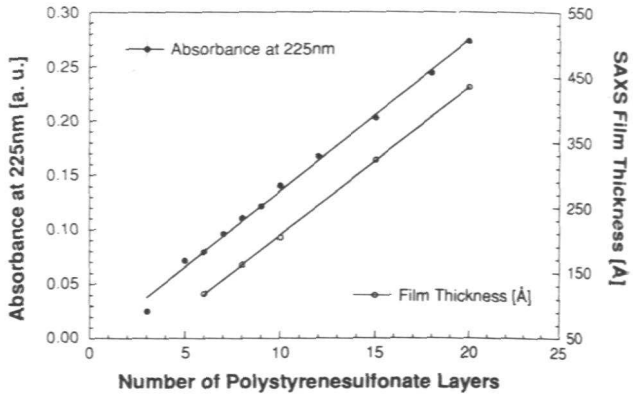

Figure 2.6-1 Film Thickness and Absorbance as a function of the number of deposited layers [38]

ISAM films are constructed as a result of the irreversible adsorption of a charged polymer on to the oppositely charged surface. Polymer is adsorbed until the effective surface charge has been reversed. This change in surface charge as alternating layers are deposited has been experimentally verified. Okubo and Suda measured the ζ potential of colloidal silica spheres as layers of cationic poly(4-vinyl-N-n-butylpyridinium bromide) and PSS were deposited.[39] Figure 2.6-2 shows the ζ potential for the bare silica spheres at just below –40 mV; however once the first cationic layer is deposited, the ζ potential increases to approximately +40 mV.

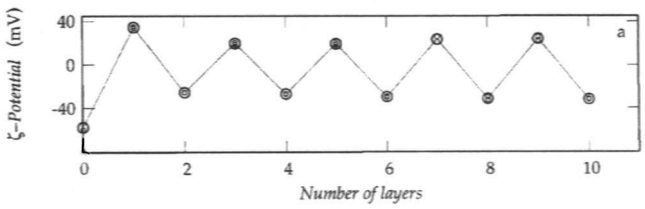

Figure 2.6-2 – Measurements of the ζ potential of colloidal particle spheres as layers of polycations and polyanions are deposited[39]

The value for ζ potential then alternates between +40 and –40 mV as additional layers are deposited. A constant increase in film thickness has been observed when the level of charge overcompensation is constant, as in Figure 2.6-2.[40] However, this consistent charge reversal and thus successful build-up of layers does not imply complete coverage on the surface of the film. Polymer only adsorbs until it is repelled by previously adsorbed polymer segments that are similarly charged, despite the fact that additional binding sites may be available.[41,42]

The internal structure of ISAM films has been studied by several different groups and through several different techniques. Lvov et al. examined films constructed with poly(vinyl sulfate) (PVS) and PAH using SAXS. The absence of diffraction peaks corresponding to the layer pair thickness implied that these ISAM films are not composed of discrete polymer layers, but rather interpenetrating layers.[43] Using measurements of advancing contact angles, Yoo et al. determined that the contact angle of the uppermost deposited layer depended on both the thickness of the top layer and the layer immediately beneath it. If a thick layer is deposited over a thinner layer, the properties of the thicker layer dominate. However if a thin layer is deposited over a thicker layer, chains from the thick layer penetrate the thin layer, modifying the surface contact angle. Films constructed with two thin layers showed essentially no dependence on which species (anion or cation) was present as the outer layer, signifying that the thin layers were highly intermingled. They verified their contact angle measurements with a surface labeling technique, which measured the available carboxylic groups on the surface and this gave similar results.[44] Schlennoff and Dubas also observed that layers were highly interpenetrated in their experiments using radiolabeled salt ions.[40]

While ISAM films are not stratified, there are several methods by which discrete layers may be built up. These methods include post deposition processing, fabricating films with solid particles and polymers, and making extremely thin layers. Lvov et al. fabricated ISAM films with discrete layering using 45 nm diameter silica particles and PDDA.[45] It is important to note that having discrete stratified layers is not a prerequisite for having orientation in films, which is essential for using ISAM films for NLO applications. The corollary that orientation does not imply stratification also holds true.

The general ISAM process is exceptionally straightforward, but there are a number of processing variables which influence the final film. These variables include the polymer solution concentration, solvent, and polymer molecular weight. However, these have fairly small effects on film formation. Other variables, such as salt concentration in the dipping solutions, which affects the fundamental electrostatics driving film formation, have much larger and marked effects on film thickness and structure. In addition, the pH plays an important role for films made using weak polyelectrolytes, as the pH determines the polymer's degree of charge. Salient studies addressing these effects will now be reviewed.

2.6.1 **Polymer Concentration.**

For general polyelectrolyte adsorption on an oppositely charged substrate, the typical adsorption isotherm reaches a limit at a relatively low polymer concentration. One example for PSS on silica is shown in Figure 2.6-3.

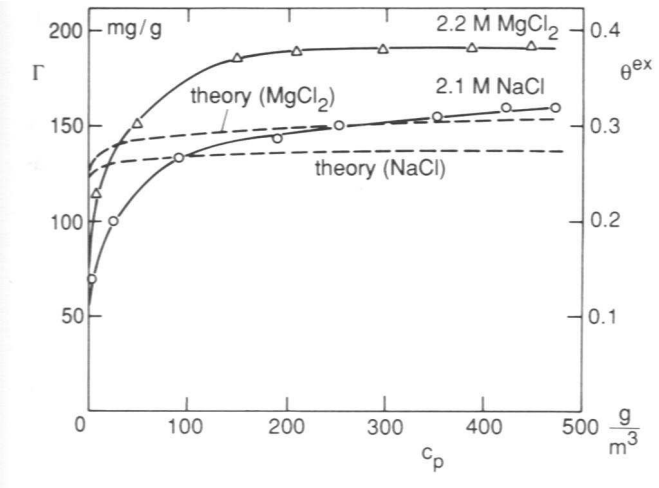

Figure 2.6-3 – Adsorption of PSS on silica as a function of the polymer concentration, c_p [46]

Above a concentration of roughly 200 g/m^3 there was little or no dependence on concentration. This corresponds to a solution concentration on the order of 10^{-6} M on a repeat unit basis. Above this critical threshold for complete coverage, there is no dependence on concentration. Similar results are observed for multilayer films. Houska and Brynda examined the deposition of heparin, a biological polymer, on an albumin treated surface.[47] Their results for adsorbed heparin as a function of heparin solution concentration are shown in Figure 2.6-4. Here the plateau region begins at a

concentration of roughly 0.3 mg/ml, which is roughly 10^{-4} M heparin. Increasing the polymer concentration by two orders of magnitude results in no significant increase in adsorbed amount.

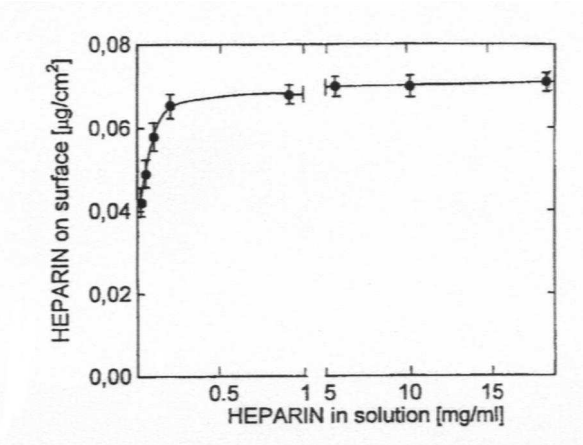

Figure 2.6-4 – Adsorbed amount of heparin on an albumin treated surface as a function of the heparin concentration in solution. The adsorbed amount is roughly constant above a polymer concentration of 0.3 mg/ml heparin.[47]

Dubas and Schlenoff also examined the effect of polymer concentration. However, they measured the thickness of 5 adsorbed layer pairs of poly(diallyldimethylammonium chloride) (PDDA) and PSS using ellipsometry.[48] The results (Figure 2.6-5) again show a steep increase followed by a plateau. Film thicknesses only vary by 10 nm over a concentration range of roughly 5-50 mM on a repeat unit basis.

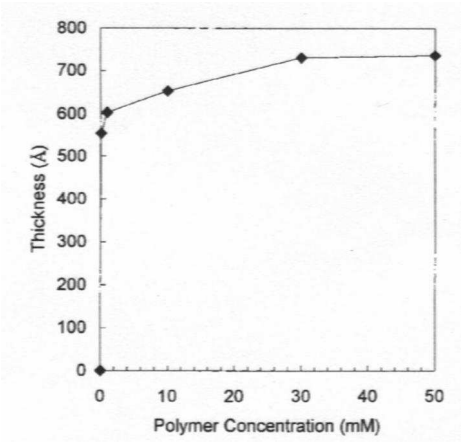

Figure 2.6-5 – Thickness results for 5 layer pairs of deposited PDDA and PSS as a function of the dipping solution's polymer concentration. A deposition time of 5 minutes was used for both species.[48]

Typical solution concentrations for polymer / polymer ISAM systems are generally on the order of 10^{-2} M on a repeat unit basis.

2.6.2 **Kinetics of the ISAM Process**

The general kinetics of adsorption can be broken down into three main components: the rate of mass transfer of the polymer to the surface, the rate of attachment, and the rate of any surface rearrangements that may occur. Dijt found that the convective flux of polymer molecules to be proportional to the diffusion coefficient (D), polymer concentration (c_p) and Reynolds number (R):[49]

$$J \propto D^{\frac{2}{3}} c_p \, \mathrm{Re}^{\frac{1}{3}} \tag{2.45}$$

While the details of this flux model will not be discussed, the principle conclusion is that for mass transfer limited adsorption, there will be a clear dependence on the polymer concentration on the time for adsorption. Additionally, if the diffusion rate is limiting, then as the Reynolds number approaches zero (no fluid velocity) the time for adsorption of a monolayer should become infinitely large.

Ferreira and Rubner fabricated 5 bilayer films of poly(thiopheneacetic acid) (PTAA) and PAH.[50] The adsorption of the next PTAA monolayer was conducted at 3 polymer concentrations (0.01 M, 0.001 M, 0.0001 M all on a repeat unit basis) at which the absorbed amount is a function of polymer concentration. The absorption was monitored with measurements of the absorbance at 420 nm. These data (shown in Figure 2.6-6) show that all three isotherms reach their plateau value in approximately 10 minutes, with little or no dependence on the polymer concentration in solution. This implies that the adsorption of the polymer layer is not transport limited and, rather, is limited by the attachment of the polymer to the surface.

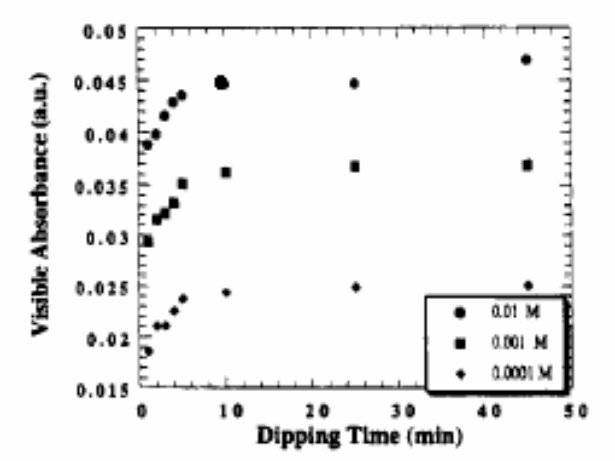

Figure 2.6-6 – Absorbance of a depositing PTAA layer on 5 PTAA / PAH bilayers as a function of polymer solution concentration and dipping time[50]

2.6.3 **Rinsing**

In the ISAM process, a rinsing step is typically employed between polyelectrolyte immersions. Hoogeveen et al. examined the effect of rinsing on films made with polyvinlyimidazole (PVI^+) and poly(acrylic acid) (PAA).[51] Figure 2.6-7 compares films made with and without rinsing.

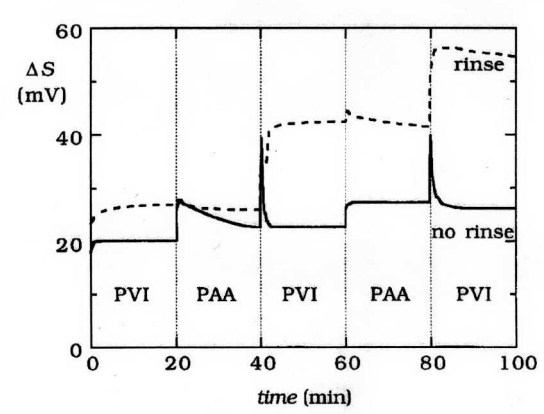

Figure 2.6-7 - Effect of rinsing on the deposition of PVI / PAA ISAM films. Rinsing promotes stability of the depositing film and results in an increase in the adsorbed amount (proportional to ΔS, the change in the reflectometer signal)[51]

Adsorption measurements were performed using optical reflectometry combined with stagnation-point flow-cell. The ΔS shown on the y-axis, the change in the reflectometer signal, is proportional to the adsorbed amount of materials. The solid line compares to films made without rinsing to films made with rinsing (dashed line). The changes during the rinsing process itself are not shown; however, they are negligible. The most obvious

observation is that rinsing results in the adsorption of significantly more material. The authors hypothesize that rinsing removes some loosely bound polymer as well as promotes rearrangement of the uppermost layer, providing a stabilizing effect on the growing film.

Lvov et al. have also examined the role that intermediate washings has on film formation.[52] Using a quartz crystal microbalance (QCM) the change in resonance frequency as a substrate is moved from aqueous PSS or PAH solutions to a pure water bath was measured (results in Figure 2.6-8). The ΔF presented in the figure is proportional to the amount of mass deposited per step. During the water-rinsing step the frequency increase was 70-80% of the frequency change observed during the adsorption step, signifying that rinsing removed a large portion of the adsorbed polymer.

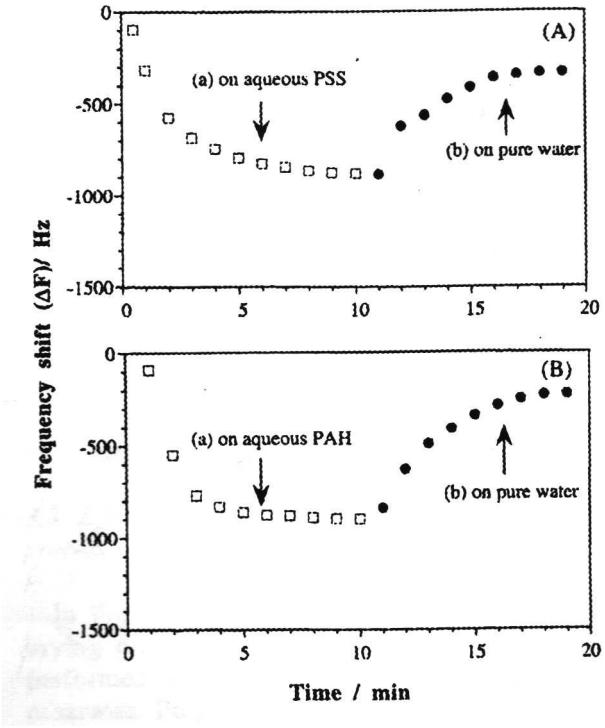

Figure 2.6-8 - QCM results showing desorption of mass as a substrate is moved from a polymer solution to pure water[52].

In a second experiment films made of poly(ethyleneimine) (PEI) and PSS were rinsed with either a 20 second immersion or a 5 minute washing. Multiple layers of polymers were deposited and the QCM results can be seen in Figure 2.6-9.

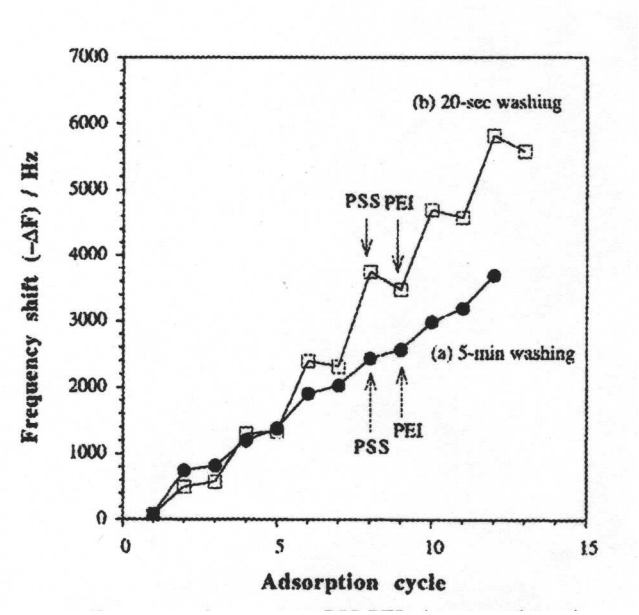

Figure 2.6-9 - QCM results for ISAM films made with PEI and PSS with 2 different rinsing times, one 20 seconds, which is insufficient for removing all the loosely bound polymer, resulting in thicker, rougher films. The other is a 5 minute rinse, which promotes stable growth.[52]

In the 20 second rinsing case a decrease in the absorbed amount is seen as the substrate was immersed in the PEI solution. This implies that previously adsorbed PSS was being removed from the film surface. Despite this desorption, films rinsed for only 20 seconds showed larger amounts of adsorbed materials, with a corresponding larger value for surface roughness. Films made with the 5 minute rinsing time did not show any decreases in adsorbed mass, implying that the loosely bound chains seen desorbing in the 20 second case were successfully removed by the rinsing step in the 5 minute case.

2.6.4 **Effect of Intermediate Drying Steps.**

In many layer-by-layer deposition systems, compressed nitrogen gas is used to dry the films for physical characterization. The effect that drying has on film deposition and structure was first examined by Decher et al. who determined that intermediate drying steps do not influence the thickness of the polymer layers. However, they do report that drying causes a rearrangement within the film, affecting the surface roughness and the internal configuration of the film. The notion of a surface rearrangement resulting from drying was tested by preparing a substrate with 8 layers of PSS and PAH. An upper layer or PSS was deposited on these 8 bilayers, the film was dried, and the layer thickness was measured to be 45 +/- 2 Å. This sample was re-exposed to the PSS

solution, dried and the thickness of the uppermost layer had increased to 83 Å. These results imply that drying causes a surface rearrangement, allowing additional polyelectrolyte to be deposited on a surface that had already reached its equilibrium coverage amount.[53]

Lvov et al. quantified the effect of drying using QCM while studying the deposition of PSS-PAH films.[52] Curve 1 in Figure 2.6-10 represents a film that was only dried after the 1st, 8th and 16th deposition step. Following the 16th step, the film was dried after every deposition step (shown in Curve 2). The -ΔF presented in the figure is proportional to the amount of mass deposited per step. Curve 1, where the films were dried only 3 times over the course of 16 deposition steps, has a –ΔF of 360 Hz, while curve 2 (dried after every step) has a –ΔF of 600 Hz. This supports the results of Decher et al. who demonstrated that more material is deposited when films are dried. Lvov et al. also used non-contact atomic force microscopy (AFM), a form of scanning probe microscopy, to compare surfaces dried in air *vs.* those dried in a stream of nitrogen. Results from their AFM analyses suggest that the films dried in the nitrogen stream have a surface orientation that corresponds to the direction of nitrogen flow on the surface.[52]

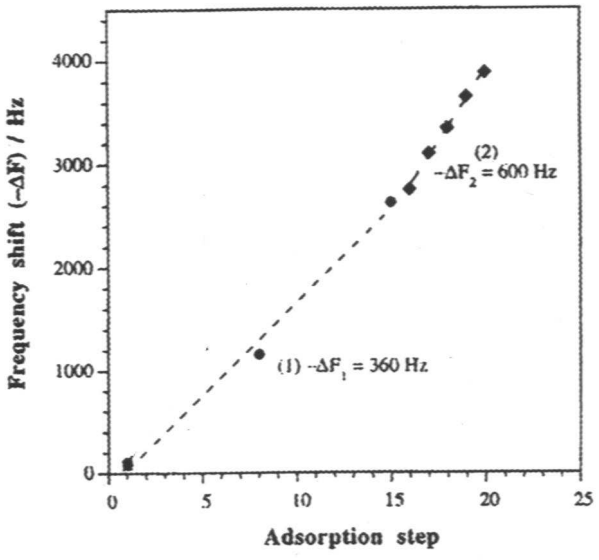

Figure 2.6-10 – QCM results for the deposition of PSS-PAH. Curve 1 represents drying every 8 adsorption steps while curve 2 represents drying every step. The Frequency shift is proportional to the amount of material deposited[52]

Cochin and Laschewsky also examined the effect of drying on film formation and arrangement. Figure 2.6-11 shows the absorbance as a function of bilayers for films that

were dried after every deposition cycle, following the 8th cycle, the films were stored in air overnight and deposition resumed the following day. The absorbance data for these films show two distinct linear regimes, one from 1-8 cycles and a second from 9 onwards. The greater slope after the overnight storage (between cycles 8 and 9) is believed to result from a surface rearrangement. The authors propose that a slow accumulation of hydrophobic groups at the surface of the film is occurring via film rearrangement. This then results in a greater amount of deposition once the cycles are again started. To test this hypothesis, a series of films were made with a period of extended storage in water. This should cause a rearrangement in the film where hydrophobic groups would retreat from the surface, hence, lowering the amount deposited per cycle once deposition resumed. This was experimentally verified. The obvious conclusion from this work is that, for the highest degree of layer-to-layer consistency, films should be made without any extended opportunities for rearrangement.[54]

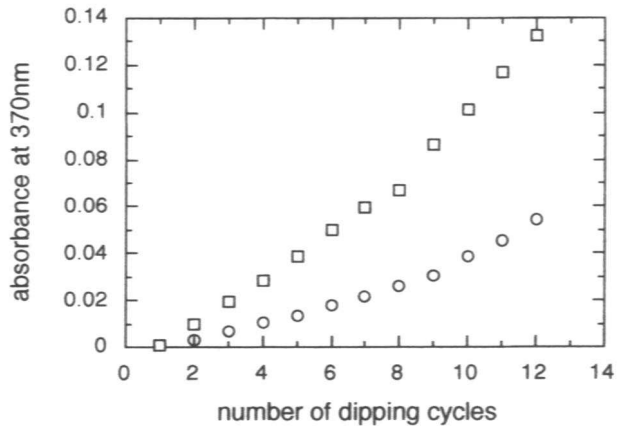

Figure 2.6-11 – Absorbance of a layer-by-layer film as with the number of layers deposited. The film is dried after every cycle and is stored in air overnight following the 8th cycle.[54]

2.6.5 **Polymer Molecular Weight.**

Rubner et al. examined the role of polymer molecular weight on film thicknesses using films fabricated from polyaniline and PSS. Between PSS molecular weights of 5,000 and 1,000,000 the thickness of films remained in the 35-40 Å range.[55] These results are supported by the work of Decher et al. in which neutron reflectometry was used to probe the internal structure of PAH / PSS films. The film thickness increased by

less than 3% as the degree of polymerization was increased from 900 to 5,000.[56] van Ackern et al. used a similar methodology to examine the role polymer molecular weight plays in film formation.[57] Films were fabricated using PAH of molecular weights of 9800 and 58000 as the polycation and 1,4-diketo-3,6-diphenylpyrrolo-[3,4-c]-pyrrole-4,4'-disulfonic acid (DPPS) as the anion. Figure 2.6-12 shows the absorbance for these films as a function of the number of bilayers deposited.

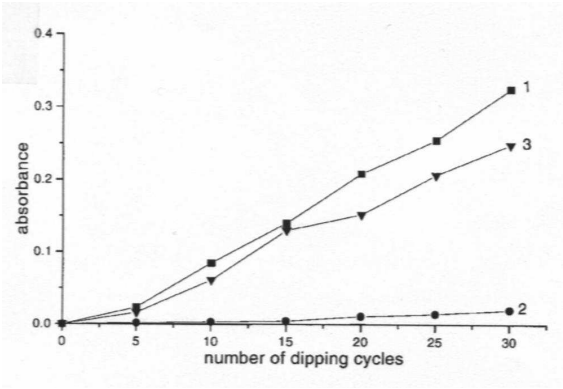

Figure 2.6-12 – Absorbance as a function of the number of bilayers for PAH / DPPS films demonstrating the weak effect of molecular weight on depostion. Curve 1 uses PAH with a Mw of 9800 and Curve 3 corresponds to a Mw of 58000.[57]

Curve 1 corresponds to films made with a PAH M_w of 9800 and curve 3 corresponds to the 58000 case. Any dependence on molecular weight is fairly weak. None of these papers examined films made with oligomers, in which below a critical molecular weight, deposition may not proceed successfully.[58]

The effect of polymer molecular weight has also been explored for branched dendritic polyelectrolytes. Blinznyuk et al. found that the thickness of a single monolayer of dendritic polyelectrolyte scaled with the molecular weight of the polymer. Polyamidoamine dendimers in which even generations are amine functionalized while odd generations are functionalized with carboxylic acid groups were deposited on a negatively charge silicon surface or a positively charged silane modified silicon surface respectively. For a single monolayer on a charged surface they determined that thickness (d) (measured by scanning probe microscopy) scaled with molecular weight according to $d \propto M^{(.27)}$. [59] However, multilayer films consisting of odd and even generations of the same polyamidoamine dendrimers show weak or no scaling behavior. Films made with generation 4 dendimers (Mw 14,215) had bilayer thicknesses of 2.8 +/- 0.4 nm while

films made with generation 10 dendimers (Mw 934,720) had bilayer thicknesses of 3.8 +/- 0.6 nm.[60]

2.6.6 **Effect of pH on ISAM Films.**

The pH of the dipping solutions for ISAM formation can have a large effect on the thickness and interpenetration of the resulting film. For strong polyelectrolytes, adding base or acid to adjust the pH will increase the ionic strength.[58] The ionic stength, I_{eff}, for a 1:1 polyelectrolyte is a function of the polymer concentration (c_{poly}), molarity of added salt and the solution pH / pOH. The general relation for ionic strength as a function of charged species in solution is given below:

$$I = \frac{1}{2}\sum_i c_i (z_i^2) \tag{2.46}$$

Assuming counterion condensation occurs, this relationship for solution containing polyelectrolyte and salt is shown below in equation 2.47.[61]

$$I_{eff} = \frac{1}{6} c_{poly} + c_{NaCl} + 10^{-pH} + 10^{-pH} \tag{2.47}$$

The Debye length, κ^{-1}, the characteristic length over which electrostatic interactions are felt is given below in terms of this effective ionic strength for water at 25°C:[62]

$$\kappa^{-1} = \frac{0.0304}{\sqrt{I_{eff}}} nm \tag{2.48}$$

Increasing the ionic strength by increasing pH will, as discussed in the following section, lead to thicker layers.

For weak polyelectrolytes in which the polymer's charge is a function of the solution pH, the effect of pH is significantly more profound. Rubner et al. examined this effect using poly(acrylic acid) and poly(allylamine hydrochloride), two weak polyelectrolytes.[63] By controlling the pH of the dipping solutions they demonstrated that it is possible to fabricate films with an extraordinary range of thickness; from below 10 Å per bilayer to over 120 Å per bilayer. They also report pH conditions in which deposition would not occurr. By measuring the contributions of each polymer to the thickness, the effect of pH on thickness of each polymer layer has been measured for pH values of 2 to 9. This is shown in Figure 2.6-13.

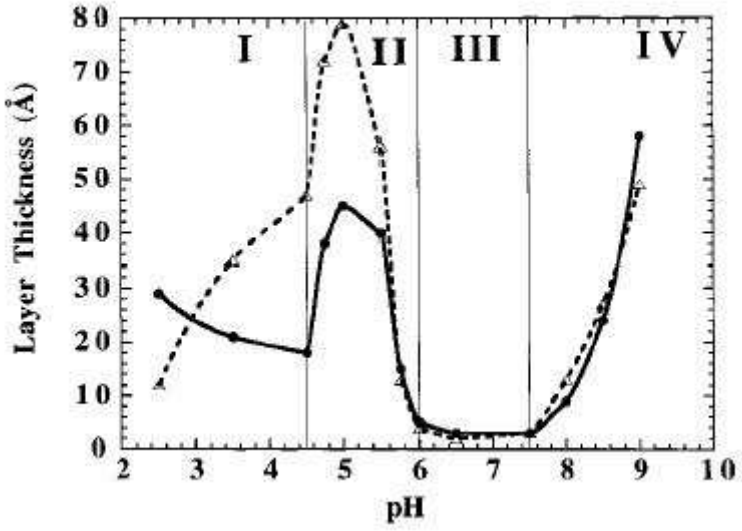

Figure 2.6-13 – Thickness contributions of PAH (dashed line) and PAA (solid line) as a function of pH. In these experiments both polyelectrolytes were at the same pH.[63]

The authors have proposed four regions, in which the pH behavior of the individual polyelectrolytes can account for the changes in film thickness observed. Region I corresponds to the PAA chains increasing in charge density, while the PAH chains are relatively fully charged. As the charge density of the PAA chains increases, the thickness contribution of the PAA decreases and the PAH thickness increases results from the increase in surface charge density. Regions II and IV both correspond to a fully charged species being alternately deposited with a nearly fully charged species. In region II, the PAH chains are fully charged, while in region IV, the PAA chains are the ones fully charged. These conditions (fully charged being deposited with nearly fully charged) result in very thick bilayers. Finally region III represents the area in which both polymers are essentially fully charged, and overall bilayer thicknesses are quite low.

2.6.7 **Effect of Salt on ISAM Films.**

Given that the deposition of ISAM films is an electrostatic process, the addition of salts to the deposition solutions would, for the reasons previously discussed, have a profound effect on the structure of the ISAM films. Dubas and Schlenoff made films of PSS / PDDA with salt concentrations (NaCl) ranging between 0 –2 M.[48] A nearly linear relationship for film thickness as a function of salt concentration was observed for salt concentrations between 0.2 - 2M (see Figure 2.6-14).

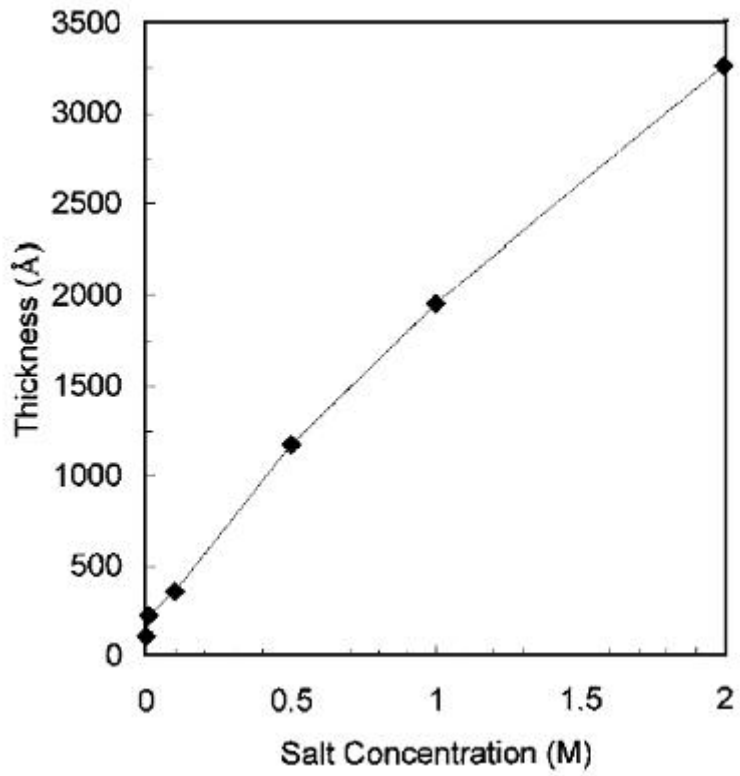

Figure 2.6-14 –Thickness of PSS / PDDA films (10 layers) made with added NaCl.[48]

This linear dependence of thickness on salt concentration was also observed for films made of PSS and PAH by Lösche et al.[56] Decher and Schmitt report being able to 'tune in' a desired layer thickness to within 0.5 Å with the addition of salts.[64] Very high salt concentrations can cause the desorption of the polymer layers, creating an upper limit on salt concentration for film formation. This is of particular importance for weak polyelectrolytes.[58] Dubas and Schlenoff report that for films made with PDDA and poly(acrylic acid) at pH 11, layer thickness decreased for salt concentrations about 0.3 M and film formation does not occur over 0.6 M.[65]

2.7 Layer-by-Layer Films with Monomeric Dyes

Traditional ISAM films consist of two oppositely charged polyelectrolytes; however, the method can be extended to incorporate other molecules. Cooper et al. demonstrate that this is possible by incorporating the monomeric dyes copper phtalocyanine tetrasulfonic acid (CPTA), Alcian Blue, and Congo Red into films using poly(L-lysine) as the polycation. These films showed the expected linear relationship between absorbance and the number of layers deposited.[66]

Ariga et al. investigated the deposition of Congo Red and other monomeric dyes with PDDA with QCM. Using the estimates of film thicknesses from QCM as well as calculations of dye dimensions, the authors suggest how the dye molecules may be oriented in the films. For Congo Red, based on chromophore dimensions and estimates of the layer thickness, they surmise that the molecule forms a well-packed monolayer in which the molecules assume a tilted orientation.[67]

Yamada et al. deposited films of PDDA and the monomeric chromophore Eriochrome Black T and measured the SHG of these films. They show an increase in the second harmonic intensity for the first 5 bilayers deposited, followed by a plateau.[68]

2.8 **Layer-by-Layer Films Built via Covalent Bonds**

The work of Marks et al. presents a unique method for the creation of layer-by-layer NLO materials.[69] While this work does not specifically address the ISAM method, this layer-by-layer method has resulted in films with promising $\chi^{(2)}$ values. Using reactive stilbazole chromophores, inorganic / organic multilayer thin films are constructed. One example from Marks' early work is shown below in Figure 2.8-1.

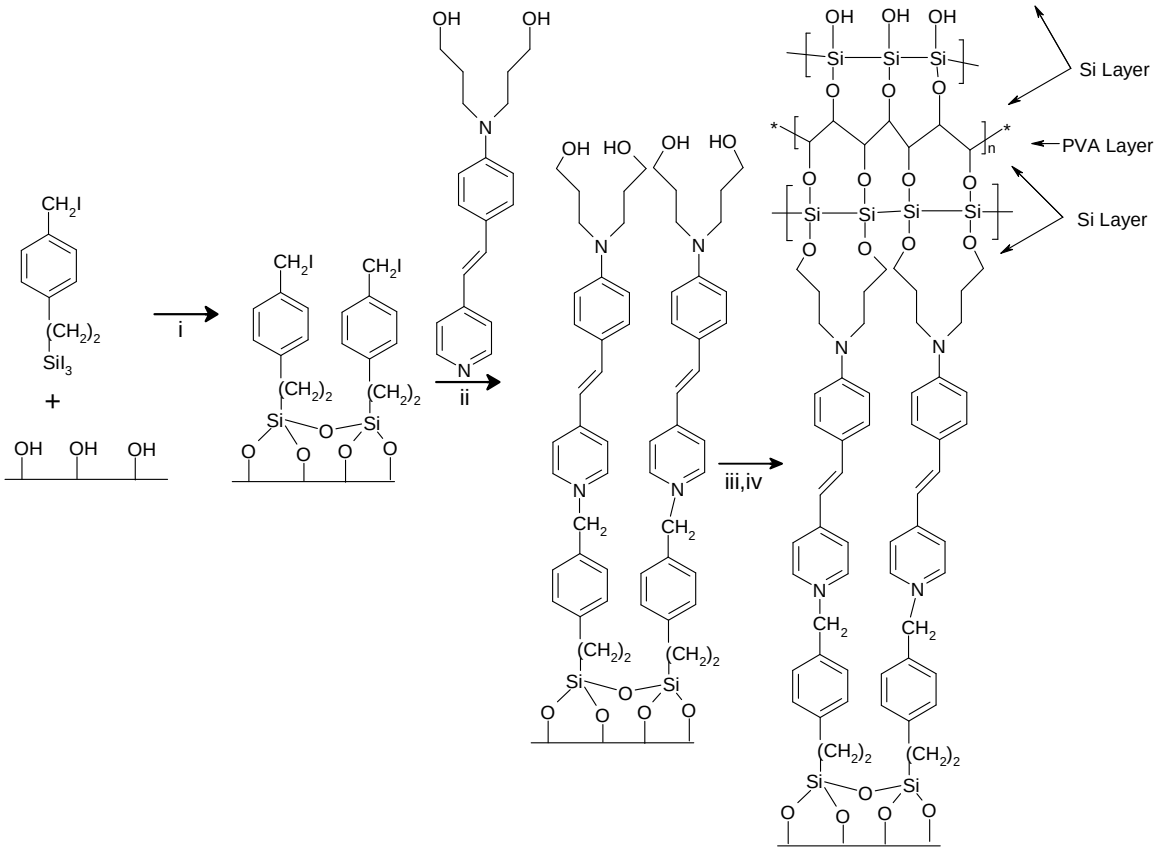

Figure 2.8-1 - Schematic of a hybrid organic / inorganic covalent deposition system for layer-by-layer NLO films[69]

The polymeric layer, poly(vinylalcohol) (PVA), is introduced to provide structural stability. The multilayer film had a $\chi^{(2)}$ value of 2 x 10^{-7} esu. More recently, using a similar methodology, Marks et al. fabricated films with a $\chi^{(2)}$ of 5.3 x 10^{-7} esu and an r_{33} of approximately 80 pm/V.[70] The principle drawback of covalent layer-by-layer deposition schemes is that they often require organic solvents and film formation occurs slowly. The multilayer structure shown in Figure 2.8-1 required 1 day for 5 multilayers to be deposited.[69] The time requirement necessary for an adequately thick film for use in a device (1-10 μm) is prohibitively long.

In addition to using covalent bonds as a method for building layer-by-layer films, there are other interactions that can be used to drive film formation that merit mention. Kunitake uses self-assembling bilayer membranes of amphiphilic lipids where organization is driven by hydrophobic interactions and hydrogen bonding.[71] These self-assembling bilayers form spontaneously when the appropriate lipids are dissolved in water. The lipid bilayers could then be transferred to a substrate. Hammond et al.

demostrates the use of hydrogen bonding to selectively deposit ISAM films of weak polyelectrolytes.[72] By treating a substrate with different functional groups (carboxylic acid and oligoethylene glycol) preferential deposition of PAH / poly(acrylic acid) on the oligo(ethylene glycol) treated areas was observed. ISAM films of linear poly(ethyleneimine) / poly(acrylic acid) were shown to preferentially deposit on the carboxylic acid functionalized regions.

2.9 **ISAM Films for Nonlinear Optics**

The electrostatic layer-by-layer is a highly versatile film fabrication method. Lvov et al. first applied this method for constructing films for non-linear optic applications.[73] The chromophore poly{1-[4-(3-carboxyl-4-hydroxyphenylazo)benzene sulfoamido]-1,2-ethandiyl, sodium salt} (PCBS) was used as the NLO active substituent while PAH and PEI were used as polycations.

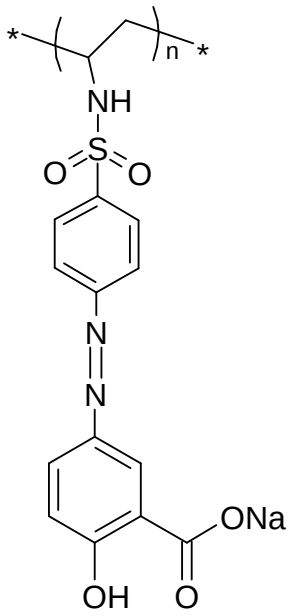

Figure 2.9-1 - Structure of the azo dye chromophore, PCBS

Films were constructed using a variety of layering schemes. Deposition was monitored by both QCM and UV-absorbance measurements, both of which increased linearly as the number of layers deposited increased. The simplest architecture used in these films consisted of alternate layers of PDDA and PCBS (pH values not given). Bilayer thicknesses of 1.8 nm / bilayer were estimated from QCM measurements. The intensity

of the second harmonic increased for the first 4 bilayers deposited and then decreased for bilayers 5-7. For a film in which the chromophore is regularly oriented layer-to-layer a quadratic dependence of the second harmonic intensity ($I_{2\omega}$) on thickness is expected.

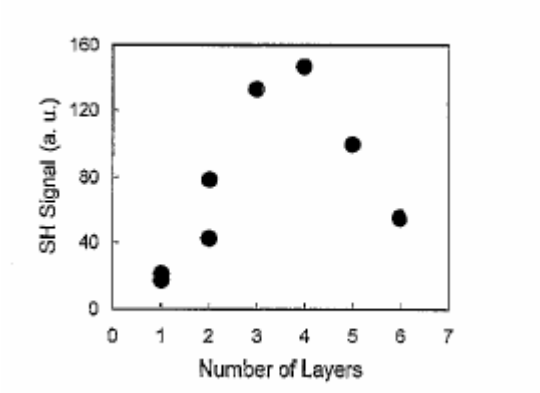

Figure 2.9-2 - Intensity of the second harmonic for layer by layer films of PDDA / PCBS. Quadratic scaling of the second harmonic is not observed for these films, with an observed decrease in the second harmonic intensity observed as layers 6 and 7 are deposited.[73]

The authors postulate that the first layers are oriented due to the influence of the solid substrate, which weakens as additional layers are deposited. Chapter 4 provides more insight as to why quadratic scaling was not observed. A different film assembly consisting of layers of [PEI / PCBS / PDDA / PSS] showed lower SHG intensities due to the lower density of chromophores. They also conducted thermal studies of the SHG intensity and showed that the SHG intensity decreased as the temperature increased.

Roberts et al. deposited alternate layers of stilbazolium-substituted polyepichlorohydrin (SPECH, see Figure 2.9-3 for structure) and PSS to construct multilayer films.[74] Dipping times of 50 minutes in the SPECH solution and 20 minutes in the PSS solution were used. Measurements of the second harmonic intensity showed quadratic scaling of the second harmonic intensity for up to 36 bilayers. As additional layers were deposited, the second harmonic reached a plateau. Lindsey et al. fabricated films using SPECH and the custom polycation C-ACCORD (Figure 2.9-3 shows the structure of C-ACCORD).[75]

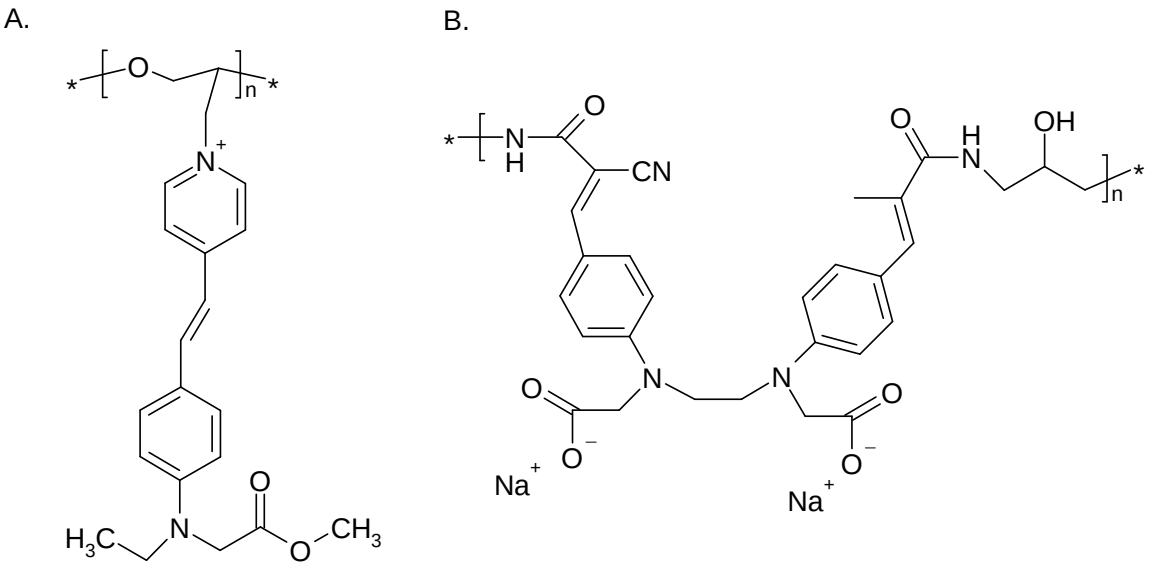

Figure 2.9-3 - Structure of the polymers used by Roberts, *et al*. Polymer A : S-PECH Polymer B:C-ACCORD[74]

This system is unique because both cationic and anionic substituents are chromophoric in nature. However C-ACCORD contains the chromophore in the polymer backbone, while SPECH is a side-chain chromophore. Films of PDDA / C-ACCORD were fabricated; however, these displayed no second harmonic generation. Films deposited using S-PECH and C-ACCORD films showed quadratic scaling of the second harmonic intensity for the first 10 bilayers deposited, followed by a plateau.

The authors note that despite UV-absorbance measurements showing that layer formation of the S-PECH layers is essentially complete in 10 minutes, they display no signs of being oriented until nearly 50 minutes. The authors postulate that the polymer absorbs in a metastable configuration, and orientation develops as the polymer chains rearrange on the surface.

Laschewsky et al. have also employed the ISAM method for fabricating NLO films, with varied levels of success. Using a custom ionene-type polycationic chromophore, only very low levels of SHG were obtained with a number of polyanions.[76]

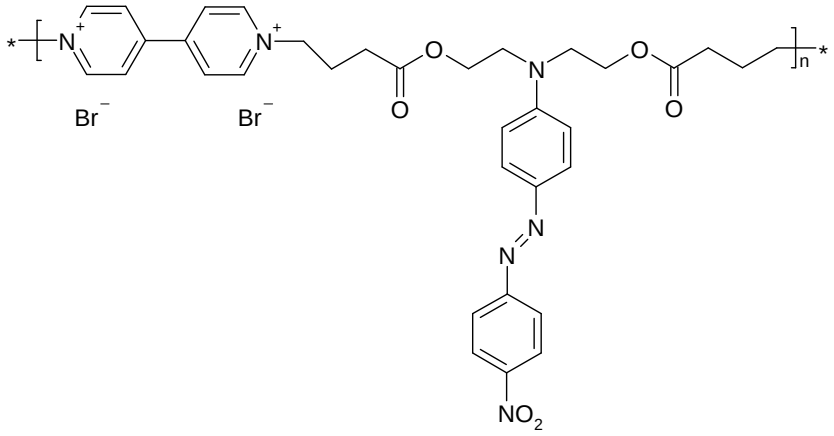

Figure 2.9-4 - Structure of the custom ionene-type polycationic chromophore used by Laschewsky, *et al*. Polar order was not observed in films of this chromophore and several different polyanions.[76]

A separate study complexed a copolymer containing an azo-chromophoric sidegroup with a charged β-cyclodextrin sleeves.[77] This system is schematically shown in Figure 2.9-5.

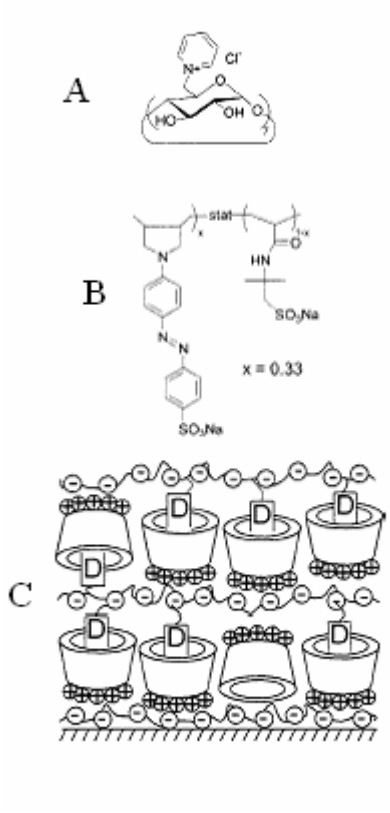

Figure 2.9-5- Laschewsky deposition scheme using a charged cyclodextrins (A) complexed with a custom chromophore (B). The cyclodextrin sleeves complex with the chromophoric side groups and layer-by-layer deposition can occur as shown in (C).[77]

In this system the chromophoric side groups of the polycation formed a complex with the charged cyclodextrin rings in solution. The complexation with the cyclodextrin rings

caused the surface charge reversal and the next layer of polycation could be deposited. The second harmonic intensity increased quadratically for the first 20 layers deposited then continued to increase, albeit in a sub-quadratic manner (shown in Figure 2.9-6).

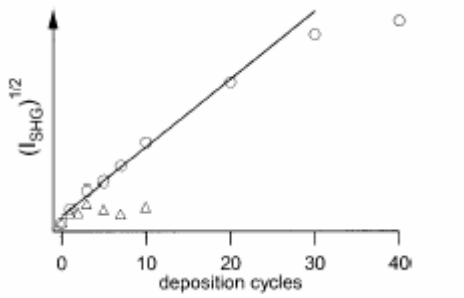

Figure 2.9-6 - The square root of the second harmonic intensity for the layer-by-layer deposition of a charged dye complexed with charged cyclodextrin rings. For up to 30 bilayers a quadratic scaling of the second harmonic intensity is observed with increasing film thickness, meaning that the chromophore molecules are equally oriented in those layers.[76]

Thermal stability experiments on these cyclodextrin complexed films showed a loss of only 20% of the SHG intensity upon heating to 100°C. 90% of the SHG intensity was recovered upon cooling to ambient temperatures. Measurements of the $\chi^{(2)}$ values for the cyclodextrin complexed films gave a value of 114 pm/V. However, it is noted that this value is enhanced due to resonance effects.

The deposition of ISAM films for NLO has also been demonstrated by Heflin et al. using the chromophores PCBS and PS-119 (see Figure 2.9-7 for structure) and PAH as the polycation for deposition.[78] These films showed linear growth of both absorbance and thickness as the number of layers deposited increased.

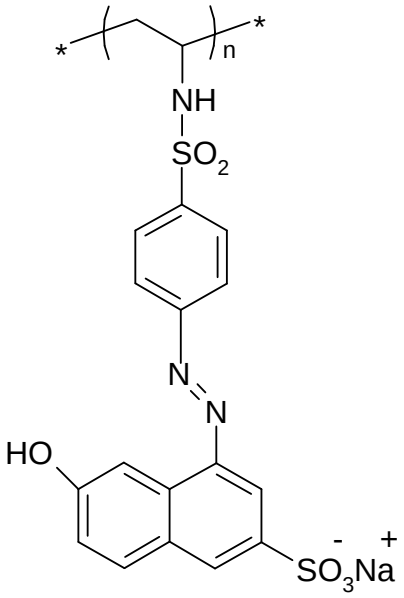

Figure 2.9-7 - Structure of the chromophore PS-119

For PAH / PS-119 films, the SHG intensity varied quadratically on the number of layers deposited for films up to 100 bilayers. This is equivalent to a quadratic dependence on thickness, as the thickness increases linearly with the number of layers deposited. This is shown in Figure 2.9-8; however, the y-axis is the square root of the second harmonic intensity, resulting in a linear relationship.

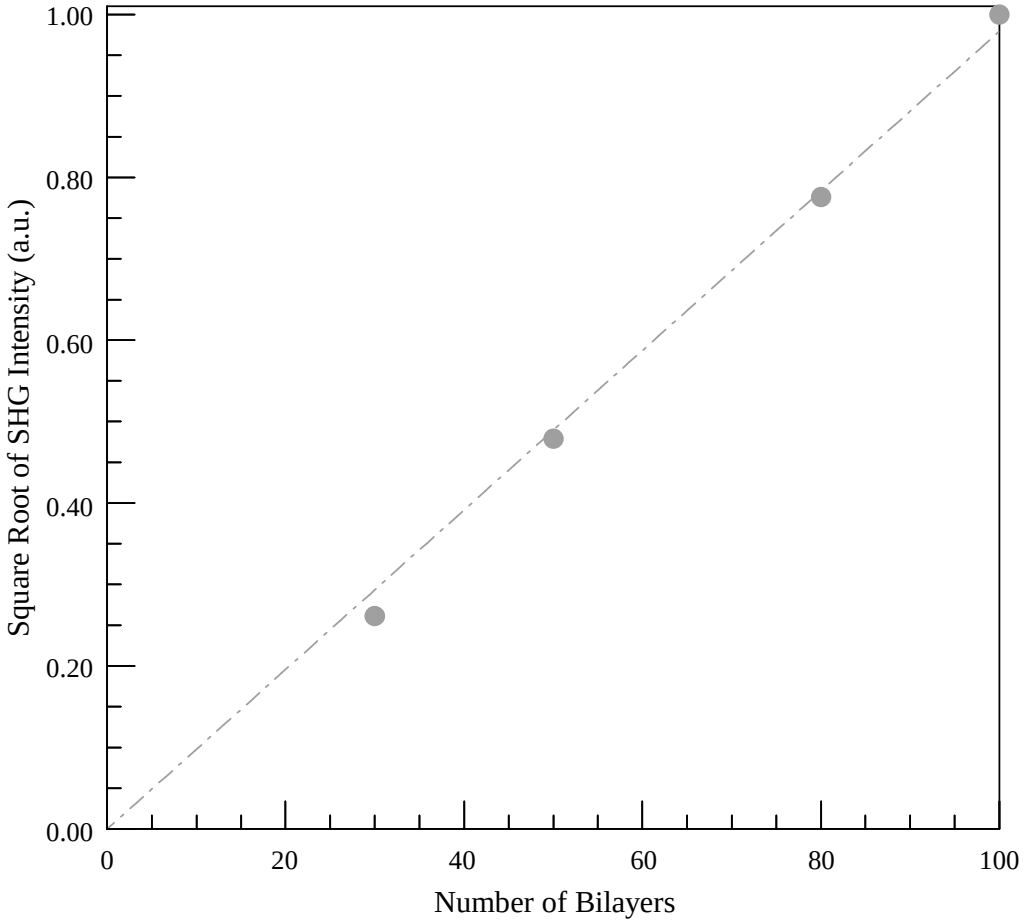

Figure 2.9-8 - The square root of the second harmonic intensity as a function of the number of layers deposited for the PS-119 / PAH system[3]

The observed quadratic scaling is significant because it means that the orientation of the chromophores molecules is the same for each successive layer. This is in contrast to much of the literature in this area, where the second harmonic intensity either decreases or increases in a sub-quadratic fashion as additional layers are deposited. Values of $\chi^{(2)}$ were measured to be 1.34 X 10^{-9} esu, roughly 70% that of quartz.

Lenahan et al. used the ISAM method to construct films of PDDA and several custom chromophore molecules.[79] Structures of the custom chromophores are shown in Figure 2.9-9.

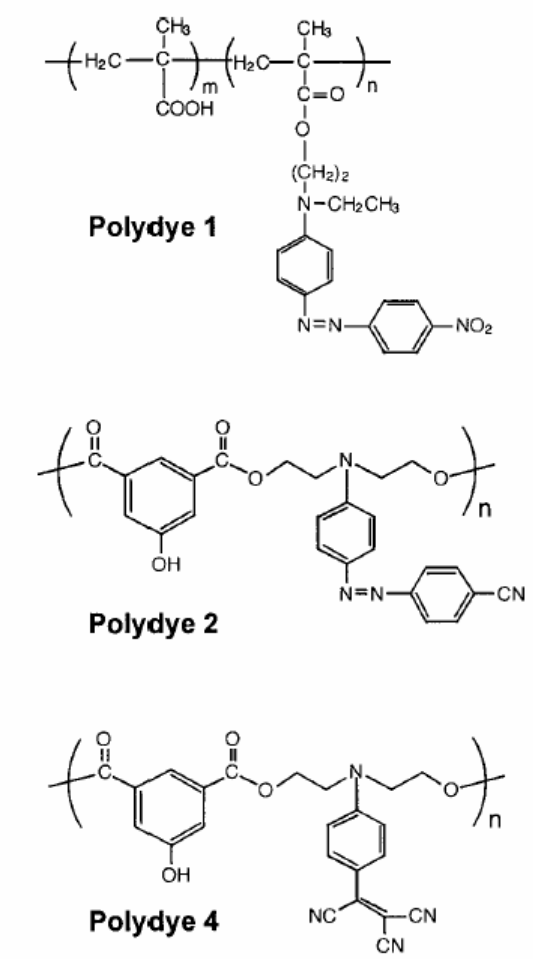

Figure 2.9-9 - Structures of the custom chromophores deposited with PDDA by Lenahan, et al.[79]

The dependence of the second harmonic intensity on film thickness is not presented as SHG data is only presented for 1 film with a given number of bilayers (15 bilayers of PDDA / polydye 1 and 52 bilayers of PDDA / polydye 2). However, of more interest is the use of SHG to probe the orientation of the chromophore molecules. Comparison of the SHG intensity observed for the s-polarized fundamental to that of the p-polarized fundamental allows for a comparison of the $\chi^{(2)}_{zxx}$ and $\chi^{(2)}_{zzz}$ components of the $\chi^{(2)}$ tensor. Equation 30 relates these quantities to the average tilt angle (relative to the surface normal) of the chromophores in the film, θ.

$$\frac{\chi^{(2)}_{zzz}}{\chi^{(2)}_{zxx}} = 2\cot^2\theta \qquad (2.49)$$

Using this technique the average tilt angle of PS-119 chromophores in the 68 bilayer PS-119 / PAH standard film was measured to be 35°. This is in comparison to an average tilt angle of 39° for typical poled polymer systems.

The thermal stability of PAH / PS-119 films was also studied by Heflin et al.[80] In this study, the temperature of films was raised to 150°C, and a 25% reduction in SHG intensity was observed. The films was held at 150°C for 15 hours, with no further reductions in the SH intensity. Upon cooling back to room temperature, the SHG returned to its initial values prior to heating. Additionally, no loss of orientation had been observed for films stored at room temperature for over one year.

Figura thoroughly examined the PAH / PS-119 system, including a focus on the effects of pH and salt concentration on the NLO behavior of the films.[3] For the PAH / PS-119 system, Figura reports that the amount of dye deposited as well as the bilayer thickness increases as the amount of salt increases and as the pH decreases. Values between 5Å and 30Å were reported for bilayer thicknesses. The orientation of the chromophore molecules in the film was shown to improve as the layers became thicker. For example, with no added salt at a pH of 2.5 the average tilt angle away from the surface normal was ~73°, while for pH 1.5 this angle was ~56°. The intensity of the second harmonic also increases as the salt concentration is increased or the pH is decreased. Calculations of $\chi^{(2)}$ show that the susceptibility decreases as the layers become thicker. Figure 2.9-10 shows how $\chi^{(2)}$ depends on both pH and salt concentration for PS-119 / PAH films. Figure 2.9-11 recasts the data of Figure 2.9-10 combining both salt and pH effects using the Debye length. For optimal $\chi^{(2)}$ values, films should be deposited under conditions that encourage layers to form in a flat and thin conformation.

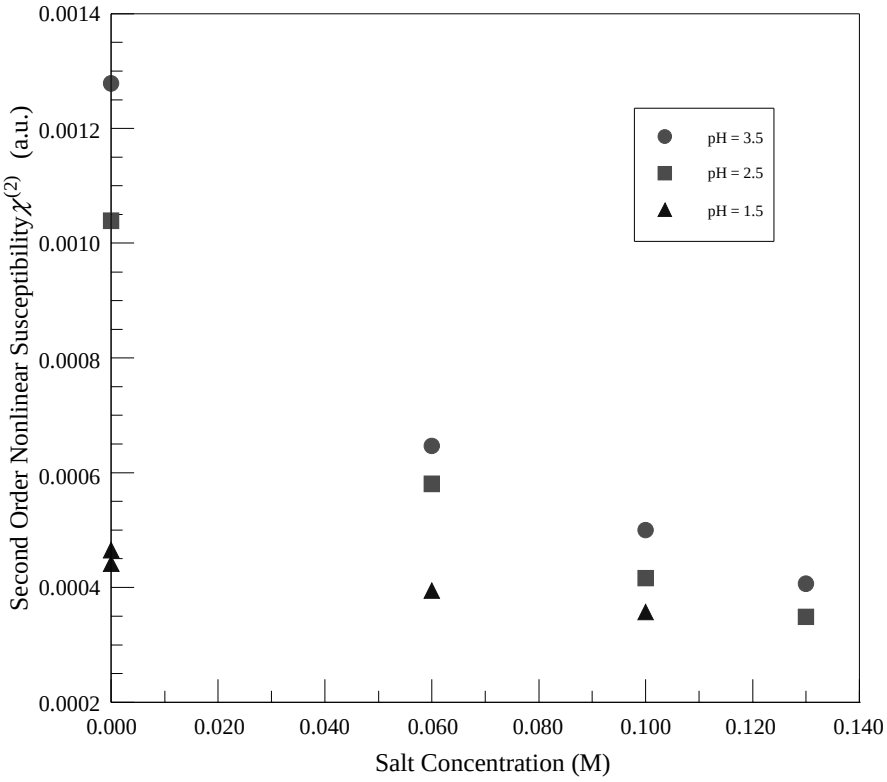

Figure 2.9-10 -Values of $\chi^{(2)}$ for PAH / PS-119 films as a function of the salt concentration and pH^3

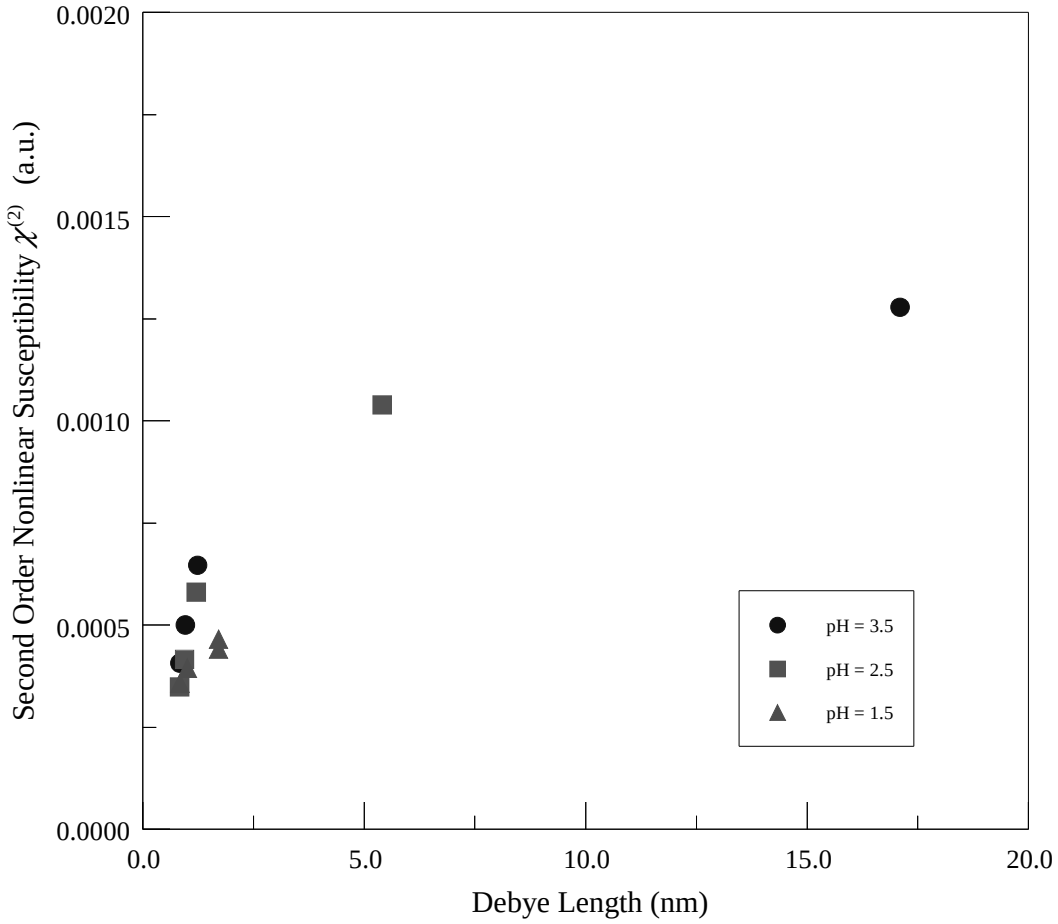

Figure 2.9-11 -Second order susceptibility, $\chi^{(2)}$ as a function of the Debye length for PS-119 / PAH ISAM films[3]

[1] Franken, P.; Hill, A.; Peters, C.; Weinreich, G.; *Phys Rev. Lett.* **7** (1961) 118-119.
[2] Wilson, J. Hawkes, J. F. B. *Optoelectronics: An Introduction*. Ed. P. J. Dean. Prentice Hall, Englewood Cliffs, New Jersey, 1983.
[3] C. Figura, Thesis, Virginia Polytechnic Institute and State University, 1999
[4] Boyd, Robert W. *Nonlinear Optics*. Academic Press, New York, New York, 1992.
[5] Baldwin, George C. *An Introduction to Nonlinear Optics*. Plenum Press, New York, New York. 21.
[6] Biaggio, I. 'Non-Local Contributions to Degenerate Four Wave Mixing in Noncentrosymmetric Materials', *Phys. Rev. Lett.* **82** (1997) 193-196.

[7] Dagani, R. 'Devices Based on Electro-Optic Polymers Begin To Enter Marketplace' *C & E News* March 4, 1996, 22-27
[8] Shi, Y.; Zhang, C.; Zhang, H.; Bechtel, J.; Dalton, L.; Robinson, B.; Steirer W. 'Low (Sub-1-Volt) Halfwave Voltage Polymeric Electro-optic Modulators achieved by Controlling chromopore Shape' *Science* **288** (2000) 119-122.
[9] Ohmer, Melvin C. and Pandey, Ravindra. 'Emergence of Chalcopyrites as Non-Linear Optical Devices' *MRS Bulletin*. July 1998, 16-20
[10] van der Vorst, C.; Horsthuis, W.; Möhlmann, G. *Nonlinear Optical Side-Chain Polymers and Electro-Optic Test Devices*, Polymers for Lightwave and Integrated Optics. Ed. By Lawrence A. Hornak, Marcel Dekker, Inc., New York, New York, 1992.
[11] Van Cott, K.;Guzy, M.; Neyman, P.; Brands, C.; Heflin, J.; Gibson, H.; Davis, R. 'Layer-By-Layer Deposition and Ordering of Low Molecular Weight Dye Molecules for Second Order Nonlinear Optics' *Angewandte Chemie* **41** (2002) 3236-3238.
[12] Lytel, R.; *Applications of Electro-Optic Polymers to Integrated Optics.* SPIE Procedings. Ed. Nasser Peygabarian. **1216** (1990) 30-40 .
[13] Norwood, R. A., Findakly, T., Goldberg, H., A., Khanarian, G., Stamatoff, J. B., Yoon, H. N. *Optical Polymers and Multifunctional Materials.* Polymers for Lightwave And Integrated Optics. Ed. by Lawrence A. Hornak. Marcel Dekker, Inc., New York, New York, 1992.
[14] Cheng, L. T.; Tam, W.; Marder, S.; Stiegman, A.; Rikken, G.; Spangler C. 'Experimental Investigations of Organic Molecular Nonlinear Optical Polarizabilities. 2. A Study of Conjugation Dependencies' *J. Phys. Chem.* **95** (1991) 10643-10652.
[15] Blanchard-Desce, M.; Alain, V.; Bedworth, P.; Marder, S; Fort, A.; Runser, C.; Barzoukas, M.; Lebus, S.; Wortmann, R. *Chem. Eur. J.* **3** (1997) 1091-1104.
[16] Karna, S., Yeates, A. *Nonlinear Optical Materials: Theory and Modeling*. Nonlinear Optical Materials: Theory and Modeling. Ed. by Shashi P. Karna and Alan T. Yeates. ACS Symposium Series. Vol 628. American Chemical Society, Washington DC, 1996
[17] Gott, J., R. *J. Phys. B.* **4**, 116, (1971)
[18] Oudar, J. L., Chemla, D. S., *Opt. Commun*. **13**, 164 (1975)
[19] Oudar, J., L., Chemla, D. S., *J. Chem. Phys* **66**, 2664 (1977)
[20] Levine, B., F. *Chem Phys. Lett.* **37**, 516 (1976)
[21] Dulcic, A., Flytzanis, C., Tang, C., Pépin, D., Fétizon, M., Hopilliard, Y. *J. Chem. Phys.* **74**, 1559 (1981)
[22] Levine, B., F, Bethea , C. G. *J. Chem. Phys.* **65**, 2429 (1976)
[23] Samyn, C., Verbiest, T., Persoons, A. 'Second Order Non-Linear Optical Polymers' *Macromol. Rapid Commun.* **21**, 1-15 (2000)
[24] Pantelis, P., Hill, J. *Guest-Host Polymer Systems for Second-Order Optical Nonlinearities*. Polymers for Lightwave and Integrated Optics. Ed. by Lawrence A. Hornak. Marcel Dekkar, Inc, New York, New York, 1992.
[25] Mandal, B. K.; Chen, Y. M.; Lee, J. 'Cross-Linked Stable Second Order Non-Linear Optical Polymer by Photochemical Reaction' *Appl. Phys. Lett*, **58** (1991), 2459
[26] Ren, A.; Dalton, L. 'Electroactive Polymers Including Non-Linear Optical Polymers' *Current Opinion in Colloid & Interface Science* **4** (1999) 165-171
[27] Wu, J.; Binkley, E.; Kenney, J.; Lytel, R.; Garito, A. 'Highly Thermal Stable Electro-optic Response in Poled Guest-Host Polyimide Systems Cured at 360°C' *J. Appl Phys. Lett.*, 69, (1991), 7366-7368
[28] Singer, K. D., Sohn, J. E., Lalama, S. J., *Appl. Phys. Lett*, **49** (1986) 248-250.
[29] Ashwell, G. 'Langmuir-Blodgett Films:Molecular Engineering of Non-Centrosymmetric Structures for Second-Order Nonlinear Optical Applications' *J. Mater. Chem.* **9** (1999) 1991-2003
[30] Katz, H.; Scheller, G.; Putvinski, T.; Schilling, M.; Wilson, W.; Chidsey, C. 'Polar Orientation of Dyes in Robust Multilayers by Zirconium Phosphate-Phosphonate Interlayers' *Science* **254** (1991) 1485-1487
[31] Iler, R. 'Multilayers of Colloidal Particles' *J. Colloid Interface Sci.* 1966, **21**, 569.
[32] G. Decher, J.D. Hong, *Thin Solid Films*, **210/211**, (1992) p831-835.
[33] Harris, J.; Bruening, M. 'Electrochemical and in Situ Ellipsometric Investigation of the Permeability and Stability of Layered Polyelectrolyte Films' *Langmuir* **16** (2000) 2006-2013
[34] Fleer, G.; Cohen Stuart, M.; Scheutjens, J.; Cosgrove, T.; Vincent, B. *Polymers at Interfaces*. Chapman & Hall, New York, New York (1993)

[35] Decher, G. 'Fuzzy Nanoassemblies: Toward Layered Polymeric Multicomposites' *Science* **277** (1997) 1232-1237
[36] Hammond, P. 'Recent Explorations in Electrostatic Multilayer Thin Film Assembly' *Current Opinion in Colloid & Interface Science* **4** (2000) 430-442
[37] Bertrand, P.; Jonas, A.; Laschewsky, A.; Legras, R. 'Ultrathin Polymer Coatings by Complexation of Polyelectrolytes at Interfaces: Suitable Materials, Structure and Properties' *Macromolecular Rapid Communications* **21** (2000) 319-348
[38] Decher, G.; Hong, J. D.; Schmitt, J. 'Buildup of ultrathin multilayer films by a self-assembly process: III. Consecutively alternating adsorption of aninonic and cationic polyelectrolytes on charged surfaces' *Thin Solid Films* **210/211** (1992) 831-835.
[39] Okubo, T.; Suda, M. 'Alternate Sign Reversal in the z Potential and Sychnronous Expansion and Contraction in the Absorbed Multi-layers of poly(4-vinyl-N-n-butyylpyridinium bromide) cations and Poly(styrene sulfonate) Anions on Colloidal Silica Spheres' *Colloid and Polymer Science* **277** (1999) 813-817.
[40] Schlenoff, J.; Dubas, S. 'Mechanism of Polyelectrolyte Multilayer Growth: Charge Overcompensation and Distribution' *Macromolecules* **34** (2001) 592-598.
[41] Raposo, M.; Oliverira, O. 'Adsorption Mechanisms in Layer-by-Layer Films' *Brazilian Journal of Physics* **28** (1998) 392-404.
[42] Lowack, K.; Helm, C. 'Molecular Mechanisms Controlling the Self-Assembly Process of Polyelectrolyte Multilayers' *Macromolecules* **31** (1998) 823-833.
[43] Lvov, Y.; Decher, G.; Mohwald, H. 'Assembly, Structural Characterization, and Thermal Behavior of Layer-By-Layer Deposited Ultrathin Films of Poly(Vinyl Sulfate) and Poly(allylamine)' *Langmuir*. **9** (1993) 481-486.
[44] Yoo, D.; Shiratori, S.; Rubner, M. 'Controlling Bilayer Composition and Surface Wettability of Sequentially Adsorbed Multilayers of Weak Polyelectrolytes' *Macromolecules* **31** (1998) 4309-4318.
[45] Lvov, Y.; Rusling, J.; Thomsen, D.; Papadimitrakopoulos, F.; Kawakami, T.; Kunitake, T. 'High-speed Multilayer Film Assembly by Alternate Adsorption of Silica Nanoparticles and Linear Polycation' *Chem. Commun.* (1998) 1229-1230
[46] G. J. Fleer, M. A. Cohen Stuart, J. M. H. M. Scheuthens, T. Cosgrove, B. Vincent. Polymers at Interfaces. Chapman and Hall. New York, 1993.
[47] Houska, M.; Brynda, E. 'Interaction of Proteins with Polyelectrolytes at Solid / Liquid Interfaces: Sequential Adsorption of Albumin and Heparin' *Journal of Colloid and Interface Science* **188** (1997) 243-250.
[48] Dubas, S., Schlenoff, J. 'Factors Controlling the Growth of Polyelectrolye Multilayers' *Macromolecules* **32** (1999) 8153-8160.
[49] J. C. Dijt, "Kinetics of Polymer Adsorption, Desorption, and Exchange", thesis, 1993
[50] Ferreira, M.; Rubner, M. 'Molecular-Level Processing of Conjugated Polymers. 1. Layer-by-Layer Manipulation of Conjugated Polyions' *Macromolecules* **28** (1995) 7107-7114
[51] Hoogeveen, N.; Cohen Stuart, M.; Fleer, G. 'Formation and Stability of Multilayers of Polyelectrolytes'. *Langmuir* **12** (1996) 3675-3681.
[52] Lvov, Y.; Ariga, K.; Onda, M.; Ichinose, I.; Kunitake, T. 'A Careful Examination of the Adsorption Step in the Alternate Layer-by-Layer Assembly of Linear Polyanion and Polycation.' *Colloids and Surfaces A* **146** (1999) 337-346.
[53] Decher, G.; Lvov, Y., Schmitt, J. 'Proof of Multilayer Structural Organization in Self-Assembled Polycation-Polyanion Molecular Films' *Thin Solid Films* **244** (1994), 772-777.
[54] Cochin, D.; Laschewsky, A. 'Layer-By-Layer Self-Assembly of Hydrophobically Modified Polyelectrolytes' *Macromol. Chem. Phys.* **200** (1999) 609-615.
[55] Cheung, J.; Stockton, W.; Rubner M. 'Molecular Level Processing of Conjugated Polymers. 3. Layer-by-Layer Manipulation of Polyaniline via Electrostatic Interactions' *Macromolecules* **30** (1997) 2712-2716.
[56] Lösche, M., Schmitt, J., Decher, G., Bouwman, W., Kjaer, K. 'Detailed Structure of Molecularly Thin Polyelectrolyte Multilayer Films on Solid Substrates as Revealed by Neutron Reflectometry' *Macromolecules* **31** (1998) 8893-8906.

[57] van Ackern, F.; Krasemann, L.; Tieke, B. 'Ultrathin Membranes for Gas Separation and Pervaporation Prepared Upon Electrostatic Self-Assembly of Polyelectrolytes'. *Thin Solid Films* **327-329** (1998) 762-766.
[58] Bertrand, P.; Jonas, A.; Laschewsky, A.; Legras, R. 'Ultrathin Polymer Coatings by Complexation of Polyelectrolytes at Interfaces: Suitable Materials, Structure and Properties' *Macromolecular Rapid Communications* **21** (2000) 319-348.
[59] Bliznyuk, V.; Rinderspacher, F.; Tsukruk, V. 'On the Structure of Polyamiodamine Dendrimer Monolayers' *Polymer* **39** (1998) 5249-5252.
[60] Tsukruk, V. Rinderspacher, F., Blinzyuk, V. 'Self-Assembled Multilayer Films from Dendrimers' *Langmuir* **13** (1997) 2171-2176.
[61] Manning, G. 'Limiting Laws and Counterion Condensation In Polyelectrolyte Soltions. IV. The Approach to the Limit and the Extraordinary Stability of the Charge Fraction' *Biophysical Chemistry* **7** (1977) 95-102
[62] D. Shaw. "Introduction to Colloid & Surface Chemistry" Butterworth Heinemann, Boston, 1996
[63] Shiratori, S.; Rubner, M. 'pH-Dependent Thickness Behavior of Sequentially Adsorbed Layers of Weak Polyelectrolytes' *Macromolecules* **33** (2000) 4213-4219.
[64] Decher, G.; Schmitt, J. 'Fine Tuning of the Film Thickness of Ultrathin Multilayer Films Composed of Consecutively Alternating Layers of Anionic and Cationic Polyelectrolytes' *Prog. Colloid Poly. Sci.* **89** (1992) 160-164.
[65] Dubas, S.; Schlenoff, J. 'Polyelectrolyte Multilayers Containinga Weak Polyacid: Construction and Deconstruction' *Macromolecules* **34** (2001) 3736-3740.
[66] Cooper, T.; Campbell, A.; Crane, R. 'Formation of Polypeptide-Dye Multilayers by an Electrostatic Self-Assembly Technique' *Langmuir* **11** (1995) 2713-2718.
[67] Ariga, K.; Lvov, Y.; Kunitake, T. 'Assembling Dye-Polyion Molecular Films by Electrostatic Layer-by-Layer Adsorption' *J. Am. Chem. Soc.* **119** (1997) 2224-2231.
[68] Yamada, S.; Harada, A.; Matsuo, T.; Ohno, S.; Ichinose, I.; Kunitake, T. 'Optical Second Harmonic Generation in Alternately Assembled Dye-Polyion Multilayers' *Jpn. J. Appl. Phys.* **36** (1997) L1110-L1112
[69] Lin, W.; Shlomp, Y.; Lin, W.; Malik, A.; Durbin, M.; Richter, A.; Wong, G.; Dutta, P.; Marks, T. 'New Nonlinear Optical Materials: Expedient Topotactic Self-Assembly of Acentric Chromophoric Superlattices' *Angewandte Chemie*, **34** (1995) 1497-1499.
[70] van der Boom, M.; Richter, A.; Malinsky, J.; Lee, P.; Armstrong, N.; Dutta, P.; Marks, T. 'Single Reactor Route to Polar Superlattices. Layer-by-Layer Self-Assembly of Large-Response Molecular Electrooptic Materials by Protection-Deprotection' *Chem. Mater.* **13** (2001) 15-17.
[71] Kunitake, T. 'Chemistry of Self-Assembling Bilayers and Related Molecular Layers' *MRS Bulliten* **20** (1995) 22-25
[72] Clark, S.; Hammond, P. 'The Role of Secondary Interactions in Selective Electrostatic Multilayer Deposition' *Langmuir* **16** (2000) 10206-10214
[73] Lvov, Y.; Yamada, S.; Kunitake, T. 'Non-linear Optical Effects in Layer-by-Layer Alternate Films of Polycations and an Azobenzene-Containing Polyanion' *Thin Solid Films* **300** (1997) 107-112.
[74] Roberts, M.; Lindsay, G.; Herman, W.; Wynne, K. 'Thermally Stable Nonlinear Optical Films by Alternating Polyelectrolyte Deposition on Hydrophobic Substrates' *J. Am. Chem. Soc.* **120** (1998) 11202-11203.
[75]Lindsay, G.; Roberts, M.; Chafin, A.; Hollins, R.; Merwin, L.; Stenger-Smith, J.; Yee, R.; Zarras, P. 'Ordered Films by Alternating Polyelectrolyte Deposition of Cationic Side Chain and Anionic Main Chain Chromophoric Polymers' *Chem. Mater.* **11** (1999) 924-929 .
[76] Laschewsky, A.; Wischeroff, E.; Kauranen, M.; Persoons, A. 'Polyelectrolyte Multilayer Assemblies Containing Nonlinear Optical Dyes' *Macromolecules* **30** (1997) 8304-8309.
[77] Fischer, P.; Koetse, M.; Laschewsky, A.; Wischeroff, E.; Jullien, L.; Persoons, A.; Verbiest, T. 'Orientation of Nonlinear Optical Active Dyes in Electrostatically Self-Assembled Polymer Films Containing Cyclodextrins' *Macromolecules* **33** (2000) 9471-9473.
[78] Heflin, J.; Liu, Y.; Figura, C.; Marciu, D.; Claus, R. 'Second Order Nonlinear Optical Thin Films Fabricated from Ionically Self-Assembled Monolayers' *SPIE Proceedings* **3147** (1997) 10-19

[79] Lenahan, K.; Wang, Y.; Liu, Y.; Claus, R.; Heflin, J.; Marciu, D.; Figura, C. 'Novel Polymer Dye for Nonlinear Optical Applications Using Ionic Self-Assembled Monolayer Technology' *Advanced Materials* **10** (1998) 853-855.

[80] Heflin, J.; Figura, C.; Marciu, D.; Liu, Y.; Claus, R. 'Thickness Dependence of Second-Harmonic Generation in Thin Films Fabricated from Ionically Self-Assembled Monolayers' *Appl. Phys. Lett.* **74** (1999) 495-497.

3 Layer-By-Layer Deposition And Ordering Of Low Molecular Weight Dye Molecules For Second Order Nonlinear Optics*

*Version appearing as "Layer-By-Layer Deposition and Order of Low-Molecular-Weight Dye Molecules for Second-Order Nonlinear Optics" in Angewandte Chemie, Vol 41 (2002), Issue 17, pgs. 3236-3238

Abstract

This study demonstrates a hybrid deposition scheme relying on electrostatic interactions as well as covalent bonds for film growth. The hybrid scheme results in films that are nanostructured and through the inclusion of a nonlinear optical chromophore molecule, these films exhibit second order nonlinear optic properties. Materials used in the fabrication of these films were the polycation poly(allylamine hydrochloride) and Procion Red MX-5B as the chromophore. As typical for self-assembled thin films using electrostatic interactions, these films demonstrate linear growth in both thickness and absorbance as layers are deposited. The pH values of both the poly(allylamine hydrochloride) as well as the Procion Red are key processing variables for successful deposition of oriented chromophore molecules. Using measurements of second harmonic generation, a linear relationship between the number of layers deposited and the $I_{2\omega}^{1/2}$ has been observed, demonstrating the polar order. Measured values of $\chi^{(2)}$ from the SHG data as large as 11.3×10^{-9} esu, or 5.9 times that of quartz, are found.

Keywords:

chromophores • nonlinear optics • self-assembly • thin films

3.1 Introduction

Second order nonlinear optical (NLO) materials possess non-centrosymmetric structures in which there is a net orientation of an NLO-active constituent. Materials that exhibit second order NLO properties are key components in electro-optic modulators and frequency doubling devices.[1] NLO refers to the optical response of a material that relates the polarization vector P to an applied electric field E according to:

$$P = \chi^{(1)}E + \chi^{(2)}E^2 + \chi^{(3)}E^3 + \ldots \qquad (3.1)$$

where $\chi^{(n)}$ is the n-th order susceptibility. The susceptibilities for the nonlinear terms characterize the nonlinear optical response of a material. Second harmonic generation

(SHG) is one example of second order NLO phenomena and is often used as an experimental probe of the second order susceptibility $\chi^{(2)}$.

Electro-optic modulators have traditionally employed inorganic crystals such as lithium niobate ($LiNbO_3$) or potassium niobate ($KNbO_3$) that are formed under high temperatures.[2] However, organic nonlinear optic materials offer several performance advantages such as higher nonlinear susceptibilities, higher modulation rates, and potentially lower device fabrication costs.[3] Organic films exhibiting nonzero $\chi^{(2)}$ have been fabricated using a variety of methods including corona poling, Langmuir-Blodgett (LB) methods, covalent self-assembly, and, more recently, ionically self-assembled monolayers involving polyelectrolytes. Poled polymer materials are fabricated by doping a host matrix with chromophore molecules, which are then oriented by an applied electric field while the matrix is above its glass transition (T_g) temperature. The temperature of the matrix is then brought below the T_g, which locks in the orientation.[4] While poled polymer systems are capable of high second order NLO activity and are easy to fabricate, the orientation of the chromophore molecules in the host is lost over time. The randomization of the dipole orientation in poled polymer devices occurs more quickly at elevated temperatures and this severely limits the operating lifetime of these materials.[5] LB films have been made with non-centrosymmetric Z- and X-type structures that exhibit relatively high values for $\chi^{(2)}$ but their relatively poor mechanical properties have limited their application in devices.[6]

Layer-by-layer (LBL) film deposition techniques that use intermolecular interactions such as covalent bonds, electrostatic attractions, or hydrogen bonding to drive self-assembly are particularly interesting for fabricating wholly organic and organic-inorganic hybrid films that exhibit SHG. There is a large and growing body of literature on the use of LBL methods for fabricating nanostructured films for a variety of applications including organic light emitting diodes[7], humidity sensors[8], biosensors[9], photovoltaics[10], electrochromics[11], and nonlinear optic (NLO) materials.[12] The LBL technique relying on purely electrostatic interactions, referred to hereafter in this paper as the ionically self-assembled monolayer or ISAM process was first developed by Iler[13] and further elaborated upon by Decher et al.[14] This process involves the immersion of a charged substrate into solutions of polyelectrolytes of opposite charge.[14] A monolayer of

polymer adsorbs onto the surface resulting in charge reversal. The substrate is then removed from the solution, thoroughly rinsed to remove nonadsorbed polymer, and immersed in a solution of polyelectrolyte with a charge opposite to that of the adsorbed layer. A monolayer of polymer adsorbs, forming a bilayer with the first polymer, and the immersion process is repeated, building up a multilayer film. Reviews by Decher[15] and Hammond[16] describe many studies of films made with a variety of organic polyelectrolytes and nanoparticles.

With the ISAM method, NLO-active chromophores are oriented by the non-covalent interactions between soluble and deposited species to form multilayered films with compositions controlled at the nanometer length scale. Heflin et al. and Lindsay et al. demonstrated that the ISAM process can be used to create films exhibiting SHG by incorporating an NLO-active polymer as one of the constituents in a film and that these ISAM films have greater stability than poled polymer systems.[17,18] Herman and Roberts studied chromophore orientation in ISAM films and found that the orientation of the chromophore in the first layer can be influenced by hydrophobic interactions between the chromophore molecule and the substrates.[19] Furthermore, they concluded that orientation in subsequent layers is influenced by the orientation of this first layer. Dewitt and Hammond showed that the average tilt angle of the charged chromophoric group in a film and the film thickness depend strongly on the solution pH values.[20] Lee et al. showed linear growth of absorbance and thickness for films made by deposition of a polycation and a polymeric dye precursor. These films were then functionalized with the dye moiety. These films showed the expected quadratic relationship between the SHG intensity and the number of bilayers, meaning that chromophore orientation is consistent from one bilayer to the next.[21] Deposition of ordered films using reactive silane compounds has been demonstrated, but the deposition processes required organic solvents and high temperatures.[22,23]

A related approach that could be employed to fabricate NLO materials involves the use of low molecular weight dye molecules and polyelectrolytes as film constituents. Yamada et al. constructed films of poly(diallyldimethylammonium chloride) and Erichrome Black T and observed linear growth of the film during the non-covalent deposition process.[24] These films exhibited a SHG intensity that increased only for the

first 5 bilayers and then reached a plateau. This plateau after 5 bilayers was attributed to the chromophore molecules in upper layers not having the same orientation as they did in lower layers; however, the addition of layers did not perturb the orientation of previous layers. Yet to be demonstrated is a combination of low molecular weight chromophore molecules and polyelectrolytes that can be used to construct stable NLO active films with high bilayer numbers needed for electro-optic device fabrication.

This work shows that low molecular weight, non-symmetric chromophores can be stably integrated into films by a facile, layer-by-layer deposition process using both electrostatic and covalent bonding. Additionally, it is shown that this deposition process results in non-centrosymmetric films that exhibit significant SHG intensities where the square root of the SHG intensity scaled linearly with bilayer number, indicating that deposition results in a reproducible orientation of the chromophore molecules from bilayer to bilayer up to high bilayer numbers. The model chromophore used is Procion Red MX-5B (Figure 3.1-1), a reactive dye that contains a triazine ring and two sulfonic acid groups. Poly(allylamine hydrochloride) (PAH, Figure 3.1-2), was used to provide both the nucleophilic primary amine groups for reaction with the triazine ring and the protonated amine groups for electrostatic interaction with the sulfonic acid groups of PR (Figure 3.1-3).

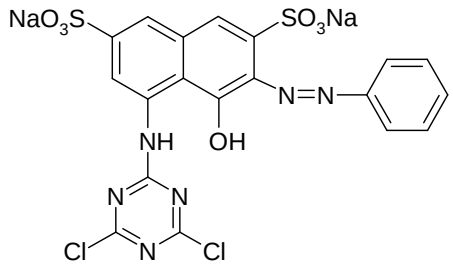

Figure 3.1-1 – Structure of Procion Red MX-5B

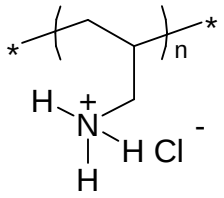

Figure 3.1-2 – Structure of poly(allylamine hydrochloride) [PAH], pK_a=8.7

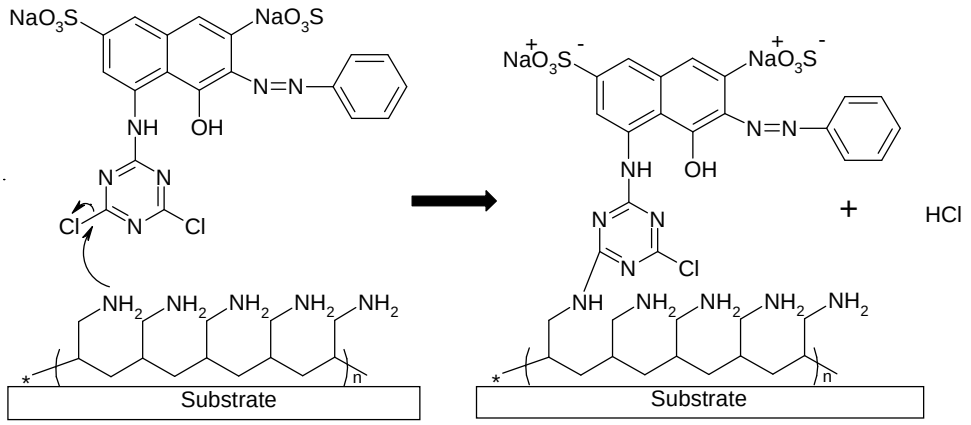

Figure 3.1-3 - Reaction between PR molecule and a previously absorbed monolayer or PAH

The pH of the PR and PAH solutions was found to be a key processing variable for achieving reproducible films with a high degree of polar ordering of the PR molecules. Conditions favoring incorporation of PR by covalent bonds resulted in films with high SHG intensity. The deposition steps involve only aqueous solutions at ambient conditions, and individual immersion times can be as low as 2 minutes/monolayer.

3.2. Experimental

3.2.1. Materials

The anionic / reactive chromophore used in this study was Procion Red MX-5B (MW = 615.34, Aldrich, lot 08423HR). The absorbance spectrum of this chromophore in DI water at a concentration of 0.03 mg/ml solution is shown in Figure 3.2-1.

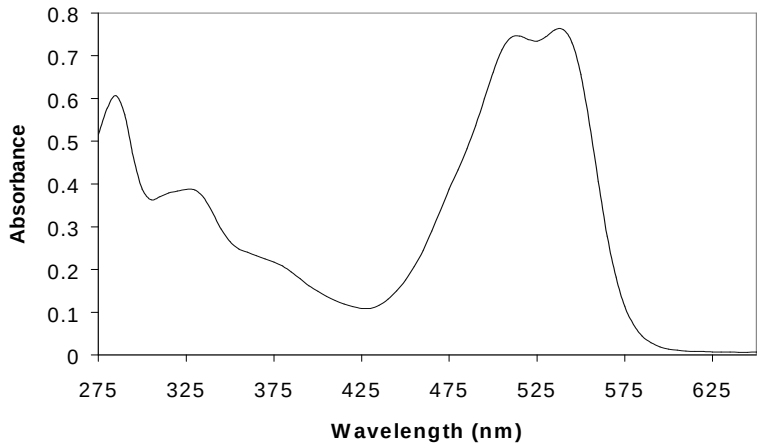

Figure 3.2-1 - Absorbance spectrum for Procion Red MX-5B, 0.03 mg/ml in deionized water. There is no appreciable absorbance above 600 nm**.**

The characteristic peak for this molecule is 538 nm, which was used for all absorbance measurements. The NLO-inactive polycation used in this study was poly(allylamine hydrochloride) (PAH; MW ~ 70,000, Aldrich). All materials were used as received without further purification. Deionized water was obtained with an ion exchange unit (Barnstead Nanopure II) and maintained a specific resistivity above 17 MΩ•cm. Glass microscope slides (Fisher Scientific) were used as the substrates on which films were deposited. They were prepared using the RCA cleaning procedure[25] in which the substrates were immersed in a solution of H_2O, H_2O_2, and NH_4OH at 70°C for 20 minutes. The slides were then rinsed and placed in an acid bath consisting of concentrated HCl, H_2O_2 and H_2O for 20 minutes and were then rinsed and baked at 130°C for at least one hour.

3.2.2. Film Deposition

PAH solutions at a concentration of 0.01 M on a monomer basis were used in all experiments. The concentrations of PR solutions were 0.025 M. The pH of the solutions was adjusted using HCl or NaOH as needed. The glass slide immersion time in PAH was 5 minutes, with the exception of the first layer, which was 10 minutes. The immersion time in PR was 10 minutes. Between immersions, the substrates were vigorously agitated and rinsed with deionized water. Slides were dried every 10 dips (which gives 5 bilayers on each side of the slide, hence 10 total bilayers) using N_2 gas. For any given set of

solution conditions, a series of 5 slides were made with a total (both sides) of 2, 10, 20, 40 and 60 bilayers.

3.2.3. Film Characterization

Absorbance measurements were made with a Hitachi U-2000 Spectrophotometer at a wavelength of 538 nm and were taken every 10 bilayers during the deposition process. Upon the completion of dipping for a given slide, 5 absorbance measurements were made along the length of the slide to characterize the homogeneity in the final absorbance value. Film thicknesses were measured using a variable angle spectroscopic ellipsometer (J. A. Woolam Ellipsometer VB-200). The amplitude factor ψ and phase factor Δ which are related to the complex Fresnel coefficients for any given film, were measured for wavelengths from 350 to 1000 nm at 10 nm intervals.[26] This wavelength range was repeated for angles ranging from 55° to 75° in 5° intervals. A portion of the substrate was roughened to scatter the light. The ellipsometric data were obtained opposite to this roughened patch, as the scattering eliminates backside reflections simplifying data analysis. Least squares analysis was used to determine the slope in absorbance vs. bilayer number graphs. The average of slopes determined from 20, 40, and 60 bilayer films is reported in Table 3.3-1. Students t-test was used to determine if differences in slope and bilayer thickness at different experimental conditions were statistically significant.

SHG measurements were performed with a standard setup using a 10-nanosecond pulse width, Q-switched Nd:YAG laser with a fundamental wavelength of 1064 nm.[27] The SHG data were averaged over 100 shots per data point, and the uncertainty in relative $\chi^{(2)}$ values is 10%. Typical spot radius and pulse energy values were 30μm and 7mJ/pulse, respectively. The film was deposited on both sides of the substrate. As a result, as the sample is rotated with respect to the incident beam, the path length between the film on opposite sides is varied, leading to interference fringes of the SHG intensity. The sample was rotated from 30° to 60° away from normal incidence using a stepper motor controlled rotation stage. The $\chi^{(2)}$ value is determined from the peak of the interference fringe in the vicinity of 45º. By comparison to Maker fringes in a quartz crystal wedge, $\chi^{(2)}$ of a film is obtained from

$$\frac{\chi^{(2)}_{film}}{\chi^{(2)}_{q}} = \frac{2l_{c,q}}{\pi d_{film}} \sqrt{\frac{I^{2\omega}_{film}}{I^{2\omega}_{q}}} \tag{3.1}$$

where l_{film} is the total path length through the film, the coherence length of quartz, $l_c = \lambda / 4(n^{2\omega}-n^{\omega})$, is 22.4 μm, and $\chi^{(2)}$ of quartz is 1.92×10^{-9} esu.

Bilayer numbers for absorbance measurements account for the film on both sides of the substrate while SHG and ellipsometry measurements are made using the film deposited on one side of the substrate.

Dynamic light scattering (DLS) was used to measure the diffusion coefficient of the PAH as a function of pH.[28] DLS measurements were performed with a DynaPro-801 TC instrument operating at a wavelength of 836 nm and a fixed angle of 90°. All experiments were conducted at 25 ± 0.2°C and all samples were filtered with a 0.02 μm Whatman Anotop syringe filter.

3.3. Results

In this study, we concentrate on how the pH of the PR and PAH solutions affect the properties of the films obtained. Successful film growth was characterized by homogeneity and a linear increase in the absorbance and thickness with the number of bilayers deposited. Absorbance data for successfully deposited films are shown in Figure 3.3-1 and Table 3.3-1. The slope characterizes the amount of dye deposited per bilayer; the standard deviation of this slope describes the reproducibility of the film deposition among replicates for a given set of experimental conditions; the correlation coefficient characterizes the reproducibility of PR deposition from bilayer to bilayer. These films displayed a linear increase in the absorbance as a function of the bilayer number.

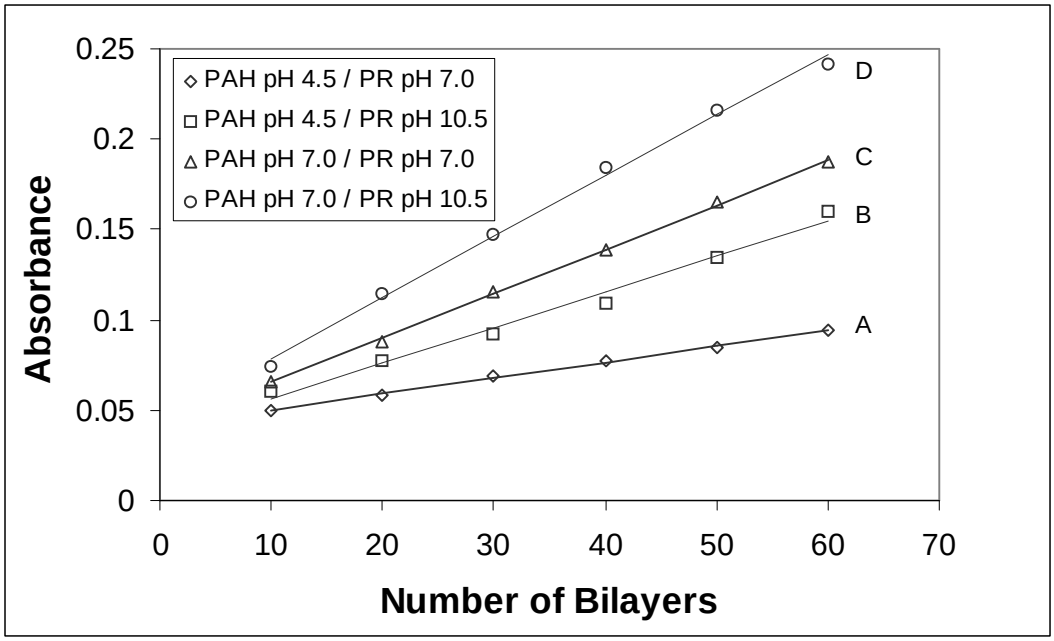

Figure 3.3-1 - Representative plots of the absorbance at 538 nm as a function of the number of bilayers deposited for 60 bilayer films. The conditions used for these slides were 10 mM M PAH (monomer basis) at pH 4.5 and pH 7; 0.025 M PR at pH 10.5 and 7 all at room temperature.

Table 3.3-1 - Summary of the slopes of the absorbance *vs.* number of bilayers and ellipsometric thicknesses for deposition of PR (0.025 M) and PAH (10 mM RU). The average of the thickness, slopes and correlation coefficients obtained for all films at a given condition are reported.

Experiment	PAH pH	PR pH	Slope (Abs/bilayer) (corr. Coefficient)	Bilayer Thickness (nm)	$\chi^{(2)}$ (10^{-9} esu)
A	4.5	7.0	$8.9\text{x}10^{-4} \pm 1.0\text{x}10^{-5}$ (0.998)	N/A[1]	N/A
B	4.5	10.5	$2.0\text{x}10^{-3} \pm 1.0\text{x}10^{-4}$ (0.992)	0.34 ± 0.02	11.2
C	7.0	7.0	$2.3\text{x}10^{-3} \pm 4.0\text{x}10^{-4}$ (0.999)	0.55 ± 0.05	1.2
D	7.0	10.5	$3.3\text{x}10^{-3} \pm 3.2\text{x}10^{-4}$ (0.998)	0.52 ± 0.06	11.3

[1] Too thin to measure

[2] For quartz, $\chi^{(2)} = 1.92\text{x}10^{-9}$ esu.

When the pH of the PAH solutions was held constant, the amount of PR deposited per bilayer increased as the pH of the PR solution was increased (compare experiments A *vs.* B and C *vs.* D, Table 3.3-1). This trend was observed until the pH of the PR solution was raised to 12.0, at which point deposition of PR failed. The best PR deposition was observed when the PR solution was at a pH of 10.5. At this optimal PR deposition condition, we found that as the pH of the PAH solution was increased from 4.5 to 7.0

(compare experiments B *vs.* D), we observed a small but statistically insignificant increase in the film thickness per bilayer ($p > 0.05$), but a significant increase in the amount of PR deposited per bilayer ($p < 0.05$). Poor film formation was observed for PAH solutions deposited at pH ≥ 8.5. This is likely due to incipient aggregation and insolubility of the PAH as the pH increased. The dramatic decrease in diffusion coefficient for pH > 7 (Figure 3.3-2) is consistent with the reduction in charge density of the PAH given its pK_a (8.7). The reduced charge density leads to reduced solubility and the formation of aggregates consisting of multiple PAH chains. Such aggregates hinder the formation of uniform, homogeneous monolayers of adsorbed PAH chains that lead to poor layer-by-layer film formation, especially when the other constituent is not a polyelectrolyte.

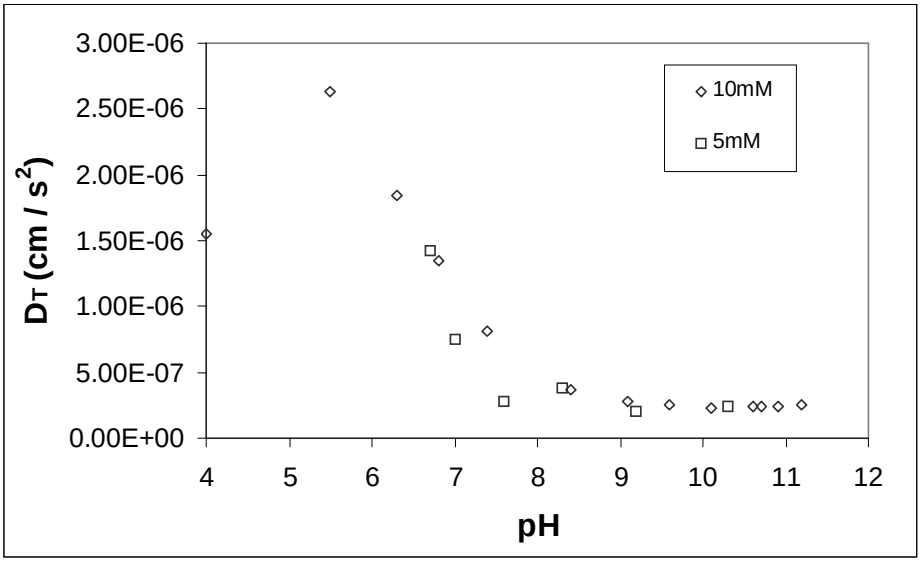

Figure 3.3-2 - Dynamic Light Scattering results for the translational diffusion coefficient of PAH in solution as a function of pH at two polymer concentrations (molarity of repeat unit) with no added salt.

When the film thickness is much less than the second harmonic coherence length of the material, the SHG intensity should exhibit a quadratic dependence on the film thickness or, correspondingly, number of bilayers. Figure 3.3-3 shows the square root of the peak second harmonic intensity as a function of the number of bilayers for the sets of films fabricated with different PAH and PR solution pH values. The linear dependence of the square root of the SHG intensity on the number of bilayers for the films fabricated with a PR solution at pH 10.5 (Figure 3.3-3, experiments B and D) demonstrates that the SHG signal is due to polar ordering in each successive bilayer of the film. If the degree of

ordering decreased in successive bilayers or if the SHG signal were due to interface effects, the SHG intensity would have a subquadratic dependence on the number of bilayers. For the films fabricated with a PR pH of 7.0, there is a much weaker dependence of the SHG intensity on the number of bilayers, indicating a lesser degree of ordering.

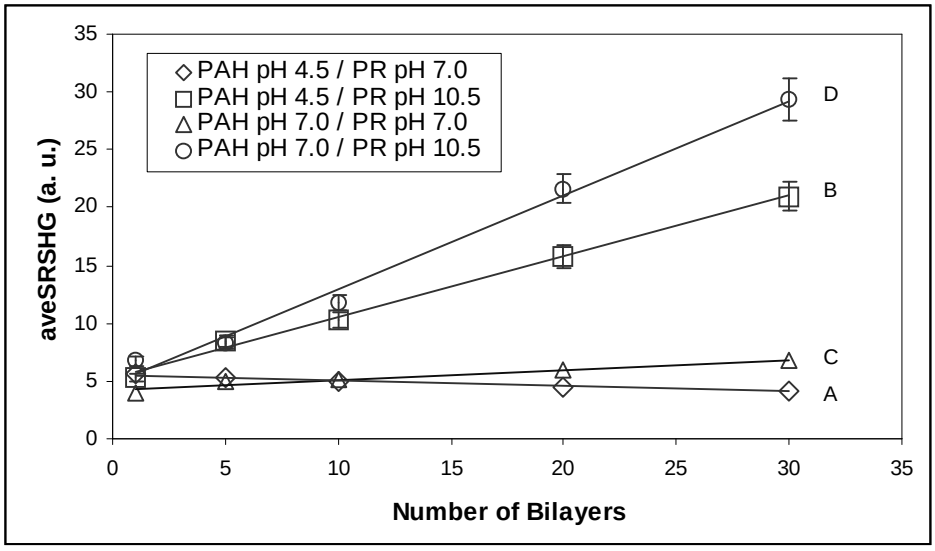

Figure 3.3-3 - Square root of the SHG intensity as a function of the number of bilayer for various PAH/Procion Red pH conditions

Koetse et al. previously reported on the fabrication of films using PR and the polycation poly[N-(3-aminopropyl)-N-(4-vinylbenzyl)-N,N-dimethylammonium chloride] [PAVDMA].[29] The structure of this polycation is shown in Figure 3.3-4 and consists of a charged ammonium group in addition to a primary amine. SHG results for this system showed that there was a lack of bulk polar order.

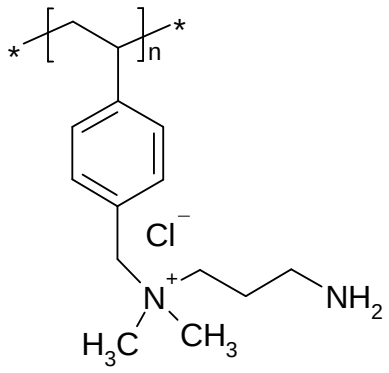

Figure 3.3-4 - Structure of the polycation poly(N-(3-aminopropyl)-N-(4-vinylbenzyl)-N,N-dimethylammonium chloride) [PAVDMA]

The growth of the self-assembled films in real time was monitored using *in situ* second harmonic generation by Charles Brands in the Department of Physics. In this case, the glass substrate was held fixed in the laser beam throughout the procedure. Because the glass cuvettes, the immersion solutions, and the substrate are all centrosymmetric, the SHG signal is due to the polar film as it grows on the substrate along with a small background signal from the air-glass and glass-liquid interfaces. The substrate was first immersed in PAH solution at pH 7.0 to produce a cationic surface. Figure 3.3-5 shows the SHG intensity as a function of time as the substrate was then immersed in a PR pH 10.5 solution. The covalent deposition of Procion Red on PAH is essentially complete in two minutes.

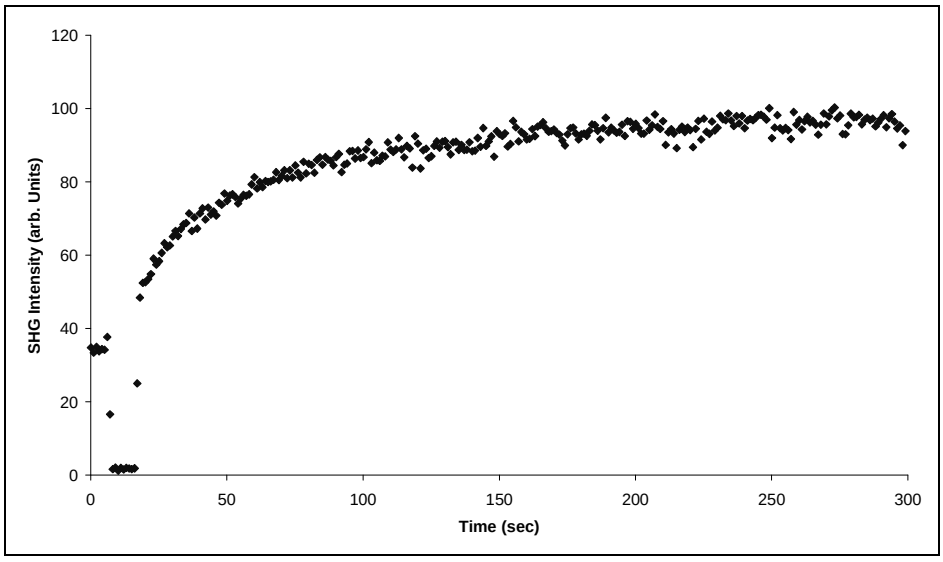

Figure 3.3-5 - *In situ* measurement of the SHG intensity as Procion Red is deposited in the film. The substrate was coated with PAH (pH 7.0) and then immersed in Procion Red (0.025 M, pH 10.5).[30]

3.4. Discussion

Ionic interactions alone are not sufficient for constructing LBL films with low molecular weight chromophores.[31] Our objective was to demonstrate that a simple layer-by-layer deposition scheme using a monomeric chromophore molecule can be used to construct films having a high net polar ordering. We used a commercially available reactive chromophore, Procion Red (PR), as a model chromophore to demonstrate this methodology. By alternating the mechanism of the deposition of each monolayer and decoupling the chromophore orientation from steric constraints of a polymer chain, we hypothesized that the PR would be deposited with a non-centrosymmetric orientation that is required for the film to display NLO properties such as SHG.

The effects of polymer type, pH, salt concentration, and other processing variables on film deposition have been studied by Decher and Schmitt[32], Lvov et al.[33], Rubner et al., and others.[34,35,36,37,38, 39,40,41] Rubner found that the thickness of ISAM bilayers made with weak polyelectrolytes can be varied by over an order of magnitude simply by varying the pH and ionic strength.[42] This is particularly relevant to the present work in that it suggests a method for controlling the conformation and thickness of the adsorbed polymer layers which is critical for controlling the orientation of deposited NLO active chromophores.

The pH determines the ionization state of the amine side groups on PAH, which affects both the conformation of the polymer upon adsorption and its subsequent reactivity with Procion Red. Efficient electrostatic deposition of PAH requires that the pH of the PAH dipping solution is maintained near or below the amino group pK_a (8.7), where the majority of the side groups will be protonated and available for interaction with the negative charges on the substrate or the sulfonate groups on the dye.[43] For efficient covalent attachment of the chromophore, the pH of the PR solution must be near or above the pK_a of the PAH amino groups. For the PAH cases studied, the amino groups on the PAH chain are essentially fully protonated. With no additional salts in these solutions, these PAH solutions were at low ionic strengths, typically 0.003 M, so there is relatively little shielding of charged groups. The positive charges along the chain strongly repel each other and are strongly attracted to the negatively charged surface. These two effects

lead to the deposition of PAH in flat, train-like layers, and the bilayer thicknesses are less than 1 nm/bilayer.

The PR solution pH also plays an important role in the film deposition process. The PR solution pH directly affects the degree of protonation of the previous deposited PAH layers, and thus affects the subsequent reaction kinetics for PR incorporation. At a pH above the pK_a of the side chain amines of PAH, the majority of the amines will be unprotonated and thus able to react with the triazine ring of PR. Additionally, the reactivity of the triazine ring on PR increases with increasing pH.[44] These two effects result in reactive deposition being favored as the pH is increased. The clearest example of the effect of PR solution pH on deposition can be seen in Figure 3.3-1 and Table 3.3-1, where the PAH pH was held constant at either pH 4.5 or 7.0, and the PR solution pH was increased from 7.0 to 10.5. The amount of dye deposited per bilayer increased as the PR solution pH was increased from 7.0 to 10.5. In fact, when the PAH pH was 4.5 and the PR pH was 7.0, very little PR was deposited at all. We believe that, in addition to a fairly low reactivity of the triazine rings at pH 7.0, the PAH layers deposited at pH 4.5 may not have a sufficiently high surface concentration to allow the deposition process to occur due to the extremely flat and thin layers that are formed.

Importantly, the pH of the deposition solutions affects the SHG intensities and the degree of polar ordering of the PR molecules in the film. Table 3.4-1 presents the data of Table 3.3-1 normalized to the PAH pH 4.5 / PR pH 10.5 case. In addition to the absorbance/bilayer and thickness data, Table 3.4-1 also contains the normalized square root of the SHG intensity ($(I_{2\omega})^{1/2}$) per bilayer.

Table 3.4-1- Relative values of the absorbance per bilayer and $(I^{2\omega})^{1/2}$ per bilayer as a function of deposition pH, both normalized to the values for PAH at pH 4.5 and Procion Red at pH 10.5.

Experiment	PAH pH	PR pH	Absorbance/ Bilayer	Bilayer Thickness	$(I^{2\omega})^{1/2}$/bilayer
B	4.5	10.5	1.0	1.0	1.0
C	7.0	7.0	1.15	1.61	0.17
D	7.0	10.5	1.63	1.53	1.55

The effect of PAH solution pH on the films can be seen by comparing experiments B *vs.* D, where the PR solution pH is held constant at 10.5. Increasing the PAH solution pH from 4.5 to 7.0 results in increases in the absorbance per bilayer. The $(I_{2\omega})^{1/2}$ per bilayer

increases by the same relative amount (~55-60%) as the absorbance. Within this pH range, the PAH is deposited as thin, flat layers. Thus, as the pH of the PAH solution is increased, $(I_{2\omega})^{1/2}$ scales proportionally with small changes amount of PR per bilayer, and the increase in $(I_{2\omega})^{1/2}$ is interpreted to be a result of simply incorporating more PR into the film.

Experiments C and D keep the PAH solution pH constant at 7.0 while varying the PR solution pH from 7.0 to 10.5. In these experiments the bilayer thickness is similar, but the absorbance per bilayer and $(I_{2\omega})^{1/2}$ per bilayer both increase as the PR pH is increased from 7.0 to 10.5. While 42% more PR is incorporated per bilayer, the value of $(I_{2\omega})^{1/2}$ per bilayer increases by over 800%. Thus, the pH of the PR solution has a dramatic effect on the orientation of the PR molecules that are incorporated in the films. We note that at pH 7, the reactivity of the PAH amine groups with the triazine ring of the PR is lower, and PR may be incorporated by a combination of electrostatic, hydrogen bond, and covalent interactions. Thus at conditions favoring covalent reaction between PR and PAH, we obtain a high degree of PR ordering, while at conditions not favoring covalent reaction between PR and PAH, the PR deposited within the films has a more random orientation. The $\chi^{(2)}$ values we obtained for deposition of PR at pH 10.5 are 11.2×10^{-9} and 11.3×10^{-9} esu (Table 1), which are six-fold greater than quartz.

The larger SHG observed in the PR pH 10.5 case serves as confirmation of the hypothesis that alternating the mechanism of deposition in these films and decoupling of the chromophore from steric constraints of a polymer backbone can provide a route to successful deposition and orientation of a low molecular weight chromophore. In our earlier studies with NLO-active polymeric dyes such as PS119,[45] which consists of a poly(vinylamine) backbone with an ionic azo dye chromophore, and poly {1-4-(3-carboxy –4-hydroxyphenylazo)-benzenesulfonamido-1,2-ethanediyl, sodium salt} (PCBS), films were made under deposition conditions leading to relatively thin bilayers (~ 0.2 nm/bilayer). In both PS119 and PCBS, the NLO-active chromophores are charged side groups on the polymer chain. Using *in situ* SHG intensity measurements, we found that the polar ordering of an adsorbed chromophore layer is reduced by subsequent adsorption of the next polyelectrolyte monolayer.[30] By decoupling the NLO-active chromophore from a polymer chain we can reduce the steric constraints to achieving

ordered films that are present when using a large chromophore side group. Additionally, by using a "bi-functional" chromophore in which the mechanism for chromophore deposition (i.e., covalent bonding) differs from the deposition of the polymeric component (electrostatic interactions), we can minimize competing intermolecular interactions that prevent the achievement of a high net polar ordering of the chromophore within the film.

3.5. Conclusions

A hybrid covalent/electrostatic deposition scheme has been demonstrated that can be used to obtain highly ordered self-assembled films. It is believed that the ordering is induced by alternating the mechanism of deposition from monolayer to monolayer and decoupling the chromophore from the steric constraints of a polymer backbone. Using Procion Red MX-5B as a model reactive/anionic monomeric NLO chromophore and PAH as the cationic polyelectrolyte, films with significant $\chi^{(2)}$ values were constructed. This deposition process is highly sensitive to the pH values of both the PAH and PR solutions. In this work we focused on the effect of pH on the film properties, and we found an operating window for optimal deposition and orientation. The PR solution pH should be high enough to favor covalent deposition. The PAH solution pH should also be as high as possible while still obtaining layer-by-layer growth of homogeneous films. While initial $\chi^{(2)}$ values are significant, these values are far from optimized because the Procion Red chromophore is far from an ideal NLO chromophore. Dr. Gibson's group in the Department of Chemistry is currently developing a triazine functionalized NLO chromophore with a higher hyperpolarizability value than Procion Red. Future deposition experiments with Procion Red and this new chromophore will further investigate the effects of ionic strength, pH, and chromophore structure. Chromophore tilt angle measurements and the thermal and temporal stability of the PR films are currently being studied. The films used in this study were relatively thin (~30 bilayers). This methodology appears suitable for making thick films (1-10 μm) necessary for electro-optic modulator devices.

---

[1] Shi, Y.; Zhang, C.; Zhang, H.; Bechtel, J.; Dalton, L.; Robinson, B.; Steier, W. 'Low (Sub-1Volt) Halfwave Voltage Polymeric Electro-Optic Modulators Achieved by Controlling Chromophore Shape' *Science* **288** (2000) 119-122.

[2] Y. R. Shen, "The Principles of Nonlinear Optics", Wiley, N.Y. 1984

[3] Dalton, L.; Harper, A.; Ghosn, R.; Steier, W.; Ziari, M.; Fetterman, H.; Shi, Y.; Mustacich, R.; Jen, A.; Shea, K. 'Synthesis and Processing of Improved Organic Second-Order Nonlinear Optical Materials for Applications in Photonics' *Chem. Mater.* **7** (1995) 1060-1081.
[4] Singer, K.; Sohn, J.; Lalama, S. 'Second Harmonic Generation in Poled Polyer Films' *Appl. Phys. Lett.* **49** (1986) 248-250.
[5] Burland, D.; Miller, R.; Walsh, C. 'Second-Order Nonlinearity in Poled-Polymer Systems' *Chem. Rev.* **94** (1994) 31-75.
[6] Ashwell, G. 'Langmuir-Blodgett films: molecular engineering of non-centrosymmetric structures for second-order nonlinear optical applications' *J. Mater. Chem.* **9** (1999) 1991-2003.
[7] Fou, A.; Onitsuka, O.; Ferreira, M.; Rubner, M.; Swieh, B. 'Fabrication and properties of light-emitting diodes based on self-assembled multilayers of poly(phenylene vinylene)' *J. Appl Phys.* **79** (1996) 7501-7509.
[8] Kleinfeld, E.; Ferguson, G. 'Rapid, reversible sorption of water from the vapor by a multilayered composite film : A nonstructured humidity sensor' *Chem Mater.* **7** (1995) 2327-2331.
[9] Caruso, F.; Furlong D.; Ariga, K.; Ichinose, I.; Kunitake, T. 'Characterization of Polyelectrolyte-Protein Multilayer Films by Atomic Force Microscopy, Scanning Electron Microscopy, and Fourier Transform Infrared Reflection-Absorption Spectroscopy' *Langmuir* **14** (1998) 4559-4565.
[10] Piok, T.; Brands, C.; Neyman, P.; Erlacher, A.; Soman, C.; Murray, M.; Schroeder, R.; Graupner, W.; Heflin, J.; Marciu, D.; Drake, A.; Miller, M.; Wang, H.; Gibson, H.; Dorn, H.; Leising, G.; Guzy, M.; Davis, RM. 'Photovoltaic Cells Based on Ionically Self-Assembled Nanostructures'. *Synthetic Metals* **116** (2001) 343-347.
[11] Laurent, D.; Schlenoff, J. 'Multilayer assemblies of redox polyelectrolytes' *Langmuir* **13** (1997) 1552-1557.
[12] Li. D.; Ratner, M.; Marks, T.; Zhang, C.; Yang, J.; Wong, G. 'Chromophoric self-assembled multilayers-organic superlattice approaches to thin-film nonlinear optical-materials' *J. Am. Chem. Soc.* **112** (1990) 7389-7390.
[13] Iler, R. ' Multilayers of Colloidal Particles' *Colloid Interface Sci.* **21** (1966) 569
[14] Decher, G.; Lvov, Y.; Schmitt, J. 'Proof of multilayer structural organization in self-assembled polycation polyanion molecular films' *Thin Solid Films* **244** (1994) 772-777.
[15] Decher, G. 'Fuzzy Nanoassemblies: Toward Layered Polymeric Multicomposites' *Science* **277** (1997) 1232-1237.
[16] Hammond, P. 'Recent Explorations in Electrostatic Multilayer Thin Film Assembly' *Curr. Opin. in Colloid & Interface Science.* **4** (2000) 430-442.
[17] Heflin, J.; Figura, C.; Marciu, D.; Liu, Y.; Clause, R. 'Thickness dependence of second-harmonic generation in thin films fabricated from ionically self-assembled monolayers' *Appl Phys Letters* **74** (1999) 495-497.
[18] Lindsay, G.; Roberts, M.; Chafin, A.; Hollins, L.; Merwin, L.; Stenger-Smith, J.; Yee, Y.; Zarras, P.; Wynne, K. 'Ordered films by alternating polyelectrolyte deposition of cation side chains and anionic main chain chromophoric polymers' *Chem Mater.* **11** (1999) 924-929.
[19] Herman, W., Roberts, M. 'The Sense of Chromophore Orientation in Films Made by Alternate Polyelectrolyte Deposition' *Advanced Materials.* **13** (2001) 744-746.
[20] DeWitt, D., Hammond, P. 'Controlling Orientation in Optically Active Multilayer Films' *Polymer Preprints* **41** (2000) 815-816.
[21] Lee, S.; Blalsubramanian, S.; Kim, D.; Viswanathan, N.; Bian, S.; Kumar, J.; Tripathy, S. 'Azo Polymer Multilayer Films by Electrostatic Self-Assembly and Layer-by-Layer Post Azo Functionalization' *Macromolecules* **33** (2000) 6534-6540.
[22] Lin, W.; Yitzchaik, S.; Lin, W.; Malik, A.; Durbin, K.; Richter, A.; Wong, G.; Dutta, P.; Marks, T. 'New Nonlinear Optical Materials : Expedient Topotactic Self-Assembly of Acentric Chromophoric Superlattices' *Angew. Chem. Int. Ed. Engl.* **34** (1995) 1497-1499.
[23] Katz, H.; Scheller, G.; Putvinski, T.; Schilling, M.; Wilson, W.; Chidsey, C. 'Polar Orientation of Dyes in Robust Multilayers by Zirconium Phosphate-Phosphonate Interlayers' *Science* **254** (1991) 1485-1487.
[24] Yamada, S.; Harada, A.; Matsuo T.; Ohno S.; Ichinose, I.; Kunitake, T. 'Optical Second Harmonic Generation in Alternately Assembled Dye-Polyion Multilayers' *Jpn. J. Appl. Phys.* **36** (1997) L1110-L1112

[25] Itano, M.; Kern, F.; Miyashita, M.; Ohmi, T. 'Particle Removal from Silicon Water Surface in Wet Cleaning Process' *IEEE Trans. on Semicond. Manu*. **6** (1993) 258-267.
[26] R. M. Azzam and N. M. Bashara. "Ellipsometry and Polarized Light" Elsevier, N. Y. 1987
[27] Neyman, P.; Guzy, M.; Shah, S.; Davis, R.; Van Cott, K.; Hang, W.; Gibson, H.; Brands, C.; Heflin, J. 'Novel Hybrid Covalent / Ionic Self-Assembly Techniques for Improved Second-Order Nonlinear Optical Films' *Mat. Res. Soc. Symp. Proc* **708** (2002) 161-166.
[28] Schaefer, D.W.; Han, C.C. In *Dynamic Light Scattering*; Pecora, R., Ed; Plenum Press: New York, 1985; Chap.5.
[29] Koetse, M.; Laschewsky, A.; Verbiest, T. 'Films Grown From Polyamines and Reactive Dyes by Alternating Polyelectrolyte Adsorption / Surface Activation (CoMPAS)'. *Mat. Sci. Eng. C.* **10** (1999) 107-113.
[30] Brands, C.; Neyman, P.; Guzy, M.; Shah, S.; Davis, R; Van Cott, K; Wang, H.; Gibson, H.; Heflin, J. 'In Situ Second Harmonic Generation Measurements of the Formation of Ionically Self-Assembled Monolayers' *SPIE Proc*. **4461** (2001) 311-318.
[31] Das, S.; Pal, A. 'Layer-by-Layer Self-Assembling of a Low Molecular Weight Organic Material by Different Electrostatic Adsorption Process' *Langmuir* **18** (2002) 458-461.
[32] Decher, G.; Schmitt, J. 'Fine-Tuning of the film thickness of ultrathin multilayer films composed of consecutively alternating layers of anionic and cationic polyelectrolytes'. *Progr Colloid Polym Sci*. **89** (1992) 160-164
[33] Lvov, Y.; Ariga, K.; Onda, M.; Ichinose, I.; Kunitake, T. 'A careful examination of the adsorption step in the alternate layer-by-layer assembly of linear polyanion and polycation'. *Colloids and Surfaces A*. **146** (1999) 337-346.
[34] Caruso, F.; Lichtenfeld, H.; Donath, E.; Möhwald, H. 'Investigation of Electrostatic Interactions in Polyelectrolyte Multilayer Films: Binding of Anionic Fluorescent Probes to Layers Assembled onto Colloids' *Macromolecules* **32** (1999) 2317-2328.
[35] Kleinfeld, E.; Ferguson, G. 'Stepwise Formation of Multilayered Nanostructural Films from Macromolecular Precursors' *Science* **265** (1994) 370-373.
[36] Yoo, D.; Shiratori, S.; Rubner, M. 'Controlling Bilayer Composition and Surface Wettability of Sequentially Adsorbed Multilayers of Weak Polyelectrolytes' *Macromolecules* **31** (1998) 4309-4318.
[37] Clark, S.; Montague M.; Hammond, P. 'Ionic Effects of Sodium Chloride on the Templated Deposition of Polyelectrolytes Using Layer-by-Layer Ionic Assembly' *Macromolecules* **30** (1997) 7237-7244.
[38] Lösche, M.; Schmitt, J.; Decher, G.; Bouwman W.; Kjaer, K. 'Detailed Structure of Molecularly Thin Polyelectrolyte Multilayer Films on Solid Substrates as Revealed by Neutron Reflectometry' *Macromolecules* **31**(1998) 8893-8906.
[39] Lowack, K.; Helm, C. 'Molecular Mechanisms Controlling the Self-Assembly Process of Polyelectrolyte Multilayers' *Macromolecules* **31** (1998) 823-833.
[40] Bertrand, P.; Jonas, A.; Laschewsky, A.; Legras, R. 'Ultrathin Polymer Coatings by Complexation of Polyelectrolytes at Interfaces : Suitable Materials, Structures and Properties' *Macromolecules Rapid Commun.* **21** (2000) 319-348.
[41] Netz, R.; Joanny, J. 'Adsorption of Semiflexible Polyelectrolytes on Charged Planar Surfaces: Charge Compensation, Charge Reversal, and Multilayer Formation' *Macromolecules*. **32** (1999) 9013-9025.
[42] Shiratori, S.; Rubner, M. 'pH-Dependent Thickness Behavior of Sequentially Adsorbed Layers of Weak Polyelectrolytes' *Macromolecules* **33** (2000) 4213-4219.
[43] Fang, M.; Kim, C.; Saupe, G.; Kim, H.; Waraksa, C.; Miwa, T.; Fujishima, A.; Mallouk, T. 'Layer-by-Layer Growth and Condensation Recations of Niobate and Titanoniobate Thin Films'. *Chem. Mater.* **11** (1999) 1526-1532.
[44] Hermanson, G. "Bioconjugate Techniques" Academic Press. N. Y. 1996
[45] Figura, C.; Neyman, P.; Marciu, D.; Brands, C.; Murray, M; Hair, S.; Davis, R.; Miller, M.; Heflin, J. 'Thermal Stability and Immersion Solution Dependence of Second Order Nonlinear Optical Ionically Self-Assembled Films' *SPIE Proc.* **3939** (2000) 214-222.

4 Effect of low molecular weight salts on the deposition and ordering of Procion dyes in a hybrid deposition system

Abstract

Hybrid deposition, a layer-by-layer technique utilizing both covalent bonds and electrostatic interactions for film formation, results in regularly oriented films suitable for second order nonlinear optic applications. This study examines deposition of PAH with three triazine functionalized chromophores; Procion Red MX-5B, Procion Orange MX-2R, and Procion Brown MX-GRN. The effect of ionic strength on the deposition process was probed through the addition of NaCl to the dye solutions. Increasing the ionic strengths resulted in screening of inter-dye electrostatic repulsions allowing for greater deposition on the surface. A packing model has been employed to describe this increased deposition. These films were also characterized for second order nonlinear optic properties with a maximum value of $\chi^{(2)}$ of 87.5 x 10^{-9} esu obtained for Procion Brown deposited with 0.5 M NaCl.

Keywords:

Layer-by-layer deposition, second order nonlinear optics, dye packing, reactive deposition

4.1 Introduction

The development of polymeric second order nonlinear optic materials is driven by performance benefits these materials possess over their inorganic counterparts. The organic materials developed by previous groups have either had $\chi^{(2)}$ values that were not sufficiently high, or poor temporal stability in the $\chi^{(2)}$ value which prevents the widespread application of organic second order nonlinear optic materials. Langmuir-Blodgett films have mechanical and thermal stabilities that aren't suitable for elecrto-optic modulator devices.[1] Poled polymer materials, while exhibiting initially high $\chi^{(2)}$ values, demonstrate temporal instability with the $\chi^{(2)}$ value decaying to zero over time.[2] Layer-by-layer films made with two oppositely charged polymers offer excellent thermal stability. [3] However, the $\chi^{(2)}$ values are currently too low for practical applications.Recently Van Cott et al. reported a new mechanism for fabricating layer-by-

layer films for second order NLO.[4] This method utilized the triazine functionalized chromophore molecule Procion Red MX-5B (PR) (Figure 4.2-1) and the polycation poly(allylamine hydrochloride) [PAH] (Figure 4.2-2). The triazine moiety on the Procion Red reacts with the amine functionality on PAH. The next layer of PAH then electrostatically couples to the negatively charged sulfonate groups on PR. The highest value of $\chi^{(2)}$ obtained for these films, 11.3 x 10^{-9} esu, was obtained when the PR was deposited at pH 10.5 and the PAH deposited at pH 7.0. Under these conditions, the PAH was deposited while highly charged, which results in a flat train-like conformation. When the previously deposited PAH is exposed to the pH 10.5 environment of the PR dye, the amine moieties are unprotonated and can react with the triazine rings on the PR dye. However, this best value for $\chi^{(2)}$ is still an order of magnitude from the benchmark for $LiNbO_3$ of approximately 200 x 10^{-9} esu.

For an organic film, the $\chi^{(2)}$ parameter is a function of several variables and is given by:

$$\chi^{(2)} = NF\beta\left\langle \cos^3\theta \right\rangle \tag{4.1}$$

where N is the number density of chromophore molecules in the film, F accounts for local field effects, β is the hyperpolarizability of the chromophore and θ is the average tilt angle of the chromophore's dipole moment in the material relative to the surface normal.[5] This relationship shows that there are several ways to enhance the $\chi^{(2)}$ of a material.

The hyperpolarizability is a function of the chromophore structure. Generally, β increases with the conjugation length and with the relative strength of the donor-acceptor pair. A chromophore with a higher β value will result in films with higher $\chi^{(2)}$ values, all other variables being constant.

A second approach to increasing the $\chi^{(2)}$ of a material is to increase the chromophore density, N, in the film. The work of Lvov and coworkers suggests one possible route towards this objective.[6] Multilayer films of the polycation poly(diallyldimethylammoniumchloride) [PDDA] and negatively charged SiO_2 nanoparticles were fabricated using several different ionic strengths for the SiO_2 suspensions. As the ionic strength of the solution increased, the bilayer thickness, and thus the deposited amount of SiO_2 particles increased. This occurred due to the increased

electrostatic shielding at higher ionic strengths, which reduced the repulsion between the negatively charged SiO_2 particles as they deposit, allowing them to pack more densely.

An analogous effect has been seen with the effect of salt on film formation in traditional polymer/polymer ISAM films.[7,8,9] At low ionic strengths the polymers absorb in flat, train-like conformations. However, as the ionic strength increases, the charges along the polymer chains are shielded which causes them to absorb in thicker layers with more loops and tails. For second order NLO applications, Figura showed that depositing bilayers of PAH and the NLO-active polymer dye PS-119 in the low ionic strength regime resulted in the highest values for $\chi^{(2)}$.[10]

The decrease in $\chi^{(2)}$ with increasing ionic strength that is observed in polymer / polymer ISAM films is not expected for films made using the hybrid deposition scheme where the polymeric 'glue' is deposited in flat thin layers and the chromophores are deposited from a high ionic strength environment. The presence of the additional ionic species in the chromophore solutions should not change the conformation of the previously deposited polymer chains for deposition times of ~ 5 minutes. Instead it should change the manner in which the charged chromophore molecules pack as they deposit.

This present study examines the effect of increasing the ionic strength of chromophore dipping solutions on the amount of deposited material, film thickness, and most importantly, the $\chi^{(2)}$ of the resulting films. A second approach to increase the $\chi^{(2)}$ was also examined, with the desired increase in $\chi^{(2)}$ coming from an increase in the chromophore's hyperpolarizability as opposed to increasing the chromophore density, N. This relationship between chromophore structure and $\chi^{(2)}$ was examined by fabricating films with three different Procion chromophores.

4.2 Experimental

The anionic / reactive chromophores used in this study were Procion Red MX-5B (Pro Red 305, Pro Chemical and Dye, Somerset, MA), Procion Orange MX-2R (Pro Strong Orange 202, Pro Chemical and Dye, Somerset, MA) and Procion Brown MX-GRN (Pro Burnt Orange 515, Pro Chemical and Dye, Somerset, MA). The Procion Red used in this study was from a different supplier than the Procion Red used in Chapter 3. The Procion Red from Pro Chemical and Dye is significantly more pure than the dye

from Aldrich, in which the major impurity is the hydrolysis product.[12] Structures of these chromophore molecules are shown in Figure 4.2-1. The characteristic absorbance peaks for these dye was determined to be: Procion Red λ_{max}=538 nm, Procion Orange λ_{max}=489 nm and Procion Brown λ_{max}=407 nm. All absorbance measurements in the layer-by-layer experiments were made at the characteristic peak for the respective chromophore molecule. The NLO-inactive polycation used in this study was poly(allylamine hydrochloride) (PAH; MW ~ 70,000, Aldrich). The structure of PAH is shown below in Figure 4.2-2. All materials were used as received without further purification. Deionized water was obtained with an ion exchange unit (Barnstead Nanopure II) and maintained a specific resistivity above 17 MΩ•cm. Fisherfinest Premium glass microscope slides (Fisher Scientific, Pittsburgh, PA) were used as the substrates on which films were deposited. They were prepared using the RCA cleaning procedure[11] in which the substrates were immersed in a solution of H_2O, H_2O_2 (Fisher Scientific, 50% H_2O_2, Certified Grade, lot 023157), and NH_4OH (EM Science, Certified, K27962605) at 70°C for 20 minutes. The slides were then rinsed and placed in an acid bath consisting of concentrated HCl (EM Science, Certified Grade, 42326), H_2O_2 and H_2O for 20 minutes and were then rinsed and baked at 130°C for at least one hour.

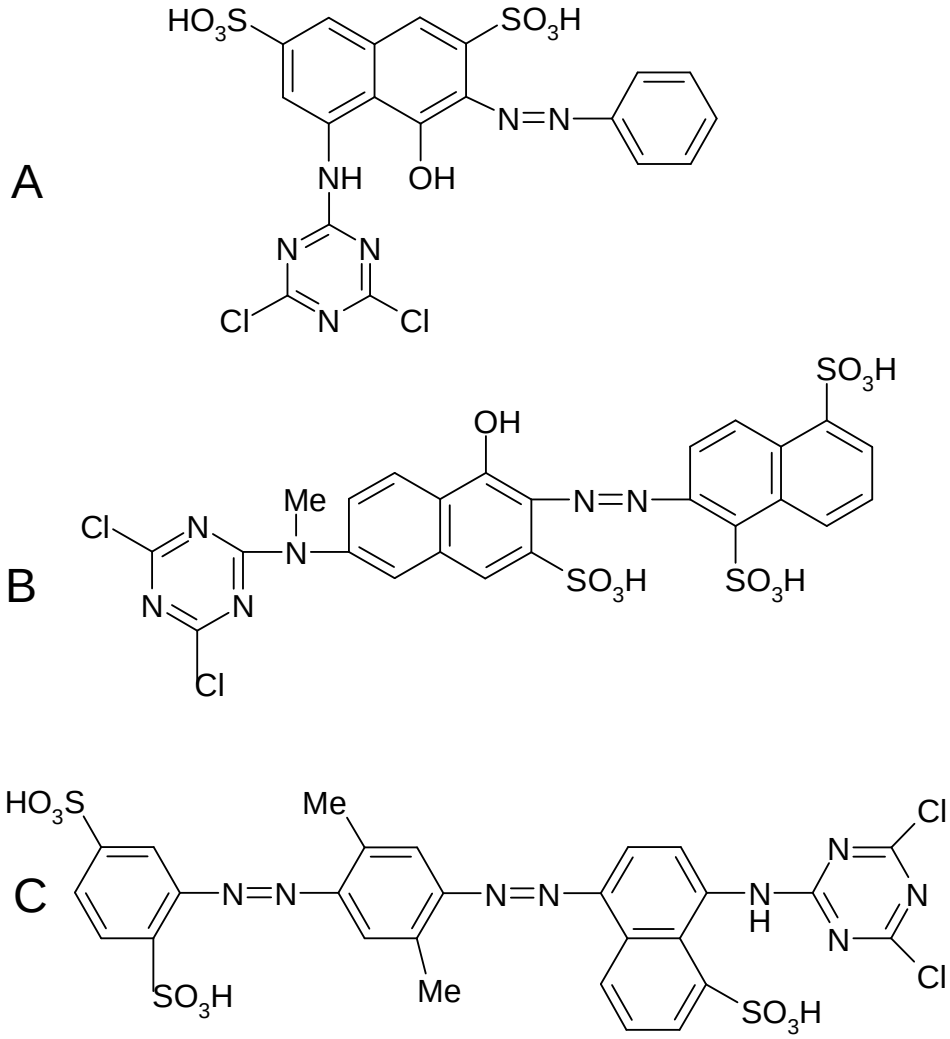

Figure 4.2-1 - Structures of the triazine functionalized chromophores used in this study. A. Procion Red MX-5B B. Procion Orange MX-2R C. Procion Brown MX-GRN

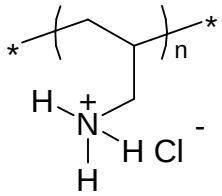

Figure 4.2-2 - Structure of the optically inactive polycation PAH

4.2.1 Dye Purification

Commercially available Procion dyes are, as a result of the manufacturing process, not pure materials.[12] The Procion Red, which was used as received was tested for Na, Fe, K, Ca, Si and S by the soil testing lab here at Virginia Tech using inductively

coupled plasma (ICP) emission spectroscopy. Results of the ICP anaylysis are shown below in Table 4.2-1. Procion Orange and Procion Brown were purified to remove any ionic salts and buffers that are in the as-received powder. Solid phase extraction with octadecysilyl functionalized silica was used to desalt the dyes (Alltech High Capacity 75 ml C18 column, lot 173801). The dye was dissolved in 50 mM ammonium acetate at ~ 10 mg/ml. This solution was filtered with a 0.45 μm syringe filter to remove any particulate impurities. The column was first washed with > 100 ml (~ 5 bed volumes) 50 mM ammonium acetate, and then the dye solution was introduced. The column was again flushed with > 100 ml of the ammonium acetate solution, allowing the column to run dry. The dye molecules bound to the column were eluted by passing 15~20 ml of methanol through the column. This solution was collected, and the methanol was removed under vacuum. Procion Red could not be efficiently purified using this technique due to its high affinity for the column packing.

Table 4.2-1 – Results of ICP emmision spectroscopy analysis for both purified and as received Procion Dyes. Data reported as part per million in solution.

Dye / Concentration	Na	Fe	K	Ca	Si	S
PR / 10.0 mg/ml	1620	0.10	0.912	2.19	2.16	610
PB / 5.0 mg/ml[1]	1180	0.21	159.5	0.87	0.45	231
PB / 4.9 mg/ml[2]	135.2	0.04	35.7	1.64	0.45	596
PO / 5.1 mg/ml[1]	1145	0.10	26.9	19.98	0.36	443
PO / 5.0 mg/ml[2]	26.9	0.05	0.9	34.5	0.38	581

[1] As received Procion Dye
[2] Purified Procion Dye

The calculated Na^+ molarity of a 5 mg/ml Procion Brown solution was 1.8×10^{-2} M, which compares well to the 5.9×10^{-3} M Na^+ calculated from Table 4.2-1.

4.2.2 Film Deposition

PAH solutions at a concentration of 0.01 M on a repeat unit (RU) basis were used in all experiments. The PAH solution pH was held at 7.0. The concentration of all dye solutions was 5 mg/ml and the pH of dye solutions was held at 10.5 in all cases. The pH was adjusted using HCl (diluted 1 N HCl, Fisher Scientific, ACS Certified, lot 024735-24) or NaOH (0.1 N NaOH, Fisher Scientific, ACS Certified, lot 024521-24) as needed. The pH was checked over the course of the deposition process - variations in excess of 0.1 pH units were uncommon. NaCl (Fisher Scientific, ACS Certified, lot 028794) was

used in all cases as the salt for varying the ionic strength of the chromophore solutions. The glass slide immersion time in PAH was 5 minutes, with the exception of the first layer, which was 10 minutes. The immersion time in the dye solutions was 10 minutes for slides made using Procion Orange and 5 minutes for Procion Brown. In solution, hydrolysis of the triazine ring is known to occurr. In order to ensure that there was still a substantial fraction of dichlorotriazine functionalized dye present, which is capable of reacting, the dipping time was shorter for Procion Brown. Between immersions, the substrates were vigorously agitated and rinsed with deionized water. Slides were dried every 10 dips (which gives 5 bilayers on each side of the slide, hence 10 total bilayers) using N_2 gas. For any given set of solution conditions, two series of 5 slides were made with a total (both sides) of 2, 10, 20, 40 and 60 bilayers.

4.2.3 Film Characterization

Absorbance measurements were made with a Milton Roy Spectronic 1201 spectrophotometer at the characteristic wavelength for a given chromophore and were taken every 10 bilayers during the deposition process. Upon the completion of dipping for a given slide, 5 absorbance measurements were made along the length of the slide to characterize the homogeneity in the final absorbance value. Point to point variations were typically < 5%.

Film thicknesses were measured using a variable angle spectroscopic ellipsometer (J. A. Woolam Ellipsometer VB-200, with WVASE32 software Version 3.361). The amplitude factor ψ and phase factor Δ which are related to the complex Fresnel coefficients for any given film, were measured for wavelengths from 350 to 1000 nm at 10 nm intervals.[13] This wavelength range was repeated for angles ranging from 55° to 75° in 5° intervals. Measurements were made on the smooth side of the frosted region of the slide, as the scattering caused by the etching eliminates backside reflections simplifying data analysis. Details of the ellipsometric models used can be found in Appendix A. Least squares analysis was used to determine the slope in absorbance vs. bilayer number graphs. The average of slopes determined from 20, 40, and 60 bilayer films is reported as the slope in various tables.

Dye aggregation in solution was characterized by Dynamic light scattering (DLS). The measurements were performed using a DynaPro-801 TC from Protein Solutions operating at a fixed scattering angle of 90° and a wavelength of 836.4 nm. All experiments were performed at 25 ± 0.2°C. Dye solutions were at 5.0 mg/ml at pH 10.5 in deionized water and no added salt. The Procion Red solution was made using the as received powder while Procion Orange and Procion Brown solutions were made using purified dyes. Prior to sample measurements, the sample chamber was flushed using deionized water filtered with a 0.02 μm Whatman Anotop syringe filter. Approximately 0.5 ml of filtered (0.02 μm Whatman Anotop syringe filter) sample was injected into the chamber. From the fluctuations in scattered light intensity, the translational diffusion coefficient (D_T) was measured. Using the Stokes-Einstein equation, this diffusion coefficient is related to the hydrodynamic radius (R_H);

$$R_H = \frac{k_b T}{6\pi\eta D_T} \tag{4.2}$$

where k_b is Boltzman's constant, T is the absolute temperature in Kelvin, and η is solvent viscosity.

SHG measurements were performed by Prof. J. R. Heflin's group in the Department of Physics at Virginia Tech with a standard setup using a 10-nanosecond pulse width, Q-switched Nd:YAG laser with a fundamental wavelength of 1064 nm.[14] The SHG data were averaged over 100 shots per data point, and the uncertainty in relative $\chi^{(2)}$ values is 10%. Typical spot radius and pulse energy values were 30 μm and 7mJ/pulse, respectively. The film was deposited on both sides of the substrate. As a result, as the sample is rotated with respect to the incident beam, the path length between the film on opposite sides is varied, leading to interference fringes of the SHG intensity. The sample was rotated from 30° to 60° away from normal incidence using a stepper motor controlled rotation stage. The $\chi^{(2)}$ value is determined from the peak of the interference fringe in the vicinity of 45º. By comparison to Maker fringes in a quartz crystal wedge, and a 68 bilayer PS-119 / PAH ISAM film, $\chi^{(2)}$ of a film is obtained from

$$\frac{\chi^{(2)}_{film}}{\chi^{(2)}_{q}} = \frac{2}{\pi}\frac{l_{c,q}}{t_{bilayer}}\frac{m}{\sqrt{I_q^{2\omega}}}\sqrt{\frac{I^{2\omega}_{standard,quartz}}{I^{2\omega}_{standard,film}}} \tag{4.3}$$

where $t_{bilayer}$ is the bilayer thickness, m is the slope of the plot of square root of the second harmonic intensity vs. number of bilayers, $I^{2\omega}_{q}$ is the intensity of the second harmonic for the quartz standard, $I^{2\omega}_{standard,quartz}$ is the second harmonic intensity for the 68 bilayer standard measured at the same time as the quartz standard, $I^{2\omega}_{standard,film}$ is the second harmonic intensity for the 68 bilayer standard measured at the same time as the films for which $\chi^{(2)}$ is being calculated, l_{film} is the total path length through the film, the coherence length of quartz, $l_c = \lambda / 4(n^{2\omega}-n^{\omega})$, is 22.4 μm, and $\chi^{(2)}$ of quartz is 1.92×10^{-9} esu. The 68 bilayer PS-119 / PAH film was originally fabricated by C. Figura and is known to be exceptionally stable. Propagation of the errors on thickness, $t_{bilayer}$, and slope m, result in the error for $\chi^{(2)}$ by

$$\sigma_{\chi}^{2} = \frac{a^{2}}{t_{bilayer}^{2}}\sigma_{m}^{2} + \frac{a^{2}m^{2}}{t_{bilayer}^{4}}\sigma_{t}^{2} \tag{4.4}$$

where a is a constant defined as:

$$a = \chi_{q}^{(2)} \frac{2}{\pi} \frac{l_{c,q}}{\sqrt{I_{q}^{2\omega}}} \sqrt{\frac{I_{standard,quartz}^{2\omega}}{I_{standard,film}^{2\omega}}} \tag{4.5}$$

Bilayer numbers for absorbance measurements account for the film on both sides of the substrate while SHG and ellipsometry measurements are made using the film deposited on one side of the substrate.

Tilt Angle Measurements

The average orientation of the chromophore molecules in the film can be probed by varying the polarization of the incident light in the SHG experiments. The experimental set-up described for the SHG experiments remain the same. The incident angle, α, is held constant at a value which produces a maximum second harmonic intensity. At this incident angle, the polarization of the incident light is varied to find the minimum and maximum value in second harmonic intensity. The maximum value corresponds to $I_{2\omega}^{s\rightarrow p}$, which is the second harmonic intensity generated from s-polarized incident light. The minimum value corresponds to $I_{2\omega}^{p\rightarrow p}$, the intensity generated from p-polarized light.

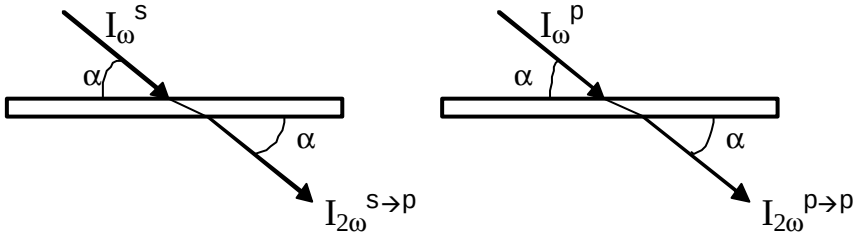

Figure 4.2-3 – Schematic illustrating $I_{2\omega}^{s\to p}$ and $I_{2\omega}^{p\to p}$.

Due to reflectance losses at the film-air interface with respect to polarization the experimentally observed value must be corrected. This is done by introducing a proportionality constant, which was calculated using the Fresnel equations for an incident angle of 50° and film refractive index of 1.6, which resulted in a value of 1.33.

$$I_{2\omega}^{p\to p} = 1.33 I_{2\omega,\text{observed}}^{p\to p} \tag{4.6}$$

These values are then used to calculate the average tilt angle, Ψ, of the chromophores in the film. The complete derivation of the equation for Ψ can be found elsewhere, however the resulting equation is:

$$\overline{\psi} = arc\cot\sqrt{\frac{1}{2}\left[\sqrt{\frac{I_{2\omega}^{p\to p}}{I_{2\omega}^{s\to p}}}\csc^2\alpha - 3\cot^2\alpha\right]} \tag{4.7}$$

an incident angle of 52° was used for all calculations.[15]

4.3 Results

As shown in previous chapters, linear growth of the absorbance as a function of the number of bilayers is an indicator of uniform layer-by-layer growth. This linear growth was observed for all films discussed in this work. The slope and standard deviation of the absorbance as a function of number of bilayers plots was calculated using a least squares regression, and is proportional to the amount of dye deposited per layer.

Procion Red Films

The first set of experiments that were conducted used the Procion Red MX-5B chromophore as received. Added salt concentrations ranging from 0 to 1.0 M NaCl were used. Table 4.3-1 shows the absorbances per bilayer as well as the film thicknesses for this series. The errors reported on the absorbance / bilayer results and thickness results are ± 1 standard deviation. Figure 4.3-1 shows the slopes increased with added NaCl concentration by as much as a factor of two, supporting the hypothesis that increased

screening allows the dye molecules to pack more densely. The thickness of 0.63 ± 0.06 nm reported for the zero salt case compares well to the thickness measurement of 0.52 ± 0.06 nm as reported in Chapter 3. The absorbance / nm, which serves as a rough indicator of the chromophore density in the film increases as the salt concentration increases from 0 M NaCl to 0.5 M NaCl. As the salt concentration increased from 0.5 M NaCl to 1 M NaCl, the absorbance / nm decreased.

Table 4.3-1 - Summary of Procion Red deposition with varying salt concentrations. All PAH solutions at 0.01 M RU and pH 7. PR solutions contain 5 mg/ml dye, the above salt concentration and are held at pH 10.5. Errors on the absorbance / bilayer and bilayer thickness values are standard deviations, while the error on $\chi^{(2)}$ is the result of the previously described error propagation.

C_{NaCl} (M)	Absorbance / Bilayer	Bilayer Thickness (nm)	Absorbance / nm	$\chi^{(2)}$ (10^{-9} esu)
0	0.0036 ± 0.0003	0.63 ± 0.06	0.0057	8.0 ± 2.0
0.05	0.0043 ± 0.0004	0.75 ± 0.14	0.0057	6.7 ± 1.2
0.10	0.0050 ± 0.0003	0.78 ± 0.14	0.0064	8.2 ± 1.7
0.25	0.0058 ± 0.0004	0.84 ± 0.11	0.0069	6.9 ± 1.1
0.50	0.0072 ± 0.0010	0.89 ± 0.05	0.0081	7.2 ± 1.5
1.0	0.0059 ± 0.0009	0.79 ± 0.11	0.0075	8.7 ± 1.2

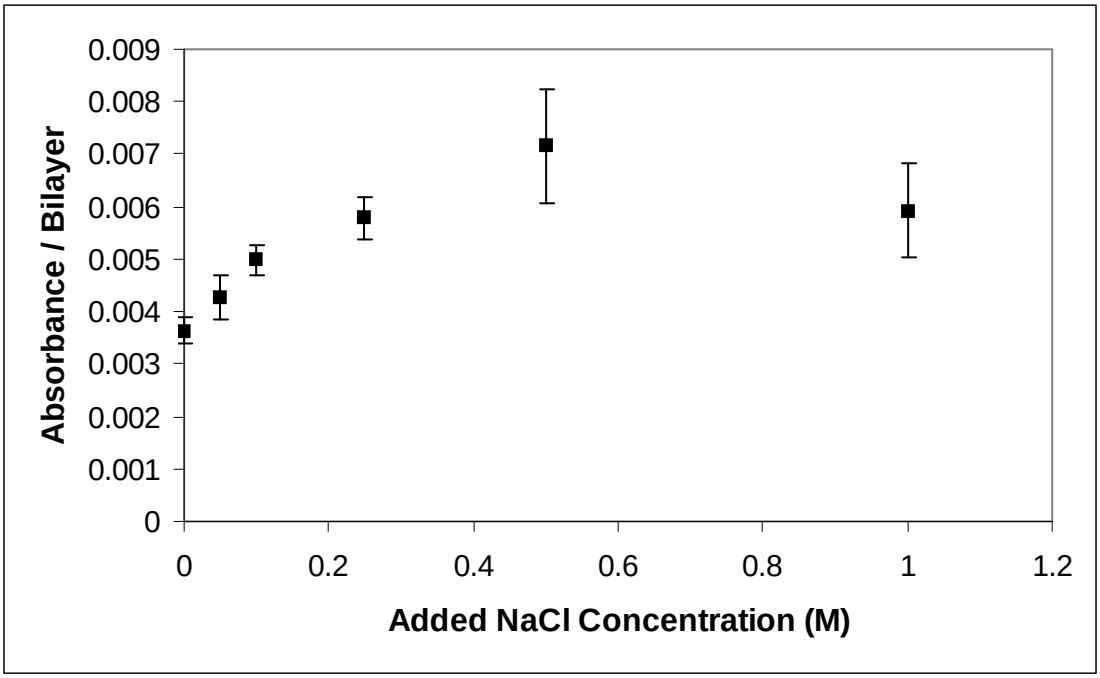

Figure 4.3-1 - Absorbance (λ=538 nm) / bilayer as a function of the salt concentration (M) for Procion Red films. PAH 10mM RU, pH 7.0, PR 5 mg/ml, pH 10.5

Results of the second harmonic generation experiments for an added salt concentration of 0.05 M NaCl are shown in Figure 4.3-2, which shows the square root of the second harmonic intensity ($I_{2\omega}^{1/2}$) as a function of the number of bilayers deposited. The linearity of this plot is typical for this series of experiments.

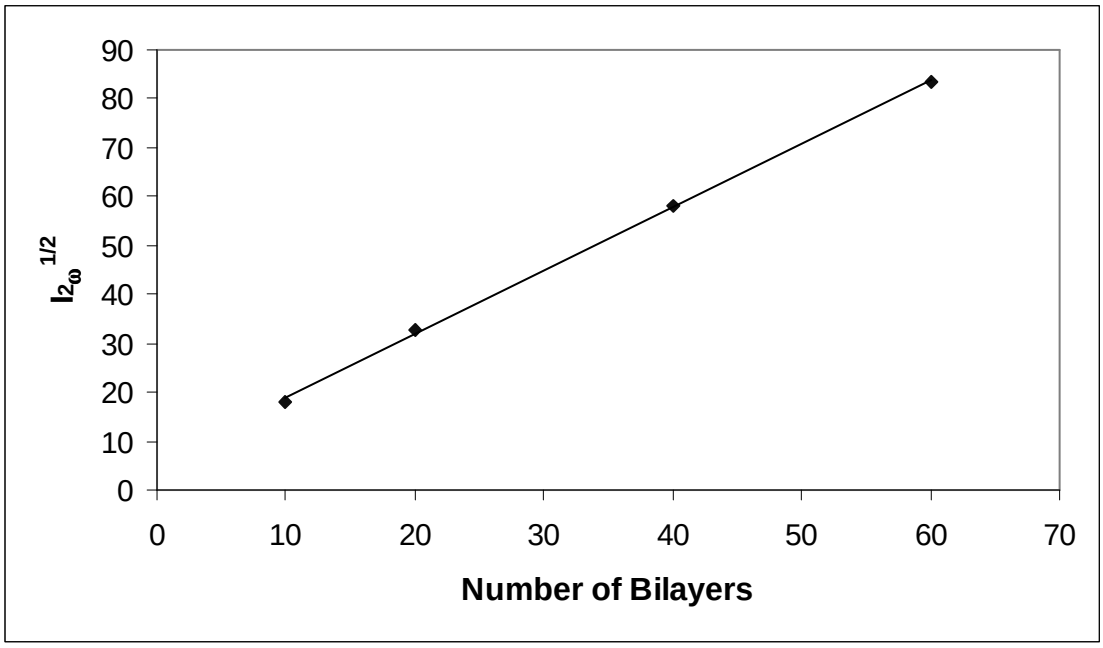

Figure 4.3-2 - Square root of the second harmonic intensity ($I_{2\omega}^{1/2}$) as a function of the number of bilayers deposited. A linear relationship signifies layer-to-layer orientation of the Procion Red chromophores. PAH 10mM, pH 7, PR 5mg/ml, 50mM NaCl, pH 10.5

The linearity of the plot shows that there is regular layer-by-layer orientation of the chromophore in the film, making it possible to calculate a $\chi^{(2)}$ value. These $\chi^{(2)}$ values are shown as a function of salt concentration in Figure 4.3-3.

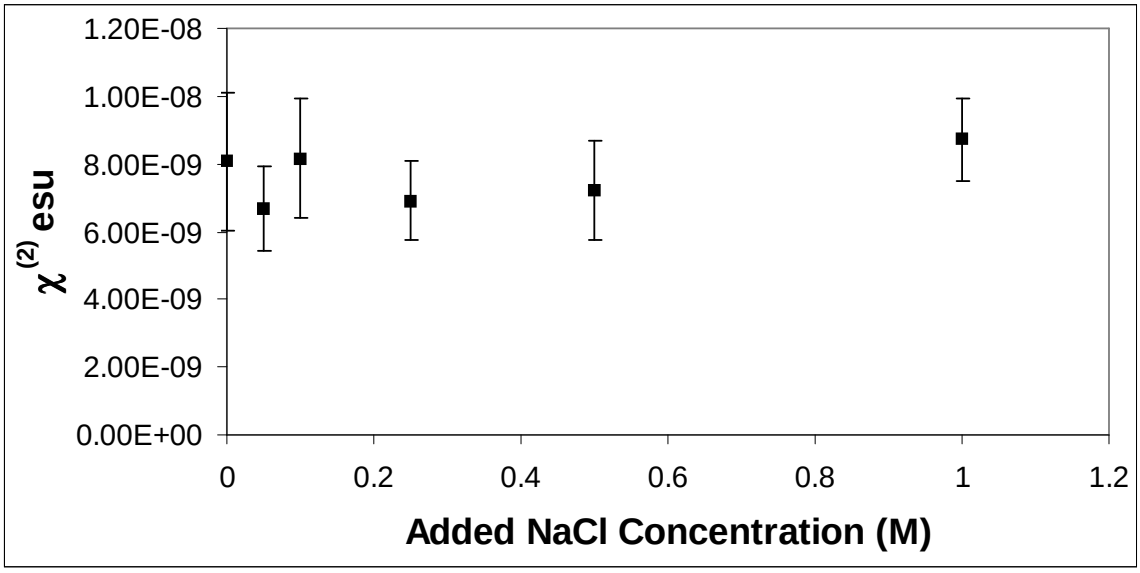

Figure 4.3-3 - $\chi^{(2)}$ values as a function of the additional NaCl concentration in the Procion Red dipping solution. The PAH solution was 10mM RU, pH 7 and the Procion Red solution was 5 mg/ml at pH 10.5

Procion Orange Films

The second set of experiments was conducted using Procion Orange MX-2R that was desalted using the aforementioned purification step. Again salt concentrations of 0 to 1.0 M NaCl were used. Table 4.3-2 contains slope and thickness data, while Figure 4.3-4 shows the slope as a function of the salt concentrations. As the salt concentration increased, a nearly linear increase in the absorbance / bilayer was observed, showing a factor of nearly 3 increase as the salt concentration increased from 0 to 1 M. The absorbance/nm remained essentially constant across all salt concentrations with the exception of the 1M NaCl case where the absorbance/nm was highest. The films made with Procion Orange displayed significant variations in point-to-point optical homogeneity and the films were noticeably inhomogeneous. These inhomogeneities are likely due to the deposition of dye aggregates. DLS was used to measure the hydrodynamic radius of the dyes in solution under the 0 M salt condition. Only Procion Orange showed a detectable (> 1 nm) hydrodynamic radius, having a component with a R_H = 23 nm as determined using the Regularization algorithm.[16] This aggregation likely occurs because the sulfonate groups a primarily found on one end of the molecule. Both Procion Red and Procion Brown had no measurable size. Since the detectable limit is radius R_H = 1 nm, this suggests that Procion Red and Procion Brown were fully soluble

and did not form aggregates. Figure 4.3-5 shows the second order susceptibility as a function of the salt concentration in solution. However, due to the relatively large point-to-point variations these values show significant amounts of error.

Table 4.3-2 - Summary of Procion Orange deposition with varying salt concentrations. All PAH solutions at 0.01 M RU and pH 7. Procion Orange solutions contain 5 mg/ml dye, the above salt concentration and are held at pH 10.5.

C_{NaCl} (M)	Absorbance / Bilayer	Bilayer Thickness (nm)	Absorbance / nm	$\chi^{(2)}$ (10^{-9} esu)
0	0.0023 ± 0.0004	0.36 ± 0.07	0.0064	18.9 ± 4.7
0.05	0.0023 ± 0.0005	0.36 ± 0.10	0.0064	14.1 ± 4.5
0.10	0.0030 ± 0.0002	0.49 ± 0.03	0.0061	15.5 ± 2.4
0.25	0.0039 ± 0.0002	0.58 ± 0.08	0.0067	16.2 ± 2.7
0.50	0.0045 ± 0.0002	0.72 ± 0.10	0.0063	17.0 ± 3.2
1.0	0.0066 ± 0.0009	0.81 ± 0.04	0.0081	12.4 ± 1.7

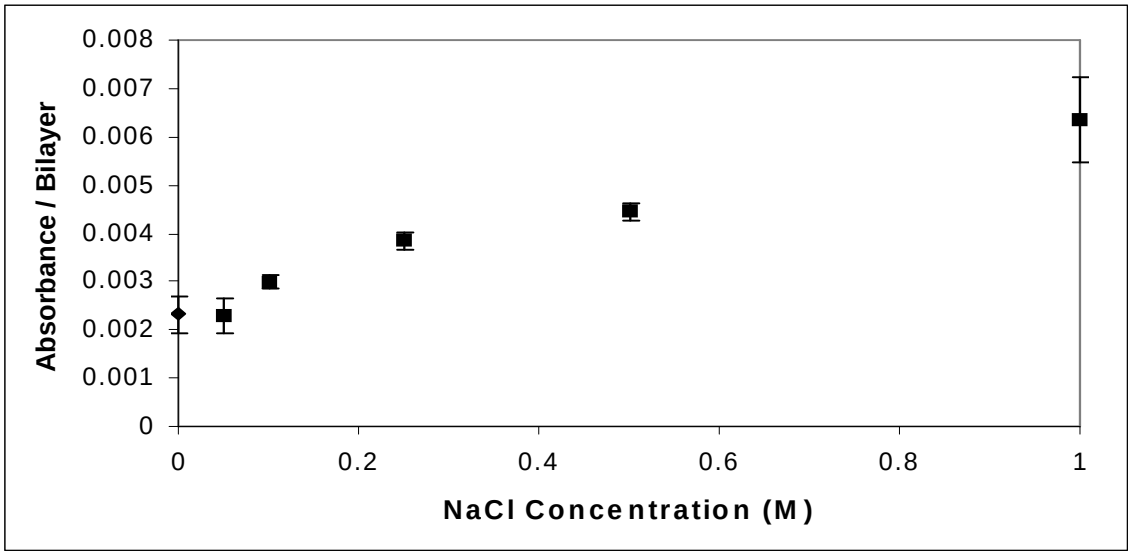

Figure 4.3-4 - Absorbance / Bilayer as a function of additional NaCl concentration in the Procion Orange deposition solutions. PAH 0.01 M RU, pH 7. PO 5 mg/ml dye, pH 10.5, with added (0-1 M) NaCl

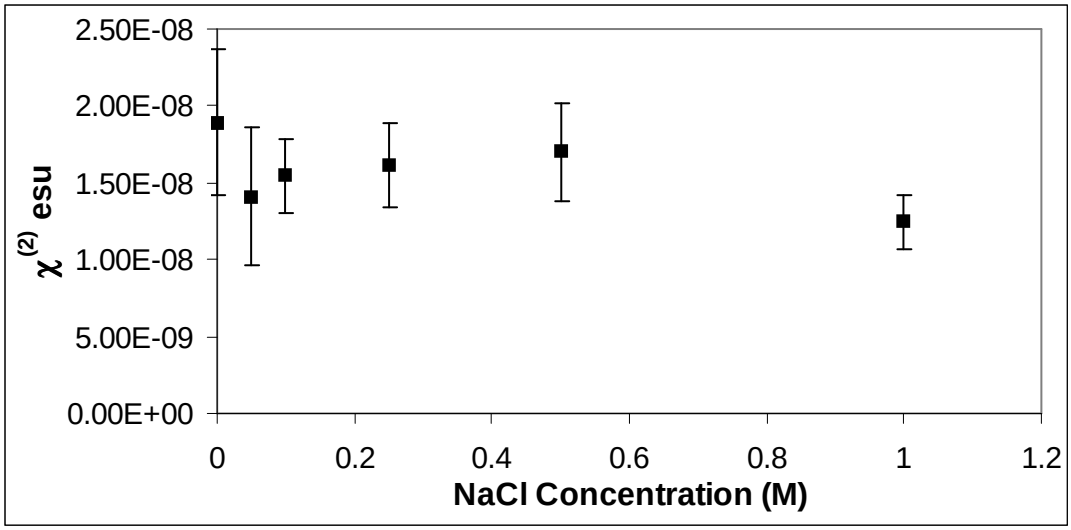

Figure 4.3-5 - Bilayer susceptibility as a function of the NaCl concentration in the Procion Orange dipping solution. PAH deposited from 0.01 M RU solution at a pH of 7, PO 5 mg/ml pH 10.5 with added NaCl.

Procion Brown Films

Finally, a series of films was made using purified Procion Brown MX-GRN deposited at varying concentrations of NaCl. These results are summarized in Table 4.3-3 and Figure 4.3-6. The general linear increase in the absorbance per bilayer as a function of the added salt concentration is observed, with an approximate factor of 3 increase observed in the absorbance / bilayer as the salt concentration increased from 0 to 1 M NaCl. The calculated absorbance / nm for these films shows very little dependence on the concentration of NaCl in the dipping solution. The $\chi^{(2)}$ of these films increase from 50.2 x 10^{-9} esu to 87.5 x 10^{-9} esu as the salt concentration increased from 0 to 0.5 M NaCl. As the salt concentration increased to 1.0 M NaCl, the $\chi^{(2)}$ decreased to 67.6 x 10^{-9} esu. These $\chi^{(2)}$ values are shown as a function of salt concentration in Figure 4.3-7 . The films become better oriented (lower tilt angle) as the salt concentration is increased from 0M to 0.5 M NaCl. A slightly higher tilt angle is observed as the salt concentration is increased to 1 M NaCl.

Table 4.3-3 – Summary of Procion Brown deposition with varying salt concentrations. All PAH solutions at 10 mM RU and pH 7. PB solutions contain 5 mg/ml dye, the given salt concentration and are held at a pH of 10.5. The thickness value reported for the 0M NaCl case was based on thicknesses of the 2 thickest slides made, as the slides with fewer bilayers were too thin to accurately measure.

C_{NaCl} (M)	Absorbance / Bilayer	Bilayer Thickness (nm)	Absorbance / nm	$\chi^{(2)}$ (10^{-9} esu)	Tilt Angle
0	0.0009 ± 0.0001	0.24 ± 0.01	0.0036	50.2 ± 1.6	49.4°
0.10	0.0012 ± 0.0001	0.37 ± 0.01	0.0032	48.9 ± 1.9	47.6°
0.25	0.0019 ± 0.0001	0.57 ± 0.02	0.0033	72.4 ± 1.9	46.5°
0.50	0.0024 ± 0.0002	0.60 ± 0.03	0.0040	87.5 ± 2.3	45.5°
1.0	0.0033 ± 0.0009	0.86 ± 0.07	0.0038	67.6 ± 2.5	46.4°

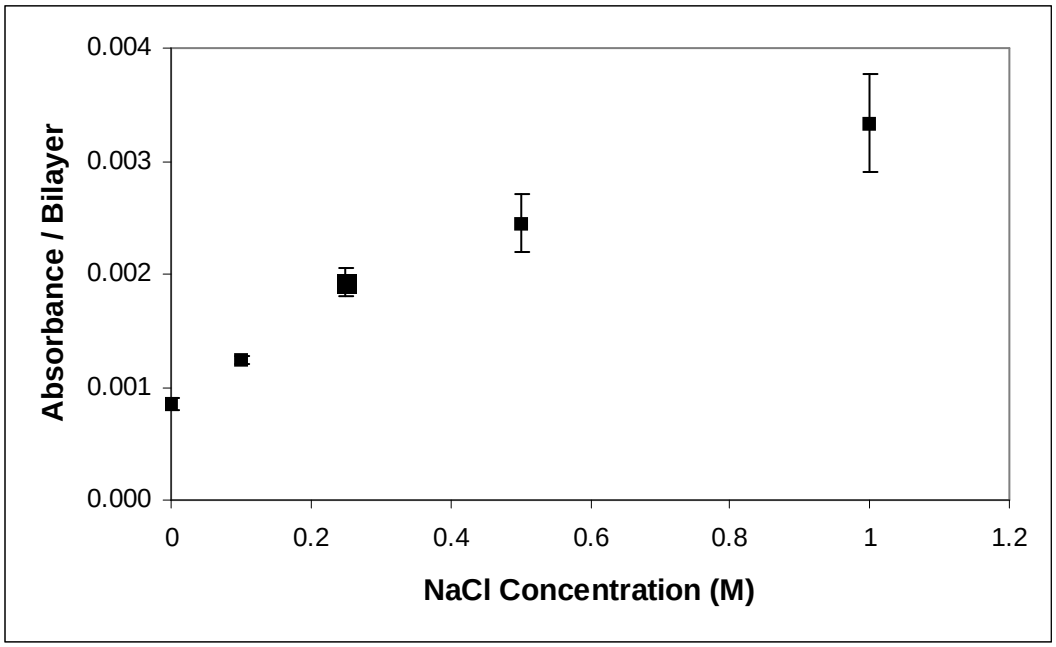

Figure 4.3-6 - Absorbance / Bilayer as a function of additional NaCl concentration in the Procion Brown deposition solutions. PAH 0.01 M RU, pH 7. PO 5 mg/ml dye, pH 10.5, with additional (0-1 M) NaCl

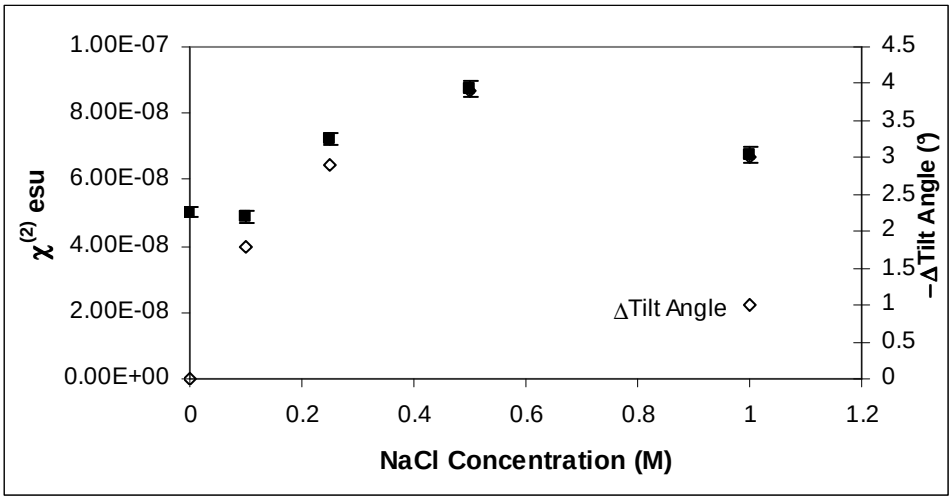

Figure 4.3-7 – $\chi^{(2)}$ as a function of NaCl concentration in the Procion Brown dipping solution. PAH deposited from 0.01 M RU solution at a pH of 7, PB 5 mg/ml pH 10.5 with added NaCl.

4.4 Discussion

4.4.1 Modeling the Effect of Ionic Strength on Deposition

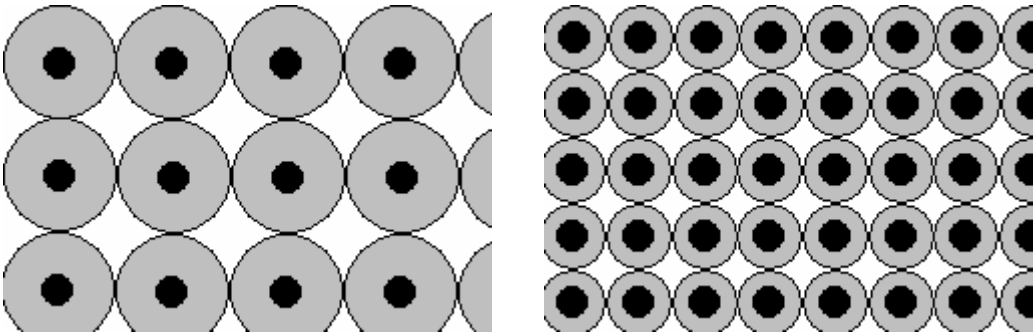

Figure 4.4-1 - Schematic description showing the higher dye density possible under high ionic strength conditions (right figure) vs. low ionic strength conditions (left figure)

As the concentration of NaCl in the dye solutions increases, the electrostatic repulsion between the charged dye molecules is increasingly screened as they deposit on the relatively uncharged layer of PAH. The Debye length characterizes the length scale over which electrostatic forces between two like charged species decay by a factor of e^{-1} in the presence of the screening ionic species. In aqueous solution, at 25°C, the Debye length is a function of the solution's ionic strength and is given by:

$$\kappa^{-1} = \sqrt{\frac{\varepsilon kT}{8\pi e^2 I_{eff}}} = \frac{0.304}{\sqrt{I_{eff}}} \tag{4.8}$$

where ε is the dielectric constant of the solvent, e is the charge of one electron, and I_{eff} is the effective ionic strength of the dye solution, which is calculated by accounting for all ionic species. For the Procion dipping solutions, this effective ionic strength is given by:

$$I_{eff} = \frac{1}{2}\left(n^2 C_{Dye} + nC_{Dye}\right) + C_{NaCl} + 10^{-pH} + 10^{-pOH} \tag{4.9}$$

where n is the valence of the Procion dye, having a value of 2 for Procion Red and 3 for Procion Brown and Orange. Contributions from any additional ionic species present in the purified dyes can be neglected due to their low levels. For large Debye lengths, or low salt concentrations (Figure 4.4-1) the charged groups on the Procion dye molecules lead to relatively long range repulsion between adjacent deposited dye molecules, limiting the amount of material that deposits on the surface. For smaller Deybe lengths, or high salt concentrations, (Figure 4.4-1) the range over which these interactions occur is much lower, allowing a great number of dye molecules to deposit on the surface.

Making the simplification that the dye molecule and its electrostatic cloud are circularly symmetric (spherical or cylindrical in shape), the effective radius of the molecule as it deposits on the surface can be taken to the sum of the molecule's hard-core radius, r_{hc}, and the Debye length, κ^{-1};

$$r_{eff} = r_{hc} + \kappa^{-1} \tag{4.10}$$

Prior to any deposition, the number of charges in a square of area $[2(r_{hc}+\kappa^{-1})]^2$ is given by:

$$n_{+\text{charges}} = D^2\sigma \tag{4.11}$$

where $D=2(r_{hc}+\kappa^{-1})$ and σ is the number of positive charges per unit area of the underlying layer. After deposition, the number of positive charges in that area is:

$$n_{+\text{charges}} = D^2\sigma - 1 \tag{4.12}$$

due to the loss of the positive charge associated with the formation of the covalent linkage between the polymer chain and the dye molecule. For layer-by-layer deposition to occur, either charge reversal must occur or the dye must deposit in patches with

sufficient negative charge density to permit the next layer of polycation to electrostatically deposit.

For charge reversal to occur due to the deposition of negatively charged dyes, the following inequality must hold true;

$$n_{-\text{charges}} > D^2\sigma - 1 \tag{4.13}$$

which states the number of negative charges ($n_{-charges}$) must exceed the number of positive charges in a given area (D^2) after deposition. The $n_{-charges}$ term depends on the number of negative charges on the dye molecule, having a value of 2 for Procion Red and a value of 3 for Procion Brown and Procion Orange. At the charge neutralization point;

$$\frac{n_{-\text{charges}} + 1}{D^2} = \sigma_{cn} \tag{4.14}$$

which, for Procion Red is;

$$\sigma_{cn} = \frac{3}{\left[2(r_{hc} + \kappa^{-1})\right]^2} = \frac{0.75}{\left[r_{hc} + \kappa^{-1}\right]^2} \tag{4.15}$$

Assuming a reasonable value of r of 0.5 nm and a κ^{-1} of 1 nm (~ 0.1 M NaCl) the charge neutralization would occur for surface amine group charge densities below 0.33 charges / nm^2. For comparison, a single PAH chain extended over 3 nm would contain approximately 12 positive charges. Assuming this chain is the only chain in a 3 nm by 3 nm box, a charge density of 1.3 charges / nm^2 results. Another estimate for the charge density can be calculated from the typical adsorbed amount in a monolayer, 0.5 mg/m^2. This monolayer coverage results in a surface charge density of 3.2 charges/ nm^2. The fact that both of these charge density estimates are well above the upper limit of 0.33 charges / nm^2 implies that if charge neutralization occurs, it is due in large part to screening of the underlying amine groups by bound ions in the Stern layer and Cl ions in the diffuse double layer. If charge reversal is not occurring, film formation may still be possible due to localized patches of negative charge in a manner analagous to what is known to occur for binding of proteins.

Assuming a packing arrangement like that shown in Figure 4.4-1, the number density of chromophore molecules that could pack on a given area is:

$$\rho = \frac{\theta_a}{\pi\left(r_{hc} + \kappa^{-1}\right)^2} \tag{4.16}$$

where θ_a is the areal packing density. This density, ρ (# chromophores / unit area), should be proportional to the absorbance per bilayer. Introducing a proportionality constant would account for the extinction coefficient on a per bilayer basis. This results in a model for the dependence on the absorbance per bilayer as a function of the Debye length of:

$$\frac{Abs}{Bilayer} = \frac{a}{\left[\left(r_{hc} + \kappa^{-1}\right)\right]^2} \tag{4.17}$$

where the "a" term is given by:

$$a = \frac{\theta_a \varepsilon}{\pi} \tag{4.18}$$

where ε is the extinction coefficient of the chromophore molecule used.

The absorbance as a function of Debye length is shown in Figure 4.4-2 for the deposition of Procion Orange. Using a least squares error fit, values for the parameters a and r were found, and the model's fit for absorbance / layer is shown in Figure 4.4-2. The model fit in Figure 4.4-2 uses a value of 8.8×10^{-3} for "a" and a value of 0.9 nm for "r_{hc}". The calculated value for "a" is 1.1×10^{-3} which uses the extinction coefficient of Procion Orange as measured in solution, 4.4×10^{-3} nm^2, and an areal packing density of 0.785. This measured extinction coefficient in solution is not expected to be the same as the extinction coefficient on the film. This is due to the fact that in solution all possible orientations are possible, while the deposited dye has a set orientation angle, and absorbs light differently.

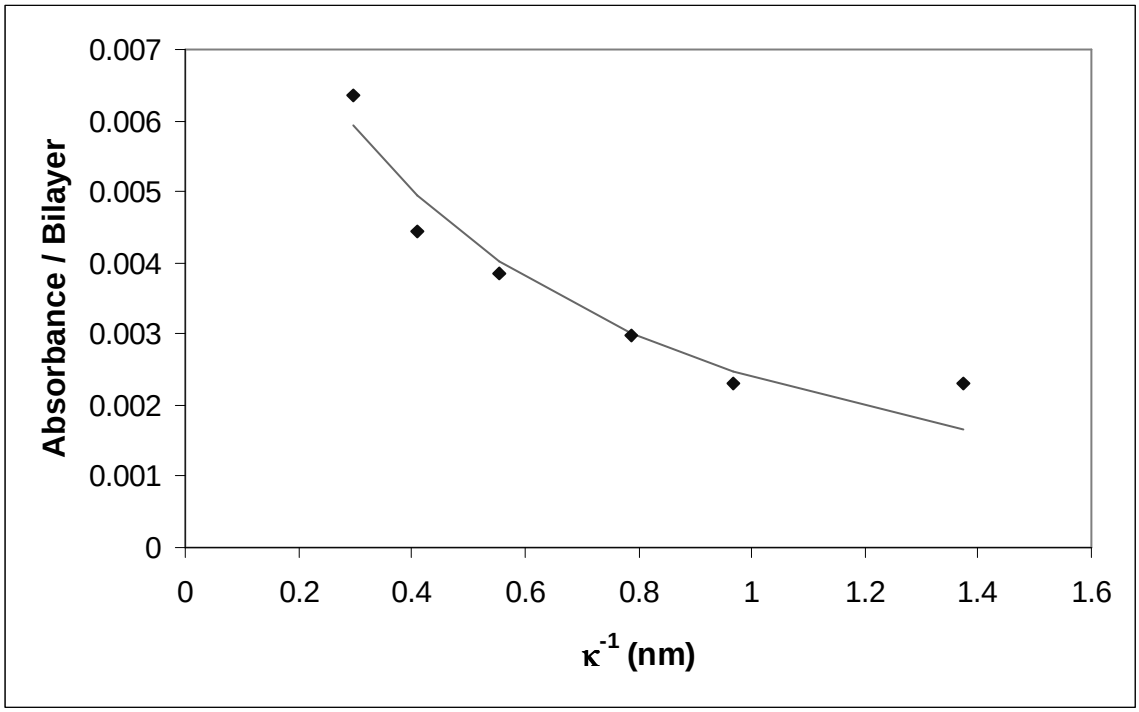

Figure 4.4-2 - Experimental and model fit for the deposition of PO as a function of Debye length. PAH deposited at 10 mM RU, pH 7, PO deposited at 5 mg/ml dye, pH 10.5 with NaCl added to change the Debye Length

Molecular modeling of the Procion Orange chromophore shows it having an end-to-end distance of ~ 2 nm. The molecular models were constructed using CS Chem3D Pro Version 3.2, which calculates the conformation of the dye by minimizing the energy of the molecule. The three dimensional structures of Procion Red (Figure 4.4-3), Orange (Figure 4.4-4) and Brown (Figure 4.4-5) that are pictured below are only first generation models. More elaborate calculations could be done in the future with modelling software such as GAUSSIAN.

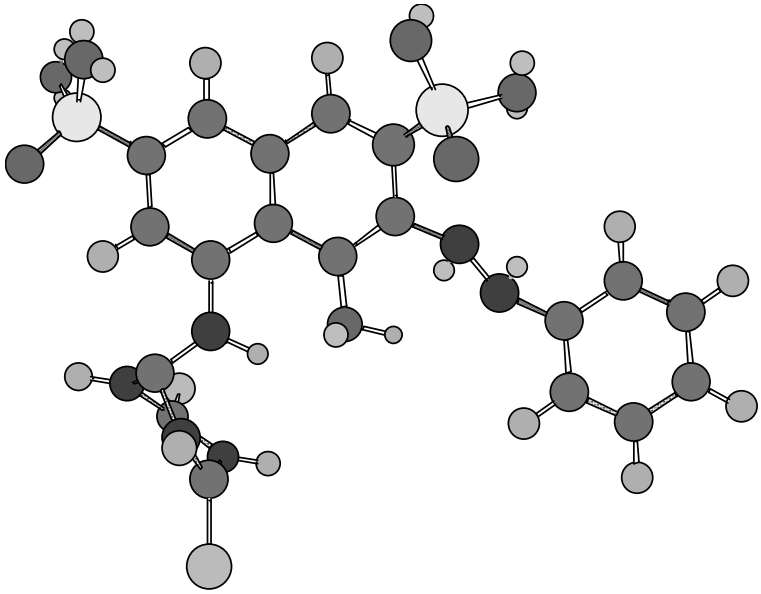

Figure 4.4-3- Molecular model of the Procion Red chromophore constructed using CS Chem3D Pro.

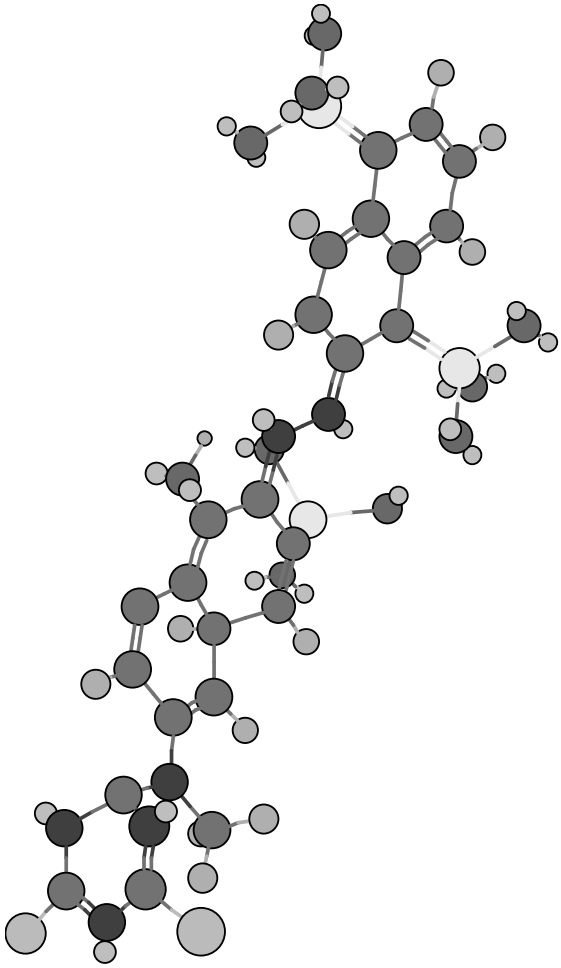

Figure 4.4-4- Molecular Model of the Procion Orange Chromophore constructed using CS Chem3D Pro. This molecule has an end to end distance of approximately 1.9 nm.

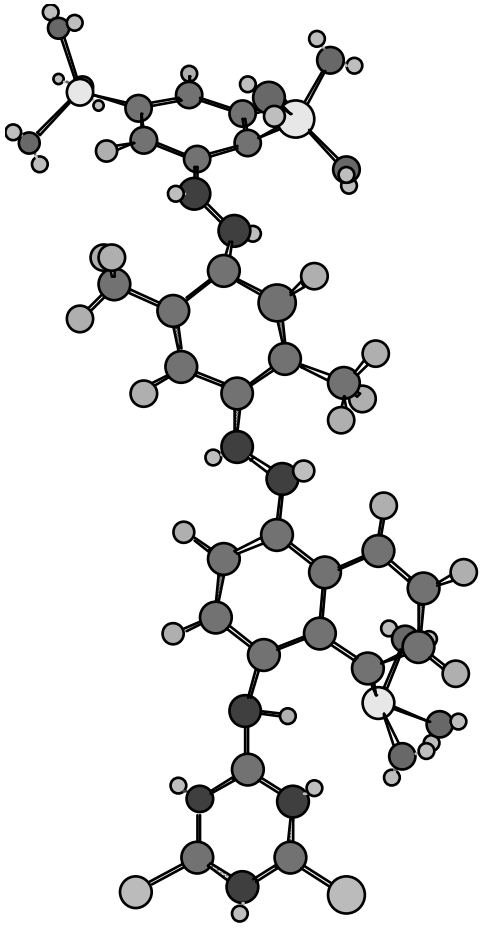

Figure 4.4-5 – Molecular Model of the Procion Brown chromophore as constructed by the CS Chem3D Pro software. This chromophore has an end to end distance of 2 nm.

Figure 4.4-6 shows the model fit for the deposition of Procion Brown. The fitted parameters for the model are an "r_{hc}" value of 0.6 nm and an "a" value of 2.8 x 10^{-3}. The calculated value for "a" for Procion Brown assuming an areal packing density of 0.785 and an extinction coefficient of 2.6 x 10^{-3} nm^2 is 6.5 x 10^{-4}. For both Procion Orange and Procion Brown the end-to-end distances and the r_{hc} values are reasonable compared to the end to end distance of ~ 2 nm for both chromophores.

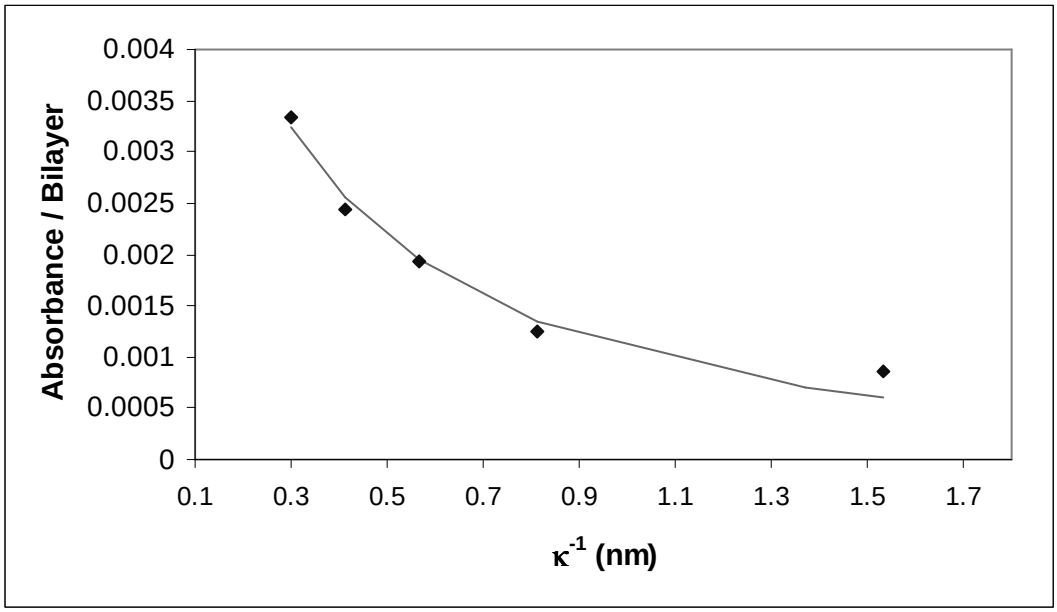

Figure 4.4-6 Experimental and model fit for the deposition of PB as a function of Debye length. PAH deposited at 10 mM RU, pH 7, PB deposited at 5 mg/ml dye, pH 10.5 with NaCl added to change the Debye Length

4.4.2 Effect of salt on $\chi^{(2)}$ and Film Properties

The addition of NaCl to the dipping solutions for all three Procion chromophores resulted in similar trends in absorbance / bilayer and bilayer thicknesses. The unpurified Procion Red resulted in an increase in both the absorbance/bilayer and bilayer thickness from 0 to 0.5 M NaCl with a lower value at 1 M NaCl. The films made with purified Procion Orange and purified Procion Brown showed a linear increase in the absorbance/bilayer and a monotonic increase in the bilayer thickness. Films made with both the Procion Orange and Procion Brown exhibited comparable bilayer thicknesses ranging between 0.2 nm and 0.9. The trend observed for thickness of the Procion Red films was likely due to ionic impurities in the as received dye. Differences between the different systems becomes apparent, however, when comparing the $\chi^{(2)}$ values.

Due to the relatively poor film homogeneity of the Procion Orange slides, the $\chi^{(2)}$ values measured will not be discussed further, as they are not entirely reliable. The poor optical homogeneity of the Procion Orange films is likely related to aggregation of the chromophores in solution, as shown by dynamic light scattering. By contrast, the films made with Procion Red and Procion Brown showed much better optical and SHG homogeneity. The $\chi^{(2)}$ values for the unpurified Procion Red slides showed no

discernible dependence on the concentration of added NaCl. Values for $\chi^{(2)}$ ranged from 6.9 ± 1.1 x 10^{-9} esu to 8.7 ± 1.2 x 10^{-9} esu. The $\chi^{(2)}$ value in the absence of salt was 8.0 ± 2.0 x 10^{-9} esu which compares well to the value of 11.3 x 10^{-9} esu observed in Chapter 3. However, for the purified Procion Brown system, a different relationship between salt concentration and $\chi^{(2)}$ was observed. In this system, $\chi^{(2)}$ increased from 50.2 ± 1.6 x 10^{-9} esu in the 0 M NaCl case to a value of 87.5 ± 2.3 x 10^{-9} esu in the 0.5 M NaCl. As the NaCl concentration increased to 1 M, the $\chi^{(2)}$ value dropped to 67.6 ± 2.5 x 10^{-9} esu. For comparison, the $\chi^{(2)}$ for quartz is 1.92 x 10^{-9} esu, and ~ 200 x 10^{-9} esu for lithium niobate. The $\chi^{(2)}$ observed for the Procion Brown films was mostly free of any resonance effects, which artificially inflate the $\chi^{(2)}$ values, as seen for Procion Red. The drop in $\chi^{(2)}$ as NaCl concentration increased from 0.5 M to 1 M was an unexpected trend, as the absorbance / bilayer increased over this range. Polarization anisotropy measurements were performed to measure the tilt angle of the chromophores in the film. The trend observed for these values was a decrease in tilt angle of 4.9° as the salt concentration went from 0 to 0.5 M. The impact that this change in tilt angle would have on the $\langle\cos^3\theta\rangle$ term depends on the absolute value of θ. This is illustrated in Figure 4.4-7 which shows $\langle\cos^3\theta\rangle$ as a function of θ. The changes in the tilt angle alone only contribute, at most, an approximate rise in $\chi^{(2)}$ of 25%, indicating that a combined effect of better orientation and a higher chromophore density may be increasing $\chi^{(2)}$ from 0 to 0.5 M NaCl. As the salt concentration increased from 0.5 M to 1 M, the tilt angle increased by 0.9°. The slight loss of orientation observed in the 1 M NaCl case may explain the lower $\chi^{(2)}$ value at this salt condition. The decrease in $\chi^{(2)}$ that is observed for Procion Brown does allow for a hypothesis to be formed as to why the films made with unpurified Procion Red show no dependence on the added salt concentration. If there exists an ionic strength above which no enhancement of the $\chi^{(2)}$ response is observed, the unpurified Procion Red solutions may be above that limit for all salt concentrations due to the ionic impurities present in the as received powder.

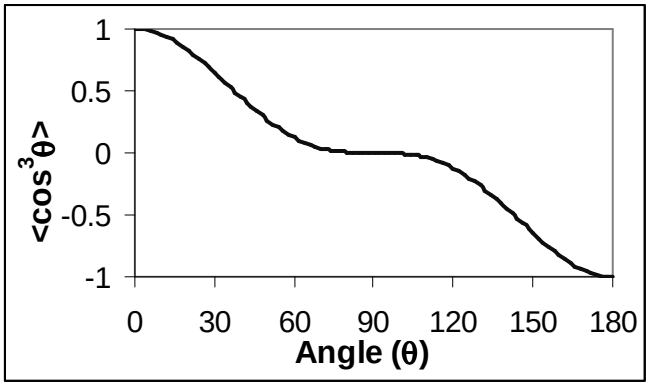

Figure 4.4-7 - $\langle\cos^3\theta\rangle$ as a function of angle, θ.

4.5 Conclusions and Future Work

The goal of this study was to determine if the $\chi^{(2)}$ response of layer-by-layer films constructed using covalent and electrostatic attachments could be increased by increasing the ionic strength of the dye solution. Increasing the ionic strength of the dipping solution reduced the inter-dye electrostatic repulsions, allowing for a higher packing density on the surface. For purified Procion Orange and Procion Brown, an increase in $\chi^{(2)}$ was observed as the salt concentration increased from 0M NaCl to 0.5 M NaCl. At salt concentrations of 1 M NaCl, the $\chi^{(2)}$ decreased below the maximum at 0.5 M NaCl. Whether this increase in $\chi^{(2)}$ is a result of the increased chromophore density, better orientation or perhaps a combination of these effects cannot be determined until measurements of the orientation angle are completed on these films. Measurements of the electro-optic coefficient, r_{33}, are pending for these films. Additionally, the thermal stability of the PAH / PB system must be tested. This study can also be used to determine which Procion chromophore should be utilized in future studies. Procion Red, the first procion chromophore used, results in optically homogeneous films, but gives relatively low $\chi^{(2)}$ values. Procion Orange, due to its tendency to aggregate in solution, resulted in optically heterogeneous films which were not of sufficient quality for detailed study. Procion Brown, however, resulted in optically clear films and also resulted in the highest $\chi^{(2)}$ values observed. This maximum $\chi^{(2)}$, $87.5 \pm 2.3 \times 10^{-9}$ esu, was observed for the deposition of Procion Brown with 0.5 M NaCl.

[1] Ashwell, G. 'Langmuir-Blodgett Films: Molecular Engineering of Non-Centrosymmetric Structures for Second-Order Nonlinear Optical Applications' *J Mater. Chem.* **9** (1999) 1991-2003.

[2] Burland, D.; Miller, R.; Walsh, C. 'Second-Order Nonlinearity in Poled-Polymer Systems' *Chem. Rev.* **94** (1994) 31-75.
[3] Heflin, J.; Figura, C.; Marciu, D.; Liu, Y.; Claus, R. 'Thickness Dependence of Second-Harmonic Generation in Thin Films Fabricated from Ionically Self-Assembled Monolayers' *Appl Physics Letters* **74** (1999) 495-497.
[4] Van Cott, K.; Guzy, M.; Neyman, P.; Brands, C.; Heflin, J.; Gibson, H.; Davis, R. 'Layer-by-Layer Deposition and Ordering of Low Molecular Weight Dye Molecules for Second Order Nonlinear Optics' *Angewandte Chemie* **41** (2002) 3236-3238.
[5] Dalton, L.; Harper, A.; Ghosn, R.; Steier, W.; Ziari, M.; Fetterman, H.; Shi, Y.; Mustacich, R.; Jen, A.; Shea, K. 'Synthesis and Processing of Improved Organic Second-Order Nonlinear Optic Materials for Applications in Photonics' *Chem. Mater* **7** (1995) 1060-1081.
[6] Lvov, Y.; Ariga, K.; Onda, M.; Ichinose, I.; Kunitake, T. 'Alternate Assembly of Ordered Multilayers of SiO_2 and Other Nanoparticles and Polyions' *Langmuir* **13** (1997) 6195-6203.
[7] Dubas, S., Schlenoff, J. 'Factors Controlling the Growth of Polyelectrolyte Multilayers' *Macromolecules* **32** (1999) 8153-8160.
[8] Losche, M.; Schmitt, J.; Decher, G.; Bouwman, W.; Kjaer, K. 'Detailed Structure of Molecularly Thin Polyelectrolyte Multilayer Films on Solid Substrates as Revealed by Neutron Reflectometry' *Macromolecules* **31** (1998) 8893-8906.
[9] Decher, G.; Schmitt, J. 'Fine Tuning the Film Thickness of Ultrathin Multilayer Films Composed of Consequtively Alternating Layers of Anionic and Cationic Polyelectrolytes' *Prog. Colloid Poly. Sci.* **89** (1992) 160-164.
[10] C. Figura, Thesis, Virginia Polytechnic Institute and State University, 1999
[11] Itano, M.; Kern, F.; Miyashita, M.; Ohmi, T. 'Particle Removal from Silicon Water Surface in Wet Cleaning Process' *IEEE Trans. on Semicond. Manu*. **6** (1993) 258-267.
[12] Van Cott, K.; Amos, T.; Gibson, H.; Davis, R.; Heflin, J. 'Characterization of the Purity and Stability of Commercially Available Dichlorotriazine Chromophores Used in Nonlinear Optical Materials' in press. *Dyes and Pigments*
[13] R. M. Azzam and N. M. Bashara. "Ellipsometry and Polarized Light" Elsevier, N. Y. 1987
[14] Neyman, P.; Guzy, M.; Shah, S.; Davis, R.; Van Cott, K.; Hang, W.; Gibson, H.; Brands, C.; Heflin, J. 'Novel Hybrid Covalent / Ionic Self-Assembly Techniques for Improved Second-Order Nonlinear Optical Films' *Mat. Res. Soc. Symp. Proc* **708** (2002) 161-166.
[15] P. Neyman, Thesis, Virginia Polytechnic Institute and State University, 2002.
[16] Ivanova, M.; Arutyunvar, A.; Lomakin, A.; Noskin, V. 'Study of DNA Internal Dynamics by Quasi-Elastic Light Scattering' *Applied Optics* **36** (1997) 7657-7663.

5. Effect of Polycation Structure on the Orientation and Deposition of a Low Molecular Weight Chromophore

Abstract

The effect of polycation structure on films fabricated using covalent / electrostatic layer-by-layer films was examined. Films were fabricated using Procion Red and poly(vinylamine hydrochloride) and poly(ethylenimine). The poly(ethylenimine) / Procion Red films showed regular chromophore orientation with a $\chi^{(2)}$ of 4.0 x 10^{-9} esu. Deposition experiments with Procion Brown and chitosan, poly(vinylamine hydrochloride) and poy(ethylenimine) were attempted. Layer-by-layer deposition occurred only for poly(vinylamine hydrochloride) / Procion Brown. These films showed some indication of polar order with a $\chi^{(2)}$ of 3.6 x 10^{-9} esu. The failure of poly(ethylenimine) and chitosan to form layer-by-layer films with Procion Brown is attributed to steric effects, preventing deposition from occurring.

Keywords

Polycation, layer-by-layer deposition, chromophore orientation, second order nonlinear optics, low molecular weight chromophore

5.1.Introduction

The development of polymeric second order nonlinear optic (NLO) materials is of interest for developing electro-optic modulator to convert electric signals into optic pulses for transmission down fiber optic fibers. Layer-by-layer deposition schemes, where thin films are fabricated through the successive deposition of thin monolayers, are one fabrication technique capable of making films suitable for these applications. Films constructed using both covalent bonds and electrostatic interactions are a particularly attractive method approach to fabricating these materials. This technique, coined hybrid deposition due to its use of two different attachment mechanisms for the layers, was first demonstrated as a viable way of fabricating NLO films by Van Cott et al.[1] The triazine functionalized chromophore Procion Red MX-5B was used with the polycation, polyallylamine hydrochloride (PAH) to build up films as shown in Figure 5.1-1. The

polymer layers are incorporated by electrostatic interactions between the charged amine groups and the sulfonate groups on the chromophores.

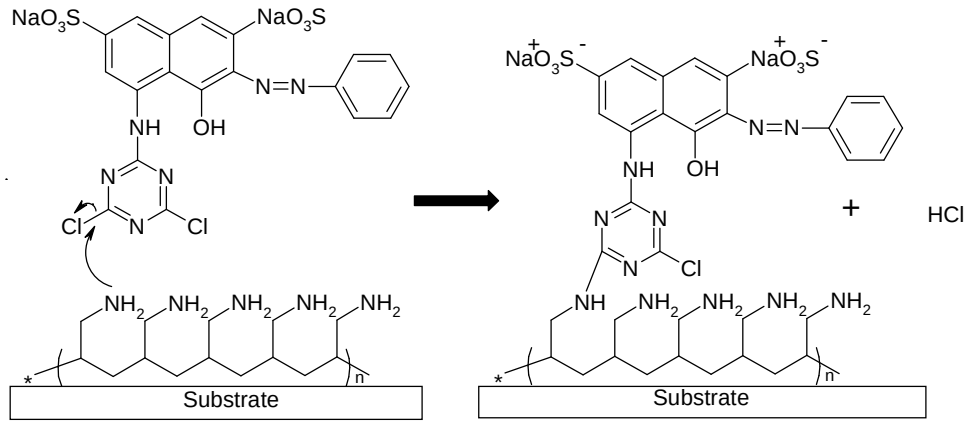

Figure 5.1-1 – Reaction mechanism for covalent / electrostatic layer-by-layer deposition. Covalent bonds couple the chromophore to the polyamine. The next layer of polyamine deposits electrostatically to the charged sulfonate groups on the dye.

One of the advantages of the chemistry used in this process is that it is fairly general in nature. The triazine ring on the chromophore is reactive to primary and secondary amines. Additionally, hybrid deposition provides one approach to incorporating NLO chromophores into films. By functionalizing an existing second order NLO chromophore with the triazine moiety, this deposition approach might be used to make oriented films with $\chi^{(2)}$ values suitable for devices.

This flexibility in chromophore choice has, in part, been demonstrated in Chapter 4. In this study, films were fabricated using PAH and three Procion chromophores, Procion Red MX-5B, Procion Orange MX-2R and Procion Brown MX-GRN. While layer-by-layer deposition occurred for all three chromophores, the Procion Orange films were not of sufficient homogeneity for optical testing, most likely due to poor solubility of the dye. The highest value of $\chi^{(2)}$ reported in that study, $87.5 \pm 2.3 \times 10^{-9}$ esu, was for films made with Procion Brown deposited with 0.5 M NaCl at a pH of 10.5. In that study PAH was used as the polycation and was deposited at pH 7.0 which gave flat, thin layers.

This hybrid approach was also explored by Koetse et al using several polyamines and either triazine or vinyl sulfone groups.[10] Layer-by-layer deposition was observed, as indicated by a regular increase in the absorbance as layers are deposited. However, regular orientation of the Procion Red chromophore was not observed when films were made with poly[N-(3-aminopropyl)-N-(4-vinylbenzyl)-N,N-dimethylammonium

chloride], a polycation possessing both a primary amine for reaction with Procion Red and a quaternary ammonium moiety.

This study examines the versatility of the hybrid deposition approach. Films were fabricated using 3 polycations, poly(vinyl amine) [a primary amine], linear polyethylenimine [a secondary amine] and chitosan [a polysaccharide with a primary amine as a side group]. The effects of polymer structure on deposition and orientation are examined, with the objective of finding the polycation that will provide the combination of highest chromophore density and greatest chromophore orientation, and thus, the highest $\chi^{(2)}$.

5.2.Experimental

The NLO active chromophores used in this study were Procion Red MX-5B (PR, Pro Red 305, Pro Chemical and Dye, Somerset, MA) and Procion Brown MX-GRN (PB, Pro Burnt Orange 515, Pro Chemical and Dye, Somerset, MA). Structures of these chromophore molecules are shown in Figure 5.2-1. The characteristic absorbance peaks for these dyes were determined to be λ_{max}=538 nm for Procion Red and λ_{max}=408 nm for Procion Brown. All absorbance measurements were made at the characteristic peak for the respective chromophore molecule. The NLO-inactive polycations used this study were poly(vinylamine hydrochloride) [PVA, M_W ~ 25,000, Polysciences, lot 520947], linear polyethylenimine [PEI, M_W ~ 25,000 Polysciences, lot 522113] and chitosan [M_W ~ 140,000, 95% degree of deacetylation, Dalwoo-chitoSan, Korea]. The structures of PVA, PEI and chitosan are shown below in Figure 5.2-2. Chitosan has a pK_a of ~ 6.5[2] while PEI has a pK_a ~ 4.8[4]. An explicit value for the pK_a of PVA is not reported in the literature; however titration results show that 50% of the polymer is charged at a pH of ~ 5.5.[3] All polycations were used as received without further purification. The PVA and chitosan are readily soluble in water. Solutions of PEI were prepared with stirring and heating (~ 60° C) with 0.1 M HCl being added dropwise until the solution was clear following the procedure of Hammond.[4]

Deionized water was obtained with an ion exchange unit (Barnstead Nanopure II) and maintained a specific resistivity above 17 MΩ•cm. Glass microscope slides (Fisher Scientific) were used as the substrates on which films were deposited. They were

prepared using the RCA cleaning procedure[5] in which the substrates were immersed in a solution of H_2O, H_2O_2, and NH_4OH at 70°C for 20 minutes. The slides were then rinsed and placed in an acid bath consisting of concentrated HCl, H_2O_2 and H_2O for 20 minutes and were then rinsed and baked at 130°C for at least one hour.

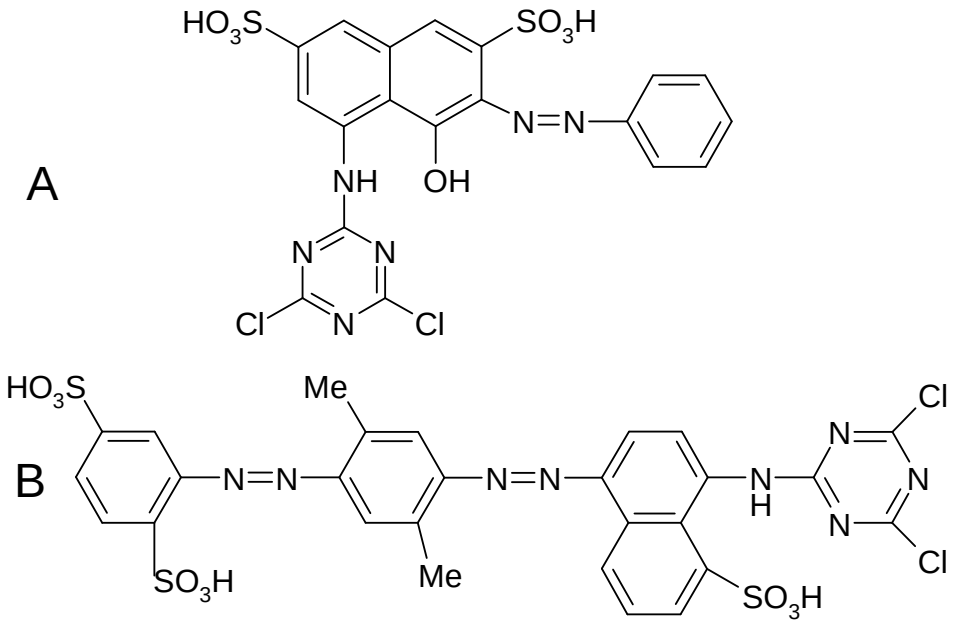

Figure 5.2-1 - Structures of the anionic chromophores (A) Procion Red MX-5B [PR] and (B) Procion Brown MX-GRN [PB]

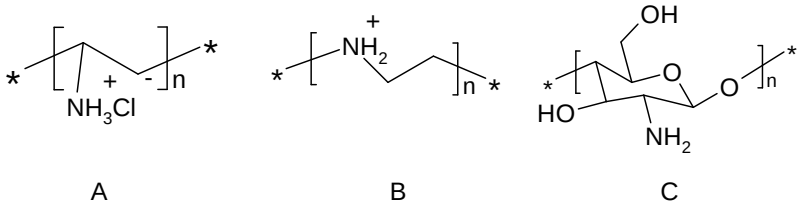

Figure 5.2-2 - Structures of the polycations (a) PVA, (b) PEI, and (c) chitosan

5.2.1. Film Deposition

Polycation concentrations of 10 mM on a monomer basis were used in all experiments. All Procion dye solutions were at 5 mg dye/ml. The Procion Red MX-5B was used as received while Procion Brown MX-GRN was purified as detailed below. Deposition pH values were chosen based on the pH at which the polycation is 50% ionized, ensuring that while the previously deposited polycation layer is exposed to the dipping solution, the amines will be unprotonated allowing for the covalent reaction

between the amine and triazine ring. Polycation solution pH values were chosen so that the polyelectrolytes would be charged, allowing for electrostatic attachment of the depositing polyelectrolyte to the covalently bound dye molecules.

Table 5.2-1summarizes the polycation pH conditions where deposition was done and shows the pH where the polycations are 50% charged.

Table 5.2-1- pH conditions for Polycation Deposition and the pH at which the polycations are 50% ionized. All PAH results from Chapter 3.

Polycation	pH at 50% Ionization	Deposition pH
PAH	8.7[6]	7.0
PVA	~5.5[3]	7.0
PEI	~4.8[4]	4.0
Chitosan	6.5	5.0

The pHs of solutions were adjusted using HCl or NaOH as needed. pH values were typically constant to ± 0.1 pH units over the course of the deposition. The glass slide immersion time in polycation was 5 minutes, with the exception of the first layer, which was 10 minutes. The immersion time in the Procion Red solutions was 10 minutes, while a deposition time of 5 minutes were used for films made with Procion Brown. Due to hydrolysis, the concentration of the dichlorotriazine functionalized dye decreases over the time needed for deposition.[7] In order to ensure there was still a substantial fraction of dichlorotriazine functionalized Procion Brown the deposition time was reduced. Between immersions, the substrates were vigorously agitated and rinsed with deionized water. Slides were dried every 10 dips (which gives 5 bilayers on each side of the slide, hence 10 total bilayers) using N_2 gas.

5.2.2. Solution Coupling Reaction Between Chitosan and Procion Brown

Chitosan was reacted with Procion Brown in solution to determine qualitatively whether covalent coupling was possible in solution without any complicating effects of a nearby glass substrate. A chitosan solution at 1.5 mg/ml was prepared. 0.05 g of Procion Brown was added to 10 mls. of the chitosan solution. The pH was adjusted to 8.5 and the solution was allowed to stir for approximately 1 hour. The solution was then transferred to dialysis tubing (Pierce SnakeSkin Dialysis Tubing, item #68100, lot DK58770A, 10,000 Molecular weight cut off). The polymer solution was dialyzed against distilled

water overnight, then again a 0.5 M NaCl solution overnight, and then distilled water until the dialysate bath was no longer visibly brown.

5.2.3. Purification of Procion Brown MX-GRN

Commercially available Procion dyes are, as a result of the manufacturing process, not pure materials.[7] Procion Brown was purified to remove any ionic salts and buffers that are in the as-received powder. Solid phase extraction with octadecysilyl functionalized silica was used to desalt the dyes (Alltech High Capacity 75 ml C18 column, lot 173801). The dye was dissolved in 50 mM ammonium acetate at ~ 10 mg/ml. This solution was filtered with a 0.45 μm syringe filter to remove any particulate impurities. The column was first washed with > 100 ml (~ 5 bed volumes) 50 mM ammonium acetate, and then the dye solution was introduced. The column was again flushed with > 100 ml of the ammonium acetate solution, allowing the column to run dry. The dye molecules bound to the column were eluted by passing 15~20 ml of methanol through the column. This solution was collected, and the methanol was removed under vacuum. Table 5.2-2 shows the results of Inductively Coupled Plasma mass spectroscopy (ICP) before and after purification for Procion Brown. This analysis was done by the Soil Testing Lab at Virginia Tech. The purification process reduced the sodium content by almost 10-fold.

Table 5.2-2- Results of ICP emission Spectroscopy analysis for both purified and as received Procion Brown. Data reported in parts per million in solution.

Dye / Concentration	Na	Fe	K	Ca	Si	S
PB / 5.0 mg/ml[1]	1180	0.21	159.5	0.87	0.45	231
PB / 4.9 mg/ml[2]	135	0.04	35.7	1.64	0.45	596

[1]As received Procion Dye
[2]Purified Procion Dye

5.2.4. Film Characterization

Absorbance measurements were made with a Milton Roy Spectronic 1201 spectrophotometer at the characteristic wavelength for a given chromophore and were taken every 10 bilayers during the deposition process. Upon the completion of dipping for a given slide, 5 absorbance measurements were made along the length of the slide to characterize the homogeneity in the final absorbance value. Film thicknesses were

measured using a variable angle spectroscopic ellipsometer (J. A. Woolam Ellipsometer VB-200, running WVASE 32 Version 3.361). The amplitude factor ψ and phase factor Δ which are related to the complex Fresnel coefficients for any given film, were measured for wavelengths from 350 to 800 nm at 10 nm intervals.[8] This wavelength range was repeated for angles ranging from 55° to 75° in 5° intervals. Measurements were made on the smooth side of the frosted region of the slide, as the scattering caused by the etching eliminates backside reflections simplifying data analysis. A Lorenz oscillator model was used to analyze the data. Details about the specific model parameters used can be found in Appendix A. Least squares analysis was used to determine the slope in absorbance vs. bilayer number graphs. The average of slopes determined from 20, 40, and 60 bilayer films is reported as the slope in various tables.

SHG measurements were performed by Prof. J. R. Heflin's in the Department of Physics at Virginia Tech group with a standard setup using a 10-nanosecond pulse width, Q-switched Nd:YAG laser with a fundamental wavelength of 1064 nm.[9] The SHG data were averaged over 100 shots per data point, and the uncertainty in relative $\chi^{(2)}$ values is 10%. Typical spot radius and pulse energy values were 30μm and 7mJ/pulse, respectively. The film was deposited on both sides of the substrate. As a result, as the sample is rotated with respect to the incident beam, the path length between the film on opposite sides is varied, leading to interference fringes of the SHG intensity. The sample was rotated from 30° to 60° away from normal incidence using a stepper motor controlled rotation stage. The $\chi^{(2)}$ value is determined from the peak of the interference fringe in the vicinity of 45º. By comparison to Maker fringes in a quartz crystal wedge, and a 68 bilayer PS-119 / PAH ISAM film, $\chi^{(2)}$ of a film is obtained from

$$\frac{\chi^{(2)}_{film}}{\chi^{(2)}_{q}} = \frac{2}{\pi}\frac{l_{c,q}}{t_{bilayer}}\frac{m}{\sqrt{I^{2\omega}_{q}}}\sqrt{\frac{I^{2\omega}_{standard,quartz}}{I^{2\omega}_{standard,film}}} \tag{5.1}$$

where $t_{bilayer}$ is the bilayer thickness, m is the slope of the square root of the second harmonic intensity vs. number of bilayers plot, $I^{2\omega}_{q}$ is the intensity of the second harmonic for the quartz standard, $I^{2\omega}_{standard,quartz}$ is the second harmonic intensity for the 68 bilayer standard measured at the same time as the quartz standard, $I^{2\omega}_{standard,film}$ is the second harmonic intensity for the 68 bilayer standard measured at the same time as the

films for which $\chi^{(2)}$ is being calculated, l_{film} is the total path length through the film, the coherence length of quartz, $l_c = \lambda / 4(n^{2\omega}-n^{\omega})$, is 22.4 μm, and $\chi^{(2)}$ of quartz is 1.92×10^{-9} esu. An analysis of the propagation of errors for calculations of the thickness, $t_{bilayer}$, and slope m, result in the error for $\chi^{(2)}$ by

$$\sigma_{\chi}^{2} = \frac{a^{2}}{t_{bilayer}^{2}}\sigma_{m}^{2} + \frac{a^{2}m^{2}}{t_{bilayer}^{4}}\sigma_{t}^{2} \tag{5.2}$$

where a is a constant defined as:

$$a = \chi_{q}^{(2)} \frac{2}{\pi} \frac{l_{c,q}}{\sqrt{I_{q}^{2\omega}}} \sqrt{\frac{I_{standard,quartz}^{2\omega}}{I_{standard,film}^{2\omega}}} \tag{5.3}$$

Details of this error analysis are given in Appendix B.

Bilayer numbers for absorbance and SHG measurements account for the film on both sides of the substrate while ellipsometry measurements were made using the film deposited on one side of the substrate.

5.3.Results

Regular layer-by-layer growth is characterized by a linear increase in the absorbance as a function of the number of bilayers deposited as shown in Figure 5.3-1. The slope of this plot, the absorbance/bilayer, is representative of the amount of material deposited in each dipping cycle. The results of the absorbance / bilayer and bilayer thicknesses values for the various deposition conditions tested are summarized in Table 5.3-1.

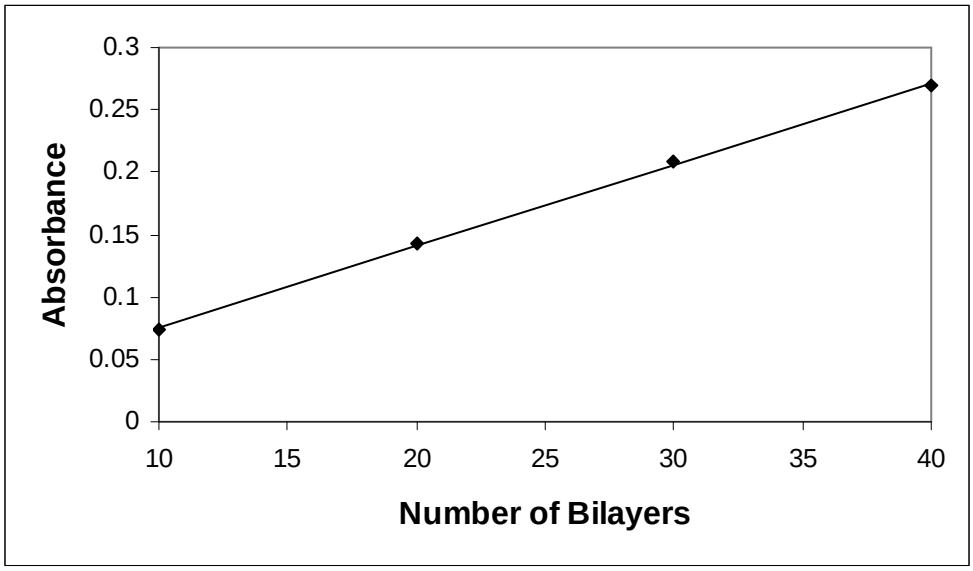

Figure 5.3-1 - Absorbance as a function of the number of bilayers deposited for 10mM RU PEI pH 4 with 5 mg/ml PR at pH 10.5. The slope, or absorbance per bilayer, characterizes the amount of material deposited in each cycle.

Table 5.3-1 - Summary of deposition results, polycations all at 10mM RU, dyes at 5 mg/ml.

Polycation	Polycation pH	Dye	Dye pH	Absorbance / Bilayer	Bilayer Thickness (nm)	Absorbance / nm
PEI	4.0	PR	10.5	0.0064 ±0.0002	0.57 ± 0.02	0.0112
PVA	7.0	PR	10.5	0.0008 ± 0.0001	-[1]	-
Chitosan	5.0	PB	10.5	N/A	-	-
Chitosan	5.0	PB	8.5	N/A	-	-
PEI	4.0	PB	10.5	N/A	-	-
PVA	7.0	PB	10.5	0.0008 ± 0.0002	0.21 ± 0.04	0.0038

[1] Too thin for measurement

The highest absorbance / bilayer occurred for the PEI pH 4.0/PR pH 10.5 case. In the chitosan/PB and PEI/PB cases, regular layer-by-layer deposition was not observed. However, a change in wetting of the glass substrate was observed following the first layer of polycation for both chitosan and PEI, implying that the polycation did absorb on the glass surface and that the subsequent reaction with PB did not occur. The thicknesses of the PVA / PR films measured were too thin to calculate reliable bilayer thicknesses. Given the relatively low absorbance / bilayer values for these conditions, it is clear that small amounts of material were deposited. The absorbance / bilayer values for PVA / PB are comparable to those obtained for the PAH / PB with the no added salt condition from Chapter 4 (0.0009 ± 0.0001).

Figure 5.3-2 shows the results of the SHG testing for PR films where successful deposition was observed. Linear scaling of the square root of the second harmonic intensity with the film thickness, which is indicative of bulk orientation, was observed for the PEI pH 4.0 / PR pH 10.5 case. The calculated $\chi^{(2)}$ for this condition is $4.0 \pm 0.6 \times 10^{-9}$ esu. By comparison, for PAH pH 7.0/PR pH 10.5, $\chi^{(2)} = 11.3 \times 10^{-9}$ esu as reported in Chapter 3. The PVA pH 7.0 / PR pH 10.5 slides showed an initial increase in the second harmonic intensity for the first 40 bilayers, but growth in the additional layers was not observed.

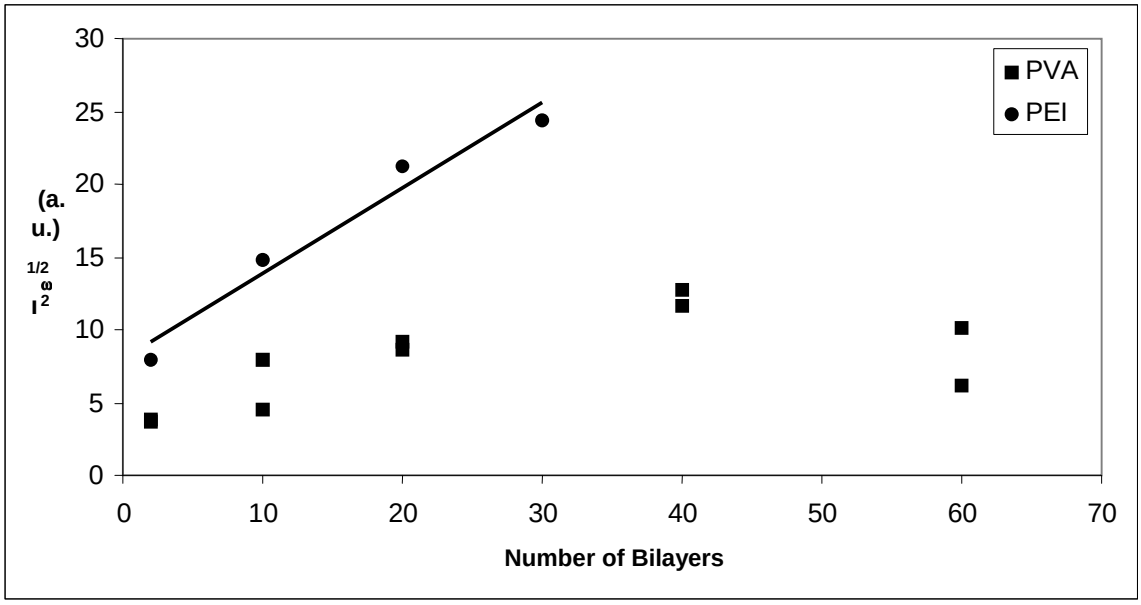

Figure 5.3-2 - Results of the SHG experiments for the experiments conducted with PR. PEI / PR shows signs of linear scaling of the square root of the SH intensity while PVA shows no signs of regular orientation

Figure 5.3-3 shows the results of the SHG testing for PB films made with PVA. The square root of the second harmonic intensity remained relatively constant over the first 20 bilayers then increased as additional layers were deposited. Assuming this increase is indicative of some bulk scaling the $\chi^{(2)}$ of this film is $3.6 \pm 0.8 \times 10^{-9}$ esu. For comparison, PB films made with no salt and PAH as the polycation had a $\chi^{(2)}$ of 50.2×10^{-9} esu.

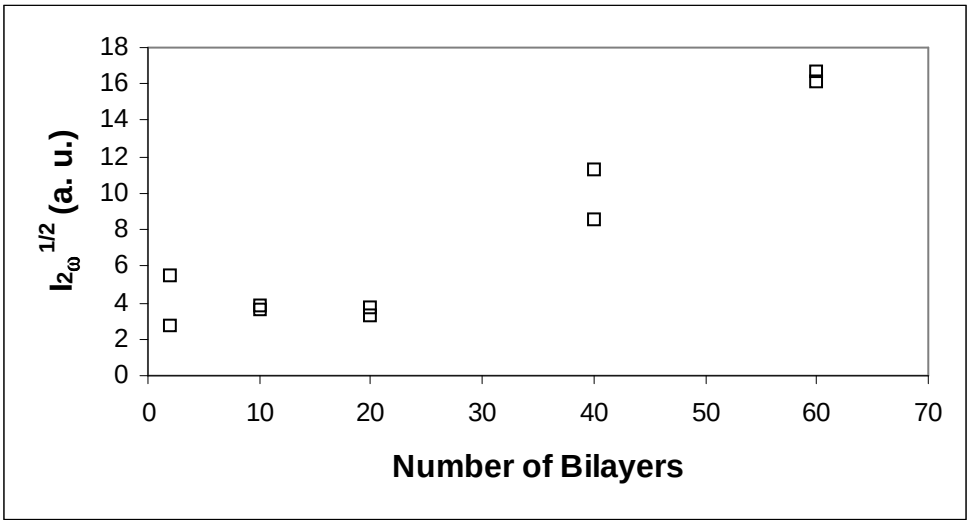

Figure 5.3-3 - Results of the SHG experiments on PVA / PB films. The films seem unoriented in the first 20 bilayers with an increase in second harmonic intensity observed for as additional layers are deposited.

5.4.Discussion

5.4.1. Layer-by-Layer Deposition with Procion Dyes

Procion Brown Films.

Deposition experiments were conducted using the Procion Brown chromophore with PVA, PEI and chitosan as the polycation. Previously, covalent / electrostatic deposition using PB as the chromophore had been successfully demonstrated using poly(allylamine hydrochloride) [PAH] as the polycation (the structure of PAH is shown in Figure 5.4-1). In this present study, layer-by-layer deposition only occurred with PVA. The amine group in PVA is directly connected to the vinyl backbone, while PAH has one additional methylene group separating the amine from the backbone. Deposition was not observed for either PEI in which the secondary amine is incorporated into the polymer backbone, or chitosan in which the primary amine exists as a side group on a glucopyranose ring. In all cases, the triazine ring should react with the amine functionalities at pH 10.5 since they should be mostly unprotonated given their pH values at 50% ionization as shown in Table 5.2-1.

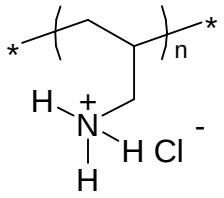

Figure 5.4-1 – Structure of poly(allylamine hydrochloride) [PAH]

To probe if the deposition process for chitosan / PB was being inhibited by the presence of the glass substrate, a solution-phase coupling reaction reaction was conducted between chitosan and Procion Brown at a pH of 8.5 to recreate one of the deposition conditions that failed. After the dialysis process was complete, the chitosan solution was brown in color, indicating that covalent coupling occurred in solution. Clearly, having the chitosan bound to the substrate interferes with this coupling reaction, perhaps by introducing an additional steric effect. The chitosan has a greater rigidity compared to PAH, and this may prevent $-NH_2$ groups from rearranging so they would be accessible for covalent coupling to occur.

Two significant and complementary conclusions can be drawn from these results; 1) the structures of PAH and PVA allow covalent coupling of PB on previously deposited polymer layers but the structure of PEI and chitosan do not and 2) the conformation of the chitosan adsorbed on the glass slide prevents layer-by-layer deposition. While the reason for these findings is not entirely clear, steric effects may play a significant effect. Koetse et al. reported on the covalent incorporation of a reactive vinyl sulfone dye Remazol Brilliant Blue with several different polycations, including PAH , chitosan and PVA.[10] Measurements of the absorbance as a function of the number of layers showed greater slopes for the PAH than for PVA and chitosan. They postulated that the amine groups in PAH were less shielded by the polymer backbone, and as a result were more accessible for covalent coupling than those of PVA and chitosan. A similar effect was observed for the reaction between poly(acrylic acid) and an aluminum oxyhydroxide surface.[11] Alexander et al. believe that steric hindrance from the poly(acrylic acid) backbone was preventing reactions between the polymer and the hydroxyl functionalities on the surface.

A similar situation may be occurring with PEI and chitosan, i.e. steric effects may be preventing the deposition from proceeding. While it is likely that some chromophore

– amine bonds formed, in those cases where deposition did not occur the surface density of bound chromophores was probably below the critical value needed for layer-by-layer deposition to continue. For polymer adsorption to occur the segmental adsorption energy, χ_s, must be greater than a critical value, $\chi_{s,critical}$. When little coupling occurs, as shown in Figure 5.4-2 (a), this results in a surface density of sulfonate groups too low for the next polycation layer to deposit. In terms of the mean field theory for polymer adsorption, a $\chi_s < \chi_{s,critical}$.

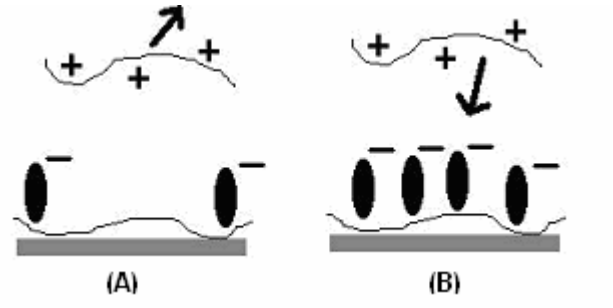

Figure 5.4-2 Schematic demonstrating how a critical level of dye deposition must occur for layer-by-layer deposition to proceed. In (B) a sufficient negative charge density exists and polyelectrolyte adsorption occurs, while in (A), the negative charge density is not sufficient

PEI is a secondary amine, which is not be as reactive as the primary amine found in PAH and PVA and it is also incorporated into the polymer backbone, further limiting the accessibility of the amine group. Despite not being able to form layer-by-layer films with PB, PEI was capable of forming films with PR. The different structure of the PB may have introduced steric effects that were not observed for the PR chromophore.

It is interesting to note that all the polycations-PVA, PEI and chitosan-were capable of forming layer-by-layer films with the polydye PCBS where the deposition was driven by only electrostatic interactions. Details of this are provided in chapter 7. However, electrostatic interactions are nonspecific and have relatively long ranges compared to covalent bonds. Covalent coupling, on the other hand, does require specific bond angles and distances for the bonds to form. If these distances and orientations are not available due to steric hindrances layer-by-layer deposition will not proceed.

Procion Red Films.

Procion Red reacts to form layer-by-layer films with PAH, PVA, and PEI. The absorbance/bilayer value for PEI / PR is nearly twice that which is observed for PAH / PR (as compared to the PAH pH 7.0 / PR pH 10.5 case presented in Chapter 3). The

thickness of the PEI / PR bilayers (0.57 ± 0.02 nm) is approximately the same as seen for PAH / PR (0.52 ± 0.06 nm). The PAH / PR absorbance/bilayer value is approximately four times the absorbance/bilayer value for PVA / PR. The PVA / PR bilayers are also thinner than those of PAH / PR, as they were to thin to accurately measure with ellipsometry.

5.4.2. Orienting a Procion Chromophore

In addition to being capable of supporting layer-by-layer deposition, there is an additional requirement that the polycation / chromophore system has a degree of net chromophore orientation. Previous work conducted with layer-by-layer films constructed using only electrostatic interactions has shown that simply having layer-by-layer growth does not a guarantee layer-by-layer orientation of the chromophore. Details of these findings can be found in Chapters 6 and 7. Previous work in Chapters 3 and 4 with the hybrid deposition approach has showed that PAH is capable of orienting both the PR and PB chromophores. In this study we find that PVA does not orient PR while PEI can provide some bulk orientation of the chromophore. The $\chi^{(2)}$ for the PEI / PR film is 4.0 ± 0.6 x 10^{-9} esu , less than half the value of the PAH / PR system. The PEI / PR films had a higher absorbance / bilayer than PAH / PR (0.0064 ± 0.0002 *vs.* 0.0033 ± 0.0003) while having a comparable bilayer thickness (0.57 ± 0.02 nm for PEI / PR vs. 0.52 ± 0.06 nm) for PAH / PR. This results in a higher chromophore density for the PEI / PR case, as shown by the absorbance/nm. However, due to the lower value of $\chi^{(2)}$ observed, it is clear that the PEI polycation does not orient the PR chromophores as well as the PAH polycation does.

The SHG scaling seen with PVA / PB implies that some orientiation may occur once several layers are depositing. If bulk scaling is being seen, the $\chi^{(2)}$ value is measured to be 3.6 ± 0.8 x 10^{-9} esu. This is fourteen times lower than the $\chi^{(2)}$ value seen for PAH / PB (no added salt) from Chapter 4. The absorbance/nm values for PVA/PB and PAH/PB (no added salt) are essentially identical. In order to account for the much lower $\chi^{(2)}$ values seen, the PVA must not be capable of the same degree of orienting that PAH is capable of.

5.5.Conclusions / Future Work

Fabrication of films via the hybrid deposition scheme occurs as a result of a covalent bond between the polyamine and the chromophore molecule. The accessibility of the amine functionality seems to be an important factor to consider in determining whether a Procion dye will couple to the previously adsorbed polycation. If sufficient coupling does not occur, layer-by-layer deposition will not proceed. The structure of the Procion dye also seems to play a role in determining if deposition occurs, in that layer-by-layer deposition occurred with PEI / PR but not with PEI / PB. This dependence of layer-by-layer deposition on particular combinations of polycations and dyes is consistent with the hypothesis that steric hindrances may be playing a significant in film formation.

The structure of the polycation also influences orientation of the chromophore. Both PVA and PEI allowed layer-by-layer deposition to occur with Procion Red. However, only films made with PEI showed regular orientation of the chromophore molecules. PEI / PR films had a $\chi^{(2)}$ of $4.0 \pm 0.6 \times 10^{-9}$ esu, roughly half that of films made using PAH / PR. These findings are significant for any future work with the hybrid deposition scheme since they suggest that future chromophore design will have to be done with possible steric hindrance effects in mind. For the present time, PAH is the most versatile polycation for both allowing deposition to occur and obtaining regular polar order. The effect of additional methylene units between the backbone and the amine group should be probed, as greater levels of orientation may be possible. However, solubility of the polycation would then become an issue. Molecular modeling may provide valuable insights in probing the accessibility and thus determining if steric factors explain why Procion Red couple couple with PEI while Procion Brown could not. Additionally, modeling may also provide insight as to why PAH couples well with Procion Brown while PEI and chitosan do not.

---

[1] Van Cott, K.; Guzy, M.; 'Layer-By –Layer Deposition and Order of Low-Molecular-Weight Dye Molecules for Second-Order Nonliner Optics' *Angewandte Chemie*, **41** (2002) 3236-3238

[2] Strand, S.; Tommeraas, K.; Varum, K.; Ostgaard, K. 'Electrophoretic Light Scattering Studies of Chitosans with Different Degrees of N-acetylation' *Biomacromolecules*, **2** (2001) 1310-1314

[3] Polymeric Materials Encyclopedia, Vol 9. CRC Press, 1999, 7095

[4] Clark, S.; Hammond, P. 'The Role of Secondary Interactions in Selective Electrostatic Multilayer Deposition' *Langmuir*, **16** (2000) 10206-10214

[5] Itano, M.; Kern, F.; Miyashita, M.; Ohmi, T. 'Particle Removal from Silicon Water Surface in Wet Cleaning Process' *IEEE Trans. on Semicond. Manu*. **6** (1993) 258-267.

[6] Fang, M.; Kim, C.; Saupe, G.; Kim, H.; Waraska, C.; Miwa, T.; Fujishima, A.; Mallouk, T. 'Layer-by-Layer Growth and Condensation Reactions of Niobate and Titanoniobate Thin Films' *Chem. Mater.* **11** (1999) 1526-1532

[7] Van Cott, K.; Amos, T.; Gibson, H.; Davis, R.; Heflin, J. 'Characterization of the Purity and Stability of Commercially Available Dichlorotriazine Chromophores Used in Nonlinear Optical Materials' in press. *Dyes and Pigments*

[8] R. M. Azzam and N. M. Bashara. "Ellipsometry and Polarized Light" Elsevier, N. Y. 1987

[9] Neyman, P.; Guzy, M.; Shah, S.; Davis, R.; Van Cott, K.; Hang, W.; Gibson, H.; Brands, C.; Heflin, J. 'Novel Hybrid Covalent / Ionic Self-Assembly Techniques for Improved Second-Order Nonlinear Optical Films' *Mat. Res. Soc. Symp. Proc* **708** (2002) 161-166.

[10] Koetse, M.; Laschewsky, A.; Verbiest, T. 'Films Grown from Polyamines and Reactive Dyes by Alternating Polyelectrolyte Adsorption / Surface Activation (COMPAS)' *Mat Sci Eng C* **10** (1999) 107-113.

[11] Alexander, M.; Beamson, G.; Blomfield, C.; Leggett, G.; Duc, T. 'Interaction of Carboxylic Acids with the Oxyhydride Surface of Aluminum: Poly(acrylic acid), Acetic Acid and Propionic Acid on Psuedoboehmite' *Journal of Electron Spectroscopy and Related Phenomena* **121** (2001) 19-32.

6. Orientation of an Anionic Chromophoric Side Group in Ionically Self-Assembled Films: Effect of pH and Polycation Choice

Abstract

Layer-by-layer deposition of polyelectrolytes is one avenue for fabricating second order nonlinear optic materials. This study examines the effect of polycation structure on the polar ordering of an anionic side group chromophore molecule. Films were fabricated using the NLO active chromophore PCBS with 3 different polycations, poly(allylamine hydrochloride), poly(diallyldimethyammoium chrloride) and poly(L-lysine). Of these films only PAH / PCBS showed regular layer-by-layer chromophore orientation. $\chi^{(2)}$ were highest when the polycation was deposited under conditions in which the chains were well charged, adsorbing in flat, thin layers. Deposition of polymer aggregates resulted in optically poor films that were not suitable for second order NLO materials.

Keywords

Layer-by-layer deposition, pH effects, optical inhomogeneity, second harmonic generation, nonlinear optics, polycation structure, chromophore orientation

6.1. Introduction

Nonlinear optical (NLO) materials that exhibit second order harmonic generation (SHG) have applications as components in frequency doubling devices and electro-optic modulators.[1] For a material to display SHG, it must be non-centrosymmetric on both the macroscopic and molecular scales. Organic NLO materials have potential advantages of faster switching rates and lower manufacturing costs over inorganic materials such as lithium niobate.[2] Current organic NLO materials such as poled polymers suffer from poor temporal stability while Langmuir-Blodgett films lack acceptable mechanical robustness. One fabrication approach that satisfies both the mechanical and temporal stability issues while providing a potentially useful level of SHG is the Ionically Self-Assembled Monolayer (ISAM) method.

The ISAM deposition process, consists of layer-by-layer deposition of polyelectrolytes of opposite charge. This technique was first introduced by Iler[3] and later elaborated upon by Decher et al.[4] Reviews by Hammond[5] and Decher[6] provide insight

into the vast array of films that can be constructed. There are two criterion that must be satisfied for an ISAM films to display SHG: 1) an NLO active chromophore molecule must be present, often incorporated as a pendant ionic side group on one of the polymers; and 2) the chromophore must be reproducibly oriented in each bilayer, i.e. possess long range polar order. The second order susceptibility ($\chi^{(2)}$) characterizes the second order NLO activity of a film and is governed by $\chi^{(2)} = NF\beta\langle\cos^3\theta\rangle$; where N is the number density of chromophores in the film, F accounts for the local electric field, β is the molecular hyperpolarizability and θ is the tilt angle of the chromophore in the film relative to the surface normal.[7] From this governing equation, a framework for designing films emerges where film deposition experiments can be designed so as to promote the maximum amount of deposition while still maintaining a high net degree of orientation.

A number of efforts are underway to develop commercially applicable NLO materials using the ISAM or ISAM-related methods. One approach includes the NLO constituent as a pendant ionic side group on a polymer backbone.[31,8,9,10] The work of Heflin et al. is of particular note due to the observed quadratic scaling of the SHG intensity with film thickness. A different approach is to use polyelectrolytes where the chromophoric substituent is incorporated into the backbone.[11] Several different approaches exist for promoting polar order. Fischer et al. complexed a side chain chromophoric group with charged cyclodextrin sleeves and maintained layer to layer polar order.[12] Van Cott et al. report a related method for fabricating oriented films using a reactive triazine-functionalized monomeric chromophore, Procion Red MX-5B.[13]

The structure of films made *via* the ISAM process depends on the processing parameters. Among the most significant parameters are the ionic strength, the pH of the polyelectrolyte solutions, and the choice of polyelectrolytes. Decher and others have reported that as the ionic strength is increased, the thickness of the resulting films also increased.[14,15,16,17,18] For strong polyelectrolytes, where the charge density is insensitive to pH, the film thickness and amount of material deposited are relatively insensitive to changes in pH.[16] For weak polyelectrolytes, where the charge density is determined by solution pH, the pH is a critical variable in defining the film's properties. The conformation of adsorbed polymer chains (loops, trains or tails) is, in part, dependent on the polymer charge density. When the polyelectrolytes are highly charged, thin and flat

layers are formed. Thick and loopy films are formed when the polymers are less charged.[17] In addition, as the surface charge density increases the amount of polyelectrolyte adsorbed also increases.[18,19] The work of Heflin et al. begins to bridge the gap between film structure and chromophoric orientation. Using ionic strength and pH variations on films constructed with the NLO polymer PS-119 and the polycation poly(allylamine hydrochloride) [PAH], they demonstrated that the susceptibility $\chi^{(2)}$ was significantly higher in films where the polymers were deposited in flat, thin layers as opposed to when polymers were deposited in thick, loopy layers.[20] Films were made PAH and PS-119 with 0.14 M NaCl which resulted in films ~ 20 times as thick with $\chi^{(2)}$ values only 25% of those of the films made with no added salt.

The role of polyelectrolyte structure is clearly demonstrated by comparing the thickness of films made with two different polycations. Using PSS and poly(diallyldiammonium chloride) Dubas et al. made films with a bilayer thickness of 27 nm compared to Lösche et al.'s bilayer thickness of 4.4 nm obtained using poly(allylamine hydrochloride) and PSS under the same deposition conditions (pH and ionic strength); the change in polycation resulted in films roughly six times thicker.[14,15,16] Laschewsky et al. demonstrate the importance of materials choice for orientation for SHG. The resulting orientation, and thus, SHG, from films made with an NLO active polycation varied greatly depending on what anionic species the films was made with. Using an anionic montmorillonite clay, an anisotropic system was obtained; however using poly(vinyl sulfate) as the anionic constituent did not result in regularly oriented layers.[21]

The effect of the NLO-inactive polyelectrolyte structure on the orientation of the chromophore moieties and the resulting SHG has not been systematically studied. In this work, three NLO-inactive polycations were chosen to evaluate these effects, each with a different response to pH. The polycations used in this study were a strong polyelectrolyte, poly(diallyldimethylammonium chloride) [PDDA]; a weak polyelectrolyte, poly(allylamine hydrochloride) [PAH] with a charge density that is strongly dependent on pH; and poly(l-lysine) [PLL] a weak polyelectrolyte that has both a charge density and a conformational dependence on pH. Measurements of the SHG, film thickness, and the amount of chromophore deposited illustrates how polycation

choice, solution pH, and the subsequent intermolecular interactions between NLO chromophores and polymers affects the orientation of the chromophores in the film.

6.2.**Experimental**

6.2.1. **Materials.**

The structures of the dye and polycations used in this study are shown in Figure 6.2-1. Poly{1-[4-(3-carboxy-4-hydroxyphenylazo)-benzensulfonamido]-1,2-ethandiyl} (PCBS, sometimes referred to as 'PAZO'; Aldrich, lot 07228DF) was used as the chromophore in all deposition experiments. The absorbance spectrum for this chromophore is shown Figure 6.2-2 and exhibits a characteristic absorption peak at 359 nm. PAH (M_w ca. 70,000; Aldrich, lot 08423HR), PDDA (100,000 < M_w < 200,000; 20 wt. % in water, Aldrich, lot 07228DF), and PLL (70,000 < M_w < 150,000; Sigma, lot 59H5907) were all used as received. These molecular weights were chosen to keep the degree of polymerization for each species as close as possible (PAH, DP ≅ 760; PDDA, 620< DP < 1240; PLL, 520 < DP < 1110). Deionized water (Barnstead Nanopure II) was used with a specific resistance above 17 MΩ·cm. Fisherbrand frosted microscope slides (Fisher Scientific, item 12-550-34) were prepared using the RCA cleaning procedure.[22] In this procedure the substrates were immersed in a solution of H_2O, H_2O_2 and NH_4OH at 70°C for 20 minutes. The slides were then rinsed and placed in an acid bath consisting of concentrated HCl, H_2O_2 and H_2O. The substrates remained in this bath for 20 minutes and were then rinsed and baked at 130°C for at least one hour.

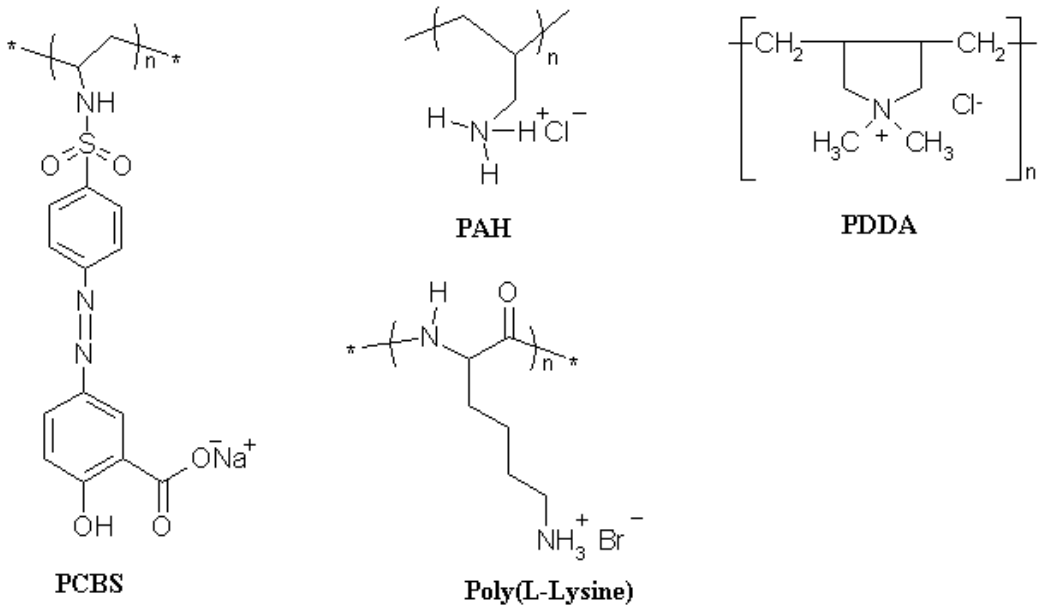

Figure 6.2-1 - Structures of polymer chromophore (PCBS) and the 3 polycations used in this work

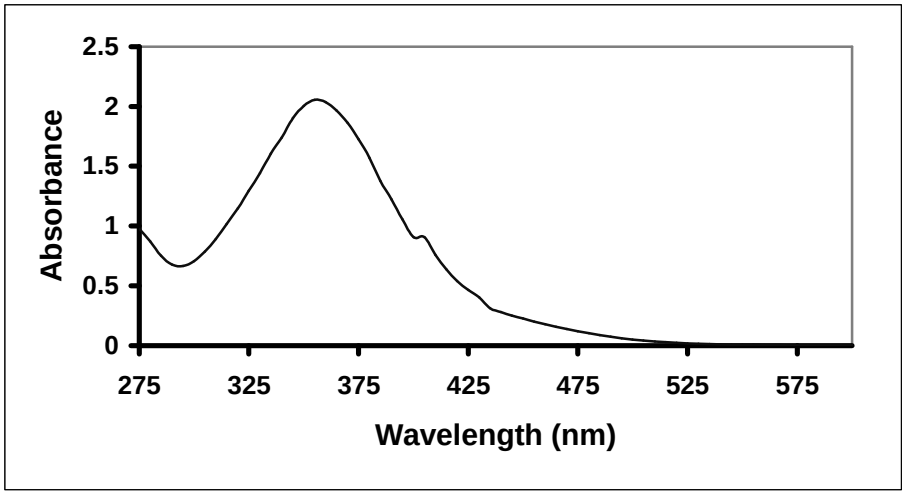

Figure 6.2-2 - Absorbance Spectrum for PCBS, 0.3 mM solution; no additional salt, 1 cm. cell

6.2.2. **ISAM Deposition.**

The concentration of all solutions in this study was 10 mM on a repeat unit (RU) basis. The pH value of the PCBS solution was adjusted to 7.0 and the pH of the PLL and PDDA solutions were adjusted to 7.0 and 11.0. Experiments with PAH were conducted at pH values of 7.0, 10.0 and 11.0. In all cases the pH was adjusted using 1 M or 0.1 M NaOH or HCl (Fisher Scientific) as necessary. The pH values of the solutions used in dipping drifted no more than +/- 0.1 pH units during the course of an experiment. An immersion time of 5 minutes was used for both solutions with the exception of the first dip in the polycation, which was 10 minutes in duration. Slides were dried every 10 bilayers (polycation/PCBS assemblies) for UV absorbance measurement using N_2 gas. Slides were made with 2, 10, 20, 40 and 80 bilayers for each of the six conditions examined. Unless otherwise specified, the total number of bilayers deposited on both sides will be cited whenever the number of bilayers deposited is specified.

6.2.3. **Film Characterization.**

ISAM films were characterized during deposition using UV-Vis spectroscopy (U-2000 Spectrophotometer, Hitachi). Absorbance values were measured at the characteristic peak for the PCBS (λ_{max}=359 nm) and were taken every 10 bilayers after the slides were dry.

Film thicknesses were measured using a variable angle spectroscopic ellipsometer (J. A. Woolam Ellipsometer VB-200). The amplitude factor ψ and phase factor Δ which are related to the complex Fresnel coefficients for a given film, were measured for wavelengths from 350 to 1000 nm at 10 nm intervals.[23] This wavelength range was repeated for angles ranging from 55° to 75° in 5° intervals. A portion of the substrate was roughened to scatter the light. The ellipsometric data were obtained opposite to this roughened patch, as the scattering eliminates backside reflections, which simplifies data analysis. The data was analyzed using a Lorenz oscillator model. Details on the

ellipsometric model can be found in Appendix A. Bilayer thicknesses are reported as the average of a minimum of three films fabricated under the same conditions.

Dynamic light scattering (DLS) measurements were performed using a DynaPro-801 TC from Protein Solutions operating at a wavelength of 836.4 nm. All experiments were performed at 25 ± 0.2°C. Prior to sample measurements, the sample chamber was flushed using deionized water filtered with a 0.02 μm Whatman Anotop syringe filter. Approximately 0.5 ml of filtered (0.02 μm Whatman Anotop syringe filter) sample was injected into the chamber. From the fluctuations in scattered light intensity, the translational diffusion coefficient (D_T) was measured. Using the Stokes-Einstein equation, this diffusion coefficient is related to the hydrodynamic radius (R_H);

$$R_H = \frac{k_b T}{6\pi\eta D_T} \tag{6.1}$$

where k_b is Boltzman's constant, T is the absolute temperature in Kelvin, and η is solvent viscosity. The regularization algorithm was used to report D_T.[24]

SHG measurements were performed with a standard setup using a 10-nanosecond pulse width, Q-switched Nd:YAG laser with a fundamental wavelength of 1064 nm.[25] The SHG data were averaged over 100 shots per data point, and the uncertainty in relative $\chi^{(2)}$ values is 10%. Typical spot radius and pulse energy values were 30μm and 7mJ/pulse, respectively. The film was deposited on both sides of the substrate. As a result, as the sample was rotated with respect to the incident beam, the path length between the film on opposite sides was varied, leading to interference fringes of the SHG intensity. The sample was rotated from 30° to 60° away from normal incidence using a stepper motor controlled rotation stage. The $\chi^{(2)}$ value was determined from the intensity of the second harmonic ($I^{2\omega}_{film}$) at the peak of the interference fringe in the vicinity of 45º. By comparison to Maker fringes in a quartz crystal wedge, $\chi^{(2)}$ of a film is obtained from

$$\frac{\chi^{(2)}_{film}}{\chi^{(2)}_{q}} = \frac{2l_{c,q}}{\pi l_{film}} \sqrt{\frac{I^{2\omega}_{film}}{I^{2\omega}_{q}}} \tag{6.2}$$

where l_{film} is the total path length through the film, $I^{2\omega}_{q}$ is the second harmonic intensity of the quartz crystal, the coherence length of quartz, $l_c = \lambda / 4(n^{2\omega}-n^{\omega})$, is 22.4 μm, and $\chi^{(2)}_{q}$ of quartz is 1.92×10^{-9} esu.

The tilt angle of the chromophore away from the normal of the substrate was determined by measuring the ratio of the SHG intensity for p-polarized vs. s-polarized incident fundamental beams.[25] The intensities, $I_{2\omega}$, of the p-polarized second harmonic from p- and s-polarized beams incident at an angle θ away from the normal to the film surface may be expressed as

$$I_{2\varpi}^{p\to p} = (3\chi_{zxx}^{(2)} \sin\theta \cos^2\theta + \chi_{zzz}^{(2)} \sin^3\theta)^2 E_{\omega}^{p\,4} \tag{6.3}$$

$$I_{2\varpi}^{s\to p} = (3\chi_{zxx}^{(2)} \sin\theta)^2 E_{\varpi}^{s\,4} \tag{6.4}$$

In addition, since the net dipole orientation of these films is normal to the surface, the non-vanishing susceptibility tensor elements for a collection of N molecules may be written as

$$\chi_{zxx}^{(2)}(-\omega,\omega_1,\omega_2) \propto \frac{1}{2} N \langle \cos\alpha \sin^2\alpha \rangle \beta_{zzz} f(\omega) f(\omega_1) f(\omega_2) \tag{6.5}$$

$$\chi_{zzz}^{(2)}(-\omega,\omega_1,\omega_2) \propto \frac{1}{2} N \langle \cos^3\alpha \rangle \beta_{zzz} f(\omega) f(\omega_1) f(\omega_2) \tag{6.6}$$

where α is the molecular tilt angle away from the normal, β_{zzz} is the hyperpolarizability along the molecular axis and the f's are local field factors. If the distribution of α's is peaked sharply about a particular angle α, the average values of these products may be taken as products of functions of the average value α. Then, the ratio of the susceptibilities may be written as:

$$\frac{\chi_{zzz}^{(2)}}{\chi_{zxx}^{(2)}} = 2\cot^2\alpha \tag{6.7}$$

This can then be expressed as a ratio of SHG intensities:

$$\alpha = \cot^{-1}\sqrt{\frac{1}{2}\left[\csc^2\theta \sqrt{\frac{I_{2\omega}^{p\to p}}{I_{2\omega}^{s\to p}} - 3\cot^2\theta}\right]} \tag{6.8}$$

6.3.**Results**

A characteristic of ISAM deposition is the linear increase of the absorbance of the film with the number of bilayers deposited. The slope of this linear relationship between absorbance and bilayer number reflects the amount of dye deposited per layer. Absorbance *vs.* the number of bilayer plots for PAH with PCBS are shown in Figure 6.3-1, while PDDA and PLL are shown in Figure 6.3-2 and Figure 6.3-3; respectively. Table 6.3-1 summarizes the absorbance slopes and standard deviations as determined by least squares regression for the polycations used at all pH conditions as well as the bilayer thicknesses. For all three polycations, the amount of chromophore deposited (as characterized by the absorbance slope) increased substantially as the pH increased. The absorbance slope for films made with PAH increased by a factor of 10 as the pH was changed from 7 to 11. For films made with PDDA, the slope increased by a factor of 3 as the pH was raised from 7 to 11. For films made with PLL, the slope increased by a factor of 13 as pH increased from 7 to 11. Accordingly, the bilayer thicknesses also increased as the pH was increased. Films made with PAH at pH 10 and 11 were respectively 30 and 47 times thicker than films made at a pH of 7. Films made with PDDA at a pH 10 and 11 were respectively 1.2 and 70 times as thick as films made at pH 7. PLL films at pH 11 were 142 times thicker than those made at a pH of 7.

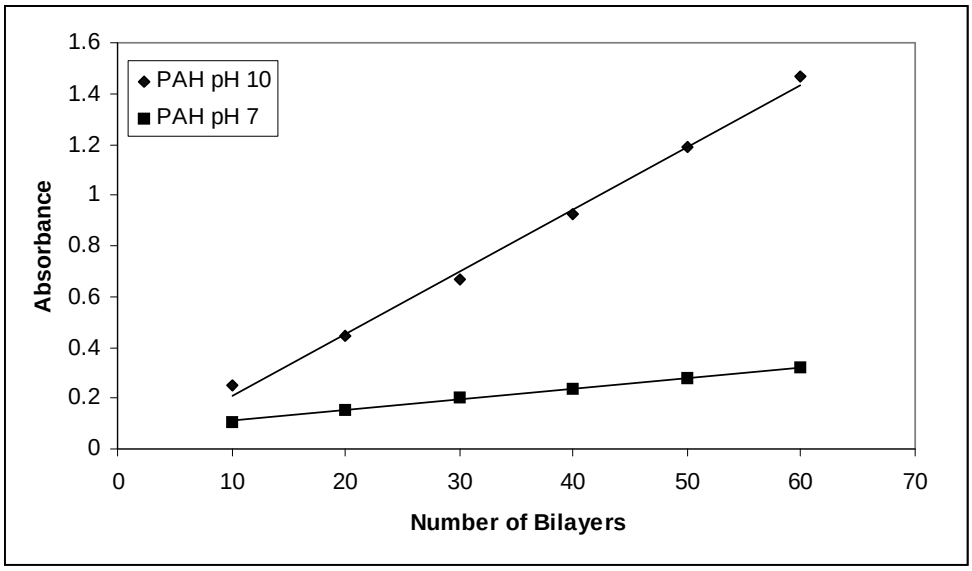

Figure 6.3-1 - Absorbance vs. number of bilayers for ISAM deposition of PCBS with PAH (10 mM RU PAH pH 7.0 / pH 10 with 10 mM RU PCBS pH 7.0)

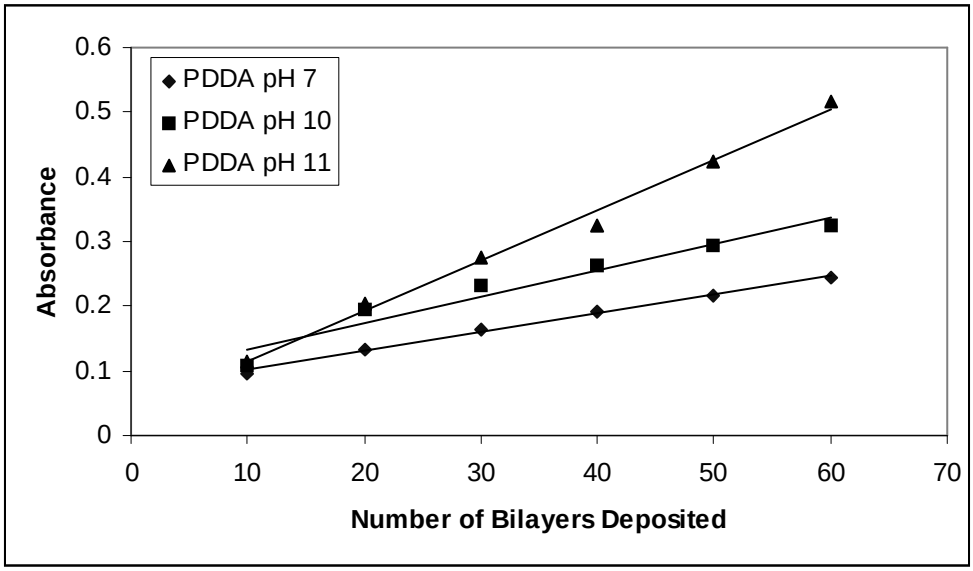

Figure 6.3-2 – Absorbance results for the deposition of PCBS with PDDA (PDDA at 10 mM RU, no added salt; PCBS 10 mM RU, pH 7, no added salt)

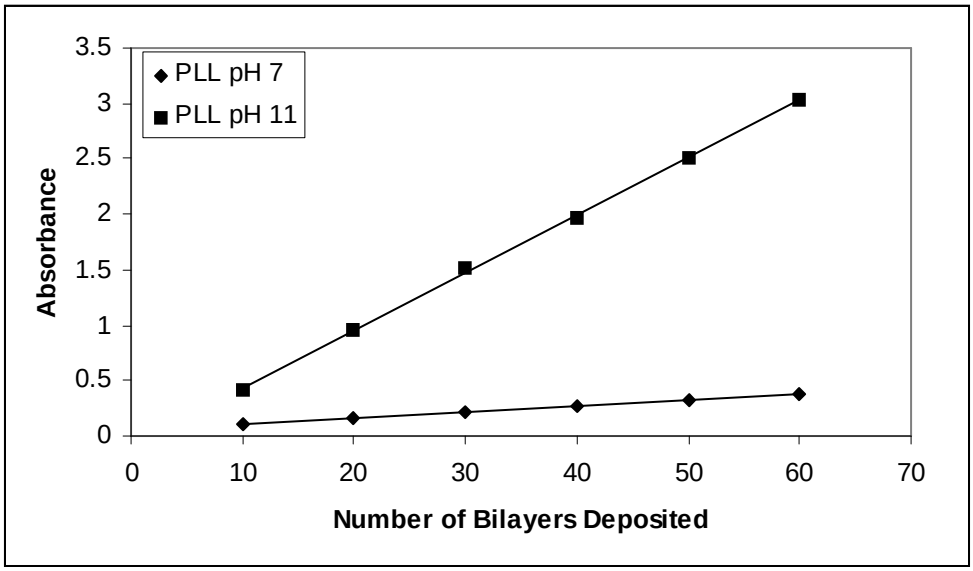

Figure 6.3-3 - Absorbance results for the deposition of PCBS with PLL (PLL at 10 mM RU, no added salt; PCBS 10 mM RU, pH 7, no added salt)

Table 6.3-1 - Slopes, bilayer thicknesses and $\chi^{(2)}$ values for films made for the three polycations and pH's (No additional salt, polycation concentration 0.01 M RU, PCBS deposition done at pH 7.0 and 10 mM RU). Reported error values represent one standard deviations of the data set.

Polycation	pH	Abs. / Bilayer	Bilayer Thickness (nm)	Abs. / nm	$\chi^{(2)}$ (10^{-9} esu)	Tilt Angle
PAH	7	0.005 ± 0.001	0.3 ± 0.1	0.0170	9.1 ± 3.4	63°
PAH	10	0.023 ± 0.003	9.2 ± 0.5	0.0025	0.95 ± 0.06	37°
PAH	11	0.050 ± 0.014	14.1 ± 1.4	0.0035	N/A[1]	N/A[1]
PDDA	7	0.003 ± 0.0002	0.16 ± 0.0	0.019	0[2]	N/A[3]
PDDA	10	0.004 ± 0.0003	0.19 ± 0.0	0.021	0[2]	N/A[3]
PDDA	11	0.009 ± 0.002	11.2 ± 0.9	0.0008	N/A[1]	N/A[1]
PLL	7	0.004 ± 0.001	0.15 ± 0.1	0.027	0[2]	N/A[3]
PLL	11	0.057 ± 0.006	21.3 ± 2.3	0.0027	N/A[1]	N/A[1]

1 - Slides not homogenous enough for SHG testing
2 - Films do not display quadratic scaling, hence the bulk $\chi^{(2)}$ is essentially zero
3 - Chromophore randomly oriented in the Film

Nonzero $\chi^{(2)}$ values are reported (Table 6.3-1) for only films made with PAH at two pH conditions. The $\chi^{(2)}$ decreased by a factor of 10 as the pH increased from 7 to 10. Figure 6.3-4 shows the linear scaling of the square root of the second harmonic intensity for these two PAH conditions as a function of the number of layers deposited. The error bars shown represent ± 10 %, the typical accuracy for the measurements. A linear relationship implies that there is bulk scaling of the chromophore in the film and that the orientation of chromophores in the film is essentially constant for each deposited layer. Films made using PDDA or PLL that were of sufficient optical homogeneity for NLO analysis showed effectively zero bulk $\chi^{(2)}$ values (Figure 6.3-5, Table 6.3-1). Films made with any of the polycations studied here at a pH of 11 were not sufficiently homogeneous for SHG testing. For comparison, the $\chi^{(2)}$ of quartz is 1.9E-9 esu.

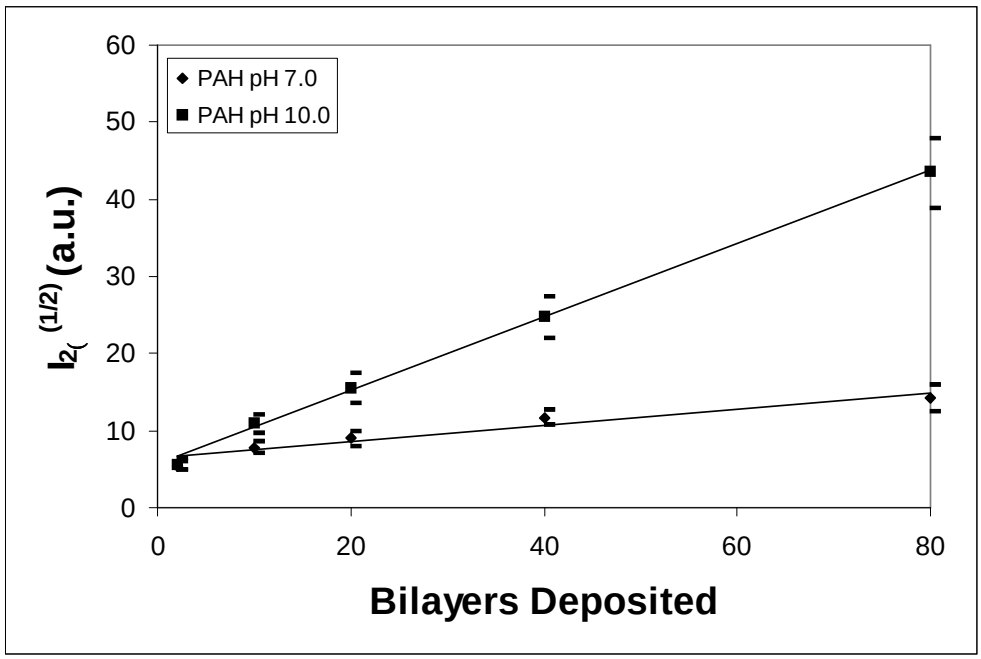

Figure 6.3-4- The square root of the second harmonic generation intensity as a function of the number of bilayers deposited of PAH / PCBS. The linear relationship indicates that these films are oriented in the bulk. The error bars shown represent ± 10%.

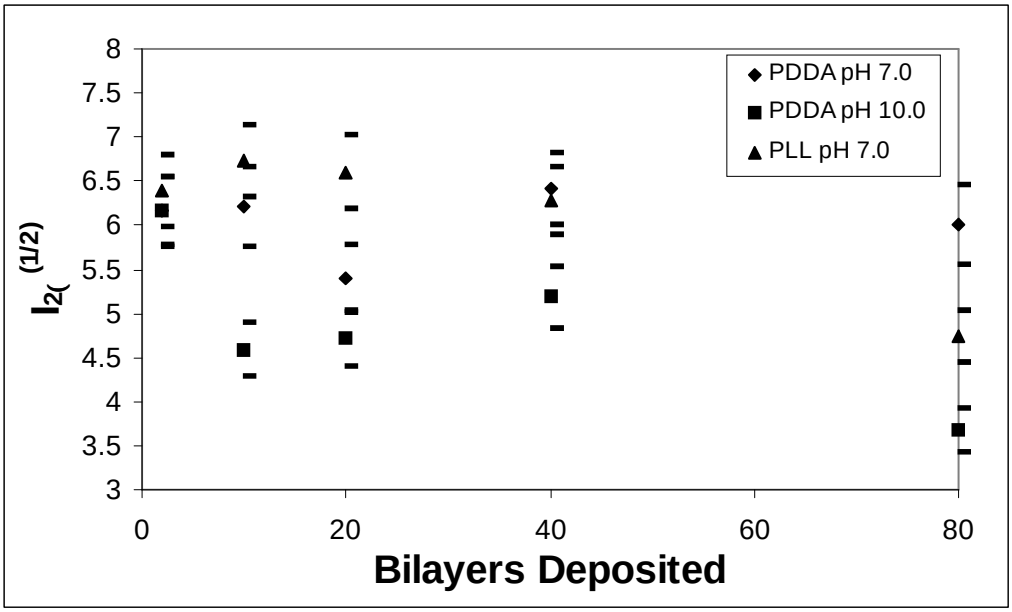

Figure 6.3-5 - Nonquadratic scaling of SHG intensity with the number of bilayers deposited for PDDA and PLL

Films made with any of the three polycations at a pH of 11 had point-to-point variations in optical homogeneity that were significant enough to preclude these films

from meaningful NLO analysis. The deposition of polymeric aggregates could account for these variations. For each polymer, dynamic light scattering was performed over a range of pH values. Over the pH values measured, only one peak was observed in the Regularizations algorithm. Figure 6.3-6 shows the translational diffusion coefficient for the polymers as a function of the solution pH. As the pH increased, the diffusion coefficients for PAH and PLL both decreased by approximately a factor of five indicating that aggregation occurred. However, the diffusion coefficient for PDDA changed by a much smaller extent, ranging from 4.0E-11 to 6.3E-11 m^2/s.

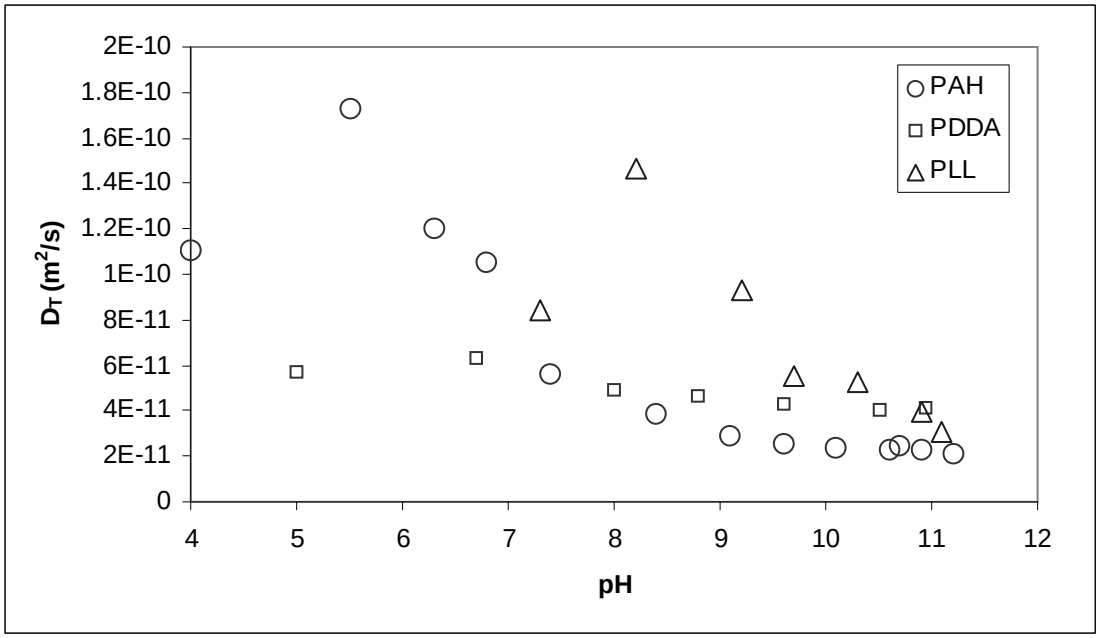

Figure 6.3-6 - DLS results for the translational diffusion coefficient (D_T) of PAH, PDDA and PLL in solution at 25°C and a concentration of 10 mM RU as a function of pH.

6.4.**Discussion**

6.4.1. **Effect of pH and Polycation on Film Deposition**

The absorbance slopes given in Table 6.3-1 clearly show a dependence of the amount of PCBS deposited depends on both the polycation used and the solution conditions. For all three polycations, the bilayer thickness and slope of the absorbance *vs*. number of bilayer plots increased significantly as the pH of the polycation solution was changed from 7.0 to 11.0. Further, optically inhomogeneous films unsuitable for NLO characterization were obtained for these polycations at a pH of 11. These effects can be understood in terms of

pH and ionic strength effects. The ionic strength of the polyelectrolyte solutions is a function of the polymer concentration, the solution pH and the concentration of any additional salts. The expression for ionic strength (Equation 6.9) has no additional salt term, as no experiments were done with added salt. The polymer's contribution to the ionic strength ($C_{poly}/6$) was calculated based on the counterion condensation theory[26] so that the overall effective ionic strength is given by:

$$I_{eff} = \frac{1}{6} C_{poly} + 10^{-pH} + 10^{-pOH} \tag{6.9}$$

The Debye length, κ^{-1} (nm), is a function of the effective ionic strength, which at 25°C in water is:

$$\kappa^{-1} = \frac{0.304}{\sqrt{I_{eff}}} \tag{6.10}$$

The polycation solution ionic strength ranged from 1.7E-3 M for the pH 7.0 condition to 2.7E-3 M for pH 11.0. These values of ionic strengths correspond to Debye lengths of 7 nm (pH 7.0) and 6 nm (pH 11.0). These values imply that changes in double layer screening between the depositing polyelectrolyte and the oppositely charged surface may not be the principle reason for the large changes seen in both the absorbed amounts and bilayer thicknesses. It is more likely that these changes are the results of the polycation's response to changes in pH value.

PAH, which has a pK_a of 8.7, is mostly unprotonated at pH 11.[27] A random coil conformation will be adopted under these conditions, due to the lack of intrachain repulsions. In addition, the polymer chains will be less soluble compared to the pH 7.0 case as evidenced by the approximately factor of 5 drop in translational diffusion coefficient by the PAH as the pH is varied from 6 to 11, which is consistent with the formation of aggregates at high pH. These two factors result in the PAH chains depositing in thick and loopy layers at high pH values. The pH 10 case is essentially identical to the pH 11 case except that the charge density is marginally higher. This led to a higher layer thickness and absorbed PCBS amount at pH 10 compared to pH 7. In the pH 7 case, the PAH chains are highly charged which leads to deposition of PAH in flat, trainlike conformations and subsequently lower values of absorbance/bilayer. These trends are consistent with the work of Rubner et al. who studied the effect of pH on the

PAH / poly(acrylic acid) system.[19] Hammond et al. performed a similar experiment using PAH at a pH of 3.5 and PCBS (denoted as PAZO) at a pH of 7.0 and fabricated films with thickness of ~ 0.7 nm / bilayer.[28] This is slightly over twice the thickness of our films fabricated at a PAH pH of 7.0. The pH 11 case showed optical inhomogeneities which likely were the result of depositing polymer aggregates. Increasing the PAH pH from 7.0 to pH 10.0 resulted in a decrease in the absorbance/nm, implying that the chromophore density in the film is lower when the polymer is deposited in a thick and loopy manner.

In the case of PLL, the 13-fold increase in absorbance/bilayer may be due to a reduced charge density and decreased solubility. During the preparation of the solution for the pH 11.0 case, the solution briefly became turbid before becoming clear again, indicating that the solubility of the PLL decreased with the increase in pH. This was not observed with the pH 7.0 solutions. Additionally, the charge density of PLL decreases with increasing pH. Under neutral conditions PLL in solution is a charged random coil. However, when the pH is increased to a value near the pK_a of 11.0, the PLL adopts an α-helical conformation.[29] The coil-to-helix transition occurs as the pH increases because the molecule becomes less charged, which allows intramolecular hydrogen bonding to dominate. The observed increase in amount of dye deposited between the helical and coil conformations has been observed for other dye systems, due presumably to an increase in charge density due to the compactness of the helical structure.[30] Deposition of highly helical PLL chains at a pH of 11 followed by a decrease to a pH of 7 when the PCBS is deposited may lead to a relatively high surface concentration of protonated amine groups. However, as the pH is increased from pH 7 to pH 11, the absorbance/nm value decreased by an order of magnitude, again implying that the chromophore density is lower in the high pH case.

For PDDA, the three-fold increase in absorbance/bilayer with increasing pH most likely results from the decreased polymer solubility at a pH of 11.0. The charge density of the PDDA does not change significantly from pH 7.0 to 11.0 since the charged group is a quaternary amine with a pK_a higher than the pH values explored in this study. However, due to the higher ionic strength at pH 11.0, the solubility of the polymer would decrease, providing a larger thermodynamic driving force for deposition, leading to

thicker and more loopy layers at a pH of 11. During the course of adjusting the pH of one of the PDDA solutions to pH 11, the solution briefly became turbid, supporting the notion that the solubility of the polymer is reduced at this pH. Films were also fabricated at a pH of 10, and the results for the absorbance / bilayer as well as the thickness fall between the pH 7.0 and pH 11.0 cases. The absorbance/nm values for PDDA / PCBS are essentially constant from pH 7 to pH 10. The value then decreased as the pH was increased to pH 11. For comparison, Advincula et al. fabricated PDDA / PCBS films using pH of 7.0 for both solutions and reported thicknesses of 0.5 nm / bilayer.[34] This is roughly three times the thickness of our films fabricated under the same experimental conditions.

6.4.2. **Effect of pH on SHG for PAH films**

A quadratic relationship is expected between the second harmonic intensity and the film thickness for films that exhibit long range (layer-by-layer) polar ordering ($I_{2\omega} \propto \left[\frac{\chi^{(2)}_{eff}\pi l}{2}\right]^2$). Figure 6.3-4 shows the square root of the second harmonic intensity ($I_{2\omega}^{1/2}$) plotted versus the number of bilayers deposited for films made with PAH. These plots should be linear if long range polar order occurs. Films made with PAH at pH values of 10.0 and 7.0 display quadratic scaling, i.e., the orientation of the chromophore molecules in the film is consistent as each additional layer is deposited. As the pH of PAH increased from 7.0 to 10.0, the $\chi^{(2)}$ values decreased from 9.1 x 10^{-9} esu to 0.95 x 10^{-9} esu. Films formed at a pH of 7 had a tilt angle of 63° from the surface normal while those formed at a pH of 10 were better oriented with a tilt angle of 37° from the normal. This compares to a tilt angle of 25° as reported by Hammond et al. for PCBS films made with PAH deposited at pH 3.5.[28] Given that the bilayer thickness in the pH 7 case is 0.3 nm, it is not unexpected that the chromophoric side group (length ~ 1.5 nm) would lie mainly in the plane of the substrate and thereby have a larger tilt angle. Despite the better orientation in the pH 10 case, the lower $\chi^{(2)}$ value can be explained by considering the relative fraction of NLO active PCBS in the film. While film thickness increased by a factor of 30 upon changing the pH from 7 to 10, the amount of chromophore incorporated in the film increased by a factor of 5. Films made at a pH of 10 have a much larger

fraction of NLO-inactive PAH relative to PCBS, resulting in a lower value of $\chi^{(2)}$ for films made at higher pH values. The PCBS concentration in the films made at pH 7.0 was nearly 7 times higher than in the films made at pH 10. This is reflected in the absorbance/nm values, as the pH 7 case had an absorbance/nm of 0.0170 while the pH 10 case had a value of 0.0025. These values support the notion that the chromophore density was significantly lower in the pH 10 case.

6.4.3. **Effect of Polycation Structure on SHG.**

Figure 6.3-5 clearly shows that quadratic scaling was not observed for films made with PLL and PDDA, which means that the orientation was not maintained in each layer. This supports the results of Lvov et al. who observed a decrease in the SHG intensity after 4 PDDA / PCBS layers were deposited.[31] The lack of bulk scaling for PLL and PDDA results in an effective $\chi^{(2)}$ value of zero for these films. The observed dependence of quadratic scaling on the NLO inactive polycation clearly demonstrates that the polycation structure dramatically affects chromophore orientation. However, the question remains as to why PAH orients PCBS in a layer-by-layer fashion while PLL and PDDA do not. The primary amines on PLL and PAH are capable of forming hydrogen bonds with the hydroxyl and undissociated carboxylate groups on the PCBS chromophore while the quaternary ammonium moieties on PDDA are not. Secondary interactions, such as hydrogen bonding, can drive self-assembly in some deposition systems.[32] The results suggest that the location of the hydrogen-bonding group or the charged group relative to the polycation backbone may play a role. The amine group on PAH is separated from the backbone by just one methylene group while the amine group in PLL is separated from the backbone by 4 methylene groups. The orienting hydrogen-bonding group may be less correlated with the backbone in PLL compared to PAH, thereby decoupling the orientation of the chromophoric side group from the orientation of the polymer backbone. Another possible reason that PLL may not be orienting the chromophoric groups as well is that there may be competition for hydrogen bonding with the PCBS chromophore between two hydrogen-bonding sites on the PLL (the amide

group and the amine group). This competition may hinder orientation of chromophore molecules.

6.4.4. **Dye Aggregation in Films.**

The state of aggregation of dye molecules in ISAM films can be determined by the red or blue shifts of the characteristic absorbance peaks. When the dipole moments of the chromophore molecule are parallel, a blue shift occurs and the aggregates are termed H-type aggregates. J-type aggregates are characterized by a red shift and occur where dye molecules' dipoles are in-line rather than parallel.[33] Several authors have examined the formation of aggregates in layer-by-layer films constructed of PCBS and PDDA. Lvov et al. observed a considerable red-shift of the absorbance band in the film compared to that of the dye in solution.[31] Dante et al. reported a red shift in the absorbance band that increased with the number of layers.[34] Films made with PEI and PCBS showed an initial red shift which was followed by a blue shift as the number of layers deposited increased. Our films made with PDDA at a pH of 7.0, the condition most comparable to the work of Dante, *et al*., showed a red shift with no apparent dependence on the number of layers deposited. Similar results were observed in films made with PDDA at a pH of 10. The films made with PAH at a pH of 7 showed a red shift at low bilayer numbers (2,10, and 20) with no shift or a blue shift at higher bilayer numbers (40, 80). At a pH of 10, PAH films showed a red shift at all bilayer numbers. Films made with PLL at a pH of 7.0 showed a large red shift in the first deposited layer (20 nm) and a lower red shift at higher number of bilayers (8 nm at 80 bilayers). There does not appear to be any definitive correlation of dye aggregation as characterized by red or blue shifts and long range polar order in these films.

6.5.**Conclusions**

The orientation of an anionic side-group chromophore in a film built *via* layer-by-layer deposition of polyelectrolytes depends strongly on the structure of the NLO-inactive polycation used. In this work, PAH was shown to orient the chromophore in PCBS, while PLL and PDDA could not. Where bulk $\chi^{(2)}$ measurements could be made, SHG was largest in films with relatively thin bilayers consisting largely of flat, trainlike

conformations that form when the polyelectrolytes are highly charged as they deposit. $\chi^{(2)}$ values of 9.1 x 10^{-9} esu and 0.95 x 10^{-9} esu were measured in the pH 7.0 and pH 10.0 cases, respectively. Better orientation of chromophores was obtained in the thicker films made when the PAH was deposited at pH 10.0. However, the concentration of NLO active material in the thicker films was considerably lower than the thinner pH 7.0 case (~1/7 as much for pH 10.0 than pH 7.0). This results in the lower $\chi^{(2)}$ values. Further work will probe the effect of polycation structure, specifically the relationship between orientation and the distance separating the hydrogen bonding ammonium group and the backbone based on the hypothesis that hydrogen bonding is needed for chromophore orientation.

---

[1] Boyd, R. "Nonlinear Optics" Academic Press, New York, 1992

[2] Lytel, R. 'Applications of Electro-Optic Polymers to Integrated Optics' *SPIE Proceedings*, 1990, 1216, 42-52.

[3] Iler, R. 'Multilayers of Colloidal Particles' *J. Colloid Interface Sci.***21** (1966) 569.

[4] Decher, G.; Lvov, Y.; Schmitt, J. 'Proof of multilayer structural organization in self-assembled polycation polyanion molecular films' *Thin Solid Films* **244** (1994) 772.

[5] Hammond, P. 'Recent Explorations in Electrostatic Multilayer Thin Film *Assembly' Curr. Opin. in Colloid & Interface Science*. **4** (2000) 430-442

[6] Decher, G. ' Fuzzy Nanoassemblies: Toward Layered Polyelectrolyte Multicomposites' *Science*. **277** (1997) 1232-1237

[7] Dalton, L.; Harper, A.; Ghosn, R.; Steier, W.; Ziari, M.; Fetterman, H.; Shi, Y.; Mustacich, R.; Jen, A.; Shea, K. 'Synthesis and Processing of Imporved Organic Second-Order Nonlinear Optic Materials for Applications in Photonics' *Chem. Mater*. **7** (1995) 1060-1081.

[8] Wang, X.; Balasubramanian, S.; Li, L.; Jiang, X.; Sandman, D.; Rubner M.; Kumar, J.; Tripathy, S. 'Self-assembled second order nonlinear optical multilayer azo polymer' *Macromolecular Rapid Communications* **18** (1997) 451-459.

[9] Lenahan, K.; Wang, Y.; Liu, Y.; Claus, R.; Heflin, J.; Marciu, D.; Figura, C. 'Novel Polymer Dyes for Nonlinear Optical Applications Using Ionic Self-Assembled Monolayer Technology' *Adv. Materials*, **10** (1998) 853-855.

[10] Heflin, J.; Liu, Y.; Figura, C.; Marciu, D.; Claus, R. 'Second Order Nonlinear Optical Thin Films Fabricated from Ionically Self Assembled Monolayers' *Proc. SPIE*, **3417** (1997) 10-19.

[11] Lindsay, G.; Roberts, M.; Chafin, A.; Hollins, R.; Merwin, L.; Stenger-Smith, J.; Yee, R.; Zarras, P.; Wynne, K. 'Ordered Films by Alternating Polyelectrolyte Deposition of Cationic Side Chain and Anionic Main Chain Chromophore Polymers' *Chem. Mater*., **11** (1999) 924-929.

[12] Fischer, P.; Koetse, M.; Laschewsky, A.; Wischerhoff, E.; Jullien, L.; Persoons, A.; Verbiest, T. 'Orientation of Nonlinear Optical Active Dyes in Electrostatically Self-Assembled Polymer Films Containing Cyclodextrins' *Macromolecules*, **33** (2000) 9471-9473.

[13] Guzy, M.; Heflin, J.;Neyman, P.; Brands, C.;Davis, R.; Gibson, H.; Van Cott, K. 'Layer-By-Layer Deposition And Ordering Of Low Molecular Weight Dye Molecules For Second Order Nonlinear Optics' *Angewandte Chemie*, **41** (2002) 3236-3238.

[14] Lösche, M.; Schmitt, J; Decher, G; Bouwman, W.; Kjaer, K. 'Detailed Structure of Molecularly Thin Polyelectrolyte Multilayer Films on Solid Substrates as Revealed by Neutron Reflectometry' *Macromolecules* **31** (1999) 8893-8906.

[15] Dubas, S.; Schlenoff, J. 'Factors Controlling the Growth of Polyelectrolyte Multilayers' *Macromolecules* **32** (1999) 8153-8160.

[16] Betrand, P.; Jonas, A.; Laschewsky, A.; Legras, R. 'Ultrathin Polymer Coatings by Complexation of Polyelectrolytes at Interfaces: Suitable Materials, Structure and Properties' *Macromolecular Rapid Communications* **21** (2000) 319-348.
[17] Fleer, G. J.; Cohen Stuart, M. A.; Scheutjens, J. M. H. M.; Cosgrove, T.; Vincent, B. "Polymers at Interfaces" Chapman & Hall, New York, 1993.
[18] Yoo, D.; Shiratori, S.; Rubner, M. 'Controlling bilayer composition and surface wettability of sequentially adsorbed multilayers of weak polyelectrolytes' *Macromolecules* **31** (1998) 4309-4318
[19] Shiratori, S.; Rubner, M. 'pH-Dependent Thickness Behavior of Sequentially Adsorbed Layers of Weak Polyelectrolytes' *Macromolecules* **33** (2000) 4213-4219.
[20] Figura, C.; Neyman, P.; Marciu, D.; Brands, C.; Murray, M. A.; Hair, S.; Davis, R. M.; Miller, M. B.; Heflin, J. R. 'Thermal Stability and Immersion Solution Dependence of Second Order Nonlinear Optical Ionically Self-Assembled Films' in *Organic Photonic Materials and Devices II*, Donald D. C. Bradley, Bernard Kippelen, Editors, Proceedings of SPIE Vol. 3939, 214-222 (2000)
[21] Laschewsky, A.; Wischerhoff, E.; Kauranen, M.; Persoons, A. 'Polyelectrolyte Multilayer Assemblies Containing Nonlinear Optical Dyes' *Macromolecules* **30** (1997) 8304-8309.
[22] W. Kern, *Semicond. Int*. **1984**, 94.
[23] R. M. Azzam and N. M. Bashara. "Ellipsometry and Polarized Light" Elsevier, N. Y. 1987
[24] Ivanova, M.; Arutyunvar, A.; Lomakin, A.; Noskin, V. 'Study of DNA Internal Dynamics by Quasi-Elastic Light Scattering' *Applied Optics* **36** (1997) 7657-7663
[25] Neyman, P.; Guzy, M.; Shah, S; Davis, R.; Van Cott, K.; Wang, H.; Gibson, H.; Brands, C.; Heflin, J. 'Second-Order Nonlinear Optical Responses of Ionically Self-Assembled Films: Polycation Variations and Dianionic Chromophores', *SPIE Proceedings*, **2001**, 4461, 214-226
[26] Manning, G. 'Limiting Laws and Counterion Condensation in Polyelectrolyte Solutions. IV. The Approach to the Limit and the Extraordinary Stability of the Charge Fraction.' *Biophysical Chemistry* **7** (1977) 95-102
[27] Fang, M.; Kim, C.; Saupe, G.; Kim, H.; Waraksa, C.; Miwa, T.; Fujishima, A.; Mallouk, T. 'Layer-by-Layer Growth and Condensation Recations of Niobate and Titanoniobate Thin Films'. *Chem. Mater*. **11** (1999) 1526-1532
[28] DeWitt, D.; Hammond, P. 'Controlling Orientation in Optically Active Multilayer Films' *Polymer Preprints*. **2000**, 41, 815-816
[29] Chou, P.; Scheraga, H. 'Calorimetric Measurement of Enthalpy Change in the Isothermal Helix-Coil Transition of Poly-L-Lysine in Aqueous Solution' *Biopolymers* **10** (1971) 657-680
[30] Shibata M.; Ihara, H.; Hirayama, C. 'Unique property of cyanine dyes on charged poly(L-lysine)' *Polymer*. **1993**, 34, 5, 1106-1108.
[31] Lvov, Y.; Yamada, S.; Kunitake, T. 'Non-linear Optical Effects in Layer-By-Layer Alternate Films of Polycations and an Azobenze-Containing Polyanion' *Thin Solid Films* **300** (1997) 107-112.
[32] Kunitake, T. 'Chemistry of Self-Assembling Bilayers and Related Molecular Layers' *MRS Bulliten* **20** (1995) 22-25.
[33] Advincula, R.; Fells, E.; Park, M. 'Molecularly Ordered Low Molecular Weight Azobenzene Dyes and Polycation Alternate Mulitlayer Films: Aggregation, Layer Order, and Photoalignment' *Chem. Mater*. **13** (2001) 2870-2878.
[34] Dante, S.; Advincula, R.; Frank, C.; Stroeve, P. 'Photoisomerization of Polyionic Layer-by-Layer Films Containing Azobenzene', *Langmuir* **15** (1999) 193-201.

7. The Role of Hydrogen Bonding and Polycation Structure on the Orienting of Chromophores in Electrostatic Layer-By-Layer Films

Abstract

Polycation structure is known to play a significant role in the orienting of a chromophore in films built in a layer-by-layer manner from alternately charged polyelectrolytes. Using PS-119 and poly(vinylpyridine)s it is demonstrated that the possibility of hydrogen bonding does not result in a regularly oriented film. The effect of spacing length between the charged amine group and the polymer backbone is examined through a series of films in which poly(allylamine hydrochloride), poly(vinylamine hydrochloride), chitosan and linear poly(ethylenimine) were used as the polycations. Layer-by-layer deposition was demonstrated for all four polycations, only PAH resulted in regular chromophore orientation. The precise ordering mechanism is not known; however, several possible sources are hypothesized.

Keywords

Hydrogen bonding, polycation structure, chromophore orientation, second order nonlinear optics

7.1. Introduction

The telecommunications industry relies on the conversion of electrical impulses to optic pulses for data transmission over fiber-optic cables. The next generation of electro-optic modulators will be constructed of second order nonlinear optic (NLO) materials for fast and efficient conversion. However, inorganic NLO materials such as lithium niobate ($LiNbO_3$) are difficult to fabricate and are prohibitively expensive. Polymeric materials offer benefits with both lower production costs as well as performance benefits. However, current polymeric fabrication techniques result in materials that are not suitable for applications.

The layer-by-layer ionically self-assembled monolayer (ISAM) technique is an alternate method to fabricate NLO materials. Heflin, et al. demonstrated that films made with the ISAM method involving NLO-active polyanions and an NLO-inactive polycation results in both regular layer-to-layer chromophore orientation and exceptional

thermal stability. Chapter 6 concerned films made with the poly-dye poly{1-[4-(3-carboxyl-4-hydroxyphenylazo)benzene sulfoamido]-1,2-ethandiayl, sodium salt} [PCBS] with three different polycations - polyallylamine hydrochloride (PAH), poly(diallyldiammonium chloride) [PDDA] and poly(l-lysine) [PLL]. Of these three polycations, only PAH demonstrated regular bulk orientation of the PCBS chromophores. The highest value of $\chi^{(2)}$ obtained occurred when the PAH and PCBS layers were deposited at pH 7, which resulted in thin, flat layers. These results suggested a possible relationship between chromophore orientation and hydrogen bonding since PAH could interact with PCBS electrostatically and by hydrogen bonding while PDDA could not hydrogen bond with PCBS. However, the precise mechanism that causes orientation is still not known. Additionally, through observations of film quality and dynamic light scattering, it was determined that dipping solutions of polymer aggregates led to optically inhomogeneous films unsuitable for EO devices.

To continue probing the sources of orientation in polymer-polymer ISAM films, further experiments were conducted in which additional polycations were studied for their ability to orient PCBS and the poly-dye PS-119. Poly(vinyl amine) [PVA], chitosan, and linear poly(ethylenimine) [PEI] were used to fabricate films with PCBS. To determine the role hydrogen bonding might play in the orientation of chromophores, films were fabricated using poly(4-vinylpyridine) and poly(4-vinyl-N, methylpyridinium iodide). The former is capable of forming hydrogen bonds with the chromophore while the latter is not.

7.2.**Experimental**

The NLO-active chromophores used in this study were poly{1-[4-(3-carboxyl-4-hydroxyphenylazo)benzene sulfoamido]-1,2-ethandiayl, sodium salt} [PCBS, Aldrich, lot DO 03912EW] and Poly S-119 [PS-119, Sigma, lot 85F3574]. Structures of these chromophore molecules are shown Figure 7.2-1. The characteristic absorbance peaks for these dyes were determined to be λ_{max}=359 nm for PCBS and λ_{max}=486 nm for PS-119. All absorbance measurements were made at the characteristic peak for the respective chromophore molecule. The NLO-inactive polycations used this study were poly(allylamine hydrochloride) [PAH, M_w ~ 70,000, Aldrich, lot 06305DI],

poly(vinylamine hydrochloride) [PVA, M_n ~ 25,000, Polysciences, lot 520947], linear polyethylenimine [PEI, MW ~ 25,000 Polysciences, lot 522113] poly(4-vinyl pyridine) [PVP, M_n=49,100, Polymer Source, sample # P1028-4VP], poly(4-vinyl-N-methylpyridinium iodide) [PVNMPI, M_n= 54,000, Polymer Source, sample #P231-4VPQ] and chitosan (M_w ~ 140,000, 95% degree of deacetlyation, Dalwoo-chitoSan, Korea). The structures of PAH, PVA, PEI and chitosan are shown below in Figure 7.2-2. PAH has a pKa of 8.7[1], chitosan has a pKa of ~ 6.5[2] while PEI has a pKA ~ 4.8[4]. An explicit value of the pKa of PVA is not reported in the literature; however, titration results show that 50% of the polymer is charged at a pH of 5.5.[3] Structures for PVNMPI and PVP are shown in Figure 7.2-3. All materials were used as received without further purification. The PAH, PVA and PVNMPI are readily soluble in water. Solutions of PVP and PEI were prepared stirring while heated with 0.1 M HCl being added periodically following the procedure of Hammond until the solution was clear.[4]

Deionized water was obtained with an ion exchange unit (Barnstead Nanopure II) and maintained a specific resistivity above 17 MΩ•cm. Fisherfinest glass microscope slides (Fisher Scientific) were used as the substrates on which films were deposited. They were prepared using the RCA cleaning procedure[5] in which the substrates were immersed in a solution of H_2O, H_2O_2, and NH_4OH at 70°C for 20 minutes. The slides were then rinsed and placed in an acid bath consisting of concentrated HCl, H_2O_2 and H_2O for 20 minutes and were then rinsed and baked at 130°C for at least one hour.

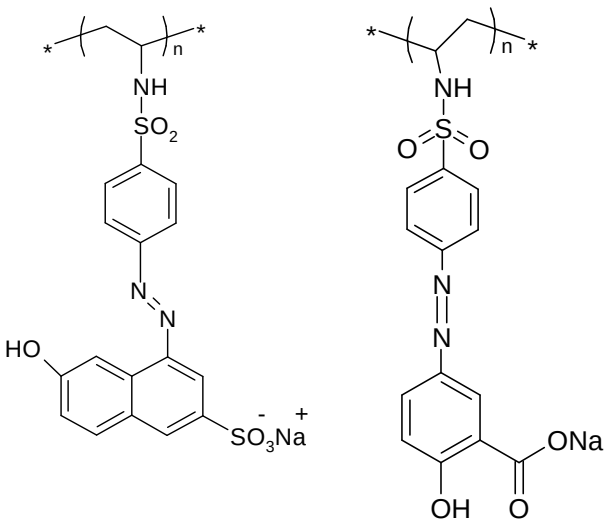

Figure 7.2-1 - Structures of the anionic chromophores, PS-119 and PCBS, used in this study

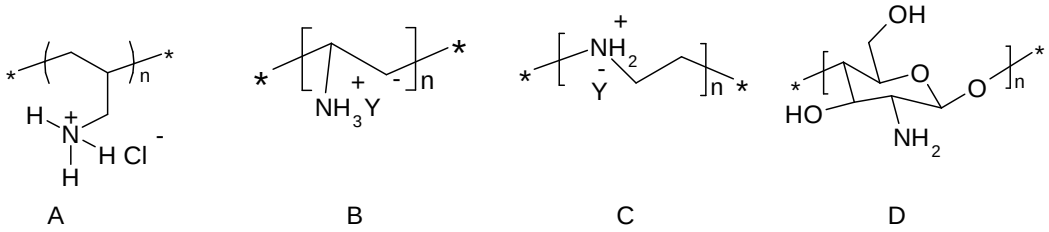

Figure 7.2-2 - Structures of the polycations (a) PAH, (b) PVA, (c) PEI, and (d) chitosan

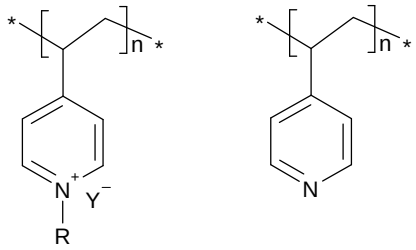

Figure 7.2-3- Structures of poly(4-vinyl-N-methyl-pyridinium iodide) and poly(4-vinylpyridine)

7.2.1. **Film Deposition**

Polymer solutions at a concentration of 10 mM on a monomer basis were used in all experiments. Deposition pH values were chosen based on the pKa of the polycation, with an attempt to ensure that the polymers were sufficiently charged in solution to support layer-by-layer growth. Table 7.2-1 summarizes the polycation pH conditions where deposition was done and shows the pH where the polycations are 50% charged.

Table 7.2-1- pH conditions for Polycation Deposition and the pH at which the polycations are 50% ionized. PVNMPI is a quaternary amine, and is charged at all pH conditions.

Polycation	pH at 50% Ionization	Deposition pH
PAH	8.7[1]	7.0
PVA	~5.5[3]	7.0
PEI	~4.8[4]	3.5; 4.25
Chitosan	6.5[2]	6.0
PVP	~4[6]	3.0; 4.0
PVNMPI	N/A	3.0; 4.5

The pHs of polymer solutions were adjusted using HCl or NaOH as needed. pH values were typically constant to ± 0.1 pH units over the course of the deposition. The glass slide immersion time in polycation was 5 minutes, with the exception of the first layer, which was 10 minutes. The immersion time in the dye solutions was 5 minutes. Between immersions, the substrates were vigorously agitated and rinsed with deionized water. Slides were dried every 10 dips (which gives 5 bilayers on each side of the slide, hence 10 total bilayers) using N_2 gas.

7.2.2. **Film Characterization**

Absorbance measurements were made with a Milton Roy Spectronic 1201 spectrophotometer at the characteristic wavelength for a given chromophore and were taken every 10 bilayers during the deposition process. Upon the completion of dipping for a given slide, 5 absorbance measurements were made along the length of the slide to characterize the homogeneity in the final absorbance value. Film thicknesses were measured using a variable angle spectroscopic ellipsometer (J. A. Woolam Ellipsometer VB-200, running WVASE 32 Version 3.361). The amplitude factor ψ and phase factor Δ which are related to the complex Fresnel coefficients for any given film, were measured for wavelengths from 350 to 800 nm at 10 nm intervals.[7] This wavelength range was repeated for angles ranging from 55° to 75° in 5° intervals. Measurements were made on the smooth side of the frosted region of the slide, as the scattering caused by the etching eliminates backside reflections simplifying data analysis. A Lorenz oscillator model was used to analyze the ellipsometric data. Complete details on the ellipsometric modeling are found in Appendix A. Least squares analysis was used to determine the slope in absorbance vs. bilayer number graphs. The average of slopes determined from 20, 40, and 60 bilayer films is reported as the slope in various tables.

SHG measurements were performed by Prof. J. R. Heflin's group in the Department of Physics at Virginia Tech group with a standard setup using a 10-nanosecond pulse width, Q-switched Nd:YAG laser with a fundamental wavelength of 1064 nm.[8] The SHG data were averaged over 100 shots per data point, and the uncertainty in relative $\chi^{(2)}$ values is 10%. Typical spot radius and pulse energy values were 30 μm and 7 mJ/pulse, respectively. The film was deposited on both sides of the

substrate. As a result, as the sample is rotated with respect to the incident beam, the path length between the film on opposite sides is varied, leading to interference fringes of the SHG intensity. The sample was rotated from 30° to 60° away from normal incidence using a stepper motor controlled rotation stage. The $\chi^{(2)}$ value is determined from the peak of the interference fringe in the vicinity of 45º. By comparison to Maker fringes in a quartz crystal wedge, and a 68 bilayer PS-119 / PAH ISAM film, $\chi^{(2)}$ of a film is obtained from

$$\frac{\chi^{(2)}_{film}}{\chi^{(2)}_{q}} = \frac{2}{\pi}\frac{l_{c,q}}{t_{bilayer}}\frac{m}{\sqrt{I^{2\omega}_{q}}}\sqrt{\frac{I^{2\omega}_{standard,quartz}}{I^{2\omega}_{standard,film}}} \tag{7.1}$$

where $t_{bilayer}$ is the bilayer thickness, m is the slope of the square root of the second harmonic intensity vs. number of bilayers plot, $I^{2\omega}_{q}$ is the intensity of the second harmonic for the quartz standard, $I^{2\omega}_{standard,quartz}$ is the second harmonic intensity for the 68 bilayer standard measured at the same time as the quartz standard, $I^{2\omega}_{standard,film}$ is the second harmonic intensity for the 68 bilayer standard measured at the same time as the films for which $\chi^{(2)}$ is being calculated, l_{film} is the total path length through the film, the coherence length of quartz, $l_c = \lambda / 4(n^{2\omega}-n^{\omega})$, is 22.4 μm, and $\chi^{(2)}$ of quartz is 1.92×10^{-9} esu. Propagation of the errors on thickness, $t_{bilayer}$, and slope m, result in the error for $\chi^{(2)}$ by

$$\sigma^2_{\chi} = \frac{a^2}{t^2_{bilayer}}\sigma^2_{m} + \frac{a^2 m^2}{t^4_{bilayer}}\sigma^2_{t} \tag{7.2}$$

where a is a constant defined as:

$$a = \chi^{(2)}_{q}\frac{2}{\pi}\frac{l_{c,q}}{\sqrt{I^{2\omega}_{q}}}\sqrt{\frac{I^{2\omega}_{standard,quartz}}{I^{2\omega}_{standard,film}}} \tag{7.3}$$

Details of the derivation of this equation are shown in Appendix B.

Bilayer numbers for absorbance and SHG measurements account for the film on both sides of the substrate while ellipsometry measurements were made using the film deposited on one side of the substrate.

7.3.**Results**

Successful layer-by-layer deposition is characterized by a linear increase in the absorbance with the number of layers deposited. An example for PEI and PCBS is shown below in Figure 7.3-1. The slope of the line, the absorbance per bilayer, characterizes the amount of chromophore deposited per cycle.

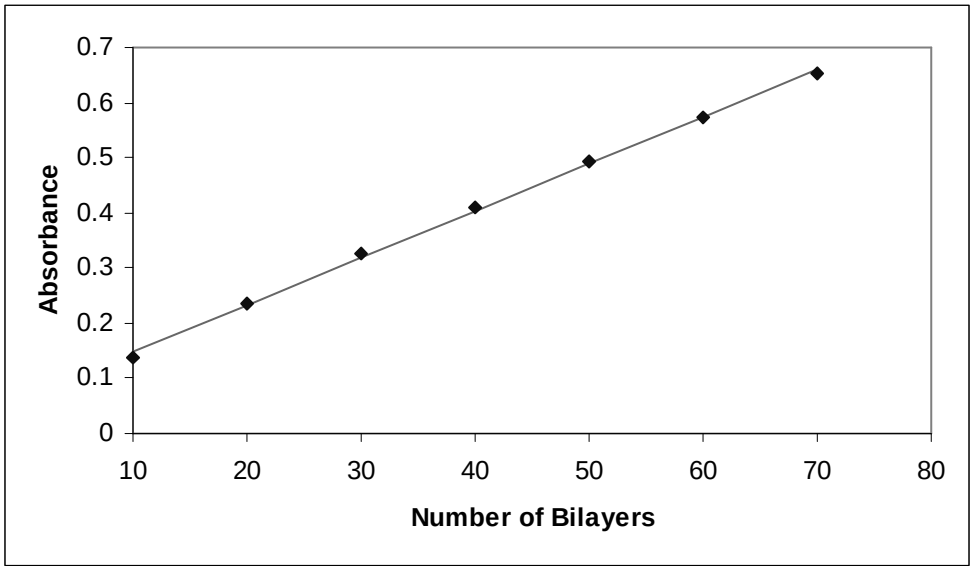

Figure 7.3-1 – Absorbance as a function of the number of bilayers deposited for films fabricated from 10mM PEI pH 4.25 and 10 mM PCBS pH 6.0 solutions.

Table 7.3-1 contains the results of deposition experiments conducted with PVNMPI and PVP. Deposition experiments were conducted with both PCBS and PS-119. Film formation did not occur in the PVP pH 4.4 / PCBS pH 6.0 case likely due to insufficient charging of the previously deposited PVP layer in the pH 6.0 PCBS solution. The results of the second harmonic generation analysis on the PS-119 films are shown below Figure 7.3-2. The films made using PVNMPI displayed quadratic scaling of the second harmonic, while those made with PVP did not. The absorbance spectra for these films were measured from 430 nm to 530 nm in order to search for any evidence of blue or red-shifts, which would suggest the formation of J- or H-aggregates in the film. However, for both polycations, the absorbance maxima did not indicate these shifts. The PVNMPI / PS-119 film had a $\chi^{(2)}$ value of 2.7 x 10^{-9} esu while the PVNMPI / PCBS film had a $\chi^{(2)}$ of 7.9 x 10^{-9} esu.

Table 7.3-1- Deposition summary for films made with PVNMPI and PVP as the polycation. PCBS or PS-119 were used as the NLO active cationic poly-dyes. All polymer solutions were at 10 mM RU.

Polycation / pH	Poly-dye / pH	Absorbance/ Bilayer	Bilayer Thickness (nm)	Absorbance / nm	$\chi^{(2)}$ (10^{-9} esu)
PVNMPI / 4.5	PCBS / 6.0	0.0071 ± 0.0001	0.25 ± 0.01	0.028	7.9
PVNMPI / 3.0	PS-119 / 3.0	0.0082 ± 0.0003	0.72 ± 0.03	0.011	2.7
PVP / 4.4	PCBS / 6.0	N/A	-	-	-
PVP / 3.0	PS-119 / 3.0	0.0109 ± 0.0004	1.12 ± 0.04	0.010	-

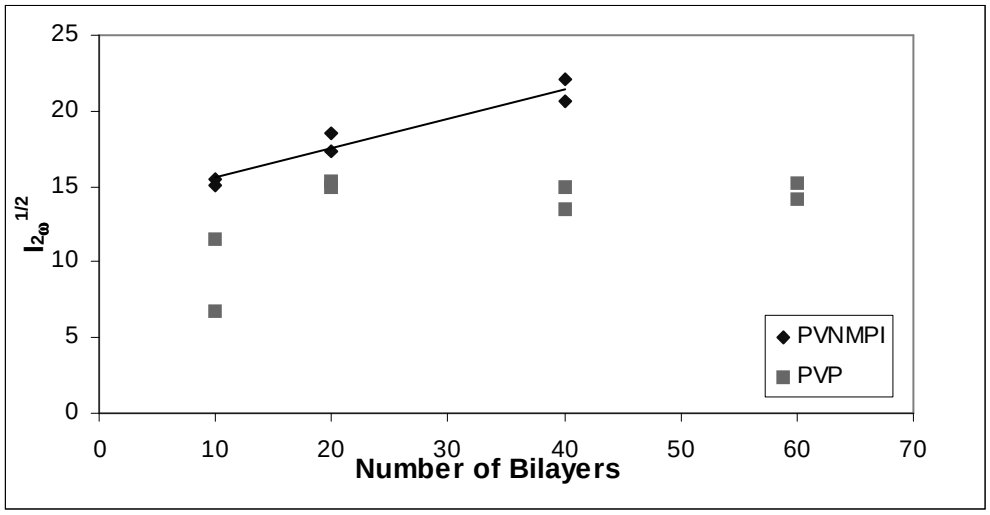

Figure 7.3-2 - Scaling of the square root of the second harmonic intensity as a function of the number of bilayers deposited for films made with PS-119 at a pH of 3 as the NLO-active component. PVNMPI and PVP were used as the optically inactive polycations (10 mM RU, pH 3)

Values for the absorbance per bilayer and film thickness values are shown below in Table 7.3-2 for films made with PAH, PVA, PEI and chitosan with PCBS. As the table shows, the greatest amount of deposition occurred with PEI at a pH of 4.25. The PEI pH 3.5 case did not display layer-by-layer growth, most likely due to insufficient charge density on the previously deposited PCBS layer while exposed to the pH 3.5 environment.

Table 7.3-2 – Summary of Deposition Results for PCBS. All polymer solutions at a concentration of 10mM on a RU basis.

Polycation	Polycation pH	PCBS pH	Absorbance / Bilayer	Bilayer Thickness (nm)	Absorbance / nm
PAH[1]	7.0	7.0	0.0050 ±0.0010	0.28 ± 0.05	0.018
PVA	7.0	7.0	0.0059 ± 0.0002	0.19 ± 0.03	0.031
PEI	4.25	6.0	0.0086 ± 0.0005	0.25 ± 0.04	0.034
PEI	3.5	7.0	N/A[2]	-	-
Chitosan	5.0	6.0	0.0057 ± 0.0002	0.18 ± 0.04	0.032

[1] Data for PAH taken from Chapter 6

[2]Layer-by-layer deposition not observed

The results of the SHG analysis are shown below in Figure 7.3-3. The square root of the second harmonic intensity is shown as a function of the number of bilayers for films made with PVA, PEI and PAH. The results of PVA, PEI, and chitosan do not show a linear increase, signifying that the PCBS chromophores are not regularly oriented in these films. As seen from Chapter 6, the PAH series do show the linear scaling, which resulted in a $\chi^{(2)}$ of 9.1 x 10^{-9} esu.

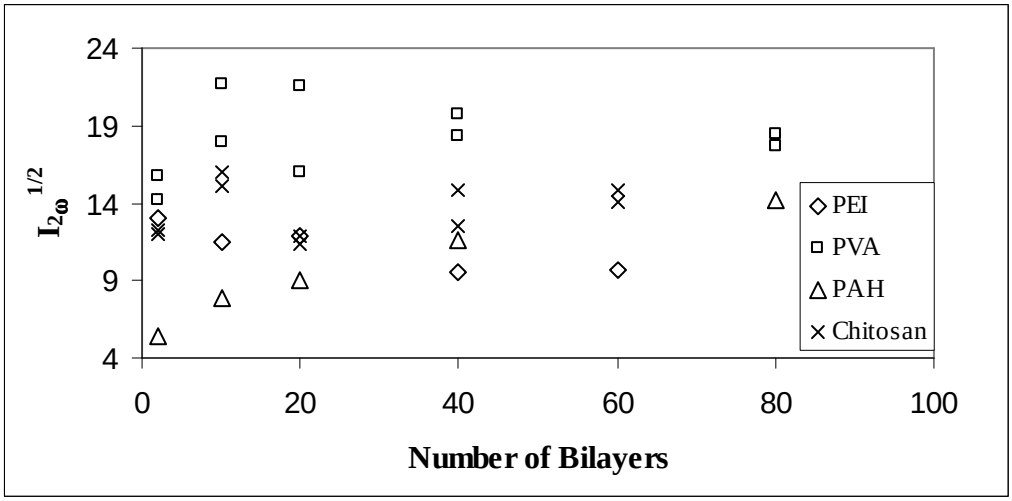

Figure 7.3-3 – Results of the SHG measurements for films made with PEI, PVA and PAH as the NLO inactive polycations with PCBS as the polydye. Films fabricated at the conditions given in **Table 7.3-2**.

7.4.**Discussion**

7.4.1. **Role of Hydrogen Bonding in Chromophore Orientation**. The previous study in Chapter 6 that compared films made with PAH, PDDA, and PLL

suggested that the combination of electrostatic and hydrogen bonding interactions might be necessary for orienting the chromophore, PCBS. PAH, which is capable of forming hydrogen bonds, oriented the PCBS chromophore, while PDDA, which cannot hydrogen bond, did not orient the chromophores. PLL, which has more than one hydrogen-bonding site, also did not orient the chromophores. To determine the role hydrogen bonding plays in chromophore orientation, two structurally similar polycations were employed, one that was capable of forming hydrogen bonds with the chromophore and one that could not. The tertiary amine in PVP is capable of hydrogen bonding and the amine is 50% ionized at a pH of approximately 4.[6] However, the quarternary ammonium moiety in PVNMPI is capable of only forming weak hydrogen bonds. Films were first fabricated using PCBS as the polycationic chromophore. However, due to solubility problems, it was not possible to fabricate PVP / PCBS films. Under pH conditions where the PCBS was soluble (pH > 5.0) the charge density on previously deposited PVP layers was not sufficient to support regular layer-by-layer growth. To overcome this effect, the polycationic dye PS-119 was utilized. Due to its sulfonate group, which is highly charged at all pHs used in this study, the dye is markedly more soluble than PCBS at low pH values, which allowed for deposition to proceed. Table 7.3-1 shows that when PS-119 was deposited at a pH of 3, regular layer-by-layer growth occurred with both PVP and PVNMPI. However, the PVP films had a greater deposited amount per bilayer than the PVNMPI films as reflected by the higher absorbance per bilayer. The chromophore densities in the film (absorbance / nm) were roughly equal due to the PVP / PS119 bilayers being thicker than the PVNMPI / PS119 bilayers. However, from the standpoint of film thicknesses the PVNMPI / PS-119 and PVP / PS-119 films are significantly thicker than the pH 7.0 PCBS films. It is possible that the more highly ionized sulfonate group in PS-119 might have led to greater polycation deposition than was the case for the more weakly ionized PCBS.

The results of the NLO analysis, shown in Figure 7.3-2 show that PVP did not result in regularly oriented films of PS-119. Instead, the intensity of the second harmonic reached a plateau after 20 bilayers, despite the absorbance readings showing that layer-by-layer deposition continued well after the second harmonic intensity leveled off. This plateau indicates that there is no bulk orientation in these films. The SHG intensity was

most likely affected by the impenetrable glass interface. This intefacial effect has been probed most carefully in a recent study by Brands.[9] PVNMPI, which was not a strong hydrogen bonding molecule, showed regular layer-by-layer orientation of the PS-119 chromophores. However, the behavior seen for PVNMPI is not mirrored in other quaternary ammonium salts, such as PDDA. While films of PVNMPI / PCBS were oriented and had a measurable $\chi^{(2)}$ of 7.9 X 10^{-9} esu, films made with PDDA / PCBS did not display bulk scaling. The deposition process for PVNMPI / PCBS resulted in a higher absorbance / bilayer (0.0071 for PVNMPI / PCBS vs. 0.003 for PDDA / PCBS) and bilayer thickness (0.25 nm for PVNMPI / PCBS vs. 0.16 nm for PDDA / PCBS) than PDDA / PCBS. The precise reason that the PVNMPI / PCBS films showed bulk scaling while the PDDA / PCBS films did not is unclear. The $\chi^{(2)}$ value obtained for PVNMPI / PCBS is experimentally not significantly different than that obtained for PAH / PCBS ($\chi^{(2)}$ = 9.1 x 10^{-9} esu).

However, one result that can be drawn is that hydrogen bonding between the polycation and a polymeric dye with a pendant charged chromophore is not necessary for chromophore orientation. In a given system, such as PAH / PCBS, hydrogen bonding may play a role, but it is not a necessity for orientation to occur.

7.4.2. **PAH / PVA / PEI / Chitosan**

The other facet of this series involves the formation of films using the structurally similar polycations PAH, PVA, PEI and chitosan. The primary amine on PAH is separated from the polymer backbone by one methylene unit while the primary amine on PVA is directly connected to the vinyl backbone. In PEI, the secondary amine is incorporated into the polymer backbone while, in chitosan, the primary amine is connected to the glucosidic backbone. All four polymers are capable of forming hydrogen bonds with the carboxyl group on PCBS. At pH 7, the PAH is highly charged, resulting in flat, thin layers.[4] The ionization behavior of PEI explains why deposition did not occur in the PEI pH 3.5 / PCBS pH 7.0 case: at a pH of 3.5, the previously deposited PCBS layer is so weakly charged that the amount of PEI that is absorbed is not sufficient to support layer-by-layer growth.[4] However, when the deposition is performed with the PEI at 4.25 and the PCBS at a pH of 6, the charge densities of both materials were high enough to support layer-by-layer growth. The greatest amount of deposition as

characterized by absorbance / bilayer occurred for PEI at a pH of 4.25 while the absorbance / bilayer of PAH, PVA and chitosan were roughly equivalent. The PAH films were the thickest which resulted in the lowest chromophore density (as implied by the absorbance / nm) of any of the films examined in this study. The PEI films had the highest chromophore density seen; however the Abs/nm values are all quite similar for the deposition of PCBS with PVA (Abs /nm =0.031), PVNMPI (Abs/nm =0.028) and PEI (0.034). The PVA and PEI films fabricated for this study had higher deposited amounts than the PDDA pH 7.0 (absorbance / bilayer = 0.003 ± 0.0002) and PLL pH 7.0 (absorbance / bilayer = 0.004 ± 0.001) films discussed in the previous chapter. The bilayer thicknesses for PVA (0.19 ± 0.03 nm) and PEI (0.25 ± 0.04 nm) are slightly thicker than those observed for PDDA pH 7 (0.16 nm) and PLL (0.15 ± 0.01 nm)

The results of the SHG experiments show that PAH is the only of these 4 polycations capable of supporting regular layer-by-layer chromophore orientation. The square root of the second harmonic intensity for PEI quickly reached a plateau and did not increase as additional layers of material were deposited. Films made with PVA showed an increase in the SHG intensity over the first few layers. However a regular increase in the intensity was not observed. The fact that PAH can orient the PCBS chromophores while PVA cannot is a relatively unexpected finding. The difference between the two polymers is simply the additional methylene group that separates the amine functionality from the polymer backbone in PAH. At this point, it is clear that electrostatic effects alone are not capable of orienting a charged pendant chromophore molecule. In fact, if electrostatic effects were the orienting factor, one would expect the levels of orientation obtained for PVA and PEI to be greater than those observed for PAH due to the position of the charged amine being more closely correlated to the position of the polymer backbone. The results obtained in this and the previous study imply that the chromophore orienting capability of PAH may be due to some combination of hydrophobic and steric effects.

Hammond suggests that secondary interactions, such as hydrophobic interactions may play significant roles on the structure of layer-by-layer films.[4] Using a substrate that was patterned with areas containing carboxylic acid (COOH) or oligoethylene glycol (EG) functionalities, layer-by-layer films were deposited using polyacrylic acid and one

of two polycations. PAH, described as a “hydrophobic” polyelectrolyte and PEI, described as a “hydrophilic” polyelectrolyte were deposited at pH 4.8where the PEI was ~50% charged and the PAH was ~95% charged. The hydrophobic PAH showed selective adsorption on the regions of the substrate patterned with EG, which was also described as “hydrophobic”. Hydrogen bonding may also play a role as PAH is capable of hydrogen bonding with the EG. The hydrophilic PEI preferentially deposited on areas of the substrate with the hydrophilic COOH functionality. If electrostatic interactions were the only forces driving deposition, this selectivity in deposition would not have been observed. In the present experiments, it is possible that the electrostatic interaction between PAH and PCBS creates a small hydrophobic complex that helps orient the chromophore in a way not possible with the less hydrophobic PVA. The secondary amine found in PEI may interact differently with the PCBS chromophore compared to the primary amine found in PAH, again preventing orientation.

Steric effects may be significant for the simple reason that, for PEI and PVA, the amine group is closer to the polymer backbone whereas in PAH the amine group is farther away from the backbone. In PEI and PVA, the relatively large chromophore molecules may be prevented from interacting with the amine groups due to the presence of the backbone. However, the amine group in PAH may be capable of orienting themselves in a position relative to the backbone that would allow for interactions to occur, potentially resulting in regular orientation. It is important to note that for all three polycations, PAH, PEI and PVA, the charged amine was sufficiently accessible to allow layer-by-layer deposition to occur.

7.5.**Conclusions**

The origins of chromophore orientation in layer-by-layer films made with charged polymers are still unknown. Electrostatic interactions certainly play an essential role in driving layer-by-layer film formation. As demonstrated by the PVP / PVNMPI series with PS-119, strong hydrogen bonding is not a prerequisite for a system to display regular layer-by-layer orientation of the chromophore molecules. The only polycations found so far that can orient an NLO polydye are PAH and PVNMPI in which the charged groups are separated from the backbone by ~ 0.25 nm for PAH and ~0.4 nm for PVNMPI. The results from the films made with PCBS and the polycations PAH / PVA /

PEI suggest that a very subtle change in polycation structure can have a significant effect on the capacity for a polycation to orient a chromophore such as PCBS. Most surprising is the comparison between PAH and PVA, in which the difference of a methylene unit between the backbone and amine group makes the difference between whether regular layer-by-layer chromophore orientation is achieved or not. The hydrophobicity of each polycation will be different and this may play a role. However, the precise mechanism remains a mystery. Future work planned to unravel this mystery includes synthesizing a polycation with two methylene units between the charged group and the polymer backbone. Molecular modeling could be used to probe any steric effects that may be interfering with orientation.

---

[1] Fang, M.; Kim, C.; Saupe, G.; Kim, H.; Waraksa, C.; Miwa, T.; Fujishima, A.; Mallouk, T. 'Layer-by-Layer Growth and Condensation Recations of Niobate and Titanoniobate Thin Films' *Chem. Mater*. **11** (1999) 1526-1532

[2] Strand, S.; Tommeraas, K.; Varum, K.; Ostgaard, K. 'Electrophoretic Light Scattering Studies of Chitosans with Different Degrees of N-acetylation' *Biomacromolecules*, **2** (2001) 1310-1314

[3] Polymeric Maters Encyclopedia, Vol 9. CRC Press, 1999, 7095

[4] Clark, S.; Hammond, P. 'The Role of Secondary Interactions in Selective Electrostatic Multilayer Deposition' *Langmuir*, **16** (2000) 10206-10214

[5] Itano, M.; Kern, F.; Miyashita, M.; Ohmi, T. 'Particle Removal from Silicon Water Surface in Wet Cleaning Process' *IEEE Trans. on Semicond. Manu*. **6** (1993) 258-267.

[6] Mika, A.; Childs, R. 'Acid / Base Properties of Poly(4-vinylpyridine) Anchored with Microporous Membranes' *Journal of Membrane Science* **152** (1999) 129-140.

[7] R. M. Azzam and N. M. Bashara. "Ellipsometry and Polarized Light" Elsevier, N. Y. 1987

[8] Neyman, P.; Guzy, M.; Shah, S.; Davis, R.; Van Cott, K.; Hang, W.; Gibson, H.; Brands, C.; Heflin, J. 'Novel Hybrid Covalent / Ionic Self-Assembly Techniques for Improved Second-Order Nonlinear Optical Films' *Mat. Res. Soc. Symp. Proc* **708** (2002) 161-166.

[9] Charles Brands. 'Second Order Nonlinear Optics in Ionically Self-Assembled Thin Films' Dept. of Physics, Thesis, Virginia Tech, 2003.

8. Conclusions and Future Work

8.1. Conclusions

This project sought to develop second order nonlinear optic (NLO) materials via layer-by-layer deposition mechanisms. Three specific research objectives were set forth:

1) Develop a hybrid deposition scheme that relies on both electrostatic interactions and covalent bonds for building layer-by-layer films
2) Probe the sources of chromophore orientation in ISAM Films
3) Determine the process variables needed to make 1-10 μm thick NLO active films with necessary optical clarity.

The progress made towards each of these goals is discussed below.

8.1.1. Hybrid Deposition

Using a layer-by-layer approach that utilizes both electrostatic interactions and covalent bonds, the deposition of oriented materials has been demonstrated. The initial study used the chromophore Procion Red MX-5B as the NLO active material. This dye molecule has two negatively charged sulfonate groups and a reactive triazine ring. The polymer poly(allylamine hydrochloride) [PAH] was used both as the polycation for electrostatic binding and as a source for amine groups with which to couple to the dye's triazine ring. The highest value of $\chi^{(2)}$ was 11.3 x 10^{-9} esu when the Procion Red was deposited at a pH of 10.5 and the PAH was deposited at pH 7.0. This was the first demonstration of covalent deposition resulting in layer-by-layer films with bulk polar ordering of an NLO-active chromophore.

With the proof-of-concept demonstrated, the effects of other factors on $\chi^{(2)}$ could be explored. For traditional films formed from oppositely charged polyelectrolytes, the ionic strength of the dipping solutions plays a significant role in film formation. Given that electrostatic interactions are required for hybrid deposition, it was reasonable to expect that changing the ionic strength of the Procion dye dipping solution could effect the $\chi^{(2)}$ of the film and so the effect of ionic strength on deposition and chromophore ordering was investigated. Additionally, the versatility of the hybrid deposition approach was demonstrated by depositing films with three different Procion chromophores – Procion Red MX-5B, Procion Orange MX-2R and Procion Brown MX-GRN. From the

structures of these three dyes, it was expected that Procion Brown would have the highest hyperpolarizability value with Procion Red having the lowest. For films made under the no salt condition with PAH, the same ordering was observed for $\chi^{(2)}$ with Procion Brown having the highest values while Procion Red had the lowest. For all three cases, PAH was used as the polycation / amine source. For all three chomophores, increasing the ionic strengths of the dipping solutions increased the amount of material deposited per bilayer. This is likely due to increased shielding of the electrostatic repulsions between neighboring dye molecules as the ionic strength increases, which allows for denser packing of the chromophore molecules on the previously deposited amine layer. Of the two dyes that made optically clear films sufficient for NLO testing, different trends in $\chi^{(2)}$ with ionic strength were observed. Procion Red films showed no discernable dependence on ionic strength, and exhibited $\chi^{(2)}$ values ranging from $6.9 \pm 1.1 \times 10^{-9}$ esu to $8.7 \pm 1.2 \times 10^{-9}$ esu. However, films made with Procion Brown showed a strong dependence of $\chi^{(2)}$ on the ionic strength of the dye dipping solution. As the concentration of added NaCl increased from 0 to 0.5 M, the $\chi^{(2)}$ increased from $50.2 \pm 1.6 \times 10^{-9}$ esu to $87.5 \pm 2.3 \times 10^{-9}$ esu. As the salt concentration increased from 0.5 M to 1.0 M the $\chi^{(2)}$ fell to $67.6 \pm 2.5 \times 10^{-9}$ esu. For comparison the $\chi^{(2)}$ value for quartz is 1.9×10^{-9} esu and the value of $\chi^{(2)}$ for lithium niobate is $\sim 200 \times 10^{-9}$ esu.

Polarization anisotropy was used to probe the orientation of the chomrophores in the Procion Brown films. As the salt concentration increased from 0 to 0.5 M NaCl, the mean tilt angles decreased by about 5°. However, as the salt concentration increased from 0.5 M to 1.0, the mean tilt angle increased by about 2°. The change in $\chi^{(2)}$ that is observed for the Procion Brown salt series is most likely due to a combination of the changing chromophore density and the changing tilt angle. Films made with Procion Orange were not of sufficient quality to warrant detailed study.

8.1.2. **Probe the Sources of Chromophore Orientation in ISAM Films**

The role polycation structure plays in both film formation and chromophore orientation was probed for Procion Red and Procion Brown using the hybrid deposition approach. In addition, the effect of polycation structure on chromophore orientation in polyer-polymer ISAM films was also studied.

Deposition experiments were conducted using poly(vinylamine hydrochloride) [PVA], poly(ethylenimine) and chitosan. Previous work had established that PAH could be used to fabricate oriented films with both of these chromophores. The most significant finding of this study is that polycation structure dramatically affects both layer-by-layer deposition and chromophore orientation. Procion Brown was incapable of forming layer-by-layer films with both PEI and chitosan. This is most likely due to steric effects limiting the accessibility of the amine groups for covalent coupling. This steric effect also depends on the chromophore used in the study, as Procion Red was capable of layer-by-layer deposition with PEI while Procion Brown was not. Both the PEI / PR films and the PVA/PB films showed indications of regular layer-by-layer orientation, but the $\chi^{(2)}$ were 93 % lower than those achieved where PAH was the optically inactive constituent.

The role of the polycation in orienting a chromophore has been more thoroughly examined for traditional polymer-polymer ISAM films were electrostatic interactions were the principle interaction assembling the films. Regular layer-to-layer chromophore orientation does not occur in every case where layer-by-layer deposition occurs. Films were made with the poly-dye PCBS, a vinyl backbone with a pendent charged chromophoric side group, and three polycations – PAH, poly(diallyldimethylammonium chlroide) [PDDA] and Poly(l-lysine) [PLL]. Regular layer-by-layer deposition occurred in all three cases. However, only PAH oriented the PCBS chromophores. Using the polymeric dye PS-119, hydrogen bonding does not appear to be the orienting interaction by comparing films made with poly(4-vinylpryridine) (PVP), which is capable of forming hydrogen bonds with the PS-119 chromophore, to films made with poly(vinyl-N-methyl-pyridinium iodide) (PVNMPI), which forms weak hydrogen bonds. The PVNMPI / PS-119 films displayed regular chromophore orientation while the PVP / PS-119 films did not.

The effect of changing the spacing between the charged group and the polymer backbone was studied using PAH, PVA and PEI. In PAH the primary amine is separated from the backbone by the presence of a methylene unit. The primary amine in PVA is directly connected to the polymer backbone. PEI consists of a secondary amine in the polymer backbone. Of these three polycations, only PAH orients the PCBS

chromophore. One theory is that there are hydrophobic interactions occurring between the PAH and PCBS that cannot occur between the other polycations and PCBS.

8.1.3. **Determine the process variables needed to make 1-10 micron thick NLO active films with necessary optical clarity**

The most important concern in making optically clear films is ensuring that all components being used are not aggregated in solution. For polymer-polymer ISAM films optically heterogeneous films resulted when the polymers were aggregated in solution, as indicated by a large hydrodynamic radius as measured by dynamic light scattering [DLS]. DLS also indicated that Procion Orange was aggregated in solution. All films made with the Procion Orange chromophore showed significant streaking and optical inhomogeneities.

8.2.**Future Work**

The best $\chi^{(2)}$ value obtained in this work was $87.5 \pm 2.3 \times 10^{-9}$ obtained for PAH deposited at pH 7.0 and Procion Brown with 0.5 M NaCl at pH 10.5. This $\chi^{(2)}$ is sufficiently high to warrant use of the automated dipper to make a thick film (1-10 μm) that would be suitable for fabricating a prototype electro-optic modulator. However, before that is done there are several additional items to explore.

One of the first tasks to complete is to determine the electro-optic coefficient, r_{33}, for Procion Brown / PAH films. Despite having a lower $\chi^{(2)}$ than lithium niobate as measured by second harmonic generation, the lower refractive index of the Procion Brown / PAH films may result in these films having better performance as switching devices. If the results of the 0 M NaCl condition are promising, the 0.5 M NaCl condition should also be measured for r_{33}. This will provide a basis from which to decide which condition would be best for continued study.

A great deal of information regarding deposition can be garnered from in-situ second harmonic generation experiments. The technique has already provided some early insights into the kinetics of film formation. The effects of dye concentration, diffusion, and convection on the time required for film formation should be thoroughly examined. Given the average thickness of a bilayer, a great number of these layers will need to be deposited to get a film of sufficient thickness for a device. If the average bilayer

thickness was 0.75 nm, ~ 1300 bilayers would be needed to obtain a total film thickness of 1 μm. Neglecting the time needed to rinse the films, at current deposition times, a 1300 bilayer film would take over 9 days to deposit. If the time required to deposit one layer can be further reduced, the total time needed for fabricating a thick film will be significantly reduced. Reducing the time needed to thick film fabrication would also reduce the amount of Procion dye needed to make the film. Due to hydrolysis, the dye will need to be replaced over the course of the deposition process, providing another reason to better understand the kinetics of deposition.

A quartz crystal microbalance (QCM) is another tool for measuring the kinetics of deposition. Instead of observing deposition through monitoring the SHG, the actual mass of material deposited on the substrate could be measured. Developing this technique would be useful as it would also allow the kinetics of deposition to be observed for the optically inactive polycation.

The thermal stability of films made *via* the hybrid deposition approach needs to be explored. While PAH / PS-119 films made years ago have maintained the same level of orientation, there is no indication as to the thermal stability of films made via hybrid deposition. The thermal stability of a PS-119 / PAH film was tested by in-situ heating of the film during a second harmonic generation experiment. This method of testing the thermal stability should certainly be used. A second method would be dielectric spectroscopy; however, care will have to be taken to eliminate parasitic capacitances during sample preparation to obtain accurate results. The potential insights into how chromophore orientation is lost and the ability to identify specific transitions, such as the β and γ transitions, may outweigh the difficulties in developing this technique. Without questions regarding stability answered, it is unclear if the hybrid deposition method is a viable route to fabricating films for devices. If there are any losses of orientation as the result of either time or thermal effects, crosslinking of the films is one route to try to offset these losses. NEXAFS and linear dichromism are two other techniques that warrant additional study.

If hybrid deposition results in thermally/temporally stable films, the design and synthesis of a custom chromophore will be likely be required to fabricate films with $\chi^{(2)}$ values higher than those of lithium niobate. The structure of a potential custom

chromophore designed by Dr. Harry Gibson in the Department of Chemistry is shown in Figure 8.2-1. The findings of the studies contained in this document have highlighted several important design concerns. Most importantly, the chromophore must be highly soluble, so as to avoid aggregating, which results in optically heterogeneous films. Secondly, the specific interaction of a chromophore with a polycation like PAH should be considered. There are no guarantees that PAH, despite its proven track record of both being capable of supporting layer-by-layer deposition and resulting in regular chromophore orientation, will be the best polycation for use with this chromophore. Molecular modeling of the "docking" of a reactive chromophore molecule to a polycation site may provide insight as to whether a chromophore / polycation pair would be capable of supporting layer-by-layer deposition.

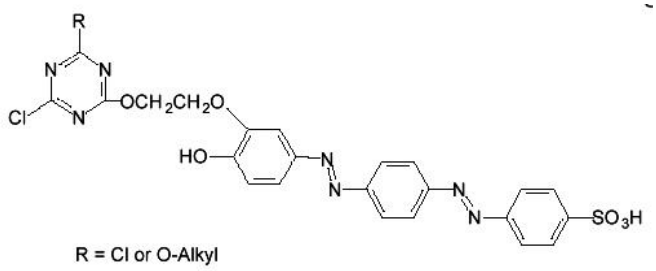

Figure 8.2-1 - Potential structure for custom synthesized chromophore molecule.

The synthesis of a new polycation may provide additional insight into the orientation mechanism at work in these layer-by-layer films. The separation distance between the charged amine group and the polymer backbone clearly has an effect on the degree of orientation obtained. PAH, with one methylene unit separating the amine group from the backbone provides the best and most consistent chromophore orientation observed. The effect on deposition and chromophore orientation by an additional methylene unit between the amine and polymer backbone, for a total of 2 units, would provide insight into the steric hindrance issue. A second way to probe the steric hindrance issue would be molecular modeling. "Docking" calculations may even be capable of predicting which dye / polycation pairs will successfully form layer-by-layer films.

Appendix A. Ellipsometry Details

Variable Angle Spectroscopic Ellipsometry (V.A.S.E.) was used to measure the film thicknesses. The ellipsometry was conducted on a J. A. Woolam VB-200 ellipsometer with WVASE32 software Version 3.361. Data was acquired at incident angles of 55°, 60°, 65°, 70°, and 75°. A wavelength range of 350 nm to 1000 nm was used in Chapters 3 and 6. Data in Chapters 4, 5 and 7 used a wavelength range of 350 nm to 800 nm. This was changed to speed up data acquisition, as the data was typically featureless between 800 nm and 1000 nm. Ellipsometry experiments are conducted on the smooth side of the slide's frosted end. This eliminates backside reflections off the glass, and simplifies data analysis.

Once the ellipsometric data has been obtained it is necessary to construct a model to determine the film thickness. The models used consisted of two layers, one for the glass substrate and a second layer which represented the bulk film. The same model was used for the glass slide for all samples. This model consists of a table of n and k values and is shown in Table A.1. Figure A.1 shows n and k as a function of wavelength.

Table A.1 – n and k values used in ellipsometry to model the glass substrate.

Wavelength (nm)	n	k	Wavelength (nm)	n	k
350	1.53	0.039	680	1.504	0.044
360	1.528	0.04	690	1.504	0.044
370	1.526	0.041	700	1.503	0.045
380	1.525	0.042	710	1.503	0.047
390	1.523	0.043	720	1.503	0.048
400	1.521	0.044	730	1.503	0.05
410	1.52	0.045	740	1.503	0.051
420	1.518	0.045	750	1.502	0.052
430	1.517	0.046	760	1.502	0.053
440	1.516	0.046	770	1.502	0.055
450	1.514	0.047	780	1.502	0.057
460	1.513	0.047	790	1.501	0.058
470	1.512	0.048	800	1.501	0.06
480	1.511	0.048	810	1.501	0.061
490	1.51	0.048	820	1.5	0.062
500	1.509	0.048	830	1.5	0.063
510	1.508	0.048	840	1.5	0.063
520	1.508	0.048	850	1.5	0.065
530	1.507	0.047	860	1.499	0.066
540	1.506	0.047	870	1.499	0.067
550	1.505	0.047	880	1.499	0.068

560	1.505	0.046	890	1.498	0.069
570	1.505	0.047	900	1.498	0.069
580	1.504	0.046	910	1.498	0.07
590	1.504	0.045	920	1.498	0.071
600	1.504	0.044	930	1.498	0.071
610	1.503	0.043	940	1.497	0.072
620	1.503	0.043	950	1.497	0.072
630	1.503	0.043	960	1.497	0.073
640	1.503	0.043	970	1.497	0.073
650	1.503	0.043	980	1.496	0.073
660	1.503	0.043	990	1.496	0.074
670	1.503	0.044	1000	1.496	0.074

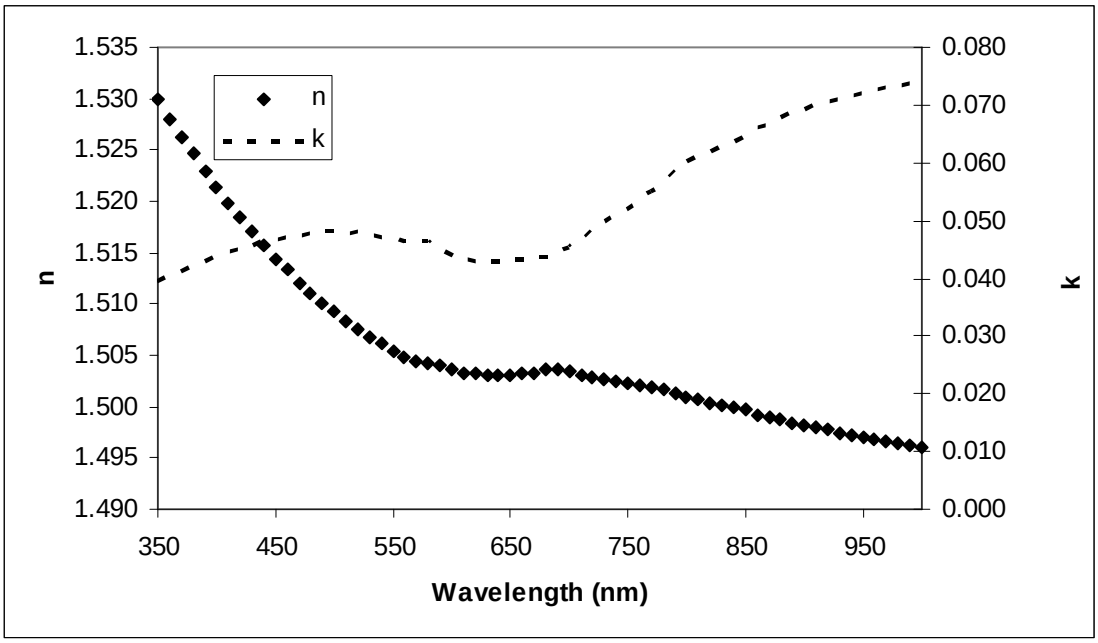

Figure A.1 –n and k values as a function of wavelength for the glass substrate

The layer that represents the film was constructed using a Lorentz oscillator model. This model, shown in equation A.1, models the absorbance behavior of a material:

$$\varepsilon = \varepsilon_1 + i\varepsilon_2 = \varepsilon_\infty + \sum_{k=1}^{n} A_k \left[\frac{1}{E + E_k + iB_k} - \frac{1}{E - E_k + iB_k} \right] \qquad \text{A.1}$$

where ε_∞ represents ε well outside the absorbance bands, A_k is the amplitude of the k^{th} absorbance, E is the photon energy, E_k is the energy of the k^{th} absorbance peak and B_k is the k^{th} peak's width. From ε, values of n and k can be calculated as shown in equations A.2 and A.3.[1]

$$n = \sqrt{\frac{\left[\varepsilon_1 + \sqrt{(\varepsilon_1^2 + \varepsilon_2^2)}\right]}{2}} \quad \text{A.2}$$

$$k = \sqrt{\frac{\left[-\varepsilon_1 + \sqrt{(\varepsilon_1^2 + \varepsilon_2^2)}\right]}{2}} \quad \text{A.3}$$

Since these films all absorb light in the range where the ellipsometry experiments are conducted this is the best model to use. The same model was used for the chromophore regardless of the polycation used or any other processing variables. For all deposition conditions these models gave "good" fits to the experimental data. The "normal fit" was used in all cases to determine the thickness of the film.

The PS-119, PCBS and Procion Red models exist as a table of n and k values with wavelength that were constructed from Lorentz model parameters. The models for Procion Brown and Procion Orange consist solely of the Lorentz parameters. The specific details of the models are given below.

PS-119

Table A.2 – n and k parameters used to model PS-119 films.

Wavelength (nm)	n	k	Wavelength (nm)	n	K
350	1.178	0.144	680	1.822	0.188
360	1.16	0.173	690	1.818	0.178
370	1.143	0.208	700	1.813	0.169
380	1.129	0.249	710	1.808	0.161
390	1.119	0.297	720	1.804	0.154
400	1.117	0.352	730	1.8	0.147
410	1.124	0.412	740	1.796	0.141
420	1.143	0.475	750	1.792	0.135
430	1.177	0.537	760	1.788	0.13
440	1.224	0.595	770	1.785	0.125
450	1.284	0.643	780	1.781	0.12
460	1.354	0.679	790	1.778	0.116
470	1.43	0.7	800	1.775	0.112
480	1.508	0.705	810	1.772	0.108
490	1.582	0.695	820	1.769	0.104
500	1.649	0.671	830	1.766	0.101
510	1.706	0.638	840	1.764	0.098
520	1.753	0.599	850	1.761	0.095
530	1.789	0.557	860	1.759	0.092
540	1.815	0.515	870	1.756	0.09
550	1.834	0.474	880	1.754	0.087
560	1.846	0.436	890	1.752	0.085
570	1.853	0.402	900	1.75	0.083

580	1.857	0.37	910	1.748	0.081
590	1.858	0.342	920	1.746	0.079
600	1.857	0.316	930	1.744	0.077
610	1.854	0.293	940	1.742	0.075
620	1.851	0.273	950	1.741	0.073
630	1.847	0.255	960	1.739	0.072
640	1.842	0.239	970	1.738	0.07
650	1.837	0.224	980	1.736	0.069
660	1.832	0.211	990	1.735	0.067
670	1.827	0.199	1000	1.733	0.066

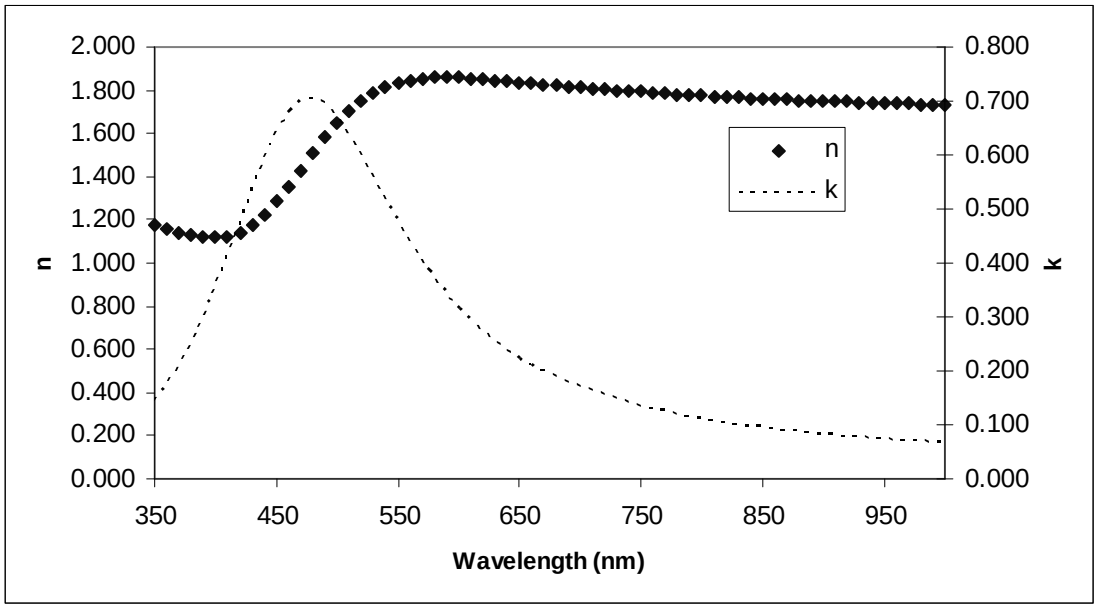

Figure A.2 –n and k values as a function of wavelength for the PS-119 model

PCBS

Table A.3 – n and k parameters used to model PCBS films.

Wavelength (nm)	n	k	Wavelength (nm)	n	k
350	1.426	0.978	680	2.034	0.159
360	1.56	1.058	690	2.031	0.155
370	1.721	1.095	700	2.028	0.152
380	1.888	1.076	710	2.025	0.149
390	2.032	1.007	720	2.023	0.146
400	2.137	0.908	730	2.02	0.143
410	2.2	0.8	740	2.018	0.14
420	2.231	0.7	750	2.016	0.137
430	2.24	0.614	760	2.014	0.135
440	2.237	0.543	770	2.012	0.133
450	2.226	0.484	780	2.011	0.13
460	2.212	0.436	790	2.009	0.128
470	2.197	0.397	800	2.007	0.126
480	2.182	0.365	810	2.006	0.124

490	2.168	0.338	820	2.004	0.122
500	2.155	0.315	830	2.003	0.12
510	2.142	0.295	840	2.002	0.118
520	2.131	0.278	850	2	0.116
530	2.12	0.264	860	1.999	0.115
540	2.111	0.251	870	1.998	0.113
550	2.102	0.24	880	1.997	0.111
560	2.094	0.229	890	1.996	0.11
570	2.086	0.22	900	1.995	0.108
580	2.079	0.212	910	1.994	0.107
590	2.073	0.205	920	1.993	0.106
600	2.067	0.198	930	1.992	0.104
610	2.062	0.192	940	1.991	0.103
620	2.057	0.186	950	1.99	0.102
630	2.052	0.181	960	1.99	0.1
640	2.048	0.176	970	1.989	0.099
650	2.044	0.171	980	1.988	0.098
660	2.04	0.167	990	1.988	0.097
670	2.037	0.163	1000	1.987	0.096

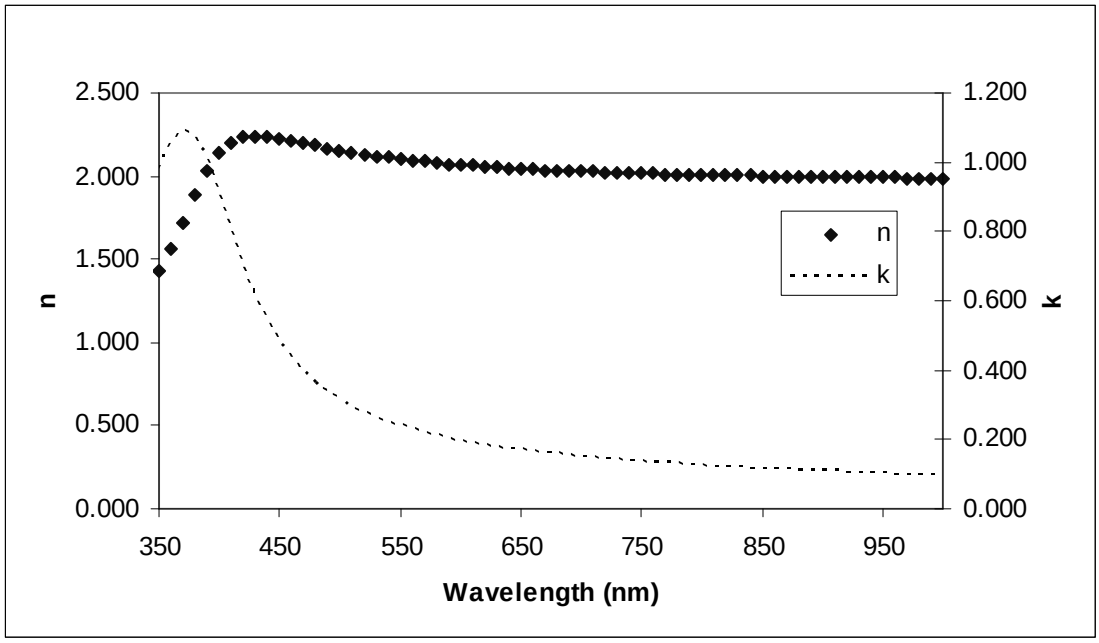

Figure A.3 –n and k values as a function of wavelength for the PCBS model

Procion Red

Table A.4 – n and k parameters used to model Procion Red films.

Wavelength (nm)	n	k	Wavelength (nm)	n	k
350	1.808	0.085	580	1.811	0.14
360	1.808	0.087	590	1.811	0.143
370	1.808	0.09	600	1.812	0.145
380	1.808	0.092	610	1.812	0.148
390	1.808	0.095	620	1.812	0.15
400	1.808	0.097	630	1.812	0.152
410	1.808	0.099	640	1.812	0.155
420	1.809	0.102	650	1.813	0.157
430	1.809	0.104	660	1.813	0.16
440	1.809	0.107	670	1.813	0.162
450	1.809	0.109	680	1.813	0.164
460	1.809	0.111	690	1.813	0.167
470	1.809	0.114	700	1.814	0.169
480	1.809	0.116	710	1.814	0.172
490	1.81	0.119	720	1.814	0.174
500	1.81	0.121	730	1.814	0.176
510	1.81	0.124	740	1.815	0.179
520	1.81	0.126	750	1.815	0.181
530	1.81	0.128	760	1.815	0.184
540	1.81	0.131	770	1.815	0.186
550	1.811	0.133	780	1.816	0.188
560	1.811	0.136	790	1.816	0.191
570	1.811	0.138	800	1.816	0.193

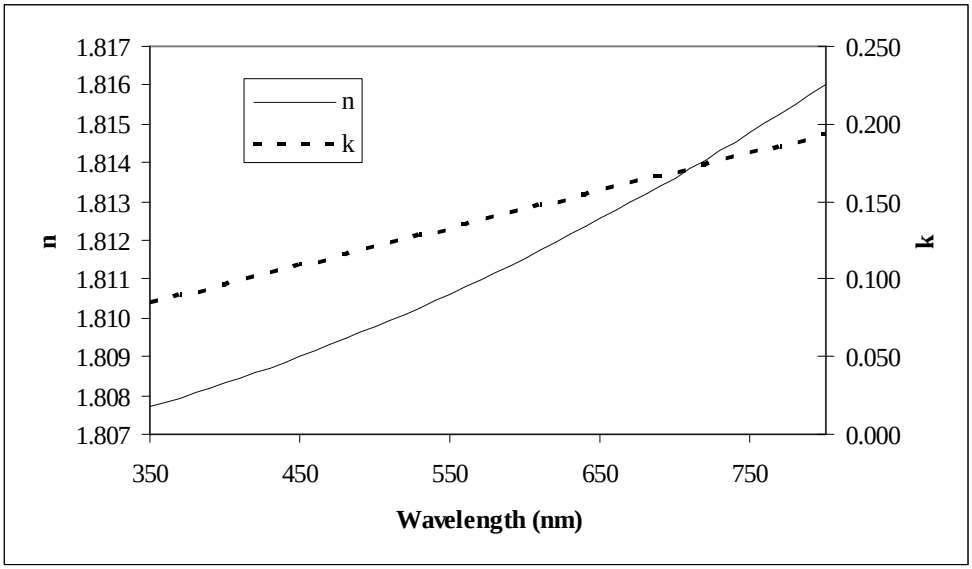

Figure A.4 –n and k values as a function of wavelength for the Procion Red model

Procion Brown Model Parameters

ε_∞ 3.2918
A_1 1.8035
B_1 0.95283
E_1 2.5535
A_2 1.2624
B_2 0.001
E_2 4.3696

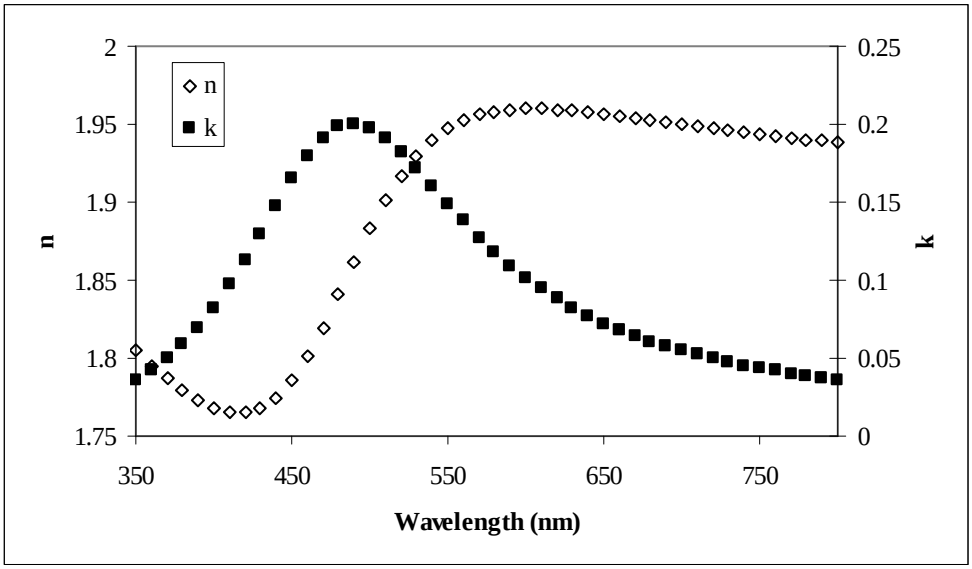

Figure A.5 –n and k values generated from the Lorentz parameters from the Procion Brown model

Procion Orange Model Parameters

ε_∞ 3.5575
A_1 1.5937
B_1 0.56065
E_1 2.4815
A_2 0.10875
B_2 0.028495
E_2 1.5035

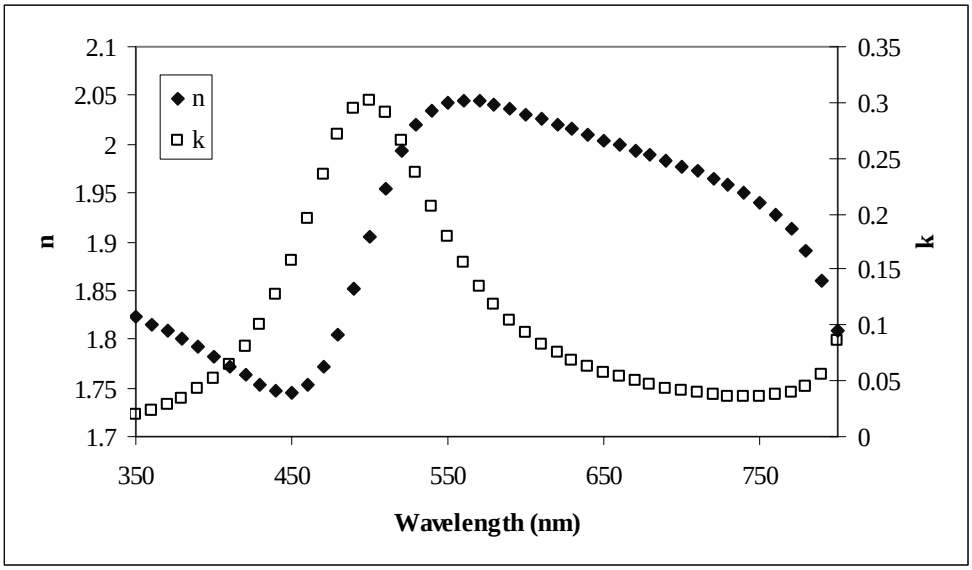

Figure A.6 –n and k values generated from the Lorentz parameters from the Procion Orange model

[1] *J. A. Woollam Ellipsometry Tutorial*. Retrieved June 20, 2003 from http://www.jawoollam.com/Tutorial/Tutorial_intro.html

Appendix B. Error Propagation Derivation

Assume x is function of the variables u and v:

$$x = f(u,v) \tag{B.1}$$

The mean of x is given by:

$$\bar{x} = \frac{1}{N}\sum_{i=1}^{N} x_i \tag{B.2}$$

$$x_i - \bar{x} = (u_i - \bar{u})\left(\frac{dx}{du}\right) + (v_u - \bar{v})\left(\frac{dx}{dv}\right) \tag{B.3}$$

$$\sigma_x^2 = \frac{1}{N-1}\sum_{i=1}^{N}(x_i - \bar{x})^2 = \frac{1}{N-1}\sum_{i=1}^{N}\left((u_i - \bar{u})\left(\frac{dx}{du}\right) + (v_u - \bar{v})\left(\frac{dx}{dv}\right)\right)^2 \tag{B.4}$$

$$\sigma_x^2 = \frac{1}{N-1}\sum_{i=1}^{N}\left[(u_i - \bar{u})^2\left(\frac{dx}{du}\right)^2 + (v_i - \bar{v})^2\left(\frac{dx}{dv}\right)^2 + 2(u_i - \bar{u})(v_i - \bar{v})\left(\frac{dx}{du}\right)\left(\frac{dx}{dv}\right)\right] \tag{B.5}$$

$$\sigma_u^2 = \frac{1}{N-1}\sum_{i=1}^{N}\left[(u_i - \bar{u})^2\right] \tag{B.6}$$

$$\sigma_v^2 = \frac{1}{N-1}\sum_{i=1}^{N}\left[(v_i - \bar{v})^2\right] \tag{B.7}$$

$$\sigma_{uv}^2 = \frac{1}{N-1}\sum_{i=1}^{N}\left[(u_i - \bar{u})(v_i - \bar{v})\right] \tag{B.8}$$

$$\sigma_x^2 = \sigma_u^2\left(\frac{dx}{du}\right)^2 + \sigma_v^2\left(\frac{dx}{dv}\right)^2 + 2\sigma_{xuv}^2\left(\frac{dx}{du}\right)\left(\frac{dx}{dv}\right) \tag{B.9}$$

If u and v are uncorrelated $\sigma_{uv} = 0$.

$$\sigma_x^2 = \sigma_u^2\left(\frac{dx}{du}\right)^2 + \sigma_v^2\left(\frac{dx}{dv}\right)^2 \tag{B.10}$$

For the calculation of $\chi^{(2)}$ we have:

$$\chi_{film}^{(2)} = \chi_q^{(2)}\frac{2}{\pi}\frac{l_{c,q}}{t_{bilayer}}\frac{m}{\sqrt{I_q^{2\omega}}}\sqrt{\frac{I_{standard,quartz}^{2\omega}}{I_{standard,film}^{2\omega}}} \tag{B.11}$$

$$\chi_{film}^{(2)} = A\frac{m}{t_{bilayer}} \tag{B.12}$$

where the A term is a collection of constants:

$$A = \chi_q^{(2)} \frac{2}{\pi} \frac{l_{c,q}}{\sqrt{I_q^{2\omega}}} \sqrt{\frac{I_{standard,quartz}^{2\omega}}{I_{standard,film}^{2\omega}}} \tag{B.13}$$

The slope (m) and standard deviation of the slope ($\sigma_{m)}$ of the square root of the second harmonic intensity vs. bilayer plots can be calculated using least squares regression. The bilayer thickness ($t_{bilayer}$) is obtained from ellipsometry results and the standard deviation of the bilayer thickness (σ_t) can be calculated from the available thickness. This allows to the calculation of the standard deviation of $\chi^{(2)}$.

$$x = \chi^{(2)} \tag{B.14}$$

From equation B.10;

$$\sigma_x^2 = \sigma_m^2 \left(\frac{dx}{dm}\right)^2 + \sigma_t^2 \left(\frac{dx}{dt}\right)^2 \tag{B.15}$$

Partial differentiation of B.12 results in:

$$\frac{dx}{dm} = \frac{A}{t_{bilayer}} \tag{B.16}$$

$$\frac{dx}{dt} = -\frac{Am}{t_{bilayer}^2} \tag{B.17}$$

Substitution of B.16 and B.17 into B.15 leads to:

$$\sigma_x^2 = \sigma_m^2 \left(\frac{A}{t_{bilayer}}\right)^2 + \sigma_t^2 \left(-\frac{Am}{t_{bilayer}^2}\right)^2 \tag{B.18}$$

Which results in a standard deviation of $\chi^{(2)}$, σ_χ of:

$$\sigma_\chi = \sqrt{\frac{A^2\sigma_m^2}{t_{bilayer}^2} + \frac{A^2 m^2 \sigma_t^2}{t_{bilayer}^4}} \tag{B.19}$$

Appendix C. Vita

Matthew Thomas Guzy entered the world on October 10, 1975 in Harrisburg, Pennsylvania, the son of Thomas and Barbara Guzy. In 1994, upon completion of high school, he entered the Pennsylvania State University and began his collegiate studies. Matt received his Bachelor of Science in Chemical Engineering in the Spring of 1998. Immediately, in the Fall of 1998, Matt began his graduate work at the Virginia Polytechnic Institute & State University. He wrapped his studies up in 2003 and began a new life in the real world.